Indole diterpenoid secondary metabolites produced by the *Epichloë festucae* var. *lolii* – *Lolium perenne* symbiosis.

A thesis
submitted in fulfilment
of the requirements of the degree
of
Doctor of Philosophy in Chemistry
at
The University of Waikato
by

Sangata Ana Fiealu Kaufononga

THE UNIVERSITY OF
WAIKATO
Te Whare Wānanga o Waikato

2019

Abstract

The indole diterpenoid intermediates of lolitrems in a crude extract of *Lolium perenne* (*L. perenne*) seed infected with *Epichloë festucae* var. *lolii* (*E. festucae* var. *lolii*) and their biological activity against porina larvae were investigated.

Liquid-liquid partitioning of the crude extract, together with a series of bench columns (normal and reversed phase) and semi-preparative High Performance Liquid Chromatography (HPLC) yielded the novel compounds A – D (**64** – **67**).

Mass spectrometry (MS) and Nuclear Magnetic Resonance (NMR) spectroscopy were used to determine the structures of these alkaloids. The indole moiety of known indole diterpenoids was modified to a six-membered ring in the novel compounds A – D (**64** – **67**), with the right side of these molecules similar to that of lolitrem B (**3**) and terpendole C (**49**). Compounds A – D (**64** – **67**) differ in the stereochemistry and substituent at C-2. The structural features of these compounds are very unusual. These contain a spiro centre that fuses the modified indole region to the right side, indicating that they may be artefacts rather than naturally occurring, which in turn, could explain why they are not detectable in the Liquid Chromatography Mass Spectrometry (LC-MS) analysis of fresh extract. However, further work would be required to confirm this.

The known alkaloids, terpendole D (**50**), 13-desoxypaxilline (**37**) and paspaline (**42**) were also isolated, together with a potential emindole analogue. This is the first report of terpendole D (**50**) from this ryegrass-endophyte association. The presence of an emindole analogue suggested that further intermediates are yet to be isolated from this association as indicated in the LC-MS analysis of the crude extract. However, due to the scarcity of the emindole analogue, complete structural confirmation was not possible.

The biological activity of paxilline (**36**), lolitrem B (**3**), 13-desoxypaxilline (**37**), paspaline (**42**), terpendole D (**50**) and compounds A (**64**) and B (**65**) on porina

larvae was determined using a semi-synthetic diet feeding bioassay. These compounds had not been previously tested on porina. Paxilline (**36**) had a dose-dependent effect on both food consumption and larval weight. Diet consumption and weight gain of porina larvae were significantly reduced by paxilline at concentrations of 2.5, 5 and 10 μg/g but not at concentrations of 1.0 μg/g, compared to dimethyl sulfoxide (DMSO) solvent control diet. Lolitrem B (**3**) had a similar effect on consumption and weight gain to that of paxilline (**36**) at concentrations of 5 and 10 μg/g but there was no indication that 13-desoxypaxilline (**37**), terpendole D (**50**), paspaline (**42**), compound A (**64**) or compound B (**65**) reduced feeding by porina larvae.

Acknowledgements

First and foremost, I will raise my voice and give thanks for the wisdom that was gifted me by the Almighty to empower me to walk on and walk strong during this journey. TO GOD BE THE GLORY, without him, I would not be able to make it to the end.

I would acknowledge my Chief supervisor Associate Professor Michèle Prinsep and my two other supervisors Dr Sarah Finch and Dr Alison Popay. Thank you for being patient with me and for all the guidance and encouragement that I received and thank you for believing that I can do it.

Thank you to Professor Alistair Wilkins for enlightening my doubts on NMR spectroscopy and to Dr Wace Made for supplying LC-MS analysis when requested, not forgetting Nicola Webb, Sweta Bhattarai, Louise Hennessy and Joanne Jensen for helping out with my porina experiments and Colin Ferguson for collecting the porina moths and supplying the eggs. Thank you also to Dr Vanessa Cave for the statistical analysis of my experimental data and Cheryl Ward for checking the formatting and the references.

I would like to express my gratitude for the great opportunity offered by AgResearch Limited in funding my study. Without this financial support, I would have not been able to fulfil the journey. In addition to that, I would like to acknowledge the University of Waikato for the Tertiary Achievement in Pacific Ako (TAPA) Awards as well as the Smethurst Trust Fund of the Methodist Women's fellowship for supporting my journey.

To Reverand Veitomoni Siufanga, the Efalata Trust and Community, Reverand Metuisela Tafuna and the Hamilton Methodist Parish, thank you for all your never-ending support. To my parents-in-law, Siosaia Kaufononga who died early this year in January and Lavelua Kaufononga, thank you for the words of encouragement and the lending hands.

My sincere thankfulness to my father, Sosefo II Siketi Mailangi and my mother Atelete Mailangi who is in heaven (Rest In Peace), thank you for moulding me to who I am today and the numerous sacrifices for me and my siblings. I am forever in debt for your unconditional love and believing in me. To my brothers (‘Atonio, Mikaele, Viliami, Lofitu and Paula Mailangi (RIP)), my sisters (Manu Kailopa Vehikite, ‘Elisapeta ‘Ofa, Malia Langilangi Mailangi, Malia Nasaleti Tausinga, Malia Sema Kaloni, Malia ‘Asopesio Latu and Tapuaki Mailangi (RIP)) and to my extended family, thank you so much.

Last but not least, this thesis is dedicated to my beloved children, Tupou, Lavelua, Sosaia and Joseph and to my devoted husband, David Kaufononga. You are my main inspiration and I cannot thank you enough for your endless support, patience and tolerance. There were many times of up and down during my journey but your vivid voices saying “*Keep going mum*” empowered me to take the extra step and to cross the finishing line. Thank you (Malo ‘aupito) and words are never enough to express my sincere gratitude for being there with me since day one.

Table of Contents

List of Figures

List of Tables

Abbreviations used

ACD	Advanced Chemistry Development
ACN	Acetonitrile
Acyl-CoA	Cholesterol acetyltransferase
ASW	Argentine stem weevil
BB	Black beetle
$CDCl_3$	Chloroform-*d*
COSY	Correlation Spectroscopy
CH_2Cl_2	dichloromethane
DMSO	dimethyl sulfoxide
ECD	Electronic circular dichroism
ESI	Electrospray ionisation
GG	Grass grub
GGDP	Geranylgeranyl diphosphate
HMBC	Heteronuclear Multiple Bond Correlation
HPLC	High Performance Liquid Chromatography
HR	High Resolution
HSQC	Heteronuclear Single Quantum Coherence
HR-MS	High Resolution Mass Spectrometry
IDTs	Indole diterpenoids
LC-MS	Liquid Chromatography Mass Spectrometry
MALDI-TOF	Matrix-Assisted Laser Desorption Ionisation-Time of Flight
MS	Mass Spectrometry
NOE	Nuclear Overhauser effect
NMR	Nuclear Magnetic Resonance
PM	Pasture mealybug
PRG	Perennial ryegrass
ppm	parts per million
RA	Root aphid
SE	Standard endophyte
TAPA	Tertiary Achievement in Pacific Ako
UoW	University of Waikato
UV	Ultraviolet

Chapter 1: Introduction

Epichloë festucae var. *lolii* (*E. festucae* var. *lolii*) is an endophytic fungus that naturally resides in *Lolium perenne (L. perenne)*, commonly known as perennial ryegrass. The fungus and ryegrass form a mutualistic, symbiotic interaction and produce an array of secondary metabolites, which are classified as peramine (**1**), ergot alkaloids (such as ergovaline (**2**)) and indole diterpenoids (such as lolitrem B (**3**)).

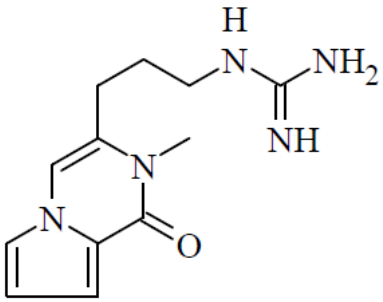

(**1**)

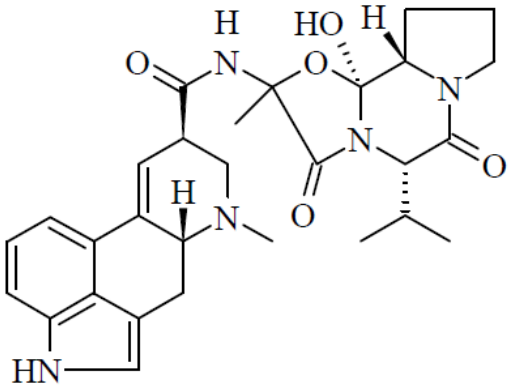

(**2**)

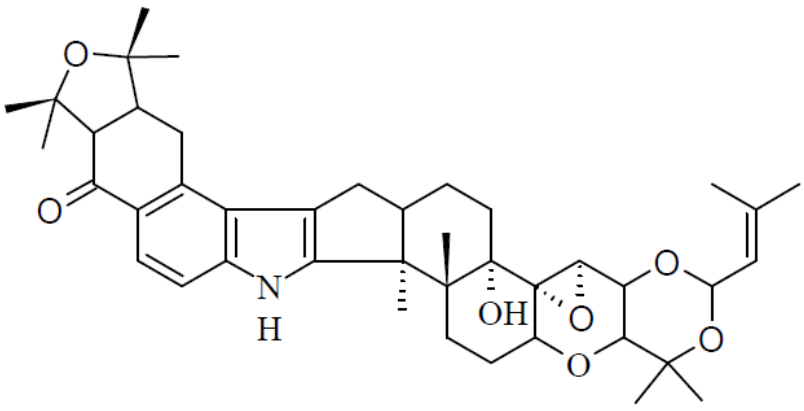

(**3**)

Some of these metabolites such as peramine (**1**), are beneficial, providing protection to the plant from insect attack, while some are detrimental to animal health. The lolitrems are the class of compounds associated with ryegrass staggers, a neurological impairment of livestock grazed on endophyte-infected perennial ryegrass. The main contributor to ryegrass staggers is lolitrem B (**3**),[1] whereas ergovaline (**2**) contributes to heat stress.

The beneficial effect of endophytes has been proven to be important in terms of pastoral agriculture, not only in New Zealand but also in Australia, the United States of America and elsewhere.[2] The naturally occurring endophyte (known as common toxic, wild-type or standard endophyte) is not ideal, due to animal health issues associated with lolitrem B (**3**) and ergovaline (**2**). Therefore, to harness the beneficial effects of endophytes while minimising the detrimental ones, endophytes can be screened to identify those with a favourable chemical profile. The selected endophyte can then be inoculated into perennial ryegrass to generate improved grass-endophyte associations. For this approach to succeed, it is essential to understand the effects of these secondary metabolites on insects and animals so that those with the highest expression of beneficial metabolites and the lowest expression of detrimental metabolites can be prioritised.

Since endophytes are seed transmitted, these grass-endophyte associations can then be sold commercially to farmers. Two such endophytic products, AR1 and AR37, have been very successful. AR1 contains no known mammalian toxins, so is therefore animal-safe. It expresses peramine (**1**) which is effective against Argentine stem weevil, a major pasture pest. AR37 does induce some ryegrass staggers despite the absence of lolitrem B (**3**), thought to be due to the presence of five epoxy-janthitrems including epoxy-janthitrem I (**4**), however, episodes tend to be of lower severity and shorter duration than those induced by the wild-type endophyte. In addition, AR37 provides resistance to a wide array of insect pests, despite the absence of peramine (**1**).[3]

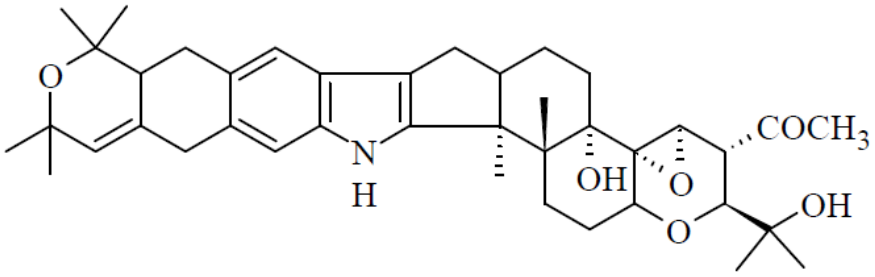

(**4**)

The implementation of such animal-safe grass-endophyte associations not only contributes to the health and welfare of the animals and of the plant hosts but also to the economy.[3] Novel endophyte strains (AR1, AR37) have benefited New Zealand financially by contributing approximately $200 million per annum through increased meat and milk production.[2,3] Recently, the AR37 novel endophyte team (AgResearch) was awarded the prestigious Pickering Medal by the New Zealand Royal Society for their extensive leadership in developing and supporting AR37 endophyte in the agricultural sector, which is estimated to contribute NZ$3.6 billion to the economy through the life of the patent.[4]

1.1 *Epichloë festucae* var. *lolii* endophyte

Epichloë festucae var. *lolii* is the new nomenclature realignment of *Neotyphodium lolii* (*N. lolii*)[5, 6] formerly known as *Acremonium lolii* (*A. lolii*)[7] and *Acremonium loliae* (*A. loliae*).[8] *Epichloë festucae* var. *lolii* is an asexual derivative of the sexual species. *Epichloë* endophytes belong to the Clavicipitaceae family and are systematic and seed transmissible fungi that form mutual symbiotic interactions with temperate grasses in the Poöideae subfamily such as perennial ryegrass.[9]

This endophyte was first identified in New Zealand in the 1940s during intensive research on ryegrass staggers.[10, 11] In 1940, Neil discovered a natural unidentified endophyte fungus which grew intracellularly in the aerial tissues of perennial ryegrass and was seed-transmitted through a female parent rather than pollen.[12] This observation had been previously reported by Sampson in England in 1935.[13] Ryegrass staggers is a seasonal mycotoxicosis of grazing livestock characterised by tremors and incoordination.[14] The staggers symptoms in livestock were observed in New Zealand in the early 1900s by Gilruth[15] in sheep, horses and cattle grazing on ryegrass in summer and autumn and especially during flowering. Animals recovered spontaneously after a change of pasture.[15] Ergot alkaloids were initially thought to be the cause of this disease, as New Zealand pasture grasses are often infected by ergot fungus *Claviceps purpurea* (*C. purpurea*) during the summer and autumn but further research showed ergot alkaloids were not the cause of ryegrass staggers.[16] A similar observation was reported by Hopkirk in 1935 when livestock developed staggers while grazing on short ryegrass growth a few days after rain during a dry autumn.[10] Consistent with this was a report of staggers by Cunningham and Hartley in 1959.[11] The pivotal observation from Fletcher and Harvey in 1981, that grass-endophyte infection was correlated with ryegrass staggers, suggested that this endophyte was involved with the staggers disease.[17] In 1984, Latch and co-workers named the endophyte as *A. loliae*,[8] which is today known as *E. festucae* var. *lolii*.[5]

The discovery of the importance of the endophytic fungus was the catalyst for grass-endophyte research in New Zealand and led to the discovery of lolitrem B (**3**) as the major cause of ryegrass staggers.[1] Furthermore, the resistance of endophyte-

infected perennial ryegrass to Argetine stem weevil was found to be due to the presence of peramine (**1**).[18] Since then, the endophyte *E. festucae* var. *lolii* in *L. perenne* has been considerably researched in New Zealand,[3] with extensive interest in the biological activities of the alkaloids expressed by the endophyte. New Zealand has led the world in understanding the role of fungal endophytes in the pasture and in their utilisation for the benefit of farmers.

1.2 Perennial ryegrass (*Lolium perenne*)

Lolium perenne, commonly known as perennial ryegrass, is a member of the subfamily Poöideae, belonging to the tribe Poaceae, genus *Lolium*.[19] It is native to Europe, North Africa and temperate Asia but has adapted to several temperate areas in the United States of America, Australia and New Zealand.[2] It was introduced to New Zealand in 1880 by English settlers.[20] Perennial ryegrass is closely related to other diploid species including *Lolium pratense* (*Schedonorus pratensis*; meadow fescue) and various species of annual ryegrass.[21] It forms a mutualistic association with the endophytic fungus *E. festucae* var. *lolii*[22] and also hosts *Epichloë typhina* (*E. typhina*) as well as *E. festucae* var. *lolii* × *E. typhina* hybrid (Lp1).[21]

Perennial ryegrass is the major forage and turf grass used in New Zealand due to its quality as feed for livestock, ease of establishment, management and adaptability to various stress conditions.[2] However, it performs poorly in hot, dry conditions and is prone to infection by the crown and stem rust disease in humid summers.[20] Naturally, perennial ryegrass occurs as diploid plants with a standard set of fourteen chromosomes and can be planted in a mixture with white clover and other pasture species.[20] Nowadays, plant breeders have successfully produced cultivars (including Grasslands Nui, Grassland Pacific and Quartet) and hybrids (such as Grassland Marsden and Grassland Greenstone) of perennial ryegrass due to the high demands of commercial activities and more specialisation within pastoral agriculture in New Zealand.[20] Plant breeders have doubled the chromosome numbers to form tetraploid types with bigger cells, more water content, larger seed and larger plants. To date, at least nineteen cultivars (classified according to

flowering time and chromosome numbers present) and at least five hybrids of perennial ryegrass are available in New Zealand.[20]

1.3 The mutual symbiosis

The relationship between *E. festucae* var. *lolii* and *L. perenne* is mutualistic, based on the benefits of exchanges of energy, nutrition, transport and defence (Figure 1.1).

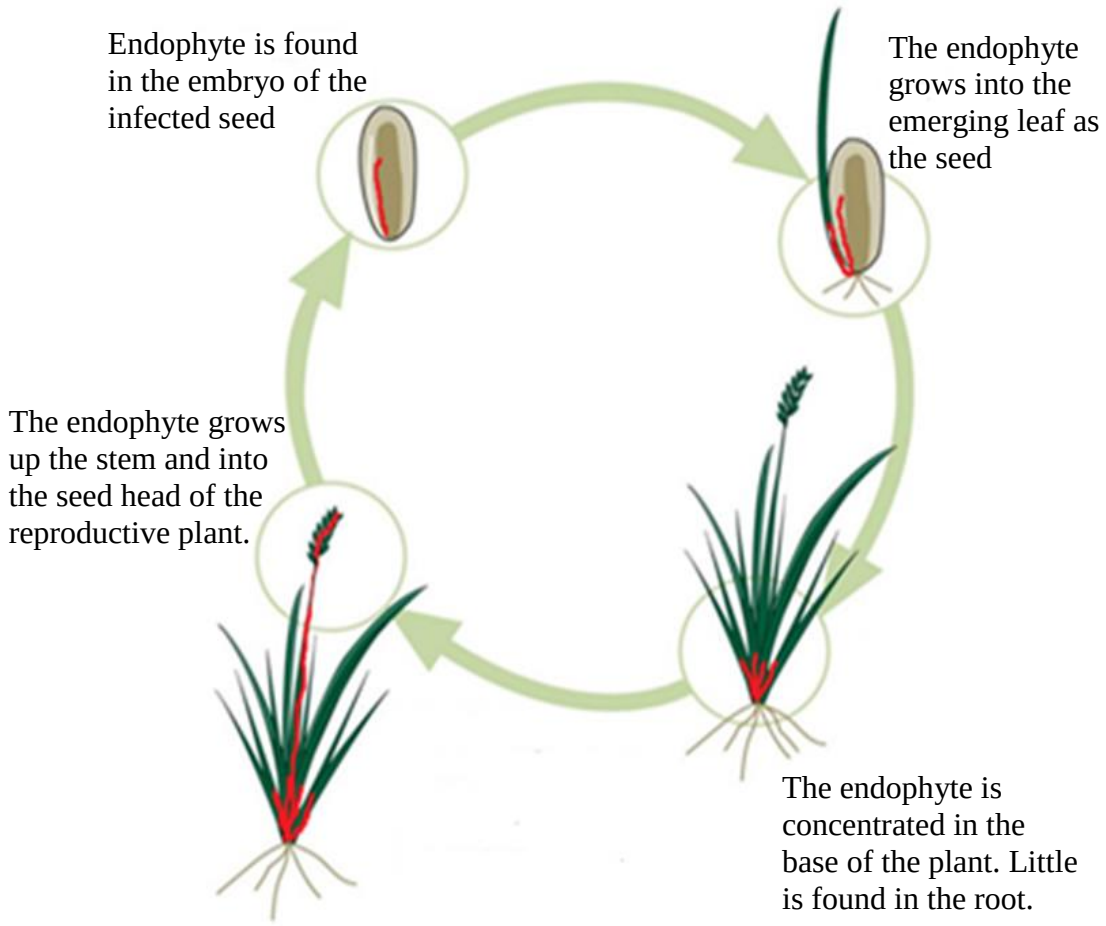

Figure 1.1: Life cycle of endophyte in perennial ryegrass. (Adapted from reference 23).

Such a relationship has no overt symptoms of infection. The above ground part of *L. perenne* harbours the endophyte. The fungus mostly resides in the apoplastic spaces, is seed-borne and grows intercellularly in the aerial parts, especially in the reproductive tiller and leaf sheaths, sparsely in leaf blades.[14] The endophyte is

concentrated in the base of the plant and only a very small amount can be detected in the root tips. It is important for the seed to be infected by endophyte in order to generate the next generation of endophyte-infected grass. The endophyte improves the agricultural value of the plant by conferring a number of biotic and abiotic advantages. However, it can also severely impair the performance of grazing livestock[24-26] due to the production of a vast array of alkaloids, some of which deter insect pests and some of which are detrimental to grazing livestock.[14] It is vital to understand the biological activities of the alkaloids produced by this association so that informed decisions can be made over what compounds are desirable and which are detrimental, to allow superior grass-endophyte associations to be developed.

1.4 Alkaloids isolated from *E. festucae* var. *lolii* – *Lolium perenne*

The most common secondary metabolites produced by the *E. festucae* var. *lolii* and *L. perenne* mutual symbiosis are peramine (**1**), ergot alkaloids and indole diterpenoids. Some of the ergot alkaloids and indole diterpenoids are active against mammals and insects, whereas peramine (**1**) specifically affects insect pests.[3] The ergot alkaloids that will be discussed below are limited to those that are expressed by *E. festucae* var. *lolii*. Further ergot alkaloids are expressed by other grass-endophyte associations but are beyond the scope of this study. As indole diterpenoids are the main metabolites studied in this research, the range of indole diterpenoids discussed is not restricted to those expressed by *E. festucae* var. *lolii* - *L. perenne* but also their structural analogues from other grass-endophyte associations.

1.4.1 Peramine (1)

Peramine (**1**) is a highly polar, pyrrolopyrazine alkaloid. It was structurally elucidated in 1986 by Gaynor and Rowan[27] and is non-toxic to livestock.[28] It was found to be fairly evenly distributed in plant tissues and did not accumulate in older tissue such as root, crown and dead leaves.[29] Peramine (**1**) is translocated from the endophyte into plant intercellular spaces where it is either metabolised or mobilised.[22]

1.4.2 Ergot alkaloids

Ergot alkaloids are complex compounds which are classified into three groups: clavines, simple lysergic acid amides and ergopeptides.[30] Ergot alkaloids share a common tetracyclic ergoline ring system methylated at nitrogen N6 and substituted at C-8 (Figure 1.2). In some of the ergot alkaloids, the sidechain (R) is comprised of amino acids.[31]

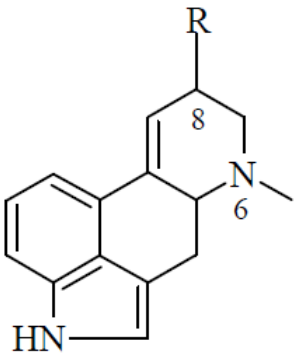

Figure 1.2: The general structure of ergot alkaloids, where R is the side chain consisting of amino acids.

Several ergot alkaloids have been reported to be expressed by *E. festucae* var. *lolii* in *L. perenne*. Ergovaline (**2**), the primary ergot peptide alkaloid, was isolated from sclerotia of *C. purpurea*,[32] *Epichloë festucae coenophiala* (*E. festucae coenophiala*) infected tall fescue[33] and also from *E. festucae* var. *lolii* (wild-type) infected perennial ryegrass.[34] It is concentrated in the stem and basal leaf sheath of intermediate aged host plants.[22]

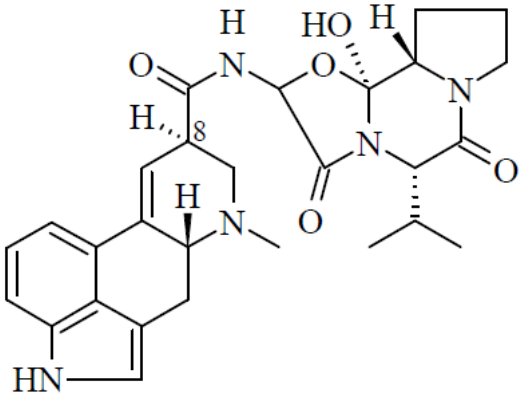

(**5**)

Ergovalinine (**5**) is the C-8 epimer of ergovaline (**2**), differing in the stereochemistry of attachment to the ergoline ring system and has also been reported from endophyte-infected perennial ryegrass.[35, 36]

The structures of ergine (**6**), a simple lysergic acid derivative and ergonovine (**7**), a related lysergyl amide, were tentatively reported in 1993 by TePaske and co-workers from endophyte-infected perennial ryegrass[37] but Lane and co-worker in 1999[36] confirmed that ergonovine (**7**) was not presented in the ryegrass. This supported the suggestion of Shelby in 1997[38] that the presence of ergonovine (**7**) in ryegrass from Tepaske's reports must have been due to contamination from *C. purpurea*.

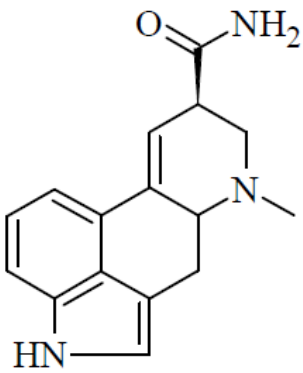

(**6**)

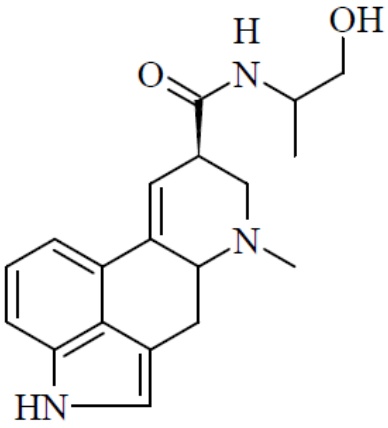

(**7**)

Chanoclavine-I (**8**) was previously reported from herbage of tall fescue (*Schedonorus arundinacea*) infected with the endophyte *Neotyphodium coenophialum* (now *E. coenophiala*) and from the seed of infected perennial ryegrass.[36, 39, 40]

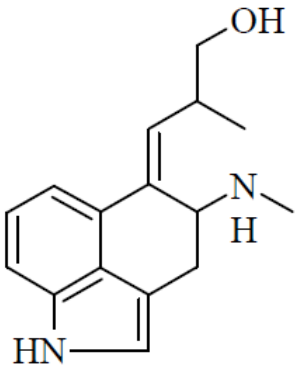

(**8**)

Ergotamine (**9**), is a very similar toxin to ergovaline (**2**) and has been identified in the seed heads of endophyte-infected tall fescue. Its presence in perennial ryegrass was due to contamination from *C. purpurea*.[41]

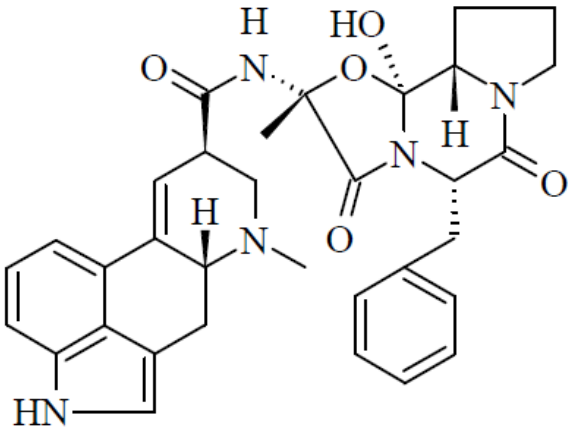

(**9**)

In 2011, a new ergot alkaloid (molecular mass 593 Da) was detected by Lehner and co-workers from perennial ryegrass hay silage associated with bovine reproductive problems but structural elucidation was not completed.[42]

1.4.3 Indole Diterpenoids

Indole diterpenoids are a structurally diverse group of natural products with a common core structure of a cyclic diterpene derived skeleton (derived from geranylgeranyl diphosphate (GGDP) (**10**) and an indole moiety (derived from tryptophan (**11**).[43]

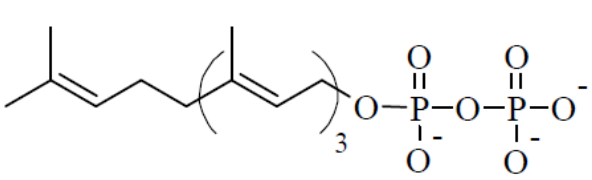

(**10**)

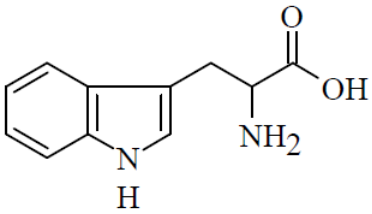

(**11**)

Many indole diterpenoids including lolitrems, paxilline analogues, paspalines, terpendoles, lolitriol, lolicines, lolilline and epoxy-janthitrems, have been isolated from the *E. festucae* var. *lolii* - *L. perenne* symbiosis and are further discussed below.[44-48]

1.4.3.1 Lolitrems

Lolitrems are lipophilic compounds which accumulate in the older tissue of the plant host, with low levels in young tissue.[22] They are distinctive since they can be detected by fluorescence and possess a characteristic ultraviolet (UV) absorbance spectrum with maxima at 268 and 280 nm.[14]

The discovery of the presence of lolitrem compounds in endophyte-infected perennial ryegrass was initiated in the early 1980s by Gallagher and his team, when they detected lolitrems A (**12**), B (**3**) and C (**13**) from material associated with ryegrass staggers.[49] The diversity of lolitrems reported from endophyte-infected perennial ryegrass is due to the structural variations at C-31, C-35, C-44, C-45, C-10, C-14, C-16 and C-27 and the stereochemistry at the A/B ring junction (labelling is shown in lolitrem A (**12**)).

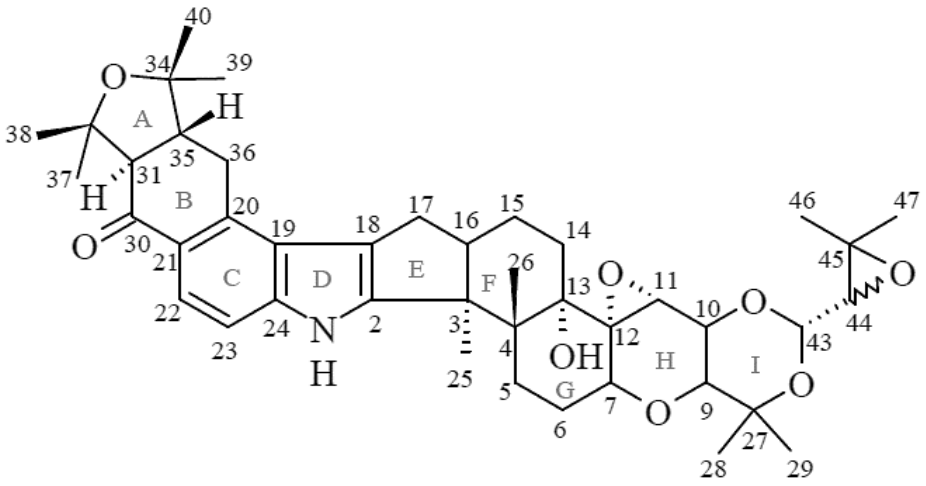

(**12**)

In 1981, Gallagher and co-workers identified lolitrem A (**12**),[1] with an epoxy moiety at C-44 and C-45, which was structurally characterised by Munday-Finch and co-workers in 1995.[50]

Lolitrem B (**3**) is the principal neurotoxin responsible for ryegrass staggers; although it is apparent that some other indole diterpenoids may also contribute to the toxicity of ryegrass.[45, 47, 51, 52] It was structurally characterised in 1984. The stereochemistry at the A/B ring junction was not defined[53] but was later determined by Ede and co-workers in 1994.[54]

Lolitrem C (**13**) was isolated in 1984 with a molecular mass of 687 g/mol[49] and a proposed structure of 44,45-dihydrololitrem B, based on Nuclear Magnetic Resonance (NMR) spectroscopy and High-Resolution Mass Spectrometry (HRMS).[53] In 1994, Miles and co-workers identified that the sample which Gallagher worked on was actually a sample of lolitrem E (**14**) but to avoid confusion, the originally proposed structure for lolitrem C (**13**) remained as assigned by Gallagher and his team (1984).[51] Lolitrem C (**13**) has not been isolated to date.

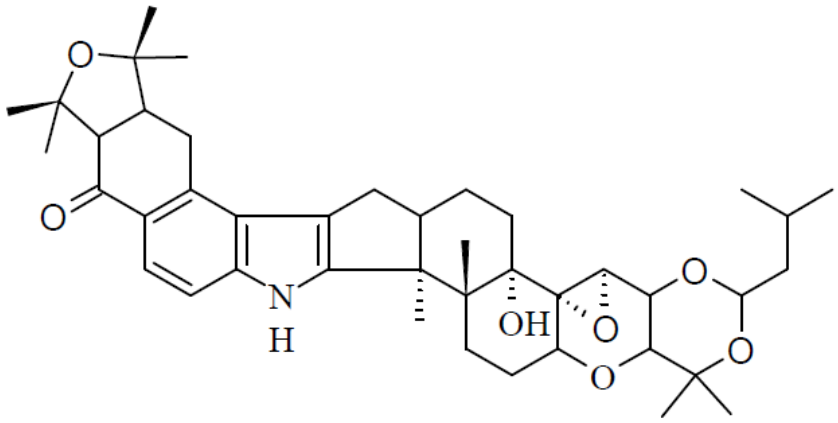

(**13**)

Lolitrem D was identified as possessing a molecular mass of 703 g/mol.[49] No further information has been reported to date.

Lolitrem E (**14**) differs from lolitrem B (**3**) in that it is an ether rather than an acetal indole diterpenoid. It was proposed as a precursor for lolitrem B (**3**) due to structural similarities.[1, 51]

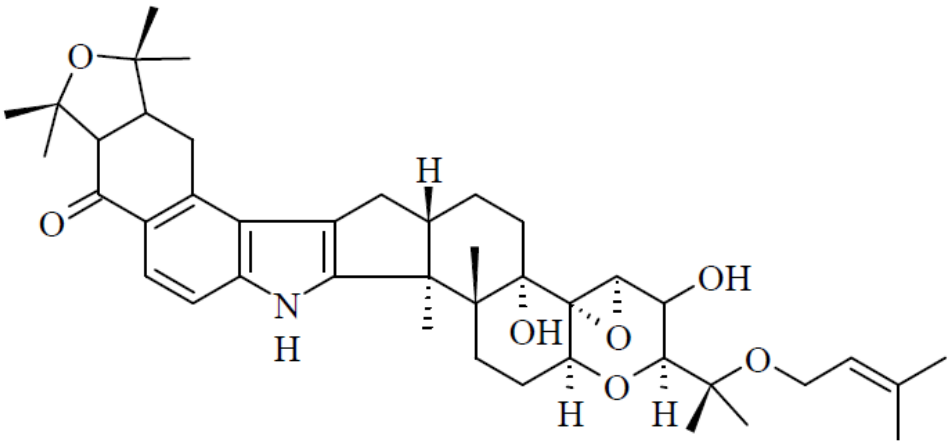

(**14**)

The other lolitrem variants were mainly discovered and isolated from *L. perenne* infected with wild-type endophyte during the course of the doctoral studies of Dr Munday-Finch.[55] The structural characterisation of each compound was achieved with mass spectrometry and NMR spectroscopy.

Lolitrem F (**15**), has similar structural features to lolitrem B (**3**) but with a *cis* H-31α, H-35α A/B ring junction while lolitrem G (**16**), is an isomer of lolitrem A (**12**) with a *cis* H-31α, H-35α A/B ring junction.[55]

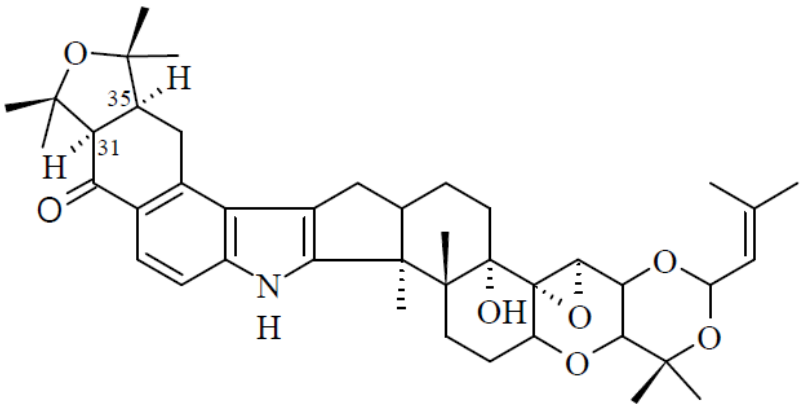

(**15**)

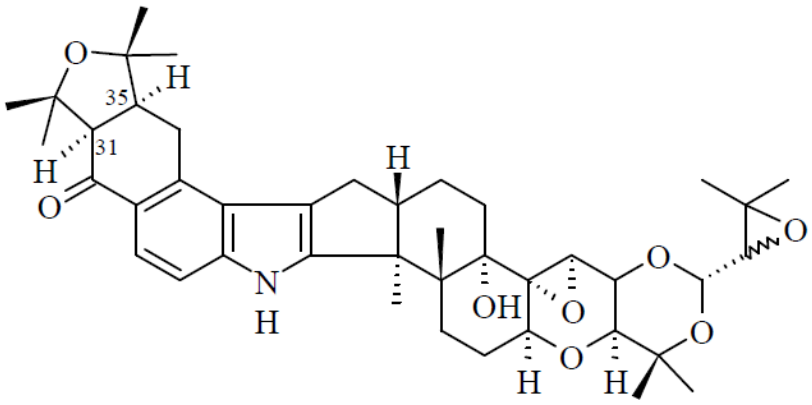

(**16**)

Lolitrem H (**17**) was isolated as lolitrem H-acetate (**18**) and identified as an analogue of lolitrem B (**3**) which had been modified by the addition of a 14-hydroxyl group. The compound was derivatised by an acetylation reaction during the isolation process.[55]

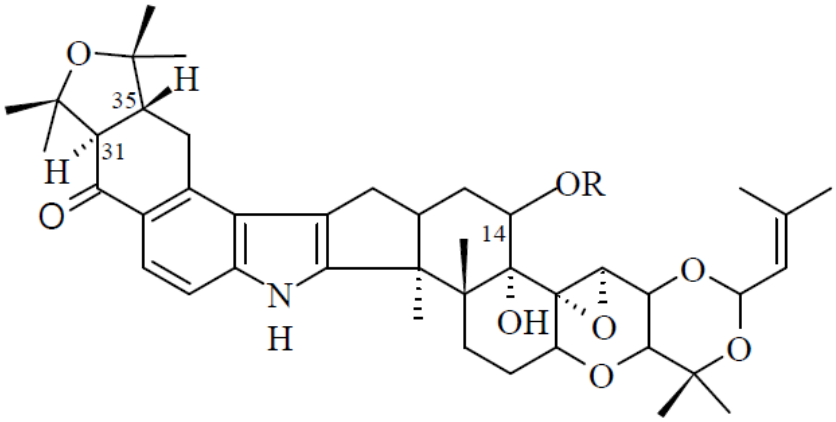

(**17**) R = H

(**18**) R = Ac

Lolitrem J (**19**), was isolated as lolitrem J-acetate (**20**). NMR spectroscopy could not confirm the actual structure of the compound, however, acetylation of lolitrem J (**19**) was carried out in pyridine and in comparison to lolitriol (**30**), the natural form of lolitrem J (**19**) was established as lolitriol 27-*O*-acetate.[55]

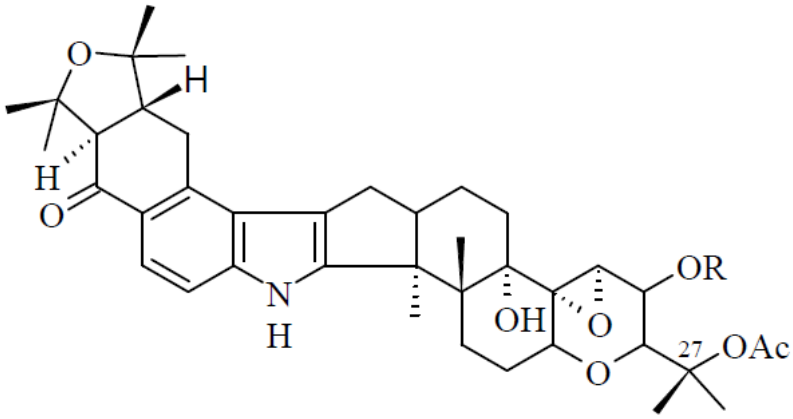

(**19**) R = H

(**20**) R = Ac

Lolitrem K (**21**) is an analogue of lolitrem B (**3**), lacking the prenyl moiety and a methyl group from ring I but with the addition of an acetate group and two olefinic protons on the H ring. It was isolated as lolitrem K-10-*O*-acetate (**22**).[55]

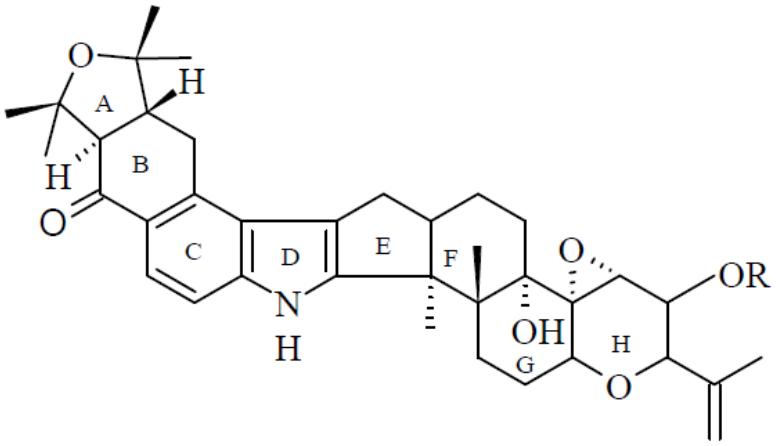

(**21**) R = H

(**22**) R = Ac

Lolitrem L (**23**) was isolated as a mixture with lolitrem G (**16**). The structure of lolitrem L (**23**) was obtained from the elimination of NMR data of lolitrem G (**16**) and by comparison with the NMR data of lolitrem E (**14**) in chloroform-*d* ($CDCl_3$). Based on the available spectroscopic data, lolitrem L (**23**) was proposed as an analogue of lolitrem E (**14**) with a *cis* H-31α, H-35α ring junction.[55]

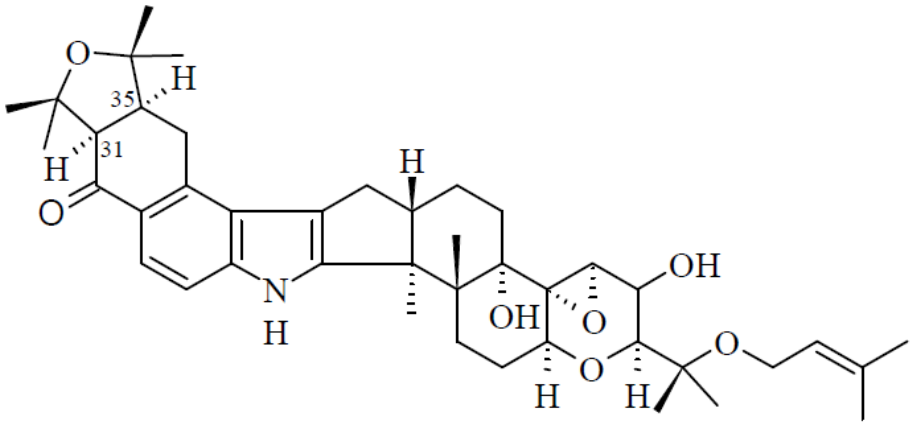

(**23**)

Lolitrem M (**24**) was identified as an analogue of lolitrem B (**3**) with modification at rings G-I, including loss of an acetate moiety from ring I. It contains a *trans* ring A/B system as in lolitrem B (**3**).[55]

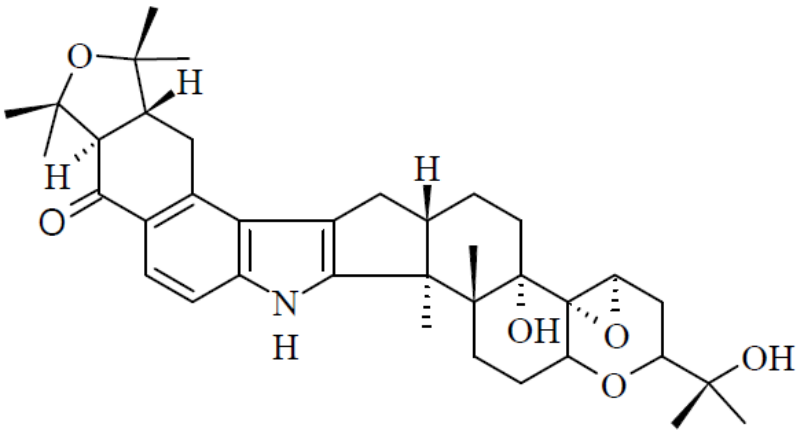

(**24**)

Lolitrem N (**25**) was isolated and elucidated as its propionate form (**26**) and identified as 35-*epi*lolitriol.[47] Another naturally occurring metabolite was 31-*epi*lolitrem N (**27**). This compound was shown to be identical to lolitriol-10-*O*-acetate (prepared from lolitrem B (**3**)) as a result of a detailed study by ^{1}H NMR spectroscopy.[47]

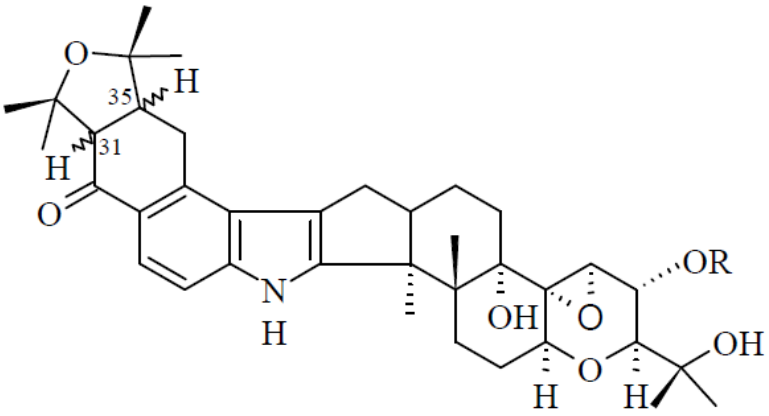

(**25**) H-31α, H-35α, R = H

(**26**) H-31α, H-35α, R = $COCH_2CH_3$

(**27**) H-31β, H-35α, R = H

A closer analysis of the NMR spectra of lolitrem B (**3**) led to the identification of another natural constituent of endophyte-infected *L. perenne* known as 31-*epi*lolitrem F (**28**)[47] and the base catalysed epimerisation of lolitrem B (**3**) afforded 31-*epi*lolitrem B (**29**).[52]

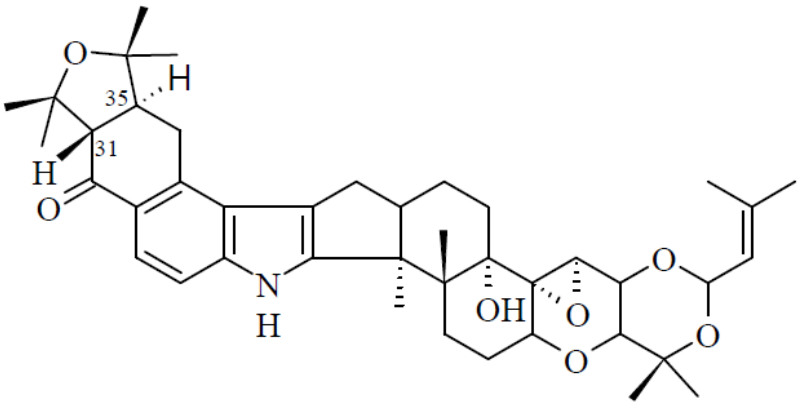

(**28**)

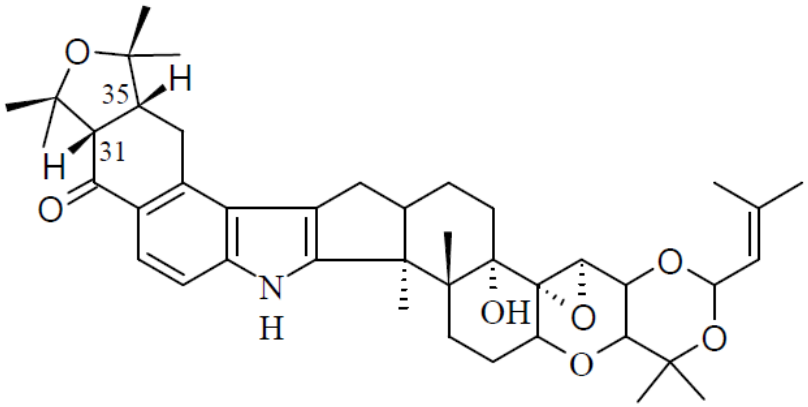

(**29**)

1.4.3.2 Lolitriol

Lolitriol (**30**) was first considered to be present in perennial ryegrass based on an unpublished observation.[56] It was suggested by Gallagher and co-workers in 1985 that it was unlikely to be formed from hydrolysis of lolitrem B (**3**) *in vivo*[57] and it was confirmed as a natural constituent of ryegrass in 1998 by Munday-Finch and co-workers.[47] It could also be formed synthetically from the acid hydrolysis of lolitrem B (**3**)[56] and was proposed as the biosynthetic precursor of lolitrems A (**12**), B (**3**) and E (**14**).

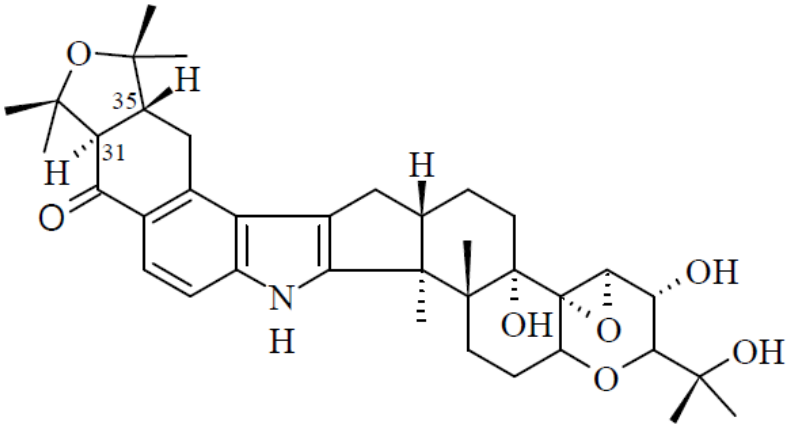

(**30**)

1.4.3.3 Lolilline

Lolilline (**31**) is a lolitrem-like analogue of paxilline (**36**) and was isolated in 1997 by Munday-Finch and co-workers from a seed extract of perennial ryegrass infected by *E. festucae* var. *lolii*.[44] It is assumed to be an intermediate for biosynthesis of the lolitrem group because its structural features are present in both lolitrems and paxilline (**36**).

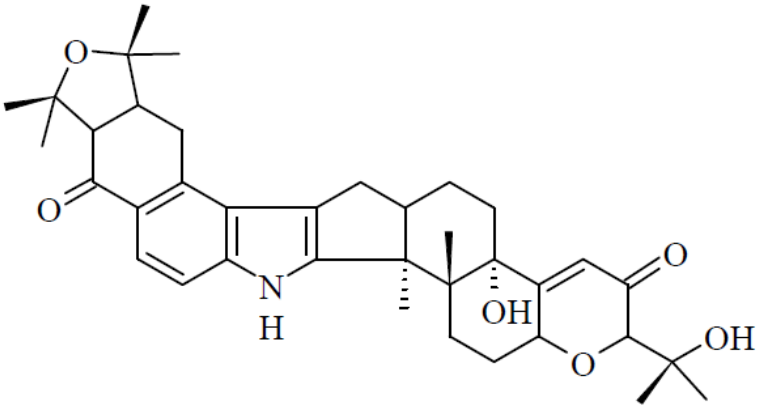

(**31**)

1.4.3.4 Lolicines

Lolicines are lolitrem-like compounds with a 2,2,5,5-tetramethyltetrahydro-furan ring *cis* or *trans* fused (C_{31} - C_{35}) to the α, β-carbons of a tetralone.[58] To date, two lolicines have been isolated from perennial ryegrass infected with *E. festucae* var. *lolii*.[47]

Lolicine A (**32**) and lolicine B (**33**) were isolated as their 11-*O*-propionate forms; lolicine A 11-*O*-propionate (**34**) and lolicine B 11-*O*-propionate (**35**) respectively, by Munday-Finch and co-workers in 1998. They might be precursors of the lolitrem group due to the similarity of their structural features to paspaline (**42**) and paspaline B (**43**) respectively.[47]

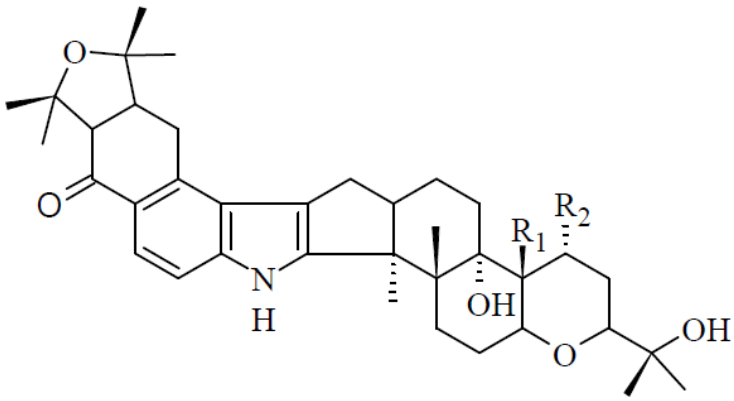

(**32**) $R_1 = CH_3$, $R_2 = H$

(**33**) $R_1 = CHO$, $R_2 = H$

(**34**) $R_1 = CH_3$, $R_2 = COCH_2CH_3$

(**35**) $R_1 = CHO$, $R_2 = COCH_2CH_3$

1.4.3.5 Paxilline

Paxilline (**36**) was originally isolated from *Penicillium paxilli* (*P. paxilli*) and has been found to be expressed by various cultures including *Emericella species*.[59, 60] It was also isolated from *Eupenicillium shearii* (*E. shearii*)[61] and ryegrass infected by *E. festucae* var. *lolii*.[45]

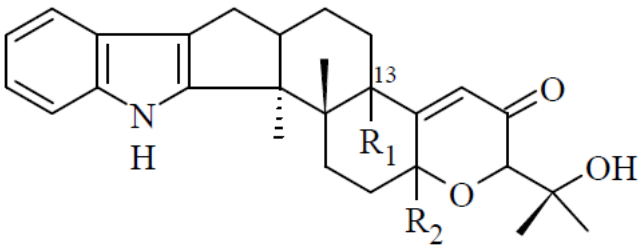

(**36**) $R_1 = OH$, $R_2 = H$

(**37**) $R_1 = R_2 = H$

(**38**) $R_1 = H$, $R_2 = OH$

(**39**) $R_1 = R_2 = OH$

Paxilline (**36**) co-occurred with lolitrem B (**3**) and every atom in paxilline (**36**) can be spatially observed at an equivalent position in lolitrem B (**3**). Therefore lolitrem B (**3**) is believed to be derived from a proximate biosynthetic precursor of paxilline (**36**) or from paxilline (**36**) itself.[56]

Other paxilline derivatives have also been isolated. One of these is 13-desoxypaxilline (**37**) which has been reported from the mycelia of the fungus *Echinopla striata* (*E. striata*) in 1988 (named as dehydroxypaxilline),[60, 62] *E. shearii*,[61] *P. paxilli*[63] and ryegrass infected by *E. festucae* var. *lolii*.[46] It is a paxilline analogue with the 13-hydroxyl group replaced by a hydrogen atom. It was isolated in the current research and biological activity against porina larvae was determined.

7α-Hydroxy-13-desoxypaxilline (**38**) was isolated from *P. paxilli* as an isomer of paxilline (**36**) together with 7α-hydroxypaxilline (**39**) and 10β-hydroxy-13-desoxypaxilline (**40**)[64] while 21-*O*-acetylpaxilline (**41**) was isolated from *E. striata*, together with paxilline (**36**).[65]

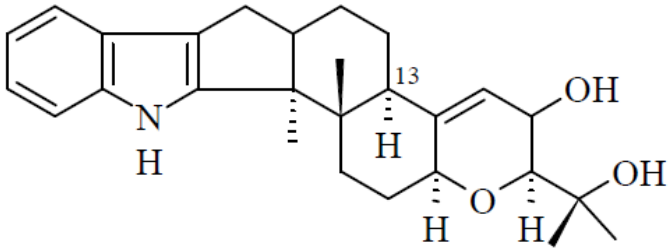

(**40**)

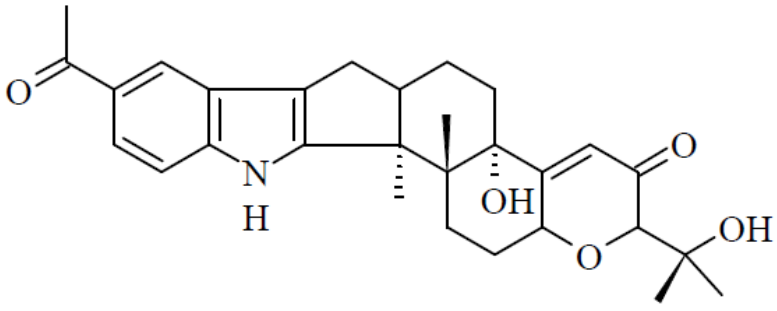

(**41**)

1.4.3.6 Paspaline

Paspaline (**42**) has been isolated from the ergot fungus *Claviceps paspali* Stevens et Hall,[66] *E. striata*,[62] *P. paxilli* Bainer,[63] *Albophoma yamanashensis* (*A. yamanashensis*),[67] sclerotia of *Aspergillus flavus* (*A. flavus*)[68] and *Aspergillus alliacus* (*A. alliacus*)[69] and from *E. festucae* var. *lolii* - *L. perenne*.[46] It was also isolated in the current research and its biological activity against porina larvae was determined.

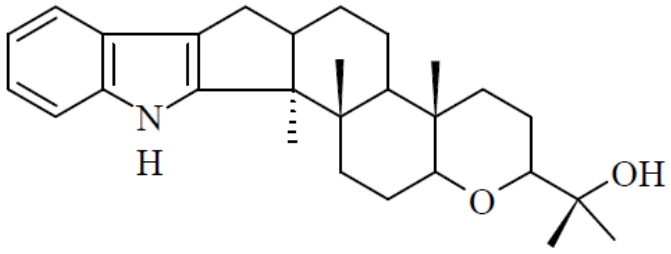

(**42**)

Other paspaline analogues have been identified from culture material. Although these analogues have not yet been isolated from *E. festucae* var. *lolii*, they are thought to be intermediates in the biosynthetic pathway to indole diterpenoids.

Paspaline B (**43**) was isolated from *P. paxilli* together with paxilline (**36**), 13-desoxypaxilline (**37**) and paspaline (**42**).[63]

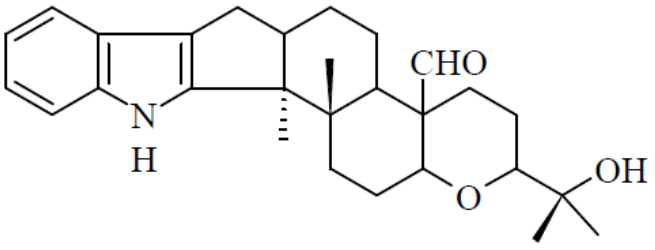

(**43**)

Paspalicine (**44**) was isolated as a congener of paspaline (**42**) from *C. paspali* Stevens et Hall and the stereochemistry of the structure was confirmed by Springer and Clardy by X-ray crystallography.[70]

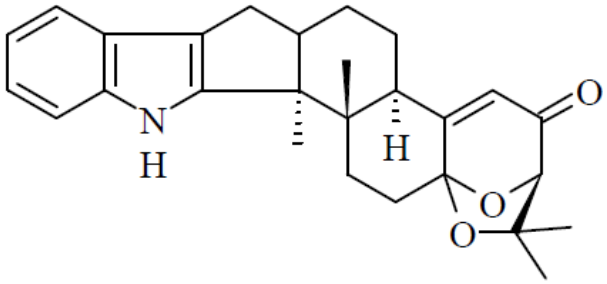

(**44**)

Paspalinine (**45**) was originally reported from *C. paspali*[66] and isolated by Cole and co-workers.[71] This compound has an additional oxygen atom compared to paspalicine (**44**). The stereochemistry of the compound was confirmed by Gallagher and co-workers.[72] It has also been isolated from the aflatoxin-producing fungi *A. flavus*[73] and *E. shearii*.[61]

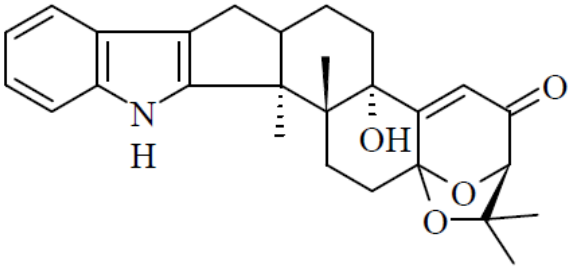

(**45**)

Emindole SB (**46**) was isolated from *E. striata*[62] and *A. yamanashensis*.[67] It is the simplest member of the indole diterpenoids and the precursor of paspaline (**42**).

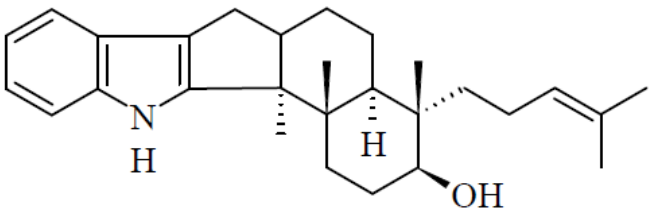

(**46**)

1.4.3.7 Terpendoles

Terpendoles are a large family of indole diterpenoids, which are structurally related to the lolitrems and paxilline (**36**). They lack the A/B rings of the lolitrems such that they are paxilline-like at the left side with the right side equivalent to various lolitrem compounds.[46] They are inhibitors of acyl-CoA: cholesterol acyltransferase, with terpendole C (**49**) being the most effective.[55] To date, thirteen terpendoles have been isolated and two variants, terpendole M (**59**)[46] and terpendole D (**50**) (from the current research) have been isolated from ryegrass infected with the wild-type endophyte.

In 1995, terpendoles A – D (**47** – **50**) were isolated by Huang and co-workers[67] and their structures determined.[74]

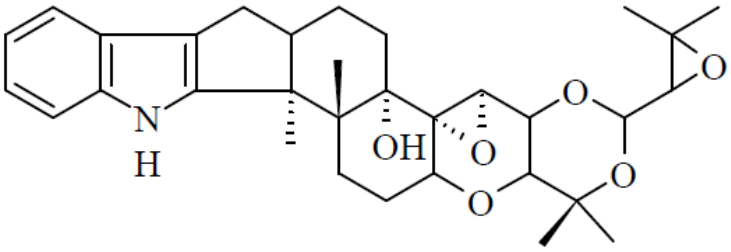

(**47**)

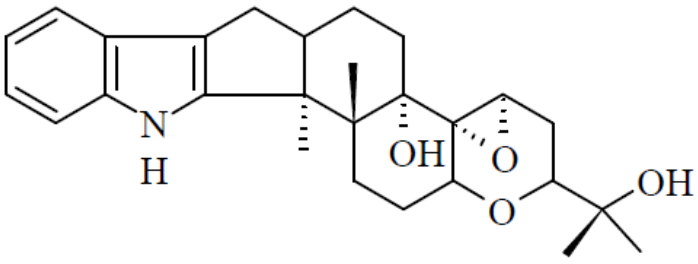

(**48**)

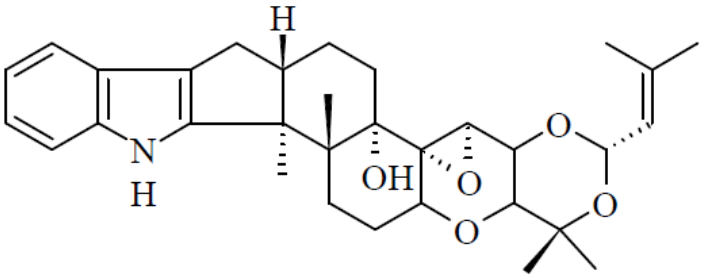

(**49**)

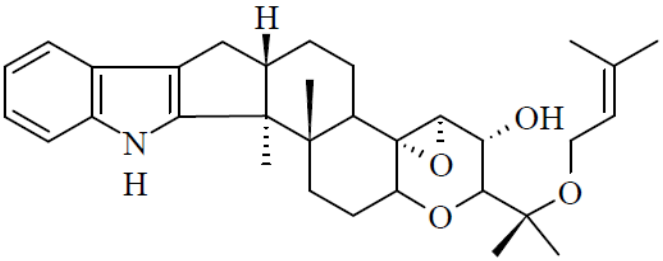

(**50**)

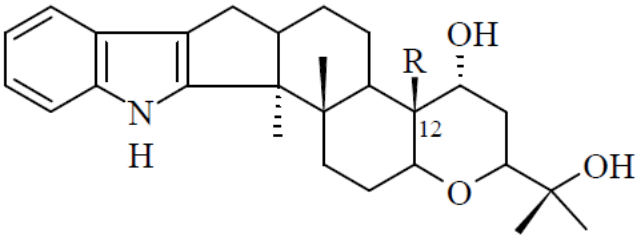

(**51**) R = CH_3

(**52**) R= CH_2OH

(**53**) R = CHO

Terpendoles E – L (**51** – **58**) were also isolated in 1995 by Tomoda and co-workers from the culture broth of *A. yamanashiensis*, although with different growth media to that used for terpendoles A – D (**47** – **50**).[74, 75] Terpendoles E – G (**51** – **53**) share a similar structure and are differentiated by the substituent at C-12.

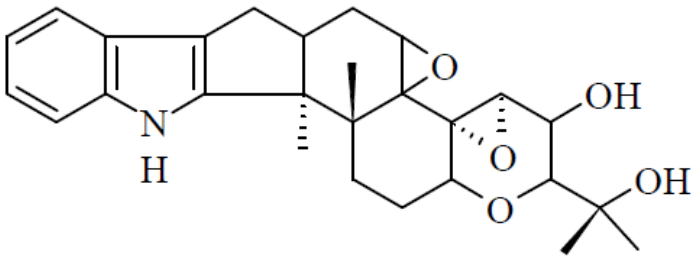

(**54**)

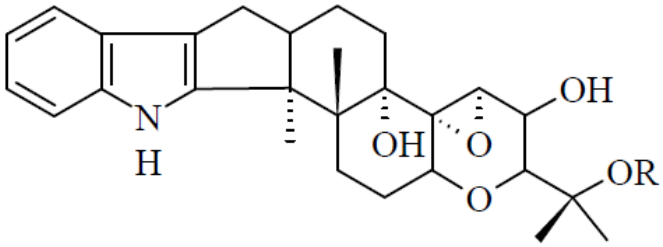

(**55**) R = H

(**56**) R =

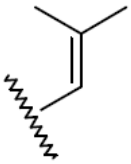

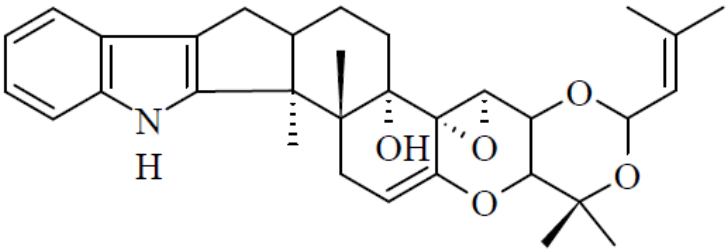

(**57**)

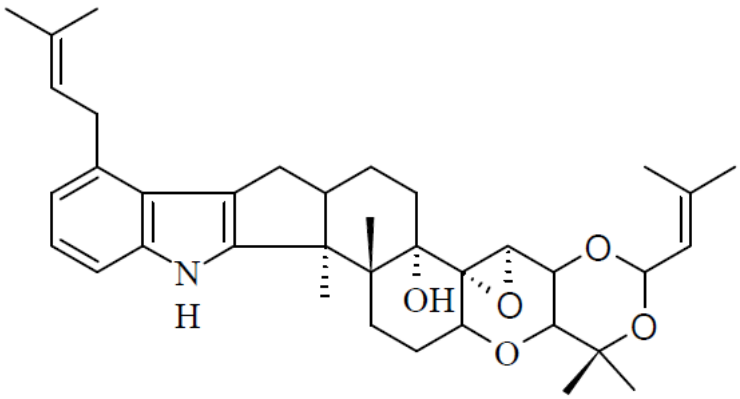

(**58**)

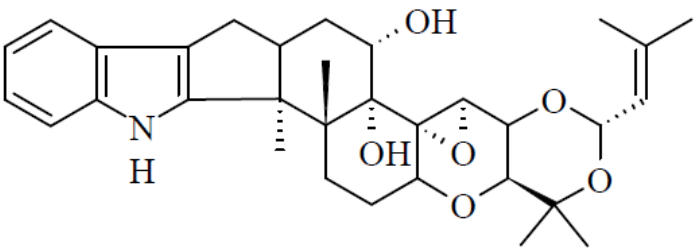

(**59**)

The isolation of terpendole M (**59**) from *E. festucae* var. *lolii* - *L. perenne* indicated the capability of the endophyte to assemble the right end (rings H-I) of the lolitrem skeleton regardless of whether A/B rings have been assembled.[46]

1.4.3.8 Epoxy-janthitrems

Epoxy-janthitrems I (**4**) and II – IV (**60** – **62**) are analogues of janthitrems (tremorgenic compounds) isolated from *Penicillium janthinellum* (*P. janthinellum*)[76] and *Aspergillus sp.*[77] They were reported from perennial ryegrass infected with the AR37 endophyte and are unique to this strain.[48, 78]

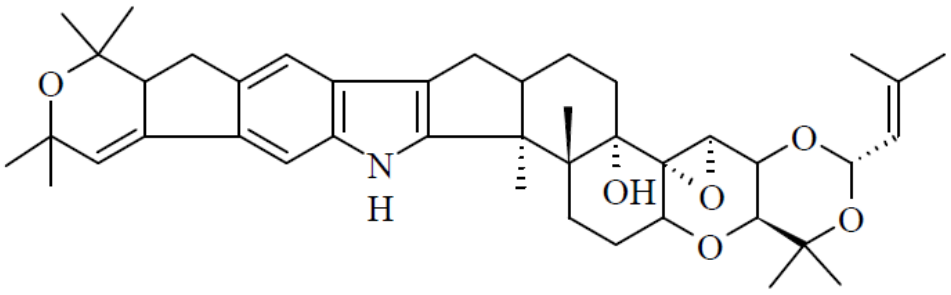

(**60**)

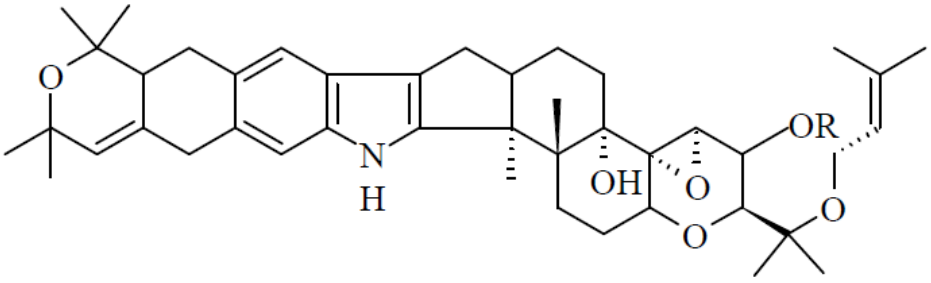

(**61**) R = H

(**62**) R = $COCH_3$

Other indole diterpenoids such as penitrems, janthitrems, aflatrem, sulphinines and shearinines have been isolated. However, because none of these compounds have been isolated from endophyte-infected perennial ryegrass, they are excluded from this review.

1.5 Biosynthesis of indole diterpenoids

The *Epichloë* fungal endophytes defend their grass host from insect and mammalian herbivory by producing bioprotective alkaloids. The occurrence of these compounds in grass-endophyte associations is dependent on the biosynthetic ability of the endophyte.[79] Genomic analysis of the Clavicipitaceae family indicated that large repeat blocks in the alkaloid biosynthetic gene can facilitate gene losses, mutations and duplications, thus enhancing the diversity of the alkaloid structures within each class.[80, 81]

A diverse array of indole diterpenoids has been biosynthesised by *Epichloë* fungal endophytes in perennial ryegrass (Figure 1.3). These compounds have a common cyclic diterpene core derived from GGDP (**10**) and an indole group derived from tryptophan (**11**) or a tryptophan precursor. The precursor for GGDP (**10**) is isopentenyl diphosphate (**63**), produced from acetyl coenzyme A (acetyl CoA).[9]

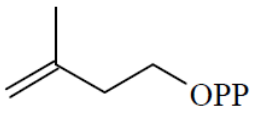

(**63**)

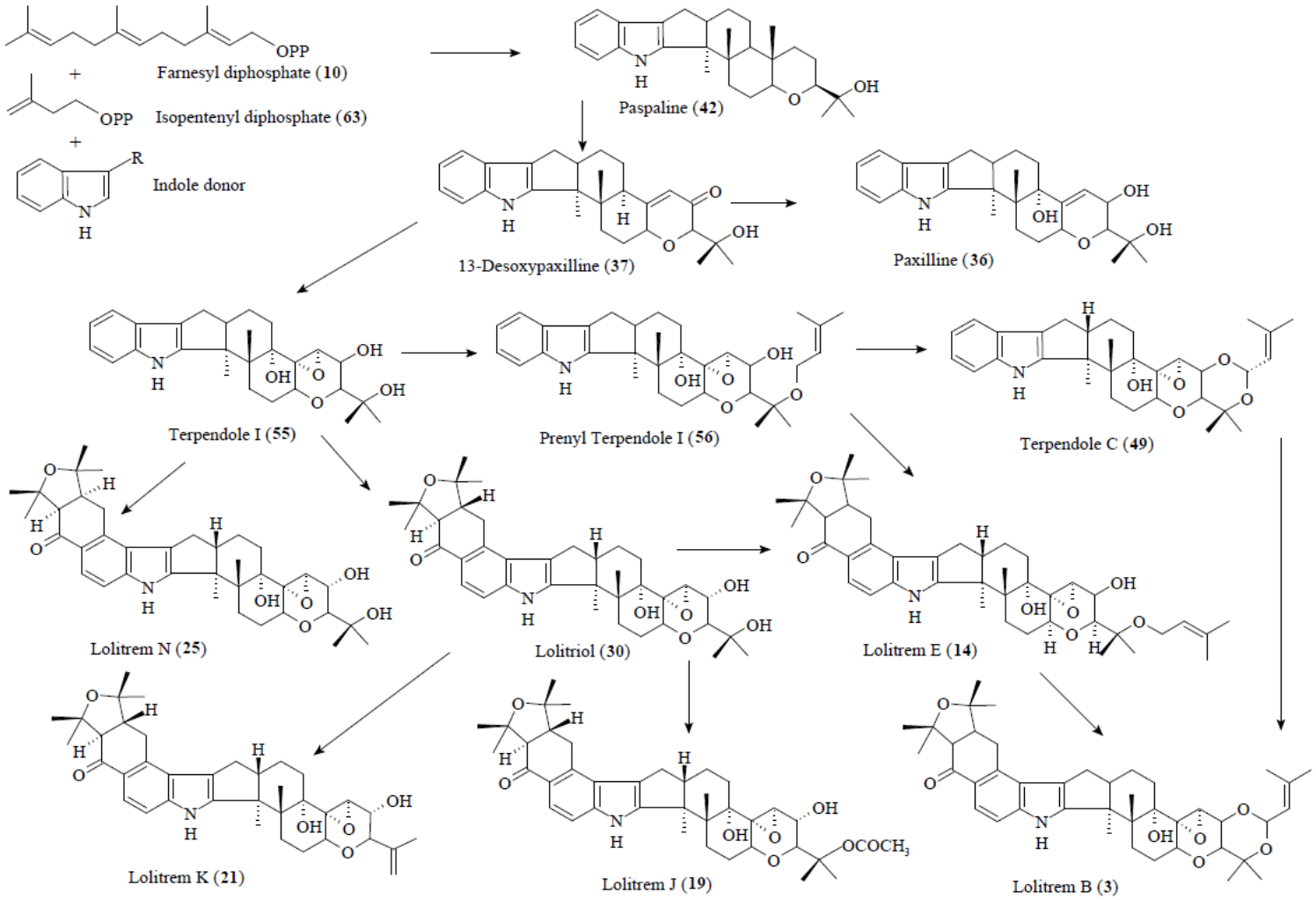

Figure 1.3: The proposed framework for the biosynthetic pathway of indole diterpenoids of *Epichloë* fungi. (Adapted from Figure 6 of reference 82).

Indole diterpenoids are biosynthesised via paspaline (**42**),[64] the key intermediate compound which provides a core structural backbone for subsequent reactions that generate the chemical diversity of indole diterpenoids.[43]

Simple indole diterpenoids such as 13-desoxypaxilline (**37**) and paxilline (**36**) are the result of modifications of paspaline (**42**) such as additional prenylations, different ring substitution and ring stereochemistry,[46] which are then further metabolised to produce more complex indole diterpenoids.[64, 82]

Paxilline (**36**) is a vital biosynthetic intermediate which is responsible for the structural backbone of complex indole diterpenes including the lolitrems.[43, 82] To convert paxilline (**36**) to lolitrem B (**3**), three structural features are required; the addition of an isoprene unit to the two appropriate and favourably disposed oxygen atoms (C-10, C-27), epoxidation of the olefinic double bond and diprenylation of the aromatic nucleus to form a bicyclic terpendole moiety.[56]

The precursors for lolitriol (**30**) include paxilline (**36**)[54, 126] and the confirmation of lolitriol (**30**) as a natural constituent supports the proposal that it is a biosynthetic precursor of lolitrems J (**20**), B (**3**) and E (**14**).[50, 51, 56, 83] Addition of a further isoprene unit to the 27-OH group of lolitriol (**30**) would generate lolitrem E (**14**), thought to be a precursor of lolitrem B (**3**).[51]

The generation of lolilline (**31**) requires two isoprene units which could be incorporated into the paxilline (**36**) skeleton at C-20 and C-21 to form the lolitrem type *trans*-fused A/B ring system of lolilline (**31**).[44]

The lolicines contain a methyl or formyl group at C-12 and are unlikely to be biosynthesised via paxilline (**36**). Their structures indicate that they may be produced by endophytes via paspaline (**42**) and paspaline B (**43**), which was strongly supported by the identification of paspaline (**42**), 13-desoxypaxilline (**37**) and terpendole M (**59**) from *L. perenne* infected with *E. festucae* var. *lolii*.[46, 47]

1.6 Biological activities of alkaloids of *Epichloë festucae* var. *lolii* - *Lolium perenne*.

The reports on biological activities of the alkaloids of endophyte-infected perennial ryegrass focus on their deterrent effects on insect pests and detrimental effects on grazing livestock. The anti-feedant potential of compounds on insects is tested by feeding bioassays which utilise semi-synthetic diets.[84] The effect often is measured by recording the weight of diet before and after insect feeding, the weight of the insect at the beginning and the end of the experiment and the number of surviving insects at the end of the experiment. Effects can also be identified by exposing the adults and/or larvae to endophyte-infected grass in a pot experiment. The effects are measured by the amount of damage to the grass host and the weight and number of surviving insects as appropriate. The tremorgenicity of alkaloids has been investigated using a mouse bioassay. Alkaloids are intraperitoneally injected into mice as a solution in dimethyl sulfoxide (DMSO) – water. Tremors are assessed regularly using a visual rating scale as described by Gallagher and Hawkes.[85]

Peramine (**1**)

The effects of endophyte-infected perennial ryegrass on the population of Argentine stem weevil and tiller damage were first observed by Mortimer.[86] A higher population of Argentine stem weevil with higher tiller damage was found on perennial ryegrass with less endophyte infection compared to ryegrass with higher endophyte infection.[87] Pot experiments were conducted to find the mechanism behind the effects of endophyte on Argentine stem weevil which showed that the presence of endophyte reduced feeding on leaf blades of perennial ryegrass by Argentine stem weevil adults[88] and also reduced oviposition[18] and survival of larvae.[88] The compound responsible for this effect was later found to be peramine (**1**) which is expressed by wild-type and AR1 endophytes. Peramine (**1**) has not been associated with a toxic effect on mammals.[27] It has been demonstrated to effectively deter adult Argentine stem weevil feeding at 0.1 ppm and larval feeding at 2 ppm in artificial diet.[89]

Ergot alkaloids

Ergot alkaloids are toxic to vertebrates and invertebrates[30] and are the major factor in *E. festucae* var. *lolii* mediated resistance to African black beetle.[35] Ergovaline (**2**) and ergotamine (**9**) deter African black beetle feeding at 5.0 µg/g while the ergopeptide epimer, ergovalinine (**5**) and other ergopeptide derivatives show moderate activities. Ergovaline (**2**) also causes heat stress in cattle[90] and sheep.[91]

Indole diterpenoids

Although indole diterpenoids possess biological effects such as insect feeding deterrence and inhibition of acyl-CoA: cholesterol acyltransferase activity,[3] the tremorgenic activity of some of these compounds indicated that they are the probable causative agents of ryegrass staggers.[44]

Lolitrem B (**3**) is the major lolitrem compound expressed by endophyte-infected perennial ryegrass seed.[51] This compound is a powerful, potent tremorgen which induces long duration tremors in mice which peak at around ten hours and last for up to three days at a dose of 4 mg/kg.[56] Tremorgenicity of lolitrems A (**12**), C (**13**), F (**15**) and 31-*epi*lolitrem F (**28**) in the mouse was equal to that of lolitrem B (**3**) at 4 mg/kg.[51, 55] This could be due to structural similarity at the intact ring I, an isoprene unit (modified) at C-43 and structural isomers at the A/B ring junction. The absence of the isoprene unit and the opening up of ring I could account for the differences in tremorgenicity seen for other lolitrems such as lolitrem M (**24**).[55] Lolitrem E (**14**) at 2 mg/kg[51] and lolitrem M (**24**) at 4 mg/kg,[55] produced no detectable tremors in mice. The orientation of only one hydrogen atom can also alter the tremorgenicity.[92] 31-*Epi*lolitrem F (**28**), with an α-face A/B ring junction is tremorgenic whereas 31-*epi*lolitrem B (**29**) with a β-face A/B ring junction, is not.[52, 55] Although much less potent, epoxy-janthitrems also induce long duration tremors in mice.[48, 78]

Simple indole diterpenoids such as paxilline (**36**),[55, 92] terpendole M (**59**),[46] 21-*O*-acetylpaxilline (**41**),[65] terpendole C (**13**)[46] and paspalinine (**45**)[71] induce short duration tremors in mice. The 13-hydroxyl group appears to be essential for tremorgenic activity. 13-Desoxypaxilline (**38**), paspaline (**42**),[92] paspalicine (**44**)[71] and terpendoles D – H (**50** – **54**) lack the 13-hydroxyl group and are not

tremorgenic.[55] However, lolitriol (**30**),[56] lolilline (**31**)[46, 93] and terpendole I (**55**) do contain the 13-hydroxyl group but are also not tremorgenic. Therefore, other structural features in addition to the 13-hydroxyl group must be required for tremorgenic activity, such as the C-10 carbonyl group in lolilline (**41**).[65]

The structural activity relationships of indole diterpenoids are very complex, but previous research has shown that an intact ring I, an isoprene unit (modified) at C-43, structural isomers at the A/B ring junction and the presence of a 13-hydroxyl group play a vital role in the tremorgenicity of the indole diterpenoids.

The potential of the indole diterpenoids to deter insects is not well understood. AR37 shows a powerful effect on a wide range of insect pests including Argentine stem weevil, pasture mealybug, black beetle, root aphids and porina larvae.[94-96] Epoxy-janthitrems have been shown to affect porina larvae in a dose-dependent manner.[78, 97] Lolitrem B (**3**) is both toxic and deterrent to Argentine stem weevil[98-100] but it showed no effect on black beetle in a choice bioassay at 5 and 10 µg/g.[35] Paxilline (**36**) has a potent effect on survival and growth of Argentine stem weevil larvae at 10 and 20 µg/g and on feeding by fruit beetle (*Carpophilus hemipterus*).[61] It also has a mild effect on weight gain and mortality of corn earworm (*Heliothis zea*) and a lesser effect on fall armyworm (*Spodoptera frugiperda*) at 25 µg/g and higher concentrations.[61, 101, 102] It has no effect on black beetle (*Heteronychus arator)* or slugs (*Deroceras* spp).[103] There is no published information on the effects of paspaline (**42**) on insect pests except for being essentially inactive against *Carpophilus hemipterus* (dried fruit beetle).[61] Effects on other insect pests are not known. To date, there is not sufficient data to be able to correlate insect bioactivity with structural features.

1.7 Common insect pests of *Lolium perenne* in New Zealand.

The common insect pests of perennial ryegrass in New Zealand are Argentine stem weevil, black beetle, pasture mealybug, root aphid, grass grub and porina larvae. Each is present in various parts of New Zealand and each has its own way of destroying the grass.[104] For example, black beetle larvae feed on roots and adults feed at the base of tillers while pasture mealybug and root aphids suck nutrients out of plants.[105] The extent of damage to the grass caused by these insects is influenced by environmental stress and grazing pressure from livestock and they are capable of causing damage in the summer-autumn period when drought and high temperatures place grass under stress.

1.7.1 Argentine stem weevil (*Listronotus bonariensis*)

Argentine stem weevil (Figure 1.4), originally from South America, has been common in all parts of New Zealand since the early twentieth century as a pest of short-term ryegrass (*Lolium multiflorum; L. boucheanum* syn. *L. hybridum*) and perennial ryegrass. It has two or three generations a year in the warmer North Island,[106] two in Canterbury and one or two generations in Otago and Southland,[107] with most pasture damage caused at the larval stage. Argentine stem weevil larvae cause most damage by mining the central part of stems which often kills the tiller and destroys the meristem which prevents the production of daughter tillers.[104] Damage is severe, especially when the pasture is growing slowly and is drought stressed. The adult weevil does not affect the persistence of established pasture but can kill seedling ryegrass at establishment.[23]

Figure 1.4: An Argentine stem weevil adult. (Adapted from reference 23).

1.7.2 Black beetle (*Heteronychus arator*)

Black beetle, also known as African black beetle, was first observed on Waiheke Island in New Zealand in the late 1930s. The root-feeding larvae have caused severe damage to ryegrass during sporadic outbreaks in the northern North Island since then.[108] It is now common in warm areas including Northland, Waikato, Bay of Plenty and coastal districts from Northland to the Manawatu on the West Coast and Hawkes Bay on the East Coast. Black beetle lives in soil and is mainly found in free draining, sandy light ash or peat soils.[23] The population depends on climatic conditions and food sources but under the conditions which favour the survival of young larvae and adults, such as low soil moisture and warm temperatures in winter and spring, their numbers can increase rapidly. An article from the *Waikato Times*, 26 August 2014, stated that over the last two consecutive years, summer droughts had favoured the build up of the black beetle populations and that they were expected to rise further if the region had a mild spring.[109]

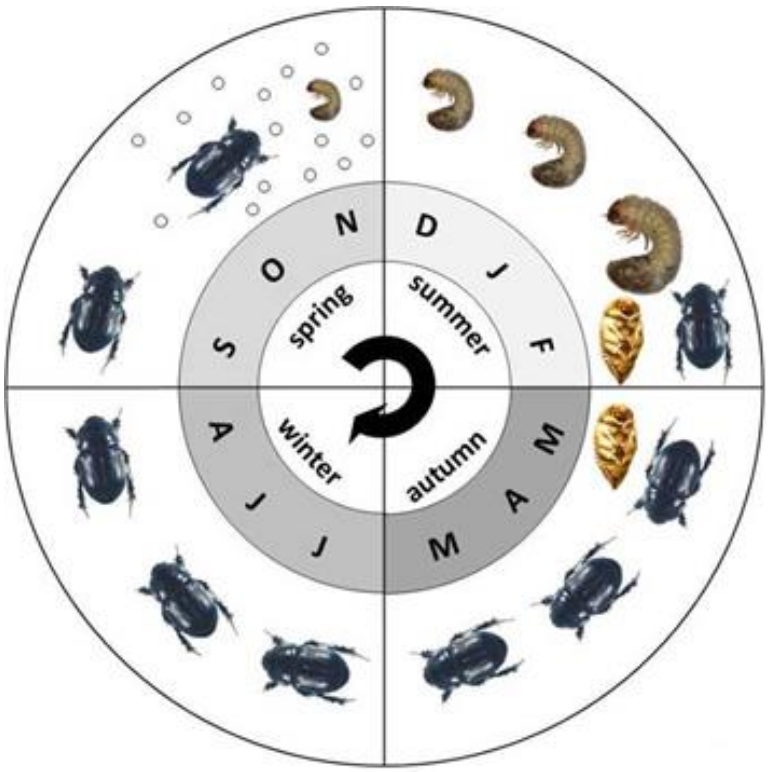

Figure 1.5: Life cycle of a black beetle. (Adapted from reference 23).

The damage to perennial ryegrass by black beetle involves seedling and tiller damage by adults and root damage by larvae at/or immediately below ground level.[110] Damage from adults usually occurs when they are active on the soil surface of newly established pastures in autumn (March – May) or spring (September – November) as shown in Figure 1.5. Extensive pasture damage occurs due to root-feeding larvae in summer (January – March) and the new generation of adults emerges in late-summer-autumn (February – March).[110, 111]

The adult black beetle is deterred from feeding on ryegrass plants infected with endophytes, such as wild-type, NEA2 or AR37, and will disperse to find better food sources, reducing the number of eggs that are laid.[105] AR1 however, provides only weak protection against black beetle.[23]

1.7.3 Pasture mealybug (*Balanococcus poae*)

Pasture mealybug (Figure 1.6) is a serious pasture pest in Canterbury and is also known to occur in Manawatu and Nelson. Outbreaks of pasture mealybug are common in autumn in Canterbury during extended dry periods. Damage tends to affect the whole paddock, causing widespread ryegrass death and poor pasture persistence.[23] The first effect of endophyte infection on pasture mealybug was reported from a glasshouse pot experiment where infestations of the insects were much higher in endophyte-free perennial ryegrass compared to the perennial ryegrass infected with wild-type endophyte.[112] The endophytes AR1, AR37, NEA2 and wild-type have high resistance to pasture mealybug. The mechanism by which endophyte-infected ryegrass affects pasture mealybug feeding has not been investigated.[113]

Figure 1.6: Pasture mealybug at the base of ryegrass. (Adapted from reference 23).

1.7.4 Root aphid (*Aploneura lentisci*)

Root aphid (Figure 1.7) is a sap-sucking insect originating from the Mediterranean but they have been common in New Zealand for many years. They may be present in the grass all year round but their population is difficult to monitor due to their tiny size. Only adult aphids and adult nymphs are visible to the naked eye. Their feeding can gradually reduce plant vigour and effects are amplified when plants are under stress from drought, low soil fertility, attack from other insects or heavy grazing.[114] They were not considered to be a significant insect pest until perennial ryegrass infected with AR37 endophyte showed resistance in comparison to wild-type infected and endophyte-free pastures.[110, 115, 116] Root aphid is also controlled by other grass-endophyte associations such as MaxP® (tall fescue)[117] and Banquet II Endo5.[105] The chemistry involved in grass-endophyte resistance to root aphids is still unknown.[113]

Figure 1.7: A root aphid. (Adapted from reference 23).

1.7.5 Grass grub (*Costelytra giveni*)

Grass grub (Figure 1.8) is an endemic species throughout most of New Zealand, although it is not common in the subtropical northern North Island. The life cycle involves three larval stages, usually completed in twelve months but which can be extended to two years depending on the weather conditions. The life cycles often coexist in the cooler soils of the southern South Island as well as in the Canterbury foothills and North Island's central plateau.[104] The larvae feed intensively on the roots of ryegrass.[118] Usually the third larval instar in March is the most damaging stage, coincident with periods of moisture stress in northern areas and low plant growth in the southern regions when the temperature drops.[104]

Figure 1.8: Grass grub beetles. (Adapted from reference 23).

1.7.6 Porina (*Wiseana cervinata*)

Porina is found throughout New Zealand and attacks pasture species such as ryegrass and white clover. The adult moths fly between October and March depending on the species and haplotype but do not feed.[23] A more detailed discussion of this pest is given in Chapter 5 of this thesis.

Different endophytes in perennial ryegrass have varying activities on insect pests due to the different alkaloid profiles expressed by the endophyte strain (Table 1.1). Endophytes in perennial ryegrass generally provide good resistance to pasture mealybug and Argentine stem weevil, although effects vary with endophyte strain and host plant genotype.

Table 1.1: Insect pest control rating for different endophytes of perennial ryegrass.[23, 119]

Species	Endophyte	Insect pests					
		[b]ASW	[d]PM	[e]BB	[f]RA	[h]GG	[i]PL
[a]**PRG**	Endophyte-free	-	-	-	-	-	-
PRG	Wild-type	****	****	***	**	-	*
PRG	AR1	****	****	*	[g] -	-	-
PRG	AR37	[c]****	****	***	****	-	***
PRG(tetraploid)	NEA2	***	(****)	***	(*)	-	[j]nt
PRG(tetraploid)	Endo5	**	(****)	***	(*)	-	(*)

a = perennial ryegrass, *b* = Argentine stem weevil, *c* = AR37 control over ASW larvae but not adult, *d* = Pasture mealybug, *e* = Black beetle, *f* = Root aphid, *g* = AR1is more susceptible to root aphid than endophyte-free, *h* = Grass grub, *i* = Porina larvae, *j* = not tested, - = no control, * = low level of control, ** = moderate control, *** = good control, **** = very good control, ( ) = provisional result.

1.8 Forage grass improvement.

In the early 1980s, the discoveries that ryegrass staggers was induced by tremorgenic neurotoxins and that positive bio-control of insect pests could be achieved by other secondary metabolites expressed by fungal endophytes in perennial ryegrass, initiated research into trying to discover better grass-endophyte associations. By inoculation of new strains of endophyte, new grass-endophyte associations can be formed that limit the impact of endophytes on animal health and welfare while maintaining good grass productivity by deterring insect pests.[3, 1, 87]

The first generation of perennial ryegrass endophyte associations was selected on the basis that the association produced peramine (**1**) and not lolitrem B (**3**). A survey of endophyte-infected perennial ryegrass around New Zealand failed to find endophyte-infected material with low or no lolitrem B (**3**), so attention was turned to international seed collections.[120] New strains of novel endophytes were found in seed collections from native habitats of perennial ryegrass in Europe that had beneficial alkaloid profiles. The exploitation of selected endophyte strains in pastoral agriculture is due to the development of techniques to isolate desirable endophytes in culture and re-inoculate them into endophyte-free germplasm.[121] As endophyte is seed-transmitted, it can be inoculated into plants and seed produced which can be sold to farmers. This has led to five novel endophytes in perennial ryegrass becoming available to farmers in New Zealand (Table 1.2).

The first endophytic product which was commercially available was Endosafe, which did not produce lolitrem B (**3**) but had good resistance against Argentine stem weevil due to the production of peramine (**1**).[122] It was released to the commercial market in 1991 but was associated with heat stress and lameness in livestock due to ergovaline (**2**) toxicity. Endosafe is no longer available in perennial ryegrass but is still retained in the market in the hybrid ryegrass 'Greenstone'. In this case, only low levels of ergovaline (**2**) are produced, with no livestock health problems encountered.[123]

Table 1.2: The key properties of endophyte strains in perennial ryegrass.

Commercial or common name	**Notable alkaloids produced**	**Key traits**	**A key region of use**
Wild-type	Lolitrems Peramine (**1**) Ergovaline (**2**)	Ryegrass staggers (negative impacts on animal health) Good [a]ASW & [b]BB resistance	Ryegrass pastures and turf in New Zealand, Australia and South Africa.
Endosafe (AR5 and AR77)	Peramine (**1**) Ergovaline (**2**)	Low ryegrass staggers and heat stress. Good ASW resistance.	Ryegrass pastures
AR1	Peramine (**1**)	No ryegrass staggers. Good ASW resistance.	Ryegrass pastures and turf in New Zealand, Australia and South Africa
Endo5	Peramine (**1**) Ergovaline (**2**)	No ryegrass staggers, some heat stress. Good ASW and BB resistance.	Ryegrass pastures in Australia
NEA2	Lolitrems Peramine (**1**) Ergovaline (**2**)	Some ryegrass staggers and heat stress. Good BB resistance.	Ryegrass pastures in New Zealand and Australia
AR37	Epoxy-janthitrems	Broad spectrum insect pest resistance, some ryegrass staggers.	Ryegrass pastures in New Zealand and Australia

a = Argentine stem weevil, *b* = black beetle. Adapted from Table 1 of reference 3.

The second generation ryegrass endophyte, AR1 was selected as a novel endophyte that produced peramine (**1**) only. This endophyte resists Argentine stem weevil and pasture mealybug without causing any ryegrass staggers.[124] It gives an improved animal performance and milk production compared with wild-type endophyte, with ryegrass herbage production and persistence that is similar to wild-type endophyte, but better than ryegrass without endophyte.[110] AR1 was commercially released to New Zealand farmers in 2001 and is now licensed in thirty one cultivars through ten companies and is exported to Australia, Chile, the United States of America, Europe and Argentina.

AR37, which does not produce lolitrem B (**3**), peramine (**1**) or ergovaline (**2**), gives similar protection to AR1 against Argentine stem weevil and pasture mealybug but has a significant effect on other insect pests.[125] This exceptional bio-protection potential of AR37 results in greater herbage production and persistence than both the wild-type endophyte and AR1.[78] AR37 can induce ryegrass staggers in sheep although episodes are less severe and of shorter duration compared to that induced by wild-type endophyte. The only known alkaloids present in AR37 are epoxy-janthitrems (predominantly epoxy-janthitrem I (**2**)).[95] AR37 was released to the market in 2007 in eleven ryegrass varieties and is the most effective endophyte for improving persistence.[105]

Additional novel endophytes in ryegrass associations in New Zealand are also available. One of the selected endophytes, NEA2, was developed by New Zealand Agriseeds and has been successfully marketed in two ryegrass cultivars to date.[126] NEA2 is a mixture of two strains that produce low levels of peramine (**1**), lolitrem B (**3**) and ergovaline (**2**). This gives moderate protection against Argentine stem weevil and strong protection against black beetle, with a reduced impact on animal health and production. A better understanding of the diversity of grass-endophyte metabolites and their effect on insects opens up new prospects for grass improvement. Investigation of grass-endophyte associations continues to reveal interactions where the underlying chemical agent(s) remains to be defined.[127]

1.9 The intention of this study

While the effects of some of the complex indole diterpenoids expressed by *E. festucae* var. *lolii* - *L. perenne* associations on insects and animal health are known, the effects of the more simple indole diterpenoids are much less understood. These compounds are generated by early steps in the biosynthetic pathway and are expressed by the wild-type endophyte as well as novel endophytes, making them of high importance. The contribution that these compounds make to plant defence against insects and their effects on livestock are of great interest in the future development of desirable grass-endophyte associations.

A bulk extract of wild-type endophyte ryegrass seed containing all those compounds that eluted before lolitrems by normal phase chromatography, was available from earlier work of Dr Sarah Finch. This extract was believed to be a good source of early-pathway compounds. The principal aims of this study were:

i) To identify, isolate, purify and structurally elucidate early-pathway diterpenoids.

ii) To test the isolated compounds against porina larvae to determine their anti-insect effects.

Chapter 2: Identification and structural elucidation of novel compounds A – D (64 – 67).

Indole diterpenoids are one of the most abundant classes of metabolites produced by perennial ryegrass infected by *E. festucae* var. *lolii*. They are lipophilic and commonly contain an indole moiety which is characterised by fragment ions at (i) *m/z* 182 [$C_{13}H_{12}N^+$] and (ii) *m/z* 130 [$C_9H_8N^+$] in their tandem mass spectra (Figure 2.1).

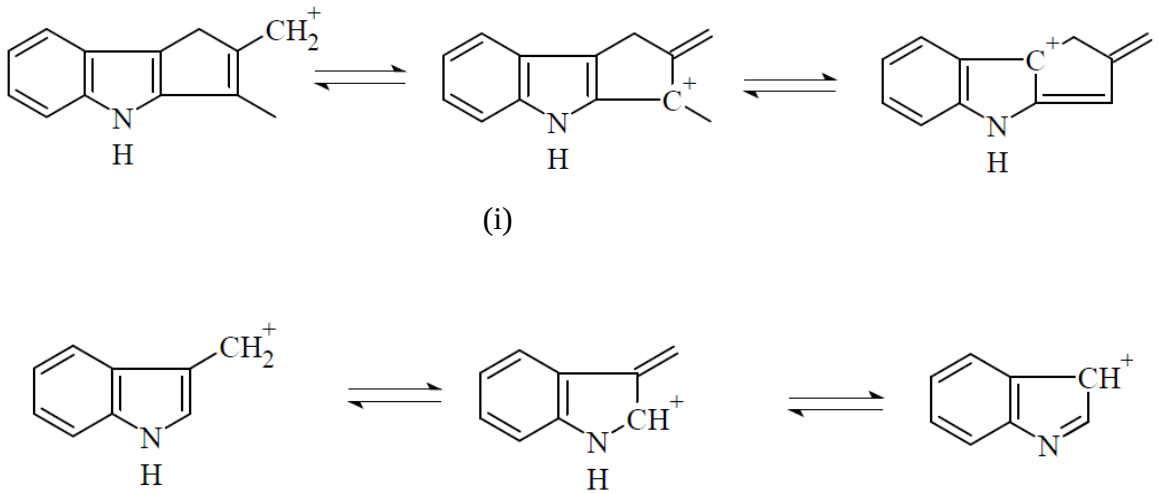

Figure 2.1: The proposed fragment ions attributed to *m/z* (i) 182 and (ii) 130 of indole diterpenoids from tandem mass spectrometry (positive ion mode).[64, 128]

The UV spectra of these compounds contain absorption maxima at 230 and 280 nm. The mass spectrometric fragment ions and UV absorptions are due to the presence of the indole moiety in the compounds.

As a starting point for this study, a pre-lolitrem fraction available from the PhD research of Dr Sarah Finch was used. She extracted *L. perenne* seed (approximately 300 kg) infected with wild-type endophyte and isolated the lolitrem compounds.[55] The term pre-lolitrem indicated that the crude fraction resulted from purification steps of the lolitrems and contained all compounds which eluted before lolitrems using normal phase flash chromatography. Based on the spectrometric features, the

crude seed extract was screened for potential indole diterpenoids. The selection of the potential indole diterpenoid intermediates prior to the isolation process was based on the fact that these compounds possess UV absorbtion maxima at around 230 and 280 nm and also exhibited at least one of these two characteristic fragment ions in tandem mass spectrometry via LC-MS. Compounds with molecular ions of *m/z* 406, 420, 422, 436, 454, 506, 522, 536 and 554 were noted as potential indole diterpenoid intermediates. However, other molecular ions of *m/z* 636 and 594 were noted, both with a high intensity fragment ion at *m/z* 536. They do not produce the characteristic fragmentation ions seen for indole diterpenoids and yielded UV absorption spectra with maxima at 215, 240 and 295 nm. This indicated that the indole region is not present, however these changes could be due to the presence of further substituents or atoms in the indole region. These compounds were later found to be modified versions of the indole diterpenoids which are described in this chapter.

The pre-lolitrem crude extract was subjected to liquid-liquid partitioning between ethanol – water (4:1) and petroleum ether (1:1). A series of normal phase flash chromatography and semi-preparative HPLC steps performed on the non-polar layer of the partition yielded two novel compounds which were named as compounds A (**64**) and B (**65**), as well as 13-desoxypaxilline (**37**) and paspaline (**42**). The presence of another unknown compound was noted but in insufficient amount for isolation and characterisation, hence a further aliquot of the crude extract was then processed using similar methods to yield the additional unknown compound C (**66**).

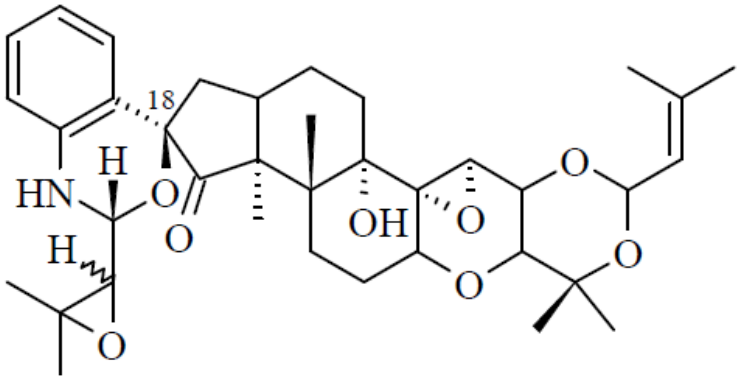

(**64**)

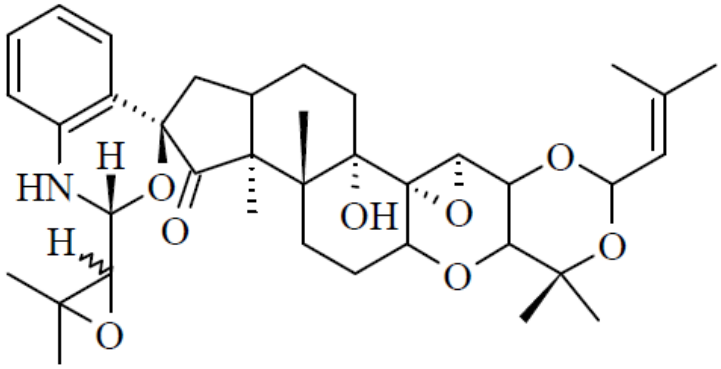

(**65**)

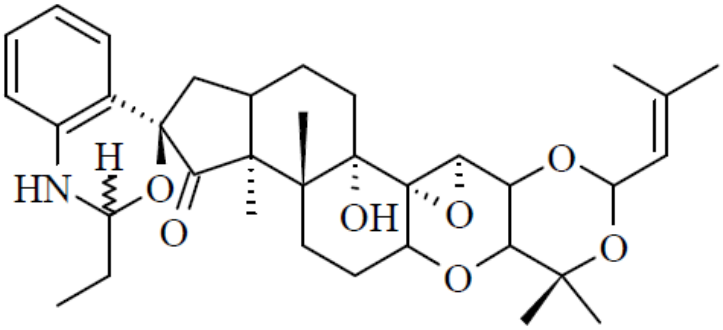

(**66**)

The presence of an analogue of compounds A – C (**64** – **66**) was also indicated from analysis of the aqueous layer of the liquid-liquid partition. Another compound (compound D (**67**)) was found to co-elute with terpendole D (**50**) in one of the subfractions.

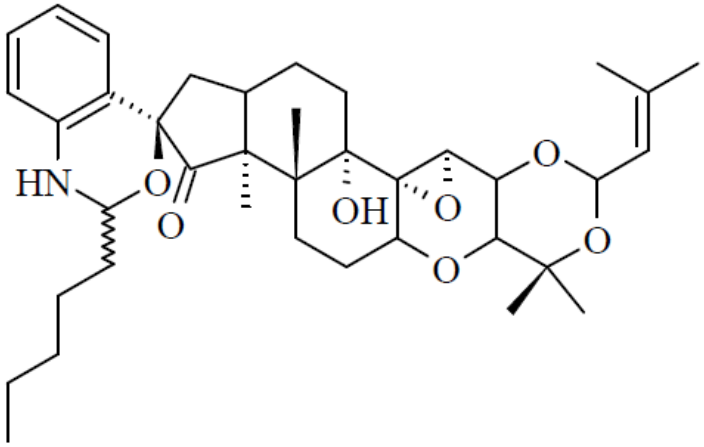

(**67**)

This is the first time for terpendole D (**50**) to be isolated from endophyte-infected perennial ryegrass. The expression of terpendoles in endophyte-infected plant material together with analogues (compounds A – D (**64** – **67**)) was confirmed by LC-MS of the crude extract. Paspaline (**42**) and 13-desoxypaxilline (**37**) were also identified in this fraction.

Compounds A – D (**64** – **67**) are unique structures. The compounds contain a modified indole region of a six membered oxygen-containing ring which is fused to the right side of the molecule via a spiro centre (C-18). This indicated that they could be artefacts which could potentially have been formed during storage of the extract and might explain why the compounds A – D (**64** – **67**) were not detected in LC-MS analysis of fresh, wild-type endophyte infected seed extract (50 mg). Further work is required to confirm whether these compounds are actually artefacts and to provide systematic and common names. Due to the complexity of the structures, the molecules are referred to as compounds A – D (**64** – **67**) in this report.

The structural elucidation of the compounds was performed using 1D and 2D-NMR spectroscopy and mass spectrometry. The isolation and structural elucidation of the novel compounds A – D (**64** – **67**) will be discussed in this chapter and that of the known compounds in Chapter 3.

2.1 Identification and structural elucidation of compound A (64).

Compound A (**64**), compound B (**65**), 13-desoxypaxilline (**37**) and paspaline (**42**) were contained in a fraction from the non-polar layer of the liquid-liquid partition of the extract (Figure 2.2). Further normal phase flash columns enabled the separation of these compounds, which were subsequently purified by semi-preparative HPLC. Compound A (**64**) was the first compound to be purified.

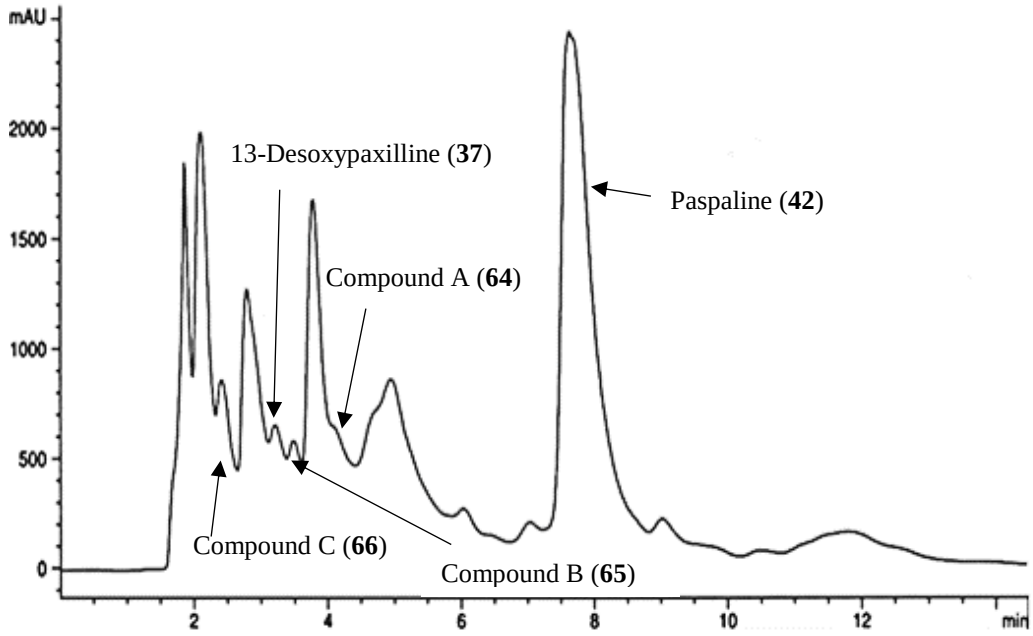

Figure 2.2: HPLC chromatogram of the non-polar layer of the crude extract with UV detection at 230 nm.

2.1.1 UV Spectroscopy

The UV absorption spectrum of compound A (**64**) contained peak maxima at 215, 240 and 295 nm (Figure 2.3), which were different to the UV maxima of 225 and 275 nm observed for 13-desoxypaxilline (**37**) and paspaline (**42**).[67] This indicated that compound A (**64**) had a different chromophore present.

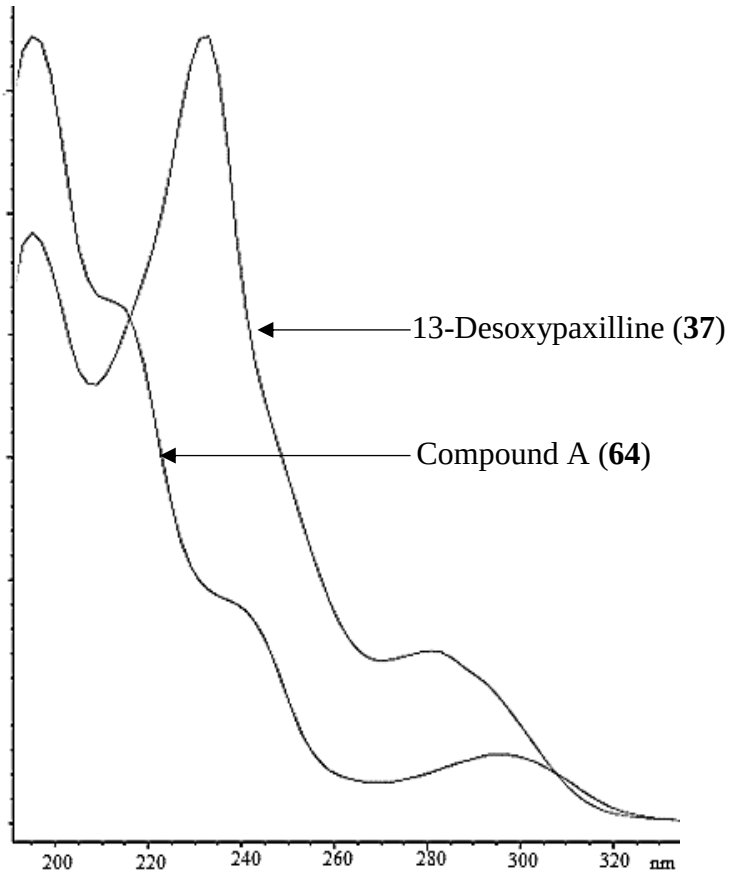

Figure 2.3: The normalised UV absorbance spectra of compound A (**64**) and 13-desoxypaxilline (**37**) obtained from HPLC.

2.1.2 Mass Spectrometry

The molecular mass of compound A (**64**) was confirmed by mass spectrometry. The high resolution mass spectrum of compound A (**64**) contained a pseudo-molecular ion at *m/z* 636.3453. This was consistent with a molecular formula of $C_{37}H_{49}NO_8$ (*m/z* 635.3458).

The tandem mass spectrum of compound A (**64**) in positive ion mode, contained the fragment ions *m/z* 618.2, 600.2, 576.3, 564.1 and 536.2 (Figure 2.4). These fragment ions are attributable to the loss of oxygen or loss of water (18 Da), two extra water molecules (36 Da), C_3H_8O (60 Da), C_4H_8O (72 Da) and $C_5H_8O_2$ (100 Da) respectively. The loss of water molecules indicated that compound A (**64**) contained at least three oxygen atoms. The common fragment ions of indole

diterpenoids at *m/z* 182 and 130 were not evident, thus indicating the indole region of compound A (**64**) could be modified.

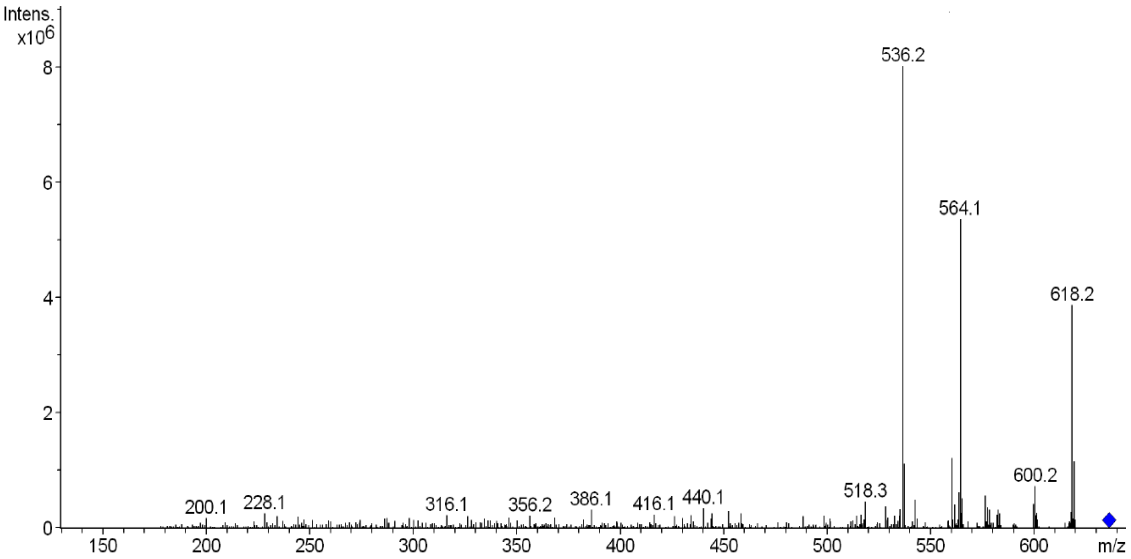

Figure 2.4: The tandem mass spectrum of compound A (**64**), *m/z* 636.3 (positive ion mode).

MS^3 fragmentation of some selected MS^2 daughter ions was further investigated and the ions observed listed in Table 2.1. The MS^3 fragmentation of the MS^2 ion at *m/z* 564.1 yielded a fragment ion at *m/z* 536.3, which would be attributable to the loss of C_2H_4 or CO (28 Da). The other resulting MS^3 fragment ions at *m/z* 600.3, 582.3, 558.4 and 518.3 would be attributable to the loss of oxygen atoms in the form of water molecules from MS^2 ions of *m/z* 618.2, 600.2, 576.3 and 536.2 respectively. This also indicated the presence of at least three oxygen atoms in compound A (**64**).

Table 2.1: The MS^2 and MS^3 fragments of *m/z* 636.3 of compound A (**64**) (positive ion mode).

Parent ion (*m/z*)	Mass loss (Da)	Attributable fragment loss	MS^2 fragment ions (*m/z*)	MS^3 ions arising from selected MS^2 ion (*m/z*)
636.3	18	H_2O	618.2	600.3
	36	2 x H_2O	600.2	582.3
	60	C_3H_8O	576.3	558.4
	72	C_4H_9O	564.1	536.3
	100	$C_5H_8O_2$	536.2	518.3

2.1.3 NMR Spectroscopy

Compound A (**64**) was structurally characterised by NMR spectroscopy with acquisition of a full range of 1D and 2D NMR experiments including ^{1}H, ^{13}C, DEPT-135, COSY, HSQC, NOE and HMBC experiments.

The ^{1}H NMR spectrum of compound A (**64**) contained thirty two signals (Figure 2.5). These signals consisted of ten singlets, six doublets, a triplet, seven doublets of doublets, three triplets of doublets, a quartet of triplets and four multiplets. The integration of these proton signals indicated the presence of forty nine protons in total. The singlet at 1.31 ppm was the most intense peak and integrated as six protons. This, therefore, could be attributed to two methyl groups.

Four aromatic proton signals comprising two doublets of triplets at 6.81 and 7.12 ppm and two doublets of doublets at 6.72 and 6.99 ppm were observed, indicating the presence of an *ortho* disubstituted benzene ring in compound A (**64**). The presence of proton signals between 3.00 – 5.00 ppm indicated that an alkene group or heteroatoms such as oxygen were likely to be present in the compound, consistent with the oxygen atoms indicated in the molecular formula. The chemical shift of one proton at 5.33 ppm was typical of that of an alkene proton.

The ^{13}C NMR spectrum (Figure 2.6) showed the presence of thirty five carbon signals and the DEPT-135 NMR spectrum (Appendix 1) contained twenty five carbon signals, with a methine resonance at 76.7 ppm which had been concealed under the solvent peak. These carbon signals were identified as representing eight methyl, five methylene, twelve methine and eleven quaternary carbons.

The presence of an aromatic ring was confirmed by the methine resonance signals at 116.6, 119.5, 122.0, 125.3 and 128.2 ppm. Four of these signals were attributable to the benzene ring. The HSQC NMR spectrum (Appendix 2) showed that the doublet at 5.33 ppm in the proton spectrum correlated to the carbon signal at 122.0 ppm, which was consistent with the presence of a protonated alkene carbon.

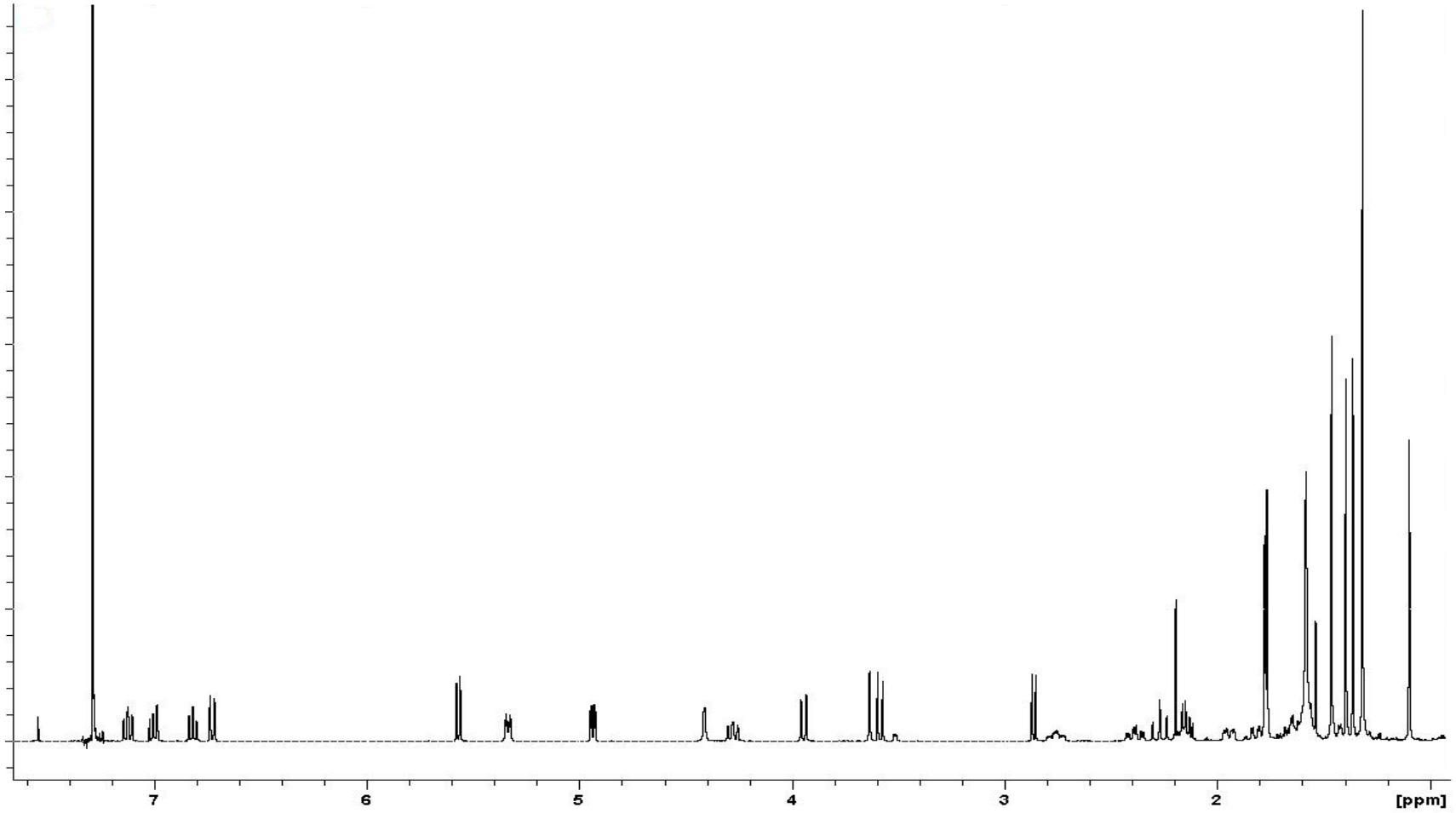

Figure 2.5: The ^{1}H NMR spectrum of compound A (**64**), ($CDCl_3$, 400 MHz).

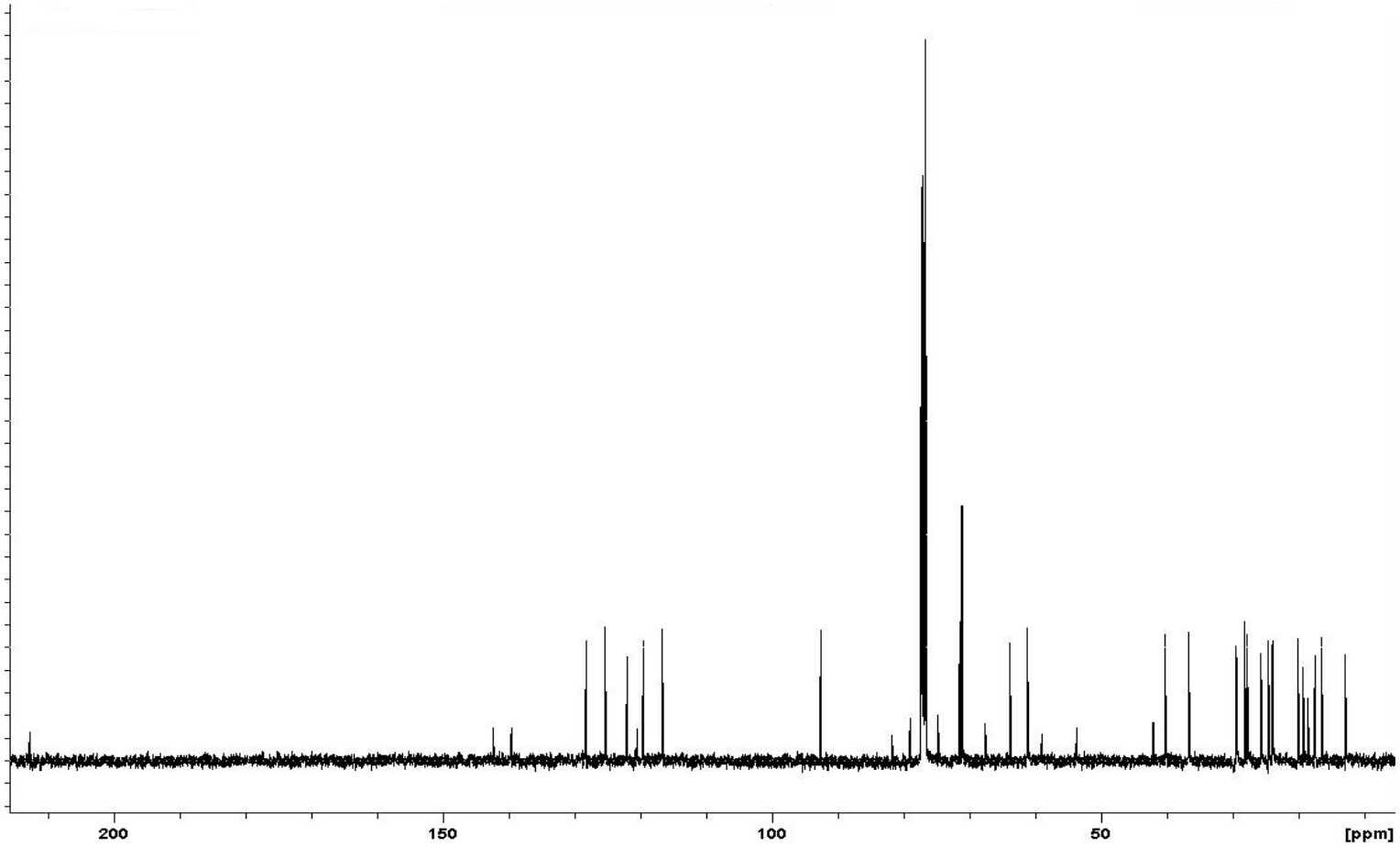

Figure 2.6: The ^{13}C NMR spectrum of compound A (**64**), ($CDCl_3$, 400 MHz).

The chemical shifts of six methine carbon signals at 61.2, 63.9, 71.1, 71.5, 76.7 and 92.6 ppm supported the idea that electronegative heteroatoms such as oxygen were present in close proximity to these carbon atoms. A quaternary carbon signal at 212.2 ppm in the ^{13}C NMR spectrum (Figure 2.6) indicated that a ketone functionality was also present in the compound.

The alkene proton resonance at 5.33 ppm displayed a COSY correlation to a proton signal at 5.56 ppm, which the HSQC NMR spectrum showed to correlate to a carbon resonating at 92.2 ppm (Appendix 2). The HMBC NMR spectrum (Appendix 3) indicated that the alkene proton at 5.33 ppm was correlated to two olefinic methyl carbons resonating at 18.6 ppm and 25.7 ppm (^3J), the attached protons of which yielded signals at 1.76 and 1.77 ppm respectively. The HMBC NMR spectrum (Appendix 3) indicated that the proton signal at 1.76 ppm was correlated to a carbon signal at 139.9 ppm (^2J) and to carbon signals at 25.7 ppm and 122.0 ppm (^3J). Similarly, the resonance at 1.77 ppm was correlated to a carbon signal at 139.9 ppm (^2J) and to signals at 18.6 ppm and 122.0 ppm (^3J). These correlations indicated that a prenyl group was present in compound A (**64**) and the chemical shifts of carbon signals at 122.0 and 139.9 ppm were consistent with the presence of a trisubstituted double bond between them.

A prenyl moiety is present in some known indole diterpenoids including lolitrem B (**3**),[50] epoxy-janthitrem II (**60**)[78] and terpendole C (**49**).[74] The chemical shifts of the prenyl moiety of lolitrem B (**3**) closely matched those of compound A (**64**) (Figure 2.7), confirming the presence of this moiety in compound A (**64**).

(i) (ii)

Figure 2.7: The ^{13}C NMR chemical shifts (ppm) in $CDCl_3$ for the prenyl moiety of (i) lolitrem B (**3**) and (ii) compound A (**64**).

The chemical shift of the methine carbon signal at 92.6 ppm was typical of that of a dioxygenated carbon, consistent with the chemical shift of the corresponding proton signal at 5.56 ppm. The HMBC NMR spectrum indicated that this proton was correlated to a methine carbon signal at 71.1 ppm and two quaternary carbon signals at 74.8 and 139.9 ppm (^3J) (Appendix 3). The intensity of the methine resonance (71.1 ppm) was double the intensity of most of the other protonated carbon signals in the ^{13}C NMR spectrum (Figure 2.6), indicating that two methine resonances could be coincident. The HSQC NMR spectrum (Appendix 2) confirmed this by showing that the signals at 3.58 and 3.94 ppm in the proton spectrum, which each represented one proton, were both correlated to this carbon signal (Figure 2.8).

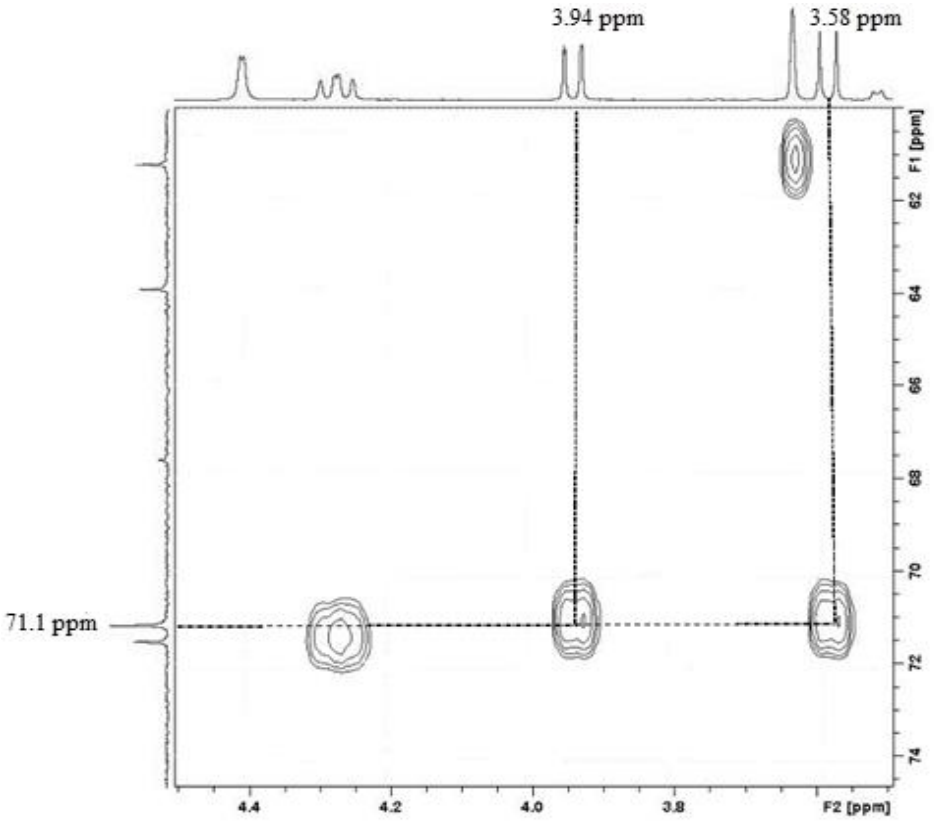

Figure 2.8: A selected region of the HSQC NMR spectrum of compound A (**64**), ($CDCl_3$ 400 MHz). (^1H, 2.50 – 5.00 ppm and ^{13}C, 60.0 – 75.0 ppm).

These proton signals had a COSY correlation to each other, indicating that both carbons at 71.1 ppm were adjacent. The doublet of doublets at 3.94 ppm indicated that this proton was not only coupled to the proton signal which resonated at

3.58 ppm but also to another signal at 3.63 ppm which was correlated to a methine carbon at 61.2 ppm in the HSQC NMR spectrum (Appendix 2).

The HMBC NMR spectrum (Appendix 3) showed that the proton signal at 3.94 ppm had correlations to methine carbon resonances at 61.2 and 71.1 ppm (^2J), 92.6 ppm (^3J) and to a quaternary carbon signal at 74.8 ppm (^3J). The proton signal at 3.58 ppm was correlated to carbon signals at 74.8 and 71.1 ppm (^2J), methine carbon signals at 61.2 and 71.5 ppm (^3J) and to the two methyl carbon signals at 16.6 and 28.3 ppm (^3J). The HSQC NMR spectrum (Appendix 2) indicated that the corresponding proton signal of these methyl carbon resonances was a singlet at 1.31 ppm which represented six protons. The correlations from this signal were to carbon signals at 74.8 ppm (^2J), 92.2 and 71.1 ppm (^3J) in the HMBC NMR spectrum (Appendix 3). These correlations indicated that a hemi-acetal ring is present in the compound, linked to the prenyl moiety by the methine carbon which resonates at 92.2 ppm (Figure 2.9).

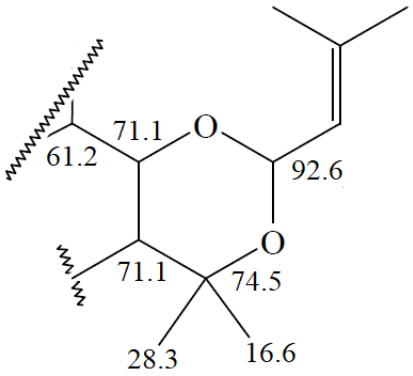

Figure 2.9: The substructure of compound A (**64**) showing a hemi-acetal ring linked to the prenyl moiety.

This substructure was linked to other parts of the molecule by COSY and HMBC correlations. The carbon at 71.5 ppm, which was attached to a proton resonating at 4.27 ppm in the HSQC spectrum (Appendix 2), was also characteristic of that of a carbon attached to an oxygen atom. The COSY NMR spectrum (Appendix 4) indicated that this proton signal was coupled to a proton resonating at 2.15 ppm (which was correlated to a methylene carbon signal at 27.8 ppm in the HSQC NMR spectrum (Appendix 2)). The 4.27 ppm proton signal was also correlated to a

quaternary carbon signal at 67.5 ppm (^2J) and to the previously mentioned methine carbon resonances at 61.2 and 71.1 ppm (^3J) in the HMBC NMR spectrum (Appendix 3).

A proton signal at 3.63 ppm which was correlated to a methine carbon signal at 61.2 ppm in the HSQC NMR spectrum (Appendix 2), had a COSY correlation to the 4.27 ppm proton (^4J). This proton signal was also correlated to the carbon signals at 71.1 and 67.5 ppm (^2J) and to a quaternary carbon signal at 79.0 ppm (^3J) in the HMBC NMR spectrum (Appendix 3). The chemical shifts of the carbon signals at 67.5 and 61.2 ppm were similar, which indicated that an oxygen atom could be attached and could be in the form of an epoxy moiety.

An epoxy group is present in nine of the known terpendoles, including terpendole C (**49**)[74] and also in the lolitrems including lolitrem B (**3**),[1] at carbons C-11 and C-12. The literature chemical shifts of the epoxy moieties in terpendole C (**49**) and lolitrem B (**3**) were 61 ppm (C-11) and 67 ppm (C-12) which matched exactly to those of the proposed epoxy group in compound A (**64**). The structure of the next ring of compound A (**64**) was therefore proposed as in Figure 2.10.

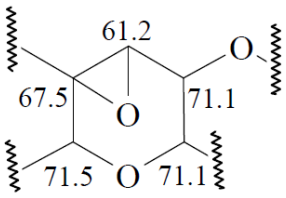

Figure 2.10: The substructure of compound A (**64**) with an epoxy group.

The proton signal at 2.38 ppm was attached to a methylene carbon at 24.0 ppm in the HSQC NMR spectrum (Appendix 2) and was also correlated to carbon signals at 27.8 and 42.1 ppm (^2J) and to a methyl carbon signal at 17.6 ppm (^3J) in the HMBC NMR spectrum (Appendix 3). The other proton attached to the carbon, which resonated at 24.0 ppm, was one which yielded a signal at 1.94 ppm and was correlated to the carbon signal at 79.0 ppm (^3J). Similarly, a methyl proton signal at 1.09 ppm was correlated to the same carbon signal at 79.0 ppm (^3J) and to carbon

signals at 53.7 ppm (^3J) and 42.1 ppm (^2J). This methyl proton was correlated to the carbon signal at 17.6 ppm in the HSQC NMR spectrum (Appendix 2). The carbon resonances at 42.1, 53.7 and 79.0 ppm were all quaternary carbons, with the chemical shift of the last one indicating the presence of a hydroxyl group. The chemical shift of this carbon matches the chemical shift of C-13 (79.0 ppm) of terpendole C (**49**),[74] as well as that of lolitrem B (**3**), which contains a hydroxyl proton. This confirmed that a hydroxyl group is present in compound A (**64**). A broad singlet signal at 1.53 ppm which was correlated to the quaternary carbon signals at 42.1 and 67.5 ppm (^3J) in the HMBC NMR spectrum (Appendix 3), was assigned to the hydroxyl proton.

A proton which yielded a signal at 1.56 ppm, was attached to the methylene carbon at 29.4 ppm from the HSQC NMR spectrum (Appendix 2) and was correlated to quaternary carbons at 79.0 (^2J) and 42.1 ppm (^3J). Similarly, a proton which yielded a signal at 1.82 ppm (attached to another methylene carbon at 20.1 ppm) was correlated to the carbon signals at 29.4 and 36.8 ppm (^2J) in the HMBC NMR spectrum (Appendix 3). Another proton signal at 2.75 ppm, correlated to the carbon resonating at 36.8 ppm, had COSY correlations to proton signals at 1.81 and 2.27 ppm. This proton (2.75 ppm), was correlated to the methyl carbon signal at 12.9 ppm (^3J) in the HMBC NMR spectrum (Appendix 3). The proton signals at 1.82 and 2.27 ppm were correlated to methylene carbons at 20.1 and 40.3 ppm respectively. The structure of the mid-region of compound A (**64**) was therefore proposed as in Figure 2.11.

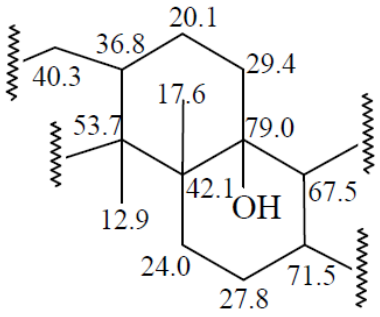

Figure 2.11: The proposed structure for the mid-region of compound A (**64**).

The compiling of all of the proposed substructures mentioned above yielded the right side of compound A (**64**), which was found to have similar structural features to some of the indole diterpenoids including lolitrem B (**3**) and terpendole C (**49**). However, the numbering systems, especially at the prenyl moieties of lolitrem B (**3**) and terpendole C (**49**), were different. The numbering system used for terpendole C (**49**) is used for compound A (**64**) (Figure 2.12). To confirm the similarity of the structural features, the NMR data for the right side of compound A (**64**) were compared to those of terpendole C (**49**) at C-3 to C-17 and C-25 to C-36 (Figure 2.12 and Table 2.2).

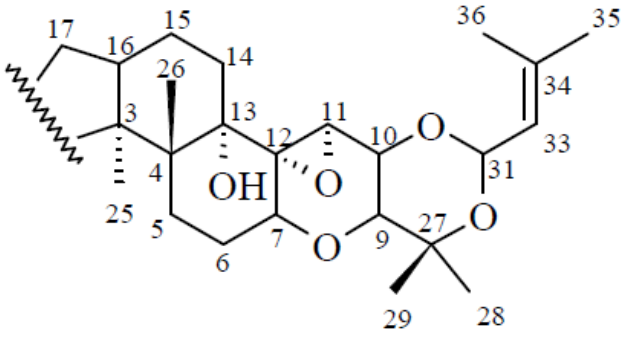

Figure 2.12: The structure of the right side of terpendole C (**49**) with carbon numbering.

Table 2.2: ^{13}C and ^{1}H NMR assignments for the right side of compound A (**64**) compared to literature values for terpendole C (**49**),[74] ($CDCl_3$, 400 MHz).

	Compound A (64)			**Terpendole C (49)[74]**	
Atom	**^{13}C (δ ppm)**		**^{1}H (δ ppm)**	**^{13}C (δ ppm)**	**^{1}H (δ ppm)**
3	53.7			50.7	
4	42.1			42.4	
5	24.0	Hα Hβ	2.38 1.94	27.4	2.72 1.35
6	27.8	Hα Hβ	2.15 1.64	28.0	2.30 1.80
7	71.5		4.27	71.5	4.35
9	71.1		3.58	71.1	3.60
10	71.1		3.94	71.2	3.94
11	61.2		3.63	61.1	3.63
12	67.5			67.8	
13	79.0			78.1	

Atom	Compound A (64)			Terpendole C (49)[74]	
	^{13}C (δ ppm)		^{1}H (δ ppm)	^{13}C (δ ppm)	^{1}H (δ ppm)
14	29.4	Hα	1.56	30.3	1.60
		Hβ	1.42		1.44
15	20.1	Hα	1.81	20.6	1.94
		Hβ	1.63		1.65
16	36.8		2.75	50.0	2.80
17	40.3	Hα	2.27	27.2	2.42
		Hβ	2.12		2.74
25	12.9		1.46	16.0	1.28
26	17.6		1.09	16.6	1.08
27	74.8			74.4	
28	16.6		1.31	18.8	1.14
29	28.3		1.31	28.3	1.32
31	92.6		5.56	92.6	5.56
33	122.0		5.33	122.0	5.33
34	139.3			139.3	
35	18.6		1.76	18.6	1.75
36	25.7		1.77	25.7	1.75

The similar structural features of the right side of compound A (**64**) and terpendole C (**49**) are reflected in the similar NMR chemical shifts. The major differences in the ^{13}C and ^{1}H NMR data for the right side of compound A (**64**) and terpendole C (**49**) were the chemical shifts of C-3, C-5, C-16, C-17 and H-5α, H-5β, H-6α, H-6β, H-17α, H-17β and H-25 respectively. This indicated that some of the functionalities at the left side of compound A (**64**) have affected these chemical shifts.

The structure of the left side of compound A (**64**) was determined from the HMBC NMR correlations of the atoms at positions C-3, C-16 and C-17. The proton signal at 2.12 ppm (H-17β) was correlated to quaternary carbon signals at 81.8 (^{2}J), 53.7 ppm (C-3) (^{3}J) and 212.2 ppm (^{3}J). This last chemical shift is typical of that of a ketone carbonyl carbon. The proton signal at 1.46 ppm (H-25) was correlated to this carbonyl in the HMBC NMR spectrum (Appendix 3) and the proton signal at 2.27 ppm (H-17α) was correlated to the carbon signals at 36.8 (C-16) (^{2}J), 20.1 (C-15) (^{3}J) and 120.5 ppm (^{3}J). The chemical shift of the carbon signal at

120.5 ppm was that of a typical aromatic carbon which was consistent with aromatic protons identified in the ^{1}H NMR spectrum (Figure 2.5).

The signals in the ^{1}H NMR spectrum of compound A (**64**) attributed to the aromatic ring system, were assigned based on COSY correlations. Proton signals at 6.99, 7.12, 6.81 and 6.72 ppm were assigned as H-20, H-21, H-22 and H-23 respectively and their corresponding carbons resonated at 125.3, 128.2, 119.5 and 116.6 ppm respectively. The proton signal at 7.12 ppm (H-21) was correlated to the proton signals at 6.99 (H-20) and 6.81 ppm (H-22) in the COSY NMR spectrum (Appendix 4), while the proton signal at 7.12 ppm (H-21) was correlated to the quaternary carbon signal at 120.5 ppm (^{3}J) in the HMBC NMR spectrum (Appendix 3). This carbon was then assigned as C-19. The proton signal at 6.99 ppm (H-20) was correlated to carbon signals at 119.5 ppm (C-22) (^{3}J) and to quaternary carbon signals at 142.3 and 81.8 ppm (^{3}J) in the HMBC NMR spectrum (Appendix 3). These quaternary carbons were assigned as C-25 and C-18 respectively for compound A (**64**).

No correlation was observed in the HSQC spectrum (Appendix 2) from a singlet proton signal at 4.40 ppm. This signal could represent either a NH or an OH proton and was correlated in the COSY spectrum (Appendix 4) to a doublet of doublets at 4.93 ppm. The proton at 4.93 ppm was assigned to H-2 and was attached to a carbon which resonated at 76.7 ppm from the HSQC NMR spectrum (Appendix 2). In the HMBC NMR spectrum, the 4.40 ppm proton signal was correlated to the carbon signals at 120.5 (C-19) and 116.6 ppm (C-23) (^{3}J), indicating that this signal was a NH proton.

In the NMR spectra of an indole moiety, the chemical shift of the NH proton usually resonates between 7.00 – 10.00 ppm with quaternary carbons at 152.0 (C-2) and 118.0 ppm (C-18), as observed for terpendoles A – D (**47** – **50**)[74] and lolitrem B (**3**).[53] However, C-2 of compound A (**64**) was a methine resonance with a much more upfield chemical shift at 76.7 ppm, indicating that the indole structure has been modified in this compound compared to that of terpendole C (**49**) (Figure 2.13).

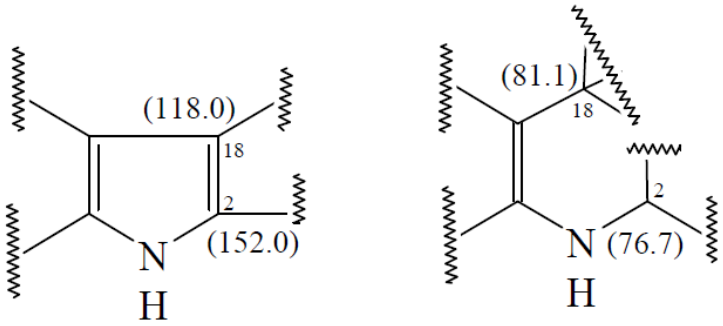

(i) (ii)

Figure 2.13: NMR chemical shifts (ppm) of C-2 and C-18 in (i) a typical indole moiety as in terpendole C (**49**), (ii) the modified indole structure in compound A (**64**).

Similarly, C-18 had a much more upfield chemical shift (81.1 ppm) than that of a typical indole group (~118.0 ppm) although still a quaternary carbon. This indicated that the double bond between C-2 and C-18 normally seen in an indole moiety is absent in compound A (**64**). The chemical shift of 81.1 ppm indicated that this carbon was most likely attached to an oxygen atom. These changes are also consistent with the much more upfield chemical shift observed for the NH proton (4.40 ppm) of compound A (**64**).

The COSY NMR spectrum indicated that the 4.93 ppm (H-2) signal was correlated to the NH proton at 4.40 ppm and to another signal at 2.86 ppm (Figure 2.14), which in the HSQC NMR spectrum correlated to a carbon which resonated at 63.9 ppm (Appendix 2). This was consistent with the absence of a double bond between C-2 and C-18 of compound A (**64**).

The HMBC NMR spectrum (Appendix 3) indicated that the H-2 resonance was correlated to the carbon signal at 63.9 ppm (^2J) and to two quaternary carbon signals at 59.0 and 81.1 ppm (^3J). The proton resonance at 2.86 ppm was also correlated to the quaternary carbon resonance at 59.0 ppm (^2J) and to two germinal methyl carbon signals at 19.3 and 24.6 ppm (^3J), the chemical shifts of which are typical of methyl carbon signals of a prenyl moiety. The protons corresponding to these carbon signals resonated at 1.36 and 1.39 ppm respectively.

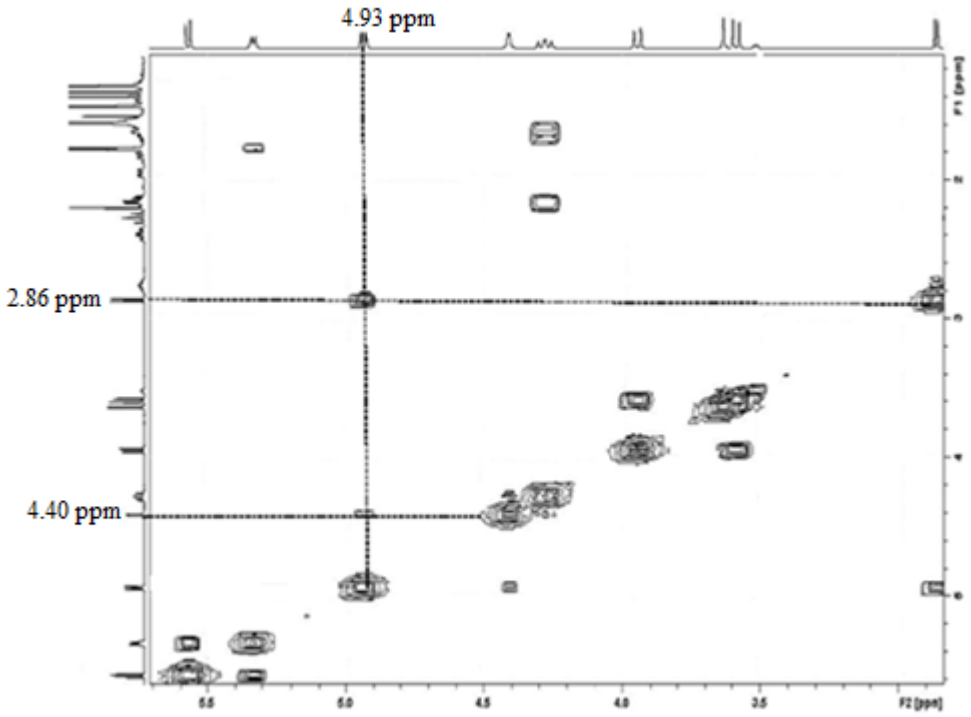

Figure 2.14: Expansion of a selected region (3.00 – 6.00 ppm) of the COSY NMR spectrum of compound A (**64**) with the correlations of 4.93 ppm (H-2) to 4.40 ppm (NH) and 2.86 ppm protons.

In comparison to the prenyl moiety that was previously identified in the compound, the chemical shifts of the carbon signals at 63.9 ppm and 59.0 ppm were much more upfield compared to those expected if a double bond were present as observed for 122.0 ppm (C-33) and 139.3 ppm (C-34). However, the chemical shifts of 61.2 ppm (C-11) and 67.5 ppm (C-12) signals closely matched the corresponding carbon resonances at 63.9 and 59.0 ppm, which indicates that an epoxy group could also be part of the proposed prenyl moiety. From the HMBC NMR spectrum (Appendix 3), the $^{1}J_{(C\text{-}H)}$ coupling constant of the 3.63 ppm (H-11) proton was approximately 178 Hz, which closely matched that of the proton signal at 2.86 ppm (175 Hz) (Figure 2.15). Hence, this was strong evidence of the presence of another epoxy group in the compound.

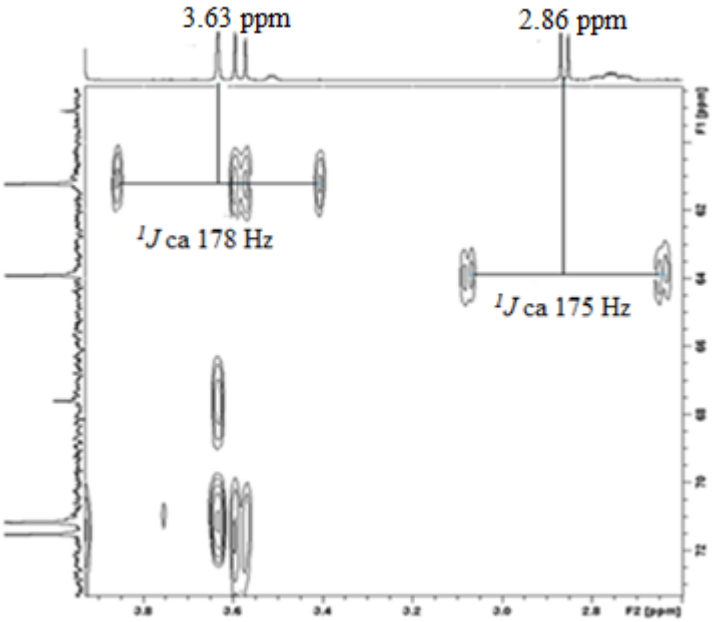

Figure 2.15: A selected region of the HMBC spectrum of compound A (**64**), with the $^1J_{(C-H)}$ coupling constants of H-11 – C-11 and H-39 – C-39 indicated. (^{1}H, 2.00 – 4.00 ppm and ^{13}C, 60.0 – 74.0 ppm).

In addition, the known compound terpendole A (**47**), contains an epoxyprenyl moiety on the right side. The moiety comprised of a methine carbon which resonated at 96.9 ppm (C-31), an oxymethine carbon signal at 64.7 ppm (C-33), an oxygenated quaternary carbon which resonated at 59.3 ppm (C-34) and two methyl carbons resonating at 17.2 ppm (C-35) and 25.0 ppm (C-36).[74] The chemical shifts of the carbon signals for C-33 to C-36 of terpenedole A (**47**) were very similar to those of the equivalent carbon resonances (63.9, 59.0, 24.6 and 12.9 ppm) of compound A (**64**) (Figure 2.16). This confirmed that an epoxyprenyl moiety was attached to the carbon resonating at 76.7 ppm (C-2) of compound A (**64**).

The molecular formula of compound A (**64**) indicated that a single oxygen atom still needed to be incorporated into the structure. In addition, the connections between the carbon signals at 76.7 (C-2), 81.8 (C-18) and 212.2 ppm still needed to be determined.

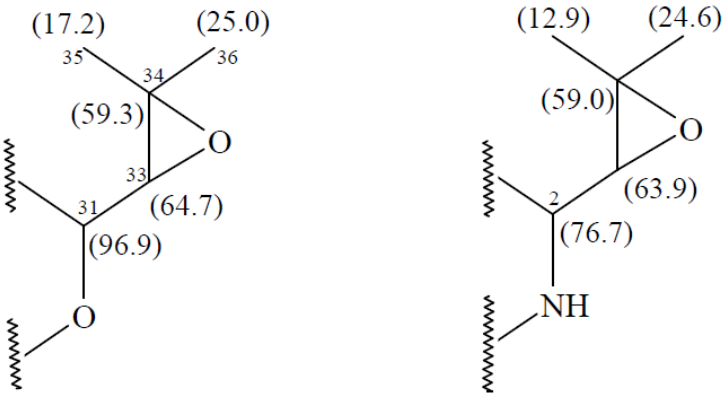

(i) (ii)

Figure 2.16: The ^{13}C chemical shifts (ppm) of (i) the epoxyprenyl moiety of terpendole A (**47**) and (ii) the substructure proposed for compound A (**64**).

From the HMBC NMR spectrum (Appendix 3) of compound A **(64)**, the $^{1}J_{(C\text{-}H)}$ coupling constant of H-2 (4.93 ppm) was 162 Hz, which closely matched that of the H-31 (5.56 ppm) proton of 163 Hz (Figure 2.17).

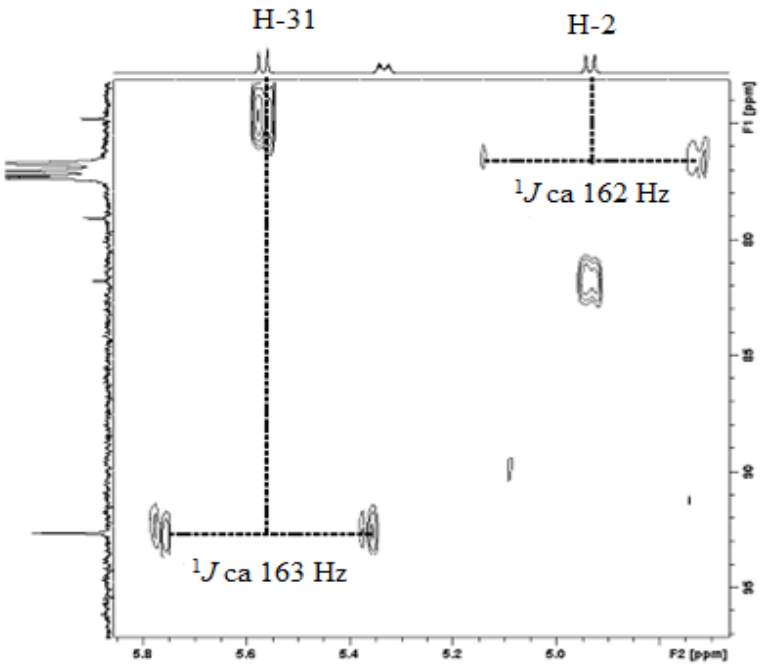

Figure 2.17: A selected region of the HMBC spectrum of compound A (**64**) showing the $^{1}J_{(C\text{-}H)}$ coupling constants of H-2 and H-31. (^{1}H, 4.00 – 6.00 ppm and ^{13}C, 70.0 – 98.0 ppm).

This indicated that the carbons resonating at 76.7 ppm (C-2) and 81.1 ppm (C-18) were connected via the remaining oxygen atom, similar to that observed between the C-31 (92.6 ppm) and C-10 (71.1 ppm) signals on the right side of compound A (**64**). The quaternary carbon at 81.8 ppm (C-18) was also directly bonded to the methylene carbon resonating at 40.3 ppm (C-17) and to the ketone carbonyl carbon resonating at 212.2 ppm. Hence, C-18 is a spiro centre, a structural feature rarely observed in related fungal metabolites and also another chiral centre in the compound.

Thus compound A (**64**) contains a unique, six membered, oxygen-containing ring. This accounted for the absence of the characteristic indole diterpenoid fragment ions at *m/z* 182 and 130 in the tandem mass spectrum (Figure 2.4) and the difference in the UV absorption spectra (Figure 2.3). The left side of compound A (**64**) is no longer an indole and is proposed as in Figure 2.18, with the carbons assigned as 212.2 (C-37), 63.9 (C-39), 59.0 (C-40), 19.3 (C-41) and 24.6 ppm (C-42).

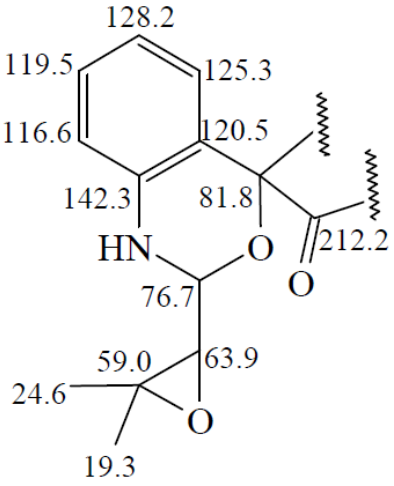

Figure 2.18: Proposed structure for the left side of compound A (**64**).

The connectivity of the atoms of compound A (**64**) was completed with the COSY correlations and the HMBC assignments mentioned in the above discussion. These correlations are summarised in Figure 2.19 and Table 2.3.

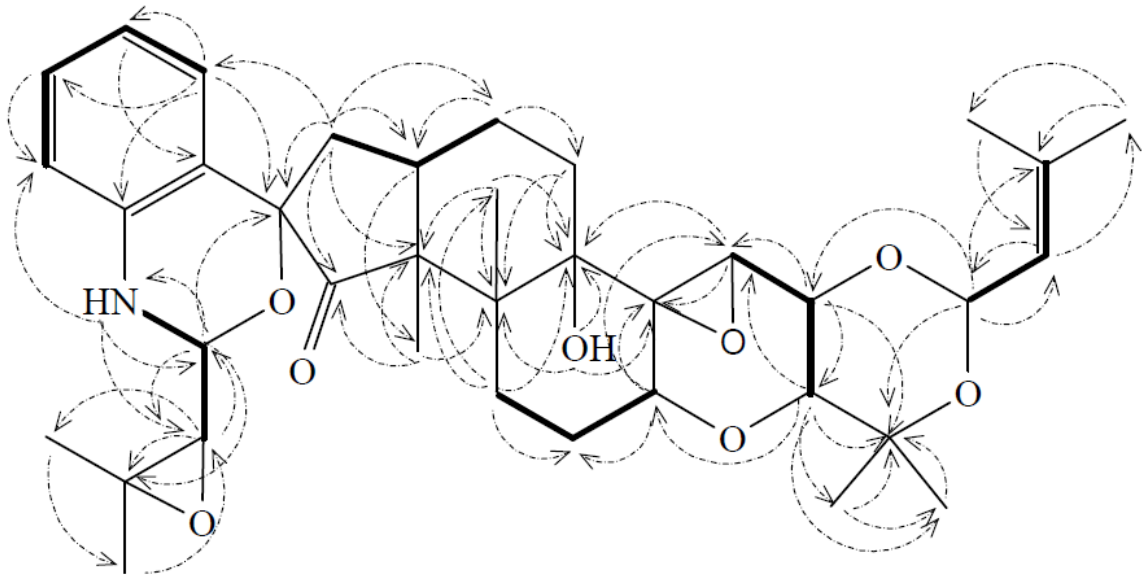

Figure 2.19: The COSY (▬) and ^{1}H - ^{13}C HMBC (- - -) correlations observed for compound A (**64**) ($CDCl_3$, 400 MHz).

Table 2.3: The COSY and ^{1}H - ^{13}C HMBC assignments for compound A (**64**), ($CDCl_3$, 400 MHz).

Atom	**^{13}C (δ ppm)**	**^{1}H (δ ppm)**	**COSY correlations**	**HMBC correlations**
NH		4.02	H-2	C-2, C-39, C-23
2	76.7	4.93	NH, H-39	C-18, C-39, C-40
5	24.0 Hα Hβ	2.38 1.94	H-5β, H-6β	C-3, C-6, C-26, C-13
7	71.5	4.27	H-11, H-6α	C-6, C-11, C-12
9	71.1	3.58	H-7	C-7, C-27, C-11, C-28, C-29
10	71.1	3.94	H-9	C-9, C-11, C-27, C-31
11	61.2	3.63	H-7, H-9	C-9, C-12, C-13
13-OH		1.53		C-13, C-4, C-12
14	29.4 Hα	1.56	H-14β	C-4, C-13
15	20.1 Hα	1.81		C-14, C-16, C-25
16	36.8	2.75	H-17α, H-7β, H-15α	C-25
17	40.3 Hα	2.27	H-17β	C-4, C-15, C-16, C-18, C-19, C-20, C-37
20	125.3	6.99	H-22, H-23	C-18, C-21, C-22, C-24
21	128.2	7.12	H-20, H-22, H-23	C-19
22	119.5	6.81	H-20, H-21	C-23

Atom	^{13}C (δ ppm)	^{1}H (δ ppm)	COSY correlations	HMBC correlations
23	116.6	6.72	H-20, H-21, H-22	C-22
25	12.9	1.46		C-37, C-3, C-4, C-17
26	17.6	1.09		C-3, C-4, C-5, C-13
28	16.6	1.31		C-9, C-27, C-29
29	28.3	1.31		C-9, C-27, C-29
31	92.6	5.56	H-33	C-33, C-10, C-34, C-27
33	122.0	5.33	H-36	C-31, C-35, C-36
35	18.6	1.76		C-33, C-34, C-36
36	25.7	1.77		C-33, C-34, C-35
39	63.9	2.86	H-2	C-2, C-40, C-41, C-42
41	24.6	1.39		C-39, C-40, C-42
42	19.3	1.36		C-39, C-40, C-41

The relative stereochemistry of some of the protons of compound A (**64**) was determined with Nuclear Overhauser Effect (NOE) experiments of selected protons. SELNOESY irradiation of the signal at 1.46 ppm (H-25) enhanced signals which resonated at 2.38 (H-5α), 1.81 (H-15α) and 2.27 ppm (H-17α), suggesting that the methyl group (C-25) was α-oriented (Figure 2.20). This α-orientation was the same as that in the equivalent methyl proton (H-25) observed for lolitrem B (**3**),[51] paxilline (**36**)[70] and the terpendoles.[74]

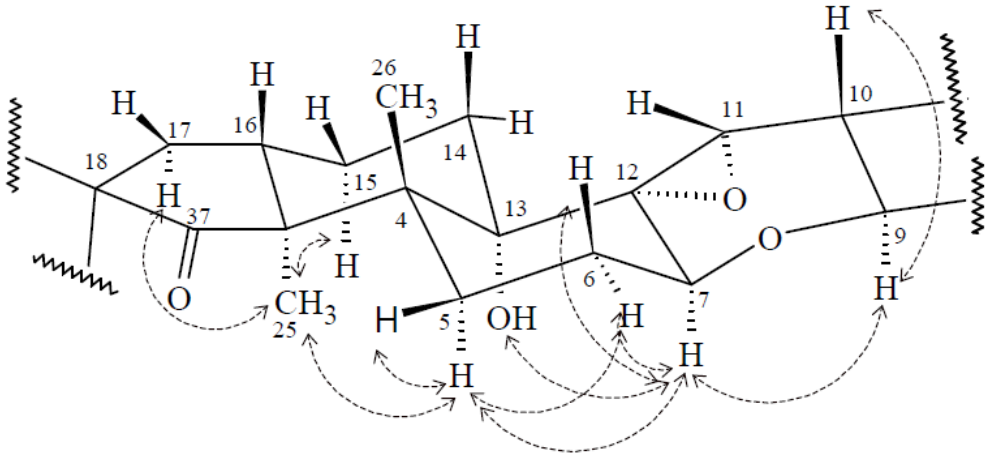

Figure 2.20: NOE of selected proton signals including H-25, H-5α, H-7 and H-9 of compound A (**64**).

Irradiation of the proton signal at 2.38 ppm (H-5α) showed NOE enhancement of the signals at 1.94 (H-5β), 4.27 (H-7) and 1.46 ppm (H-25), while the irradiation of the 4.27 ppm (H-7) signal showed enhancement of the signals at 2.15 (H-6α), 3.58 (H-9) and 1.53 ppm (13-OH). The enhancement of the proton signals arising from H-7, H-9 and 13-OH confirmed that they were α-oriented (Figure 2.20).

Irradiation of the proton signal at 3.94 ppm (H-10) showed enhancement of the signals at 3.58 (H-9), 3.63 (H-11), 1.31 (H-29) and 5.56 ppm (H-31) and irradiation of the proton signal at 3.63 ppm (H-11) caused the enhancement of signals at 3.94 (H-10), 1.42 (H-14β) and 1.09 ppm (H-26), indicating that H-10, H-11, H-29, H-14β and H-26 protons are β-oriented. The enhancement of the 3.58 ppm (H-9) signal (α-oriented) on irradiation of the 3.94 ppm (H-10) proton (β-oriented) indicated that they were *trans*-oriented to each other. The irradiation of the 1.09 ppm (H-26) proton signal enhanced the signals at 1.94 (H-5β), 1.64 (H-6β), 3.94 (H-10) 3.63 (H-11), 2.75 (H-16) and 4.93 ppm (H-2) (Figure 2.21). The irradiation of the proton signal at 2.75 ppm (H-16) enhanced proton signals at 2.12 (H-17β) and 1.09 ppm (H-26), suggesting that these protons are β-oriented. This was consistent with the β-orientation of protons with signals at 3.63 (H-11) and 2.8 ppm (H-16) of terpendole C (**49**) determined by X-ray crystallographic analysis.[74] Irradiation of 2.27 ppm (H-17α) enhanced the 6.99 ppm (H-20) and 1.46 ppm (H-25) protons. The stereochemistry of the right side of compound A (**64**) was consistent with that of lolitrem B (**3**)[51] and terpendole C (**49**).[74]

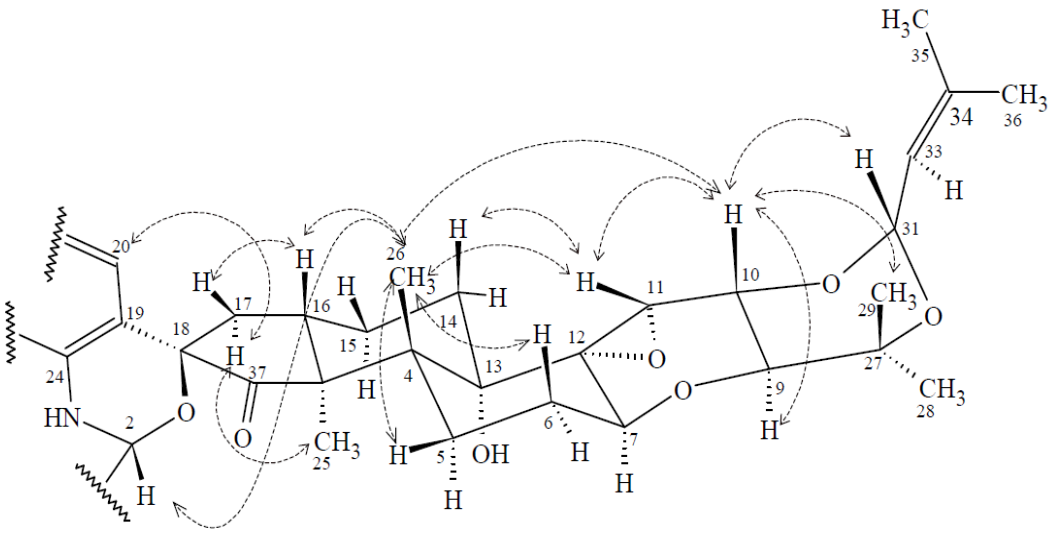

Figure 2.21: NOE of selected proton signals including H-10, H-11, H-16 and H-26 of compound A (**64**).

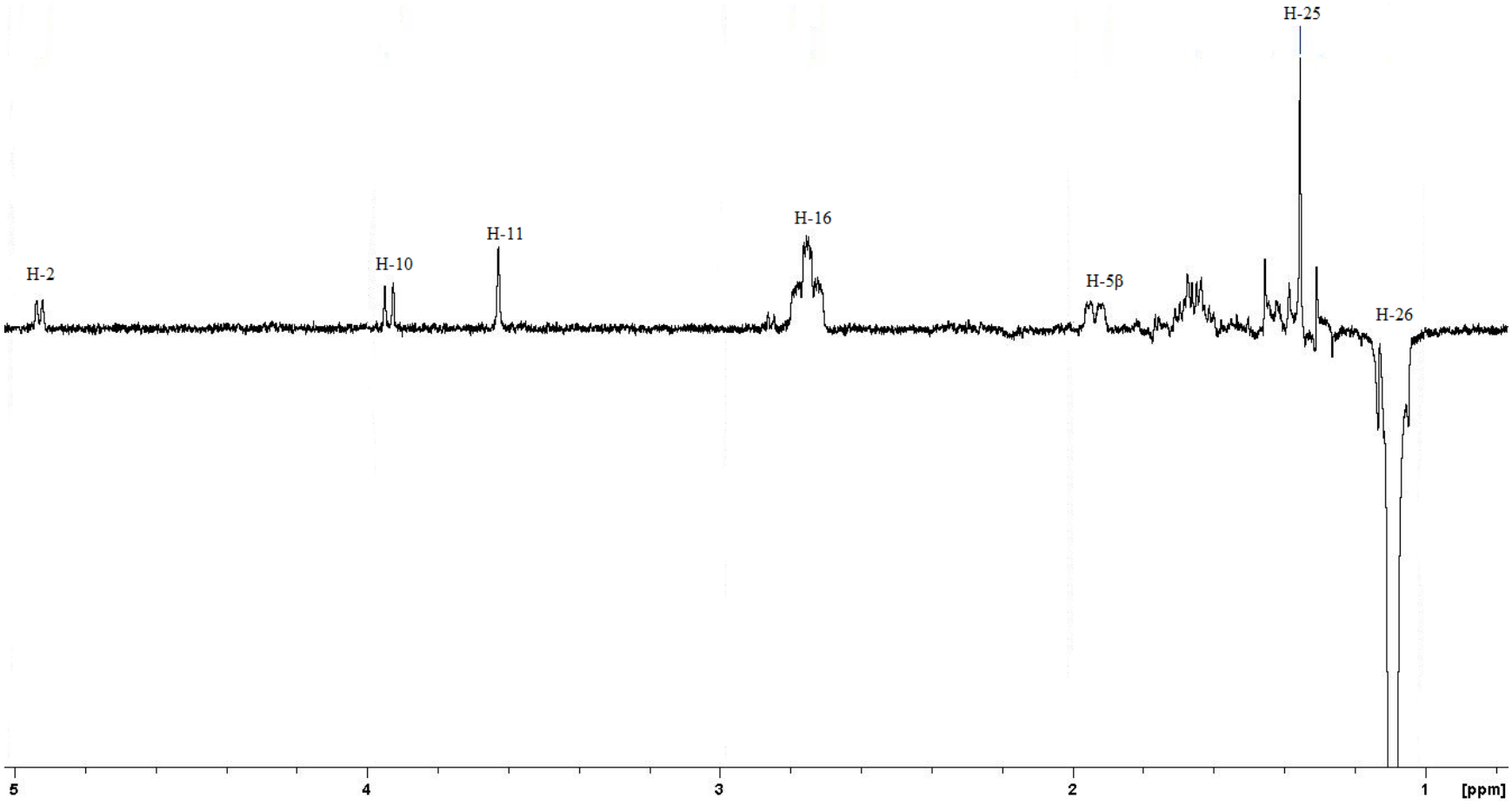

Figure 2.22: The SELNOESY NMR spectrum of compound A (**64**) when the proton signal at 1.09 ppm (H-26) was irradiated, ($CDCl_3$, 400 MHz).

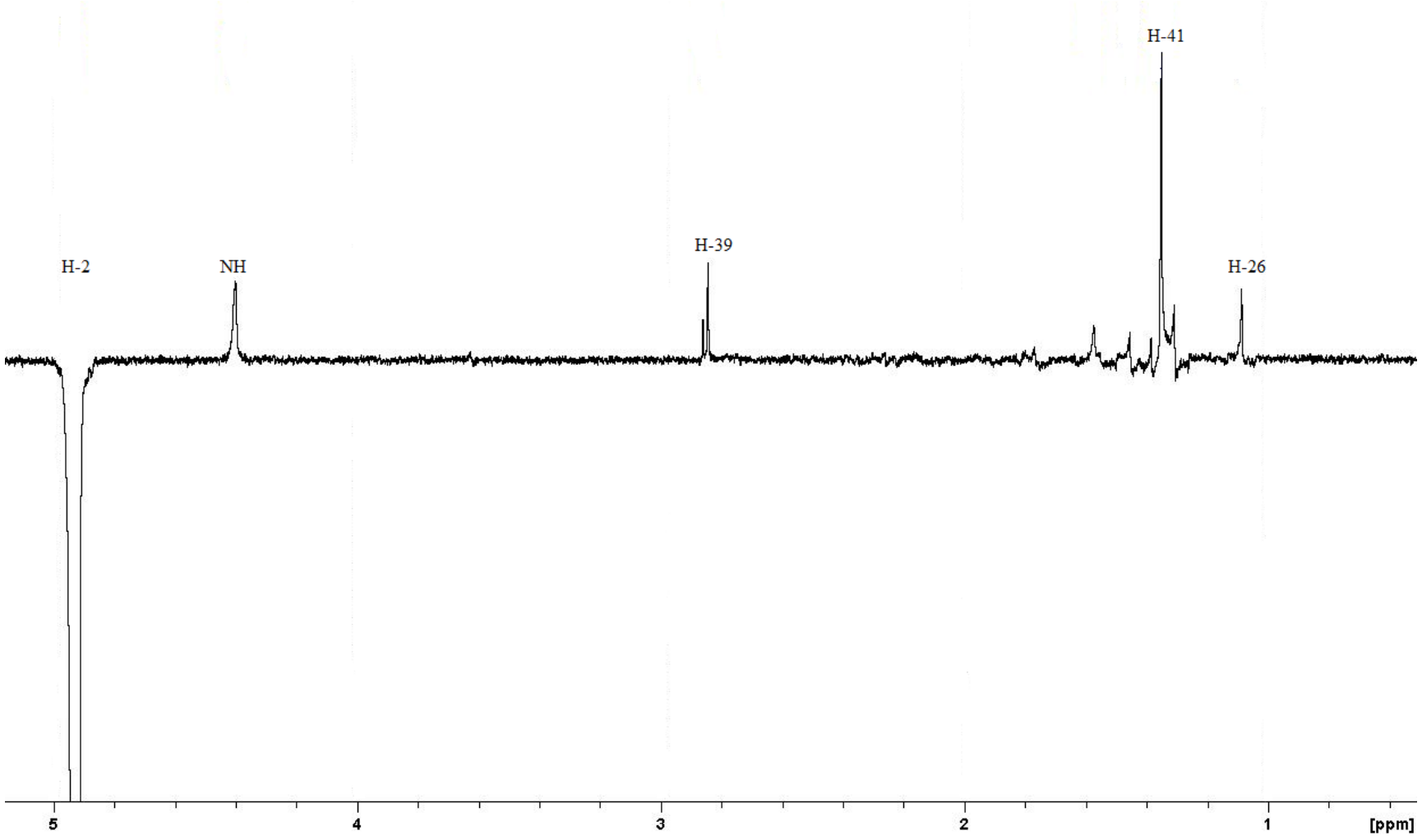

Figure 2.23: The SELNOESY NMR spectrum of compound A (**64**) when the proton signal at 4.93 ppm (H-2) was irradiated, ($CDCl_3$, 400 MHz).

The enhancement of the 4.93 ppm (H-2) signal on irradiation of the proton signal at 1.09 ppm (H-26) (Figure 2.22) was not expected due to the distance between these protons. However, the irradiation of the proton signal at 4.93 ppm (H-2) enhanced the proton signal at 1.09 ppm (H-26) (Figure 2.23) which implies that H-2 and H-26 protons are β-oriented. The orientation around the spiro centre C-18 could in fact bring the H-2 and H-26 protons close enough to enhance each other. The NOE enhancement observed between the H-17α and H-20 protons (Figure 2.21) and H-2 and H-26 protons (Figure 2.24) suggested the stereochemistry at C-18 with the aromatic ring below and the oxygen atom above the plane. Further work is needed to confirm whether this suggestion is correct. Other proton resonances at 4.40 (NH), 2.86 (H-39) and 1.36 ppm (H-42) were also enhanced at the irradiation of the H-2 proton (Figure 2.23), suggesting these protons could be β-oriented.

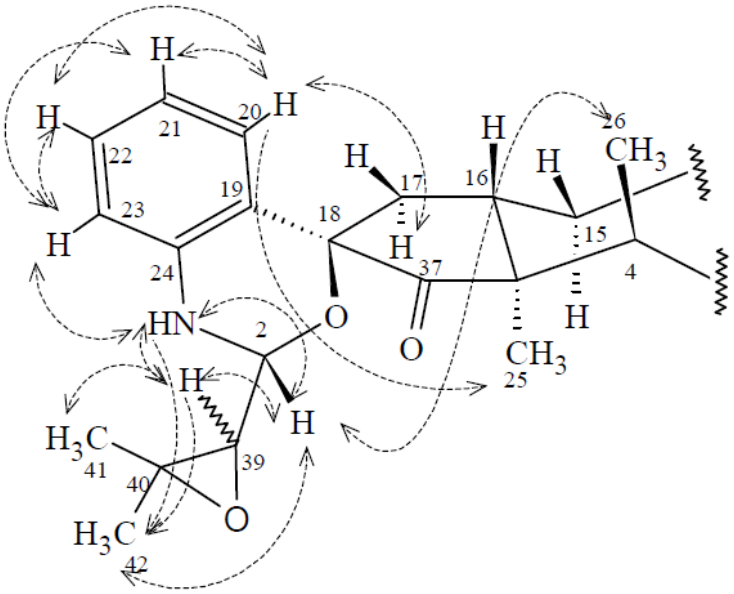

Figure 2.24: NOE of selected protons including H-26, H-2 and the proton signals of the substructure at the left side of compound A (**64**).

Irradiation of the 2.86 ppm (H-39) signal caused the enhancement of the 4.93 (H-2), 1.39 (H-41), 1.36 (H-42) and 4.40 ppm (NH) proton signals and signals at 2.86 (H-39), 6.72 (H-23), 1.36 (H-42) and 4.93 ppm (H-2) were enhanced when the NH proton signal at 4.40 ppm was irradiated. The irradiation of the aromatic proton at 6.72 ppm (H-23) enhanced the 4.40 (NH), 7.12 (H-21) and 6.81 ppm (H-22) proton

signals and irradiation of the 6.99 ppm (H-20) signal enhanced the 2.27 (H-17α), 7.12 (H-21), 6.81 (H-22) and 1.46 ppm (H-25) proton signals (Figure 2.24).

The spatial correlations mentioned above are summarised in Figure 2.25 and Table 2.4.

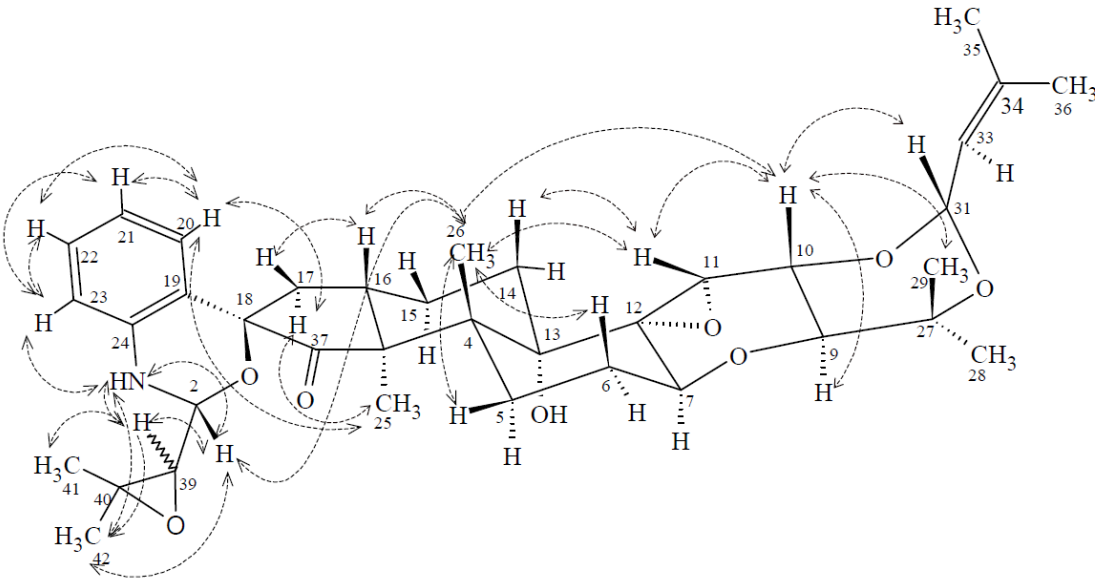

Figure 2.25: NOE correlations of selected protons in compound A (**64**).

Table 2.4: Selected NOE enhancements observed for compound A (**64**), ($CDCl_3$, 400 MHz).

^{1}H NMR (δ, ppm)	**NOE correlations (δ, ppm)**
4.40 (NH)	H-2, H-39
4.93 (H-2)	NH, H-26, H-39, H-42
2.38 (H-5α)	H-7, H-25, H-5β
2.15 (H-6α)	H-7, H-5α
4.27 (H-7)	H-9, H-6α, 13-OH
3.58 (H-9)	H-7, H-10, H-28
3.94 (H-10)	H-11, H-29, H-31
3.63 (H-11)	H-10, H-14β, H-26
2.75 (H-16)	H-17β, H-26
2.27 (H-17α)	H-20, H-25
6.99 (H-20)	H-17α, H-25, H-21, H-22
6.72 (H-23)	NH, H-21, H-22
1.46 (H-25)	H-5α, H-15α, H-16, H-17α, H-20
1.09 (H-26)	H-2, H-5β, H-6β, H-10, H-11, H-16, H-25
2.86 (H-39)	H-2, NH, H-42
1.36 (H-42)	H-2, H-39

The proposed relative stereochemistry could be confirmed by X-ray crystallography and/or computational chemistry but due to time constraints and a non-crystalline sample, these approaches were not explored. Other approaches such as the use of NMR prediction software and ChemDraw 3D modelling could be helpful in ascertaining the relative and absolute stereochemistry. Measurement of the optical rotation of compound A (**64**) is also required but has not been completed to date, due to lack of availability of a suitable polarimeter and to time constraints. Further investigation of the stereochemistry of this compound should be carried out in the future.

Based on the available information, the complete proposed structure of compound A (**64**) was then elucidated and the NMR spectra assigned as in Figure 2.26 and Table 2.5.

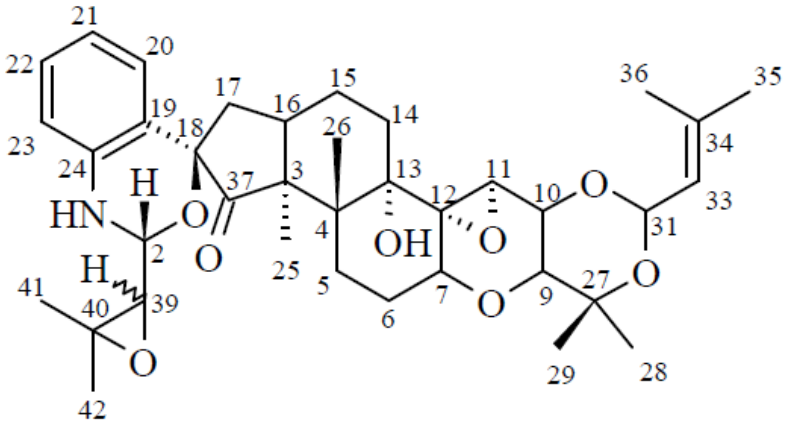

Figure 2.26: The proposed structure of compound A (**64**).

Table 2.5: ^{13}C and ^{1}H NMR chemical shift assignments for compound A (**64**), ($CDCl_3$, 400 MHz).

Atom	**^{13}C (δ ppm)**		**^{1}H (δ ppm)**	**Multiplicity (*J*, Hz)**
NH			4.40	d (2.4)
2	76.7		4.93	dd (6.7, 2.4)
3	53.7			
4	42.1			
5	24.0	Hα	2.38	td (27.9, 13.4, 4.4)
		Hβ	1.94	dd (12.5, 5.8)
6	27.8	Hα	2.15	d (5.8)
		Hβ	1.64	m
7	71.5		4.27	dd (10.9, 8.4)

Atom	^{13}C (δ ppm)		^{1}H (δ ppm)	Multiplicity (*J*, Hz)
9	71.1		3.58	d (9.5)
10	71.1		3.94	dd (9.5, 0.9)
11	61.2		3.63	s
12	67.5			
13	79.0			
13-OH			1.53	s
14	29.4	Hα	1.58	s
		Hβ	1.42	m
15	20.1	Hα	1.81	dd (12.5, 2.9)
		Hβ	1.63	m
16	36.8		2.75	qt (12.9, 2.9)
17	40.3	Hα	2.27	t (26.4, 13.4)
		Hβ	2.12	d (5.5)
18	81.8			
19	120.5			
20	125.3		6.99	dd (8.0, 1.2)
21	128.2		7.12	dt (7.1, 1.4)
22	119.5		6.81	dt (7.1, 1.2)
23	116.6		6.72	dd (7.0, 1.1)
24	142.3			
25	12.9		1.46	s
26	17.6		1.09	s
27	74.8			
28	16.6		1.31	s
29	28.3		1.31	s
31	92.6		5.56	d (6.9)
33	122.0		5.33	m
34	139.3			
35	18.6		1.76	s
36	25.7		1.77	s
37	212.2			
39	63.9		2.86	d (6.7)
40	59.0			
41	24.6		1.39	s
42	19.3		1.36	s

2.2 Identification and structural elucidation of compound B (65).

2.2.1 UV Spectroscopy

The UV spectrum of compound B (**65**) was very similar to that of compound A (**64**), with peak maxima at 215, 240 and 295 nm (Figure 2.27). This indicated that compounds A (**64**) and B (**65**) had similar chromophores and therefore could have similar structures.

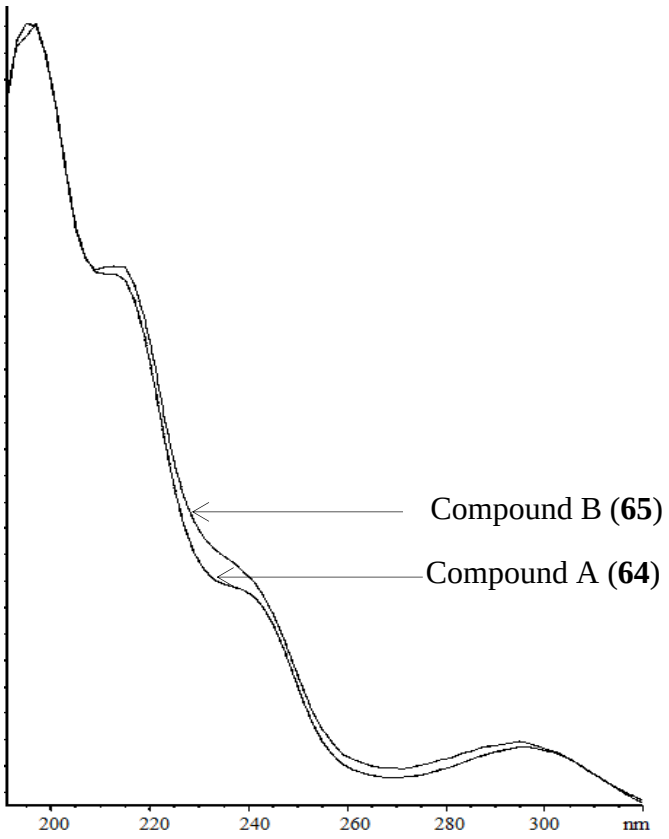

Figure 2.27: The normalised UV absorbance spectra of compound B (**65**) and compound A (**64**) obtained from HPLC.

2.2.2 Mass Spectrometry

The high resolution mass spectrum of compound B (**65**) exhibited a pseudo-molecular ion at *m/z* 636.5683 consistent with the molecular formula $C_{37}H_{49}NO_8$ (*m/z* 635.5686) and similar to that of compound A (**64**).

The tandem mass spectrum of compound B (**65**) (Figure 2.28) contained fragment ions at *m/z* 618.2, 600.2, 576.3, 564.1 and 536.2. This fragmentation pattern was the same as that observed in the MS^2 spectrum of compound A (**64**) and the MS^3 spectrum was also identical, strongly suggesting similar structural features (Table 2.6).

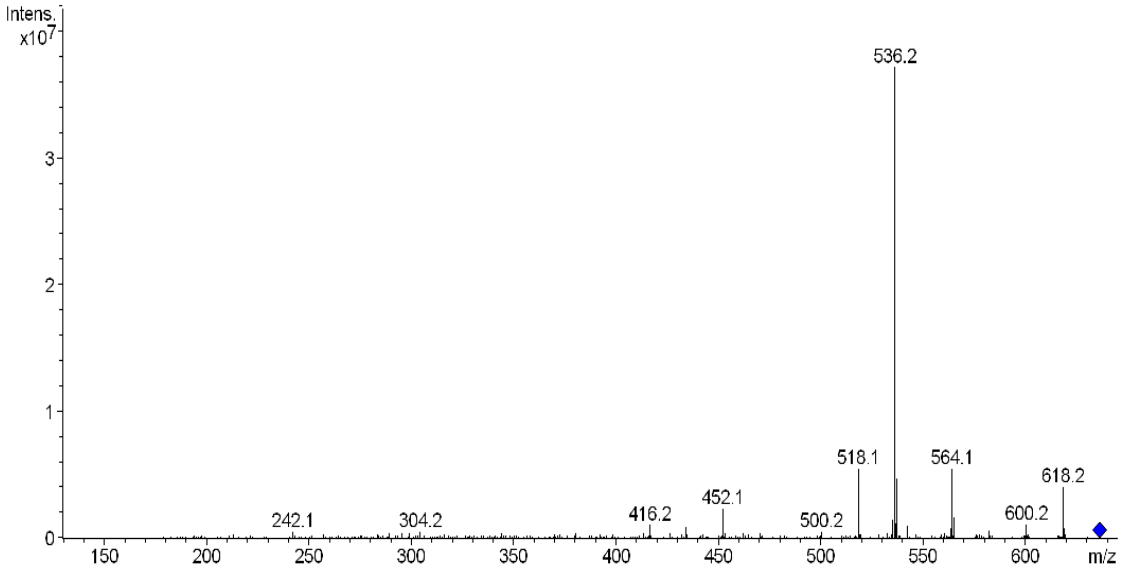

Figure 2.28: The tandem mass spectrum of compound B (**65**), *m/z* 636.7 (positive ion mode).

Table 2.6: The MS^2 and MS^3 fragments of *m/z* 636.3 of compound B (**65**).

Parent ion (*m/z*)	**Mass loss (Da)**	**Attributable fragment loss**	**MS^2 fragment ions (*m/z*)**	**MS^3 ions from the selected MS^2 ion (*m/z*)**
636.5	18	H_2O	618.2	600.4
	36	2 x H_2O	600.2	582.3
	60	C_3H_8O	576.3	558.4
	72	C_4H_8O	564.1	536.3
	100	$C_5H_8O_2$	536.2	518.3

2.2.3 NMR Spectroscopy

The ^1H NMR spectrum (Figure 2.29) of compound B (**65**) contained thirty three signals. These signals comprised of eleven singlets, seven doublets, a triplet, six doublets of doublets, three triplets of doublets, four multiplets and a triplet of

quartets. Integration of signals indicated the presence of forty nine protons in compound B (**65**).

The presence of an *ortho* disubstituted aromatic ring in compound B (**65**) was indicated by the aromatic proton signals as doublets of doublets at 6.75 and 6.97 ppm and doublets of triplets at 6.85 and 7.14 ppm in the ^{1}H NMR spectrum (Figure 2.29). The presence of proton signals between 3.00 – 5.00 ppm indicated that compound B (**65**) could contain heteroatoms such as oxygen atoms.

The ^{13}C NMR spectrum (Figure 2.30) contained twenty four carbon signals. The DEPT-135 NMR spectrum (Appendix 5) classified these carbon signals as eight methyl, five methylene, twelve methine and eleven quaternary carbons. An additional methine carbon signal at 78.8 ppm was revealed in the DEPT-135 NMR spectrum (Appendix 5) which was concealed under the solvent signal in the ^{13}C NMR spectrum (Figure 2.30). The coincidence of this methine carbon signal with that of the solvent was very similar to that of the methine signal at 76.7 ppm in compound A (**64**). In addition, the intensity of the methine resonance at 71.1 ppm was double that of most of the other protonated carbon signals, which indicates that two methine signals could be coincident, as observed in compound A (**64**).

A proton signal at 5.54 ppm was correlated to a typical alkene resonance at 5.32 ppm in the COSY NMR spectrum (Appendix 8) of compound B (**65**) indicating the presence of a prenyl moiety. From the HMBC NMR spectrum (Appendix 7), the proton signal at 5.54 ppm (which correlated to the carbon signal at 92.6 ppm in the HSQC NMR spectrum (Appendix 6)) was correlated to the carbon signals at 139.7, 74.8 and 71.1 ppm (^{3}J). Two methyl proton signals at 1.77 and 1.78 ppm, corresponding to the olefinic methyl carbons resonating at 18.6 and 25.7 ppm respectively from the HSQC NMR spectrum (Appendix 6), were correlated to the carbon signals at 139.7 (^{2}J) and 122.0 ppm (^{3}J) in the HMBC spectrum (Appendix 7). The chemical shifts of the carbon signals mentioned above matched the carbon resonances at 92.6 (C-31), 139.3 (C-34), 74.8 (C-27), 71.1 (C-10), 18.6 (C-35) and 25.7 ppm (C-36) of compound A (**64**). The similarity in chemical shifts and correlations confirmed that the prenyl moiety present in compound A (**64**) was also present in compound B (**65**).

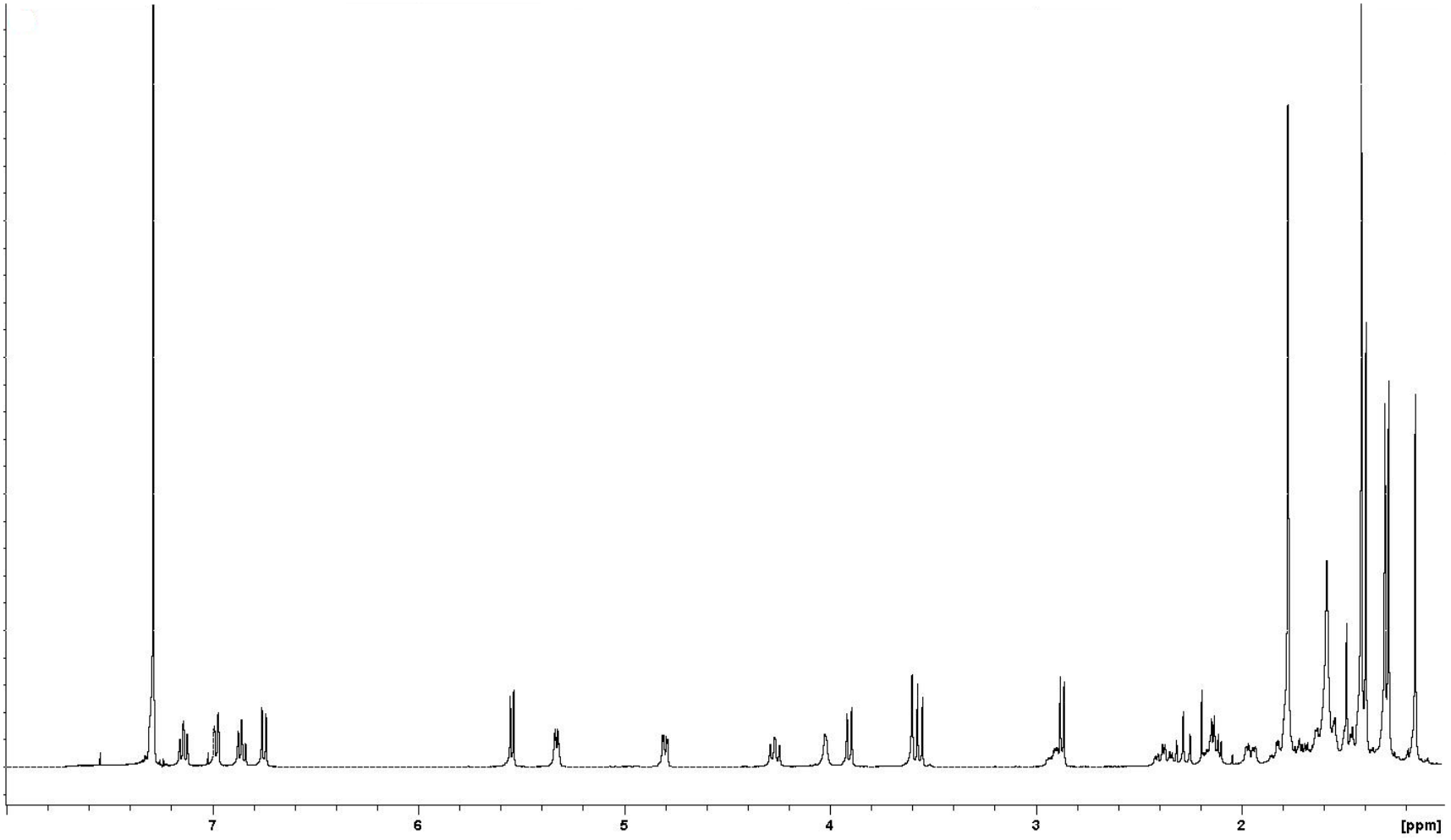

Figure 2.29: The ^{1}H NMR spectrum of compound B (**65**), ($CDCl_3$, 400 MHz).

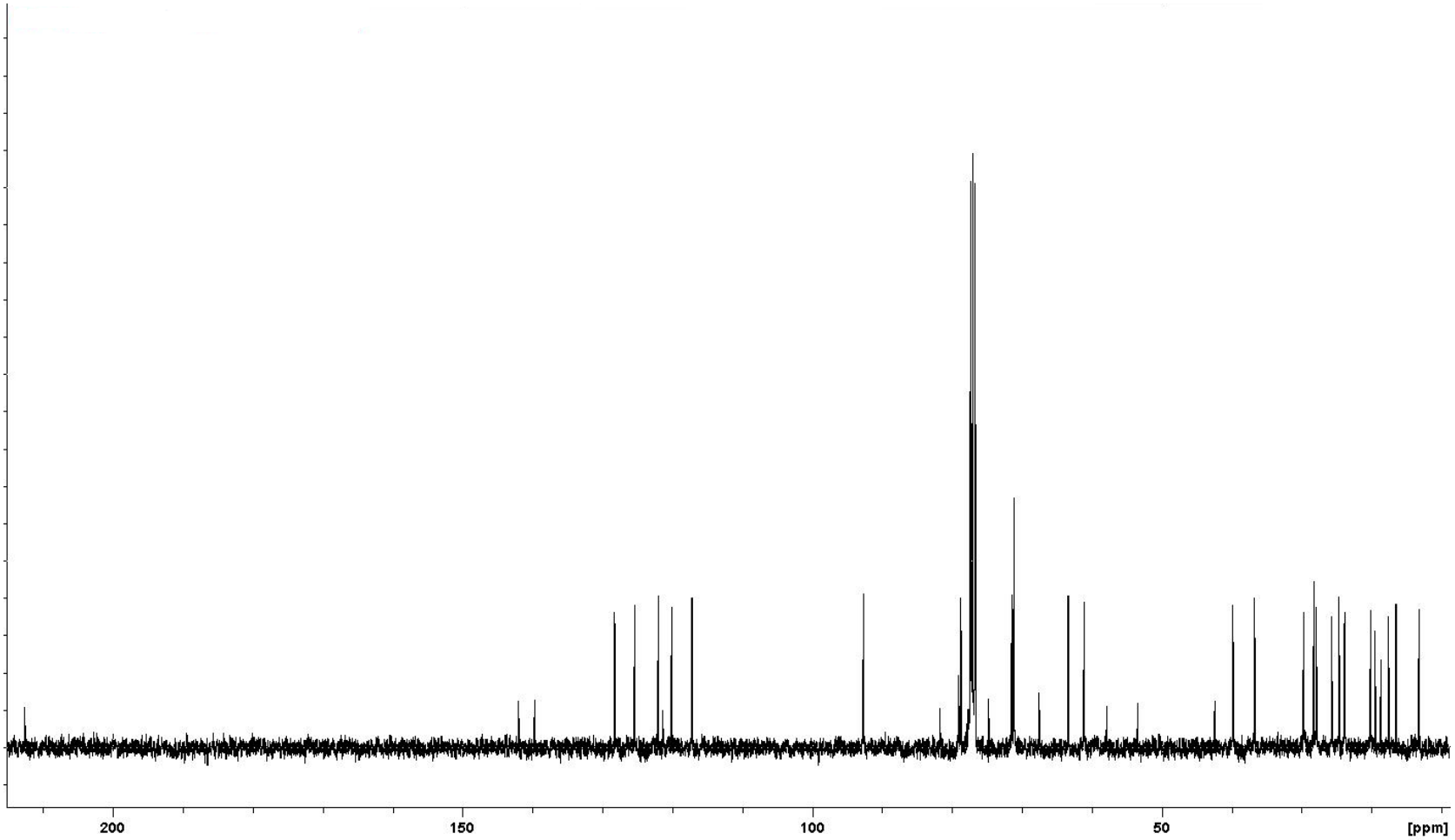

Figure 2.30: The ^{13}C NMR spectrum of compound B (**65**), ($CDCl_3$, 400 MHz).

The HSQC NMR spectrum (Appendix 6) showed that the protons which resonated at 3.56 and 3.90 ppm were correlated to the carbon signal at 71.1 ppm, consistent with two coincident methine carbons. These proton resonances coupled to each other in the COSY NMR spectrum (Appendix 8) and had similar chemical shifts to the proton signals at 3.58 ppm (H-9) and 3.94 ppm (H-10) of compound A (**64**). Therefore, the proton resonances at 3.56 and 3.90 ppm of compound B (**65**) were assigned as H-9 and H-10 respectively.

From the HMBC NMR spectrum (Appendix 7), the 3.56 ppm (H-9) proton signal was correlated to the carbon signals at 74.8 and 71.1 ppm (^2J) and 71.4, 61.1 and 16.5 ppm (^3J). The chemical shifts of these carbon resonances were consistent with the carbon signals at 74.8 (C-27), 71.1 (C-10), 71.5 (C-7), 61.2 (C-11) and 16.6 ppm (C-28) in compound A (**64**). This indicated that the hemi-acetal ring observed in compound A (**64**) could also be present in compound B (**65**). In addition, the proton signal at 3.90 ppm (H-10) was correlated to the carbon signals at 61.1 (^2J), 74.8 and 92.6 ppm (^3J). The carbon signals at 16.5 and 28.2 ppm were the two methyl carbon resonances whose associated protons were correlated to the quaternary carbon signal at 74.8 ppm, confirming the presence of the hemi-acetal ring in compound B (**65**).

The HSQC NMR spectrum (Appendix 6) indicated that the proton signal resonating at 3.59 ppm was correlated to a carbon at 61.1 ppm. This proton signal was correlated to the quaternary carbon signals at 67.5 (^2J) and 79.1 ppm (^3J) in the HMBC NMR spectrum (Appendix 7). The chemical shift of these carbon resonances matched those of the carbon signals at C-11, C-12 and C-13 of compound A (**64**). This implied that an epoxy group was present and a hydroxyl group could be attached to the carbon atom which resonated at 79.1 ppm (C-13) in compound B (**65**).

From the ^{13}C NMR spectrum (Figure 2.30), the quaternary carbon signals at 42.5, 53.4, 81.7 and 212.7 ppm were very similar to the carbon signals at C-4, C-3, C-18 and C-37 of compound A (**64**). Similarly, the methine resonance at 36.7 ppm and the methylene carbon signals at 23.9, 27.9, 29.7, 20.1 and 39.8 ppm matched those of compound A (**64**) at carbon resonances C-16, C-5, C-6, C-14, C-15 and C-17

respectively. The similarities of the carbon signals indicated that compounds A (**64**) and B (**65**) shared similar structural features.

The methyl proton signal at 1.42 ppm (H-25) was correlated to the carbon signals resonating at 42.5, 53.4, 212.7 and 36.7 ppm and the methyl proton at 1.14 ppm, assigned to H-26, was correlated to the carbon resonances at 42.5, 53.4 and 23.9 ppm in the HMBC NMR spectrum (Appendix 7). The proton signals corresponding to the carbon signals mentioned above were determined from the HSQC NMR spectrum (Appendix 6) as indicated in Figure 2.31 and Table 2.7.

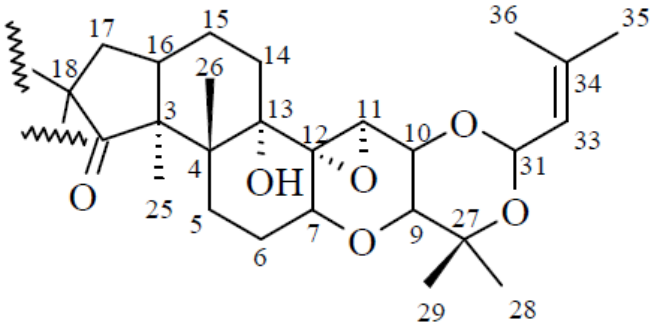

Figure 2.31: The structure of the right side of compound B (**65**).

Table 2.7: ^{13}C and ^{1}H NMR assignments for the right side of compounds B (**65**) and A (**64**), ($CDCl_3$, 400 MHz).

Atom	Compound B (65)			Compound A (64)	
	^{13}C (δ ppm)		^{1}H (δ ppm)	^{13}C (δ ppm)	^{1}H (δ ppm)
3	53.4			53.7	
4	42.5			42.1	
5	23.9	Hα	2.38	24.0	2.38
		Hβ	1.96		1.94
6	27.9	Hα	2.14	27.8	2.15
		Hβ	1.70		1.68
7	71.4		4.26	71.5	4.27
9	71.1		3.56	71.1	3.58
10	71.1		3.90	71.1	3.94
11	61.1		3.59	61.2	3.63
12	67.5			67.5	
13	79.1			79.0	
13-OH			1.50		1.53
14	29.7	Hα	1.55	29.4	1.58
		Hβ	1.46		1.42
15	20.1	Hα	1.81	20.1	1.81
		Hβ	1.62		1.63

Atom	Compound B (65)			Compound A (64)	
	^{13}C (δ ppm)		^{1}H (δ ppm)	^{13}C (δ ppm)	^{1}H (δ ppm)
16	36.7		2.91	36.8	2.75
17	39.8	Hα	2.28	40.3	2.27
		Hβ	2.10		2.12
18	81.7			81.8	
25	13.2		1.42	12.9	1.46
26	17.6		1.14	17.6	1.09
27	74.8			74.8	
28	16.5		1.28	16.6	1.31
29	28.2		1.31	28.3	1.31
31	92.6		5.54	92.6	5.56
33	122.0		5.32	122.0	5.33
34	139.7			139.3	
35	18.6		1.77	18.6	1.76
36	25.7		1.78	25.7	1.77
37	212.7			212.2	

The similar chemical shifts of the right sides of compounds A (**64**) and B (**65**) implied that the difference in the compounds could lie on the left side of the molecule. The differences in the chemical shifts were only ± 0.4 ppm for the carbon signals and ± 0.05 ppm for the proton signals, indicating that the stereochemistry of the two compounds was likely similar. However, the chemical shifts of the H-16 proton signals differed by 0.16 ppm, with H-16 slightly more downfield in compound B (**65**). Even though the chemical shifts of the C-16 carbon signals for compounds A (**64**) and B (**65**) were very similar (36.7 and 36.8 ppm respectively), the difference in the respective proton signals indicated that the orientation could be different.

The presence of an aromatic ring in compound B (**65**) was confirmed with the correlations from the proton signal at 6.97 ppm (H-20) to the signal at 7.14 ppm (H-21) and from the proton resonance at 6.85 ppm (H-22) to the proton signals at 6.75 (H-23) and 7.14 ppm (H-21) in the COSY NMR spectrum (Appendix 8). The HMBC NMR spectrum (Appendix 7), showed that the 6.97 ppm (H-20) proton signal was correlated to the carbon signals at 120.1 (C-22), 81.7 (C-18) and 142.0 ppm (C-24) (^{3}J). In addition, the 7.14 ppm (H-21) proton signal correlated to the carbon resonances at 125.4 and 120.1 ppm (^{2}J) and 121.3 ppm (C-19) (^{3}J) and

the proton signal at 6.75 ppm (H-23) correlated to the 142.0 ppm (C-24) (^2J) carbon signal.

A proton signal at 4.02 ppm, with a COSY correlation to a proton signal at 4.80 ppm was not correlated to any carbon signal in the HSQC NMR spectrum (Appendix 6) and was attributed to an NH proton. The 4.80 ppm proton signal assigned to H-2 was coupled to a proton signal at 2.87 ppm in the COSY NMR spectrum (Appendix 8) and correlated to carbon signals at 63.4 ppm (^2J) and 81.7 ppm (C-18) (^3J) in the HMBC NMR spectrum (Appendix 7), indicating that C-18 (81.7 ppm) is still a spiro carbon. The HSQC NMR spectrum (Appendix 6), showed that the proton resonance at 4.80 ppm was attached to a methine carbon, at 78.8 ppm (C-2), and the proton signal at 2.87 ppm was correlated to a methine carbon signal assigned to 63.4 ppm (C-39). The 2.87 ppm (H-39) proton signal was correlated to carbon signals at 78.8 ppm (C-2) (^2J), 57.9 ppm (^2J) and the methyl carbon resonances at 24.6 and 19.5 ppm (^3J) in the HMBC NMR spectrum (Appendix 7).

The chemical shifts of these carbon signals closely matched those of the epoxyprenyl moiety in compound A (**64**), indicating that this functional substructure was also present in compound B (**65**) as shown in Figure 2.32 and Table 2.8.

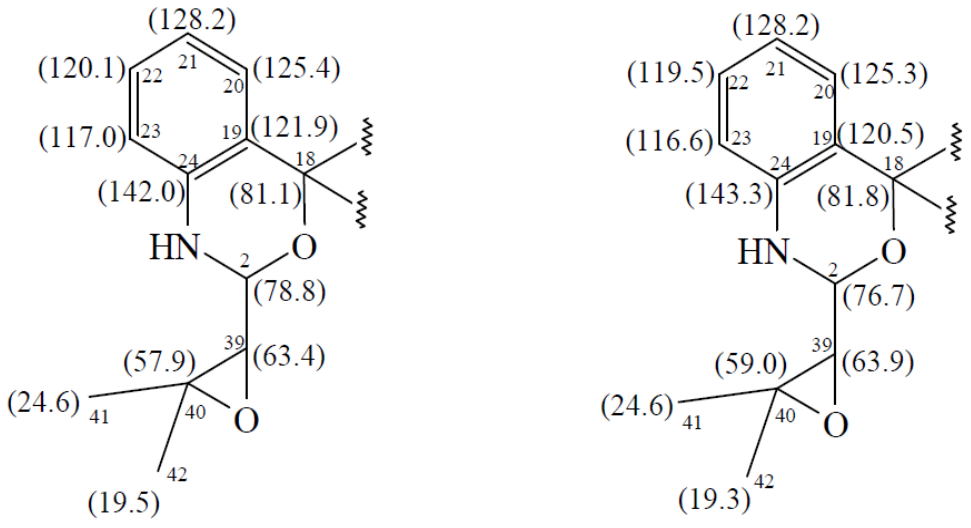

Figure 2.32: ^{13}C NMR chemical shifts (ppm) for the left side of compounds (i) B (**65**) and (ii) A (**64**), ($CDCl_3$, 400 MHz).

Table 2.8: ^{13}C and ^{1}H NMR assignments for the left side of compounds B (**65**) and A (**64**), ($CDCl_3$, 400 MHz).

	Compound B (65)		Compound A (64)	
Atom	**^{13}C (δ ppm)**	**^{1}H (δ ppm)**	**^{13}C (δ ppm)**	**^{1}H (δ ppm)**
NH		4.02		4.40
2	78.8	4.80	76.7	4.93
18	81.7		81.8	
19	121.3		120.5	
20	125.4	6.97	125.3	6.99
21	128.2	7.14	128.2	7.12
22	120.1	6.85	119.5	6.81
23	117.2	6.75	116.6	6.72
24	142.0		142.3	
39	63.4	2.87	63.9	2.86
40	57.9		59.0	
41	24.6	1.39	24.6	1.39
42	19.5	1.41	19.3	1.36

The COSY and HMBC correlations of the proton and carbon signals mentioned above are presented in Figure 2.33 and Table 2.9.

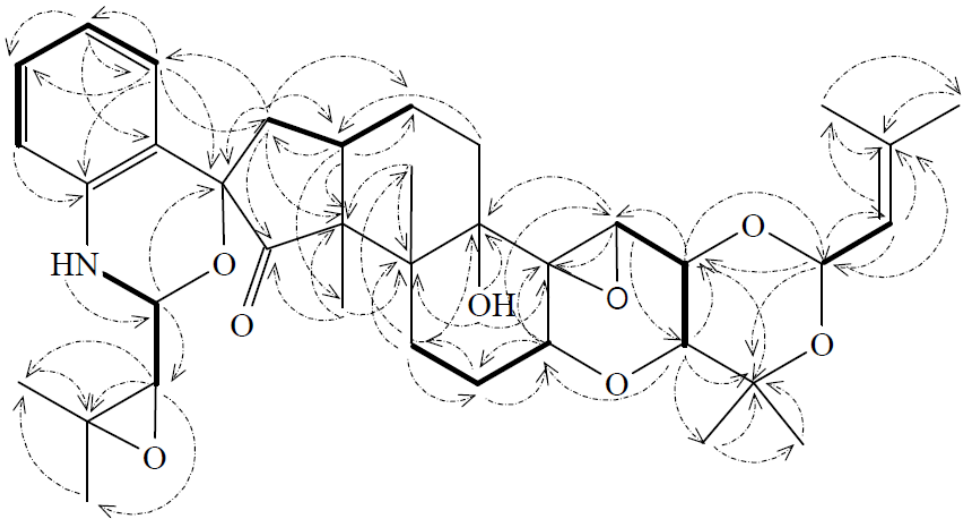

Figure 2.33: The COSY (——) and HMBC (-----) correlations of protons in compound B (**65**), ($CDCl_3$, 400 MHz).

Table 2.9: COSY and ^{1}H - ^{13}C HMBC correlations observed for compound B (**65**), ($CDCl_3$, 400 MHz).

Atom	**^{13}C (δ ppm)**	**^{1}H (δ ppm)**	**COSY correlation**	**HMBC correlation**
NH		4.02	H-2	
2	78.8	4.80	NH, H-39	C-18, C-39
5	23.9 Hα Hβ	2.38 1.96	H-6β	C-4, C-6, C-13, C-26
6	27.9 Hα	2.14	H-6β	C-7, C-5
7	71.4	4.26	H-6α, H-6β	C-6, C-11, C-12
9	71.1	3.56	H-10	C-7, C-10, C-27, C-8
10	71.1	3.90	H-9	C-27, C-31
11	61.1	3.59	H-10	C-9, C-12, C-13
13-OH		1.49		C-4, C-12, C-13
14	29.7 Hα	1.55		C-16
16	36.7	2.91	H-17β, H-15α, H-15β	C-3, C-15, C-17, C-25
17	39.8 Hα Hβ	2.28 2.10	H-17β	C-3, C-15, C-16, C-20 C-3, C-18, C-37
20	125.4	6.97	H-27, H-29	C-18, C-21, C-22
21	128.2	7.14	H-26, H-28	C-20, C-22, C-19
22	120.1	6.85	H-29	C-21
23	117.2	6.75	H-28	C-24
25	13.2	1.42		C-3, C-4, C-37, C-16
26	17.6	1.15		C-3, C-4, C-5
28	16.5	1.28		C-9, C-27, C-29
29	28.2	1.31		C-9, C-27, C-28
31	92.6	5.54	H-33	C-27, C-10, C-33, C-34
33	122.0	5.32	H-31	C-31, C-34, C-35
35	18.6	1.77		C-34, C-33, C-36
36	25.7	1.78		C-33, C-35
39	63.4	2.87	H-2	C-40, C-41
41	24.6	1.39		C-39, C-40, C-42
42	19.5	1.41		C-39, C-40, C-41

From the NMR data, the differences in chemical shifts between the two compounds were observed for the NH, H-2 and H-42 proton signals and for the C-2, C-19, C-22, C-23 and C-40 carbon resonances. The deviation in the chemical shifts indicated that the orientation of atoms could be different and that the study of the spatial orientation could determine the differences in structure.

The relative stereochemistry of the protons of compound B (**65**) was determined with NOE experiments. The enhancements of selected proton signals on the right side of the molecule matched those of compound A (**64**), indicating that the stereochemistry on the right side of compounds A (**64**) and B (**65**) is the same, consistent with the similar chemical shifts.

In the modified indole region, the irradiation of the proton signal at 4.80 ppm (H-2) caused enhancement of the proton signals at 4.02 (NH), 2.87 (H-39), 1.15 (H-26) and 1.39 ppm (H-42) and irradiation of the H-20 signal enhanced the proton signals at 2.28 (H-17α), 7.14 (H-21), 6.85 (H-22) and 1.42 ppm (H-25). These enhancements were observed for H-2 and H-20 protons of compounds A (**64**), suggesting conserved stereochemistry at C-2 in compound B (**65**). The irradiation of the 6.75 ppm (H-23) signal enhanced the 4.02 (NH), 7.14 (H-21) and 6.85 ppm (H-22) proton signals and irradiation of the 2.87 ppm (H-39) signal enhanced the 4.80 (H-2) and 1.41 ppm (H-42) proton signals (Figure 2.34 and Table 2.10). In contrast to compound A (**64**), the NH signal was not enhanced when the H-39 proton was irradiated, indicating that the orientation of H-39 could be different. In addition to that, irradiation of the 4.02 ppm (NH) proton signal of compound B (**65**) in a SELNOESY experiment did not enhance any protons, suggesting different spatial orientation to that in compound A (**64**).

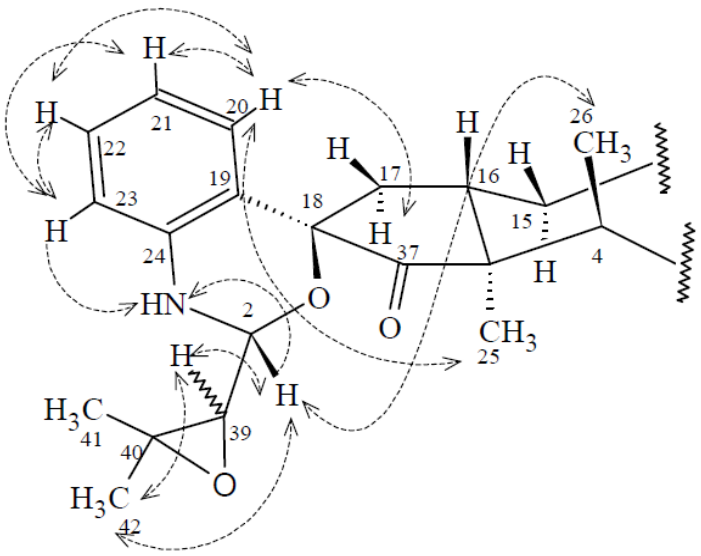

Figure 2.34: NOE of selected proton signals of the substructure at the left side of compound B (**65**).

Table 2.10: Selected NOE enhancements observed for compound B (**65**), ($CDCl_3$, 400 MHz).

^{1}H NMR (δ, ppm)	**NOE correlations (δ, ppm)**
4.02 (NH)	
4.80 (H-2)	NH, H-26, H-39, H-42
6.97 (H-20)	H-17α, H-25, H-22
6.75 (H-23)	NH, H-22
2.87 (H-39)	H-2, H-42
1.41 (H-42)	H-2, H-39

A NOESY experiment was then run and the signal at 4.02 ppm (NH) correlated to proton signals at 6.75 (H-23), 4.80 (H-2) and 2.87 ppm (H-39), similar to those in compound A (**64**). The differences between the SELNOESY and NOESY experiments for compounds A (**64**) and B (**65**) did not confirm the orientation of the H-39 proton.

Comparison of the coupling constants of selected protons including NH, H-2 and H-39 also did not provide significant evidence to differentiate the stereochemistry. The H-2 proton-proton couplings of compound B (**65**) (7.0, 2.5 Hz) and A (**64**) (6.7, 2.4 Hz) were similar and indicated that H-2 of compound B (**65**) adopted the same β-orientation in compound A (**64**). Therefore the stereochemistry of the group at C-39 of compounds A (**64**) and B (**65**) is undefined. The orientation of this group could account for the deviation in the chemical shifts observed for compounds A (**64**) and B (**65**).

The slight differences in chemical shifts of proton signals assigned to NH, H-2 and H-42 and the carbon signals assigned to C-2, C-19, C-22, C-23 and C-40, could indicate that compound B (**65**) is an isomer of compound A (**64**). Computational chemistry and modelling studies are therefore required to determine the actual stereochemistry at C-39 and to confirm the stereochemistry at C-2. Both C-2 and C-39 are chiral centres, therefore the potential stereochemistries (absolute configurations *R* and *S*) at these carbons (Figure 2.35) were studied with Advanced Chemistry Development (ACD) Labs via ChemSketch (Freeware).[129]

The first two stereoisomers of compounds A (**64**) and compound B (**65**) (i and ii) posses the (*R*) configuration at C-2, indicating that H-2 and H-26 are on the same face of the molecule (Figure 2.35). At this position, the H-2 and H-26 protons are close enough to each other to account for the NOE correlations observed between them.

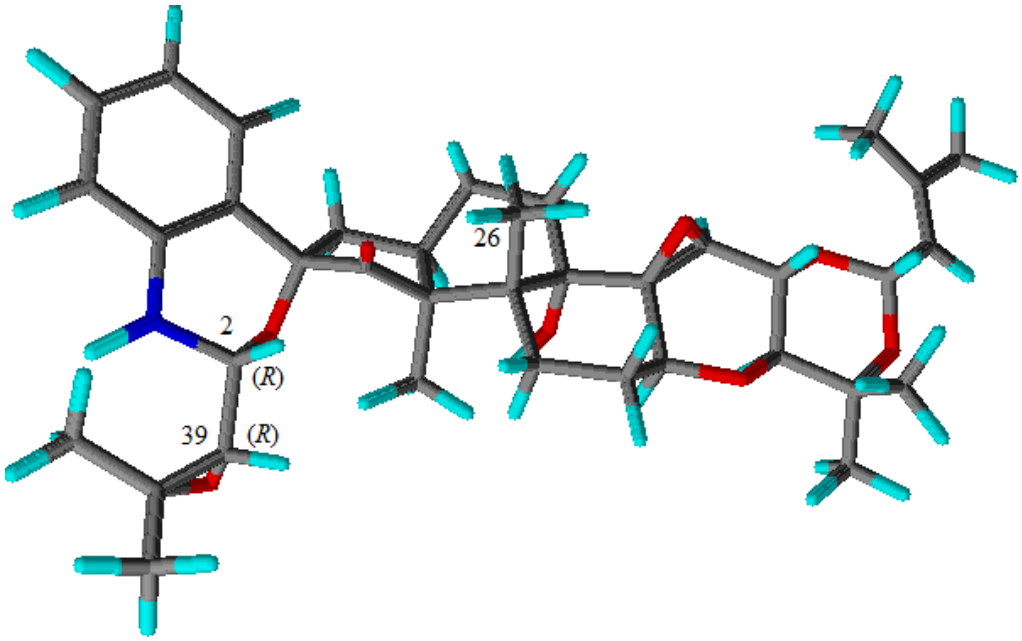

(i)

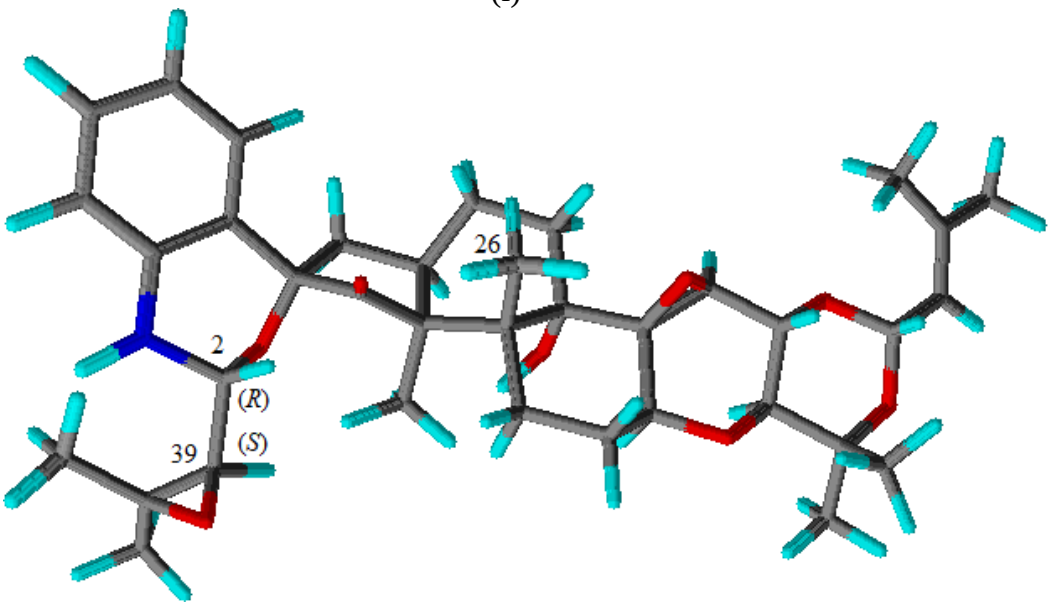

(ii)

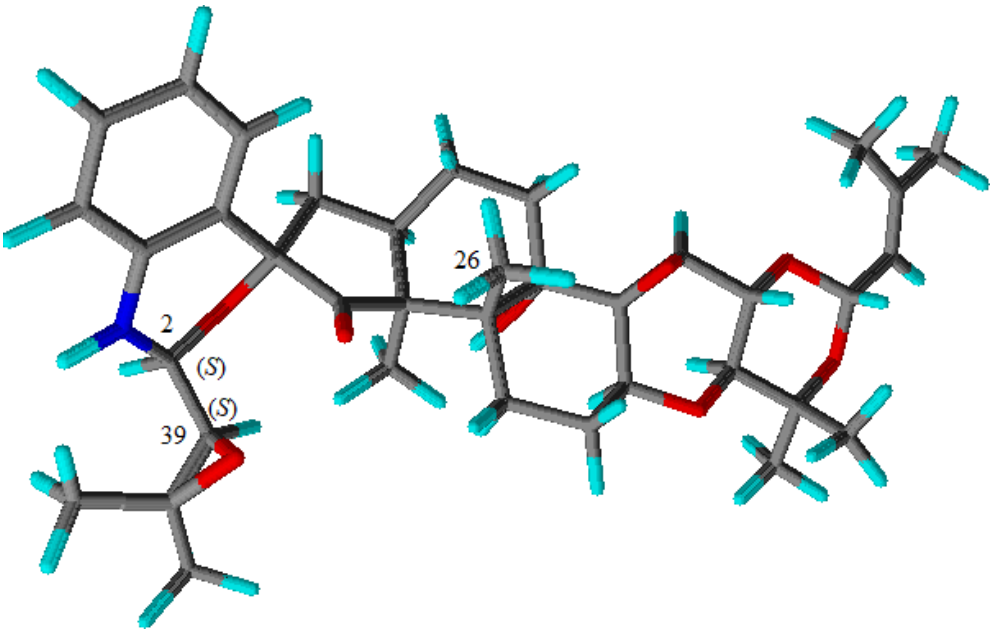

(iii)

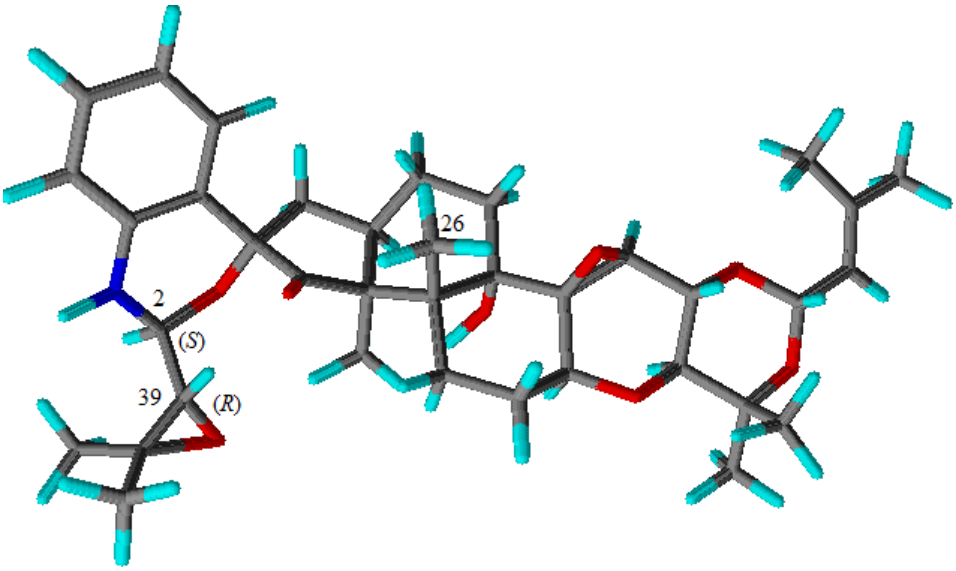

(iv)

Figure 2.35: The possible stereoisomers of compounds A (**64**) and B (**65**) at C-2 and C-39.[129]

However, when C-2 possesses the (*S*) configuration (stereoisomers iii and iv), the H-2 and H-26 protons are on opposite faces of the molecule, thus it is impossible for these protons to have any NOE correlation. Therefore this limits the possible structures for compounds A (**64**) and B (**65**) to the first two stereoisomers (i and ii). For stereoisomer (i), the H-2 proton is on the same face of the molecule as the H-39

proton and on the same face of the molecule as the epoxy group at C-39 for stereoisomer (ii) (Figure 2.36).

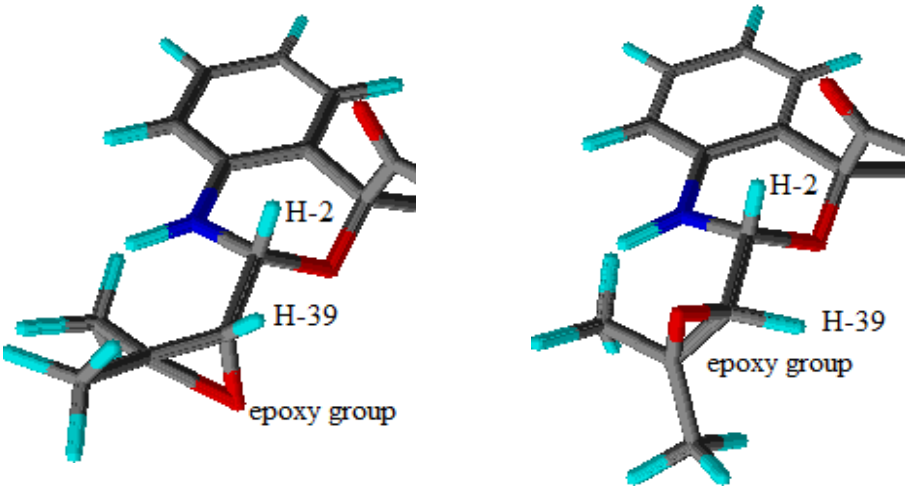

(i) (ii)

Figure 2.36: The orientations of the H-2 and H-39 protons and the epoxy group for the possible stereoisomers for compounds A (**64**) and B (**65**).

The chemical shifts of the NH and H-2 protons in compound B (**65**) are more upfield than those of the same protons in compound A (**64**) whilst that of C-2 in compound B (**65**) is more downfield than the chemical shift of C-2 in compound A (**64**) (Table 2.8). Unfortunately, there are no suitable model compounds available for this system, making it difficult to draw any firm conclusions from this data. Therefore future work is required to confirm the proposed structures.

The stereochemistry of compound A (**64**) and compound B (**65**) could also be confirmed by X-crystallography, however, neither has crystallised to date. The optical rotation could also provide some clues that could differentiate between the two compounds, but this has not been measured due to the same reason given for compound A (**64**). Hence, the complete proposed structure of compound B (**65**) and the NMR assignments are summarised in Figure 2.37 and Table 2.11.

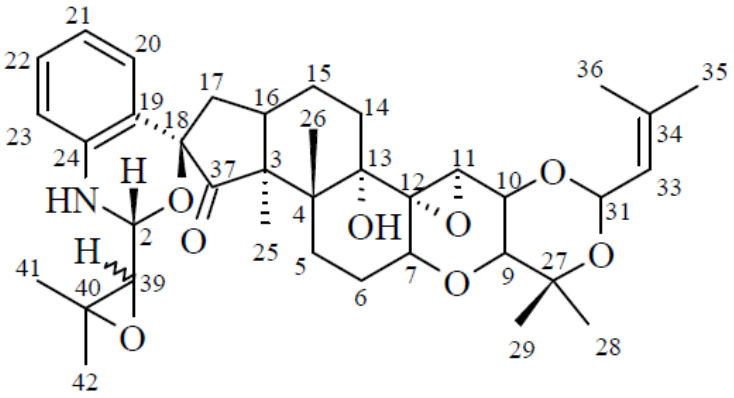

Figure 2.37: The proposed structure of compound B (**65**).

Table 2.11: ^{13}C and ^{1}H NMR chemical shift assignments for compound B (**65**), ($CDCl_3$, 400 MHz).

Atom	^{13}C (δ ppm)		^{1}H (δ ppm)	Multiplicity (*J* Hz)
NH			4.02	d (2.5)
2	78.8		4.80	dd (7.0, 2.5)
3	53.4			
4	42.5			
5	23.9	Hα	2.38	td (13.9, 5.1)
		Hβ	1.96	dd (13.5, 4.2)
6	27.9	Hα	2.14	d (5.6)
		Hβ	1.70	m
7	71.4		4.26	t (18.1, 9.2)
9	71.1		3.56	d (9.5)
10	71.1		3.90	d (9.5)
11	61.1		3.59	s
12	67.5			
13	79.1			
13-OH			1.49	s
14	29.7	Hα	1.55	s
		Hβ	1.48	m
15	20.1	Hα	1.81	dd (12.5, 2.9)
		Hβ	1.62	m
16	36.7		2.91	qt (12.9, 2.0)
17	39.8	Hα	2.28	t (26.3, 13.3)
		Hβ	2.10	d (5.6)
18	81.7			
19	121.3			
20	125.4		6.97	dd (7.9, 1.2)
21	128.2		7.14	dt (7.5, 1.4)
22	120.1		6.85	t (7.5, 1.5)
23	117.2		6.75	dd (8.2, 1.1)

Atom	^{13}C (δ ppm)	^{1}H (δ ppm)	Multiplicity (*J* Hz)
24	142.0		
25	13.2	1.42	s
26	17.6	1.15	s
27	74.8		
28	16.5	1.28	s
29	28.2	1.31	s
31	92.6	5.54	d (6.7)
33	122.0	5.32	m
34	139.7		
35	18.6	1.77	s
36	25.7	1.78	s
37	212.7		
39	63.4	2.87	d (7.0)
40	57.9		
41	24.6	1.39	s
42	19.5	1.41	s

2.3 Identification and structural elucidation of compound C (66).

Compound C (**66**) was isolated from a further aliquot of the crude extract via similar processes to those applied to the isolation of novel compounds A (**64**) and B (**65**).

2.3.1 UV Spectroscopy

The UV spectrum of compound C (**66**) was very similar to that of compound A (**64**), indicating that the UV chromophores are similar (Figure 2.38).

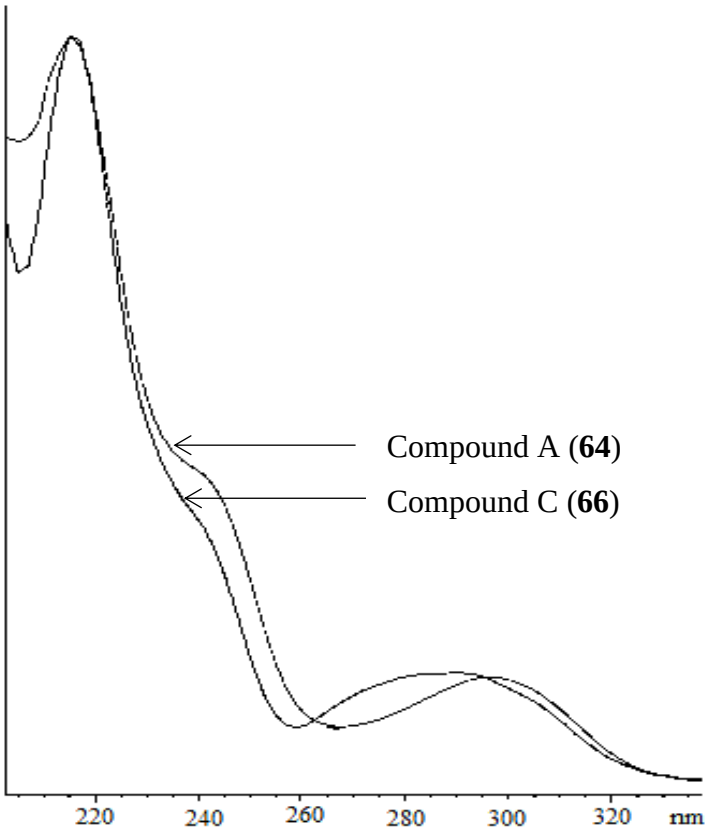

Figure 2.38: The normalised UV absorbance spectra of compounds A (**64**) and C (**66**) obtained from HPLC.

2.3.2 Mass Spectrometry

The molecular mass of compound C (**66**) was confirmed by high resolution mass spectrometry. The spectrum exhibited a pseudo-molecular ion of *m/z* 594.3686

(positive ion mode), which was consistent with a molecular formula of $C_{35}H_{47}NO_7$ (*m/z* 593.3658).

The tandem mass spectrum of compound C (**66**) in positive ion mode produced major fragment ions at *m/z* 576.2, 558.4, 536.3 and 494.2 (Figure 2.39).

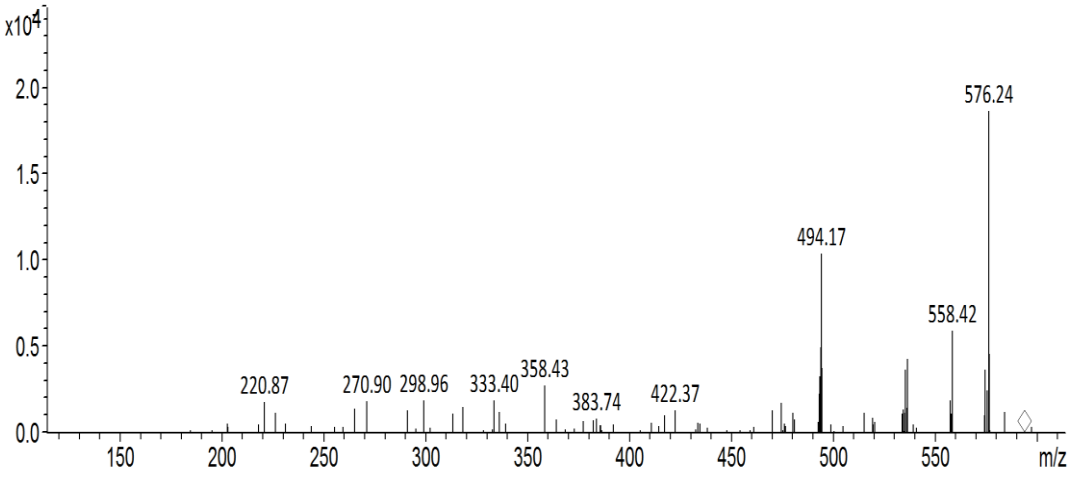

Figure 2.39: The tandem mass spectrum of compound C (**66**), *m/z* 594.3 (positive ion mode).

These fragment ions were attributable to the loss of oxygen in the form of a water molecule (18 Da), then loss of two further water molecules (36 Da), [C_3H_6O] (88 Da) and $C_5H_8O_2$ (100 Da) respectively (Table 2.12). The loss of water molecules and the $C_5H_8O_2$ group suggested that compound C (**66**) contained at least four oxygen atoms. The common fragment ions of indole diterpenoids at *m/z* 182 and 130 were not evident, indicating that compound C (**66**) likely contained the same modified indole region as for compounds A (**64**) and B (**65**).

Table 2.12: The MS^2 fragment ions of *m/z* 594.1 of compound C (**66**), (positive ion mode).

Parent ion (*m/z*)	**Mass loss (Da)**	**Attributable fragment loss**	**MS^2 fragment ions (*m/z*)**
594.1	18	H_2O	576.4
	36	2 x H_2O	558.4
	88	C_3H_6O	536.3
	100	$C_5H_8O_2$	494.2

2.3.3 NMR Spectroscopy

Compound C (**66**) was structurally characterised by NMR spectroscopy with full analysis of the 1D and 2D NMR experiments including ^{1}H, ^{13}C, DEPT-135, COSY, HSQC, NOE and HMBC experiments.

The ^{1}H NMR spectrum of compound C (**66**) (Figure 2.40) contained twenty eight proton signals consisting of nine singlets, five doublets, three triplets, two doublets of doublets, three doublets of triplets, a triplet of doublets, a triplet of quartets and four multiplets.

The presence of two doublets at 6.72 and 6.99 ppm and two doublets of triplets at 6.84 and 7.11 ppm in the ^{1}H NMR spectrum of compound C (**66**) (Figure 2.40) indicated that the *ortho* disubstituted benzene ring found in compounds A (**64**) and B (**65**) was also present in compound C (**66**). This was consistent with the similar UV absorptions of compounds A (**64**) and C (**66**) (Figure 2.38), implying that the same chromophore is present.

Proton signals at 5.56 and 5.33 ppm were identical to the proton signals of H-31 and H-33 of compound A (**64**), indicating that the prenyl moiety in compound A (**64**) was also present in compound C (**66**). Similarly, the presence of proton signals at chemical shifts 3.00 – 5.00 ppm implied that oxygenated atoms were also present in compound C (**66**).

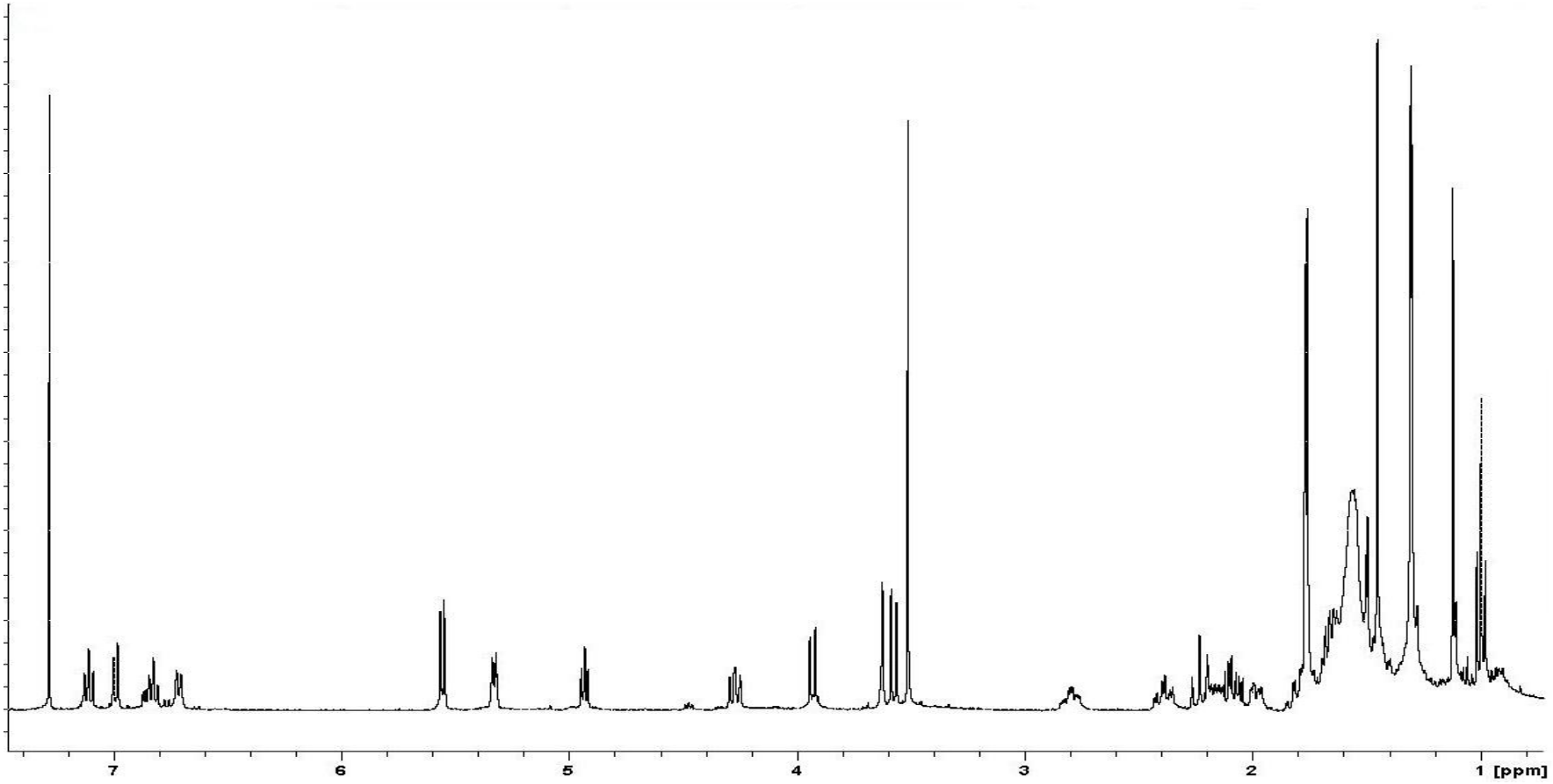

Figure 2.40: The ^{1}H NMR spectrum of compound C (**66**), ($CDCl_3$, 400 MHz).

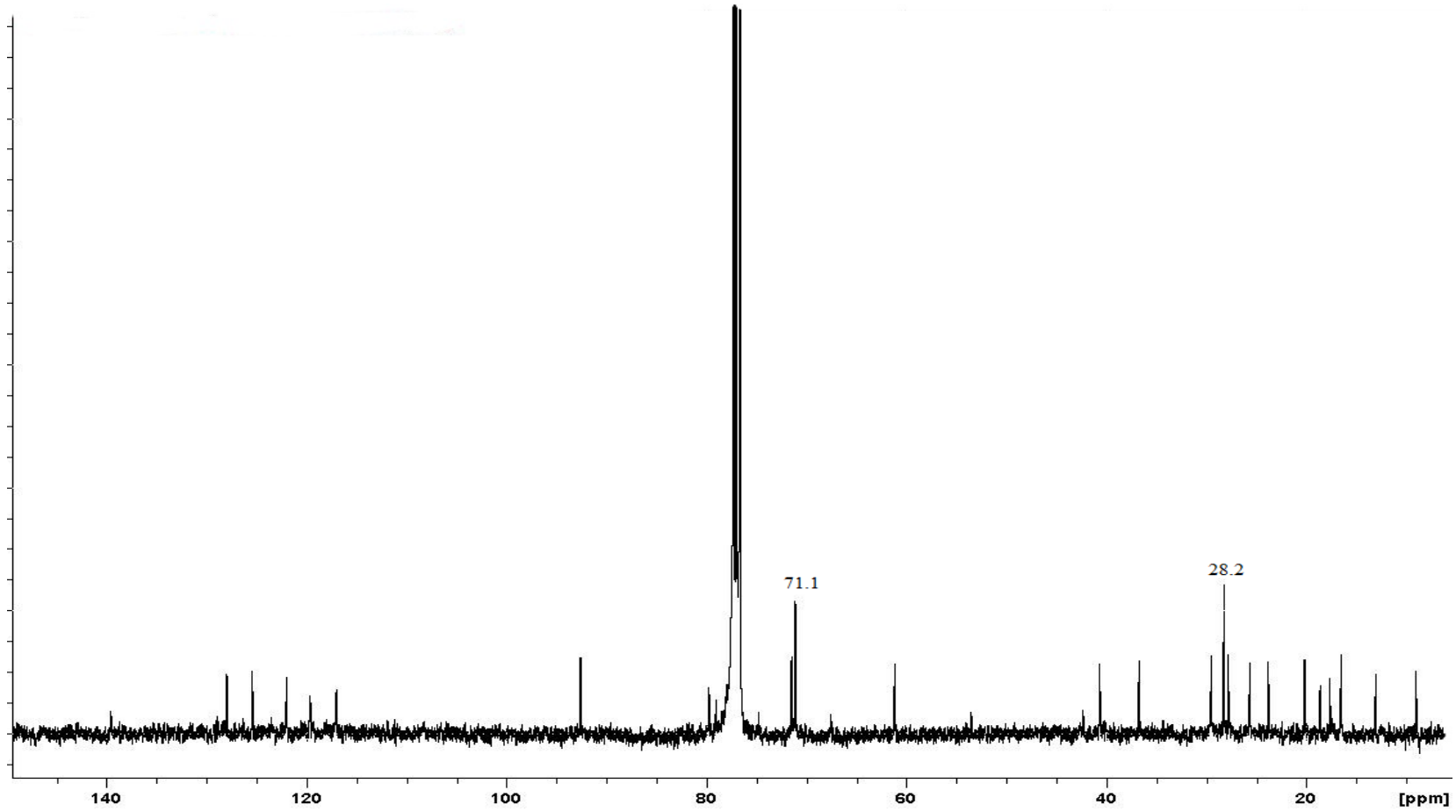

Figure 2.41: The ^{13}C NMR spectrum of compound C (**66**), ($CDCl_3$, 400 MHz).

Twenty nine carbon signals were observed in the ^{13}C NMR spectrum of compound C (**66**) (Figure 2.41), compared to the thirty five carbons suggested by the molecular formula. The DEPT-135 NMR spectrum (Appendix 9) indicated that the carbon signals comprised of seven methyl, five methylene, eleven methine and six quaternary carbons. The remaining six carbon signals, not visible in the ^{13}C NMR spectrum (Figure 2.41) were assigned based on HMBC correlations as detailed in the following discussion.

There were seven methyl carbon signals observed in the ^{13}C NMR spectrum of compound C (**66**) (Figure 2.41), one less than the eight methyl carbon signals reported for compounds A (**64**) and B (**65**). From the HSQC NMR spectrum (Appendix 10), a triplet proton signal at 1.00 ppm was observed to correlate to an upfield methyl carbon signal at 9.0 ppm. The multiplicity of the proton signal was that of a typical terminal methyl carbon bonded to a methylene carbon, which was not observed in compounds A (**64**) or B (**65**).

The carbon signals at 92.6, 122.0 and 139.6 ppm in the ^{13}C NMR spectrum (Figure 2.41) matched the carbon resonances of C-31, C-33 and C-34 in compounds A (**64**) and B (**65**), typical carbon resonances of the prenyl moiety on the right side of the molecule. The HMBC NMR spectrum (Appendix 12) indicated that the proton which resonated at 5.56 ppm (attached to the carbon resonating at 92.6 ppm) was correlated to carbon signals at 71.1 (^3J) and 74.1 ppm (^3J). A proton signal at 1.76 ppm which was correlated to a carbon signal at 18.6 ppm in the HSQC NMR spectrum (Appendix 10), was correlated to the carbon signals at 139.6 (^2J), 122.0 (^3J) and 25.7 ppm (^3J) in the HMBC NMR spectrum (Appendix 12). Similar correlations were observed for compounds A (**64**) and B (**65**), confirming that the prenyl moiety was at the right side of compound C (**66**). The carbons signals in compound C (**66**) were assigned as 92.6 (C-31), 122.0 (C-33), 139.6 (C-34), 18.6 (C-34) and 25.7 ppm (C-36).

The proton signals at 3.57 and 3.94 ppm correlated to the methine carbon signal at 71.1 ppm in the HSQC NMR spectrum (Appendix 10) are equivalent to the H-9, H-10, C-9 and C-10 signals of compound A (**64**) respectively. The intensity of carbon signals at 71.1 ppm and 28.2 ppm were similar, double the intensity of most

of the other carbon signals. This indicated that the carbon signal at 28.2 ppm represented two overlapping carbon environments.

In the DEPT-135 spectrum (Figure 2.42), the 28.2 ppm signal was differentiated as two separate signals with both a positive and a negative peak, implying that one of the coincident carbons at 28.2 ppm could be a methyl carbon while the other one could be a methylene carbon. The HSQC NMR spectrum (Appendix 10) indicated that proton signals at 1.31 ppm and 1.67 ppm correlated to the carbon signal at 28.2 ppm. The 1.31 ppm proton signal overlapped with the proton signal at 1.30 ppm and together integrated as six protons. The proton signal at 1.30 ppm was correlated to a methyl carbon signal at 16.5 ppm, hence the 1.31 ppm proton signal was correlated to 28.2 ppm in the HSQC NMR spectrum (Appendix 10).

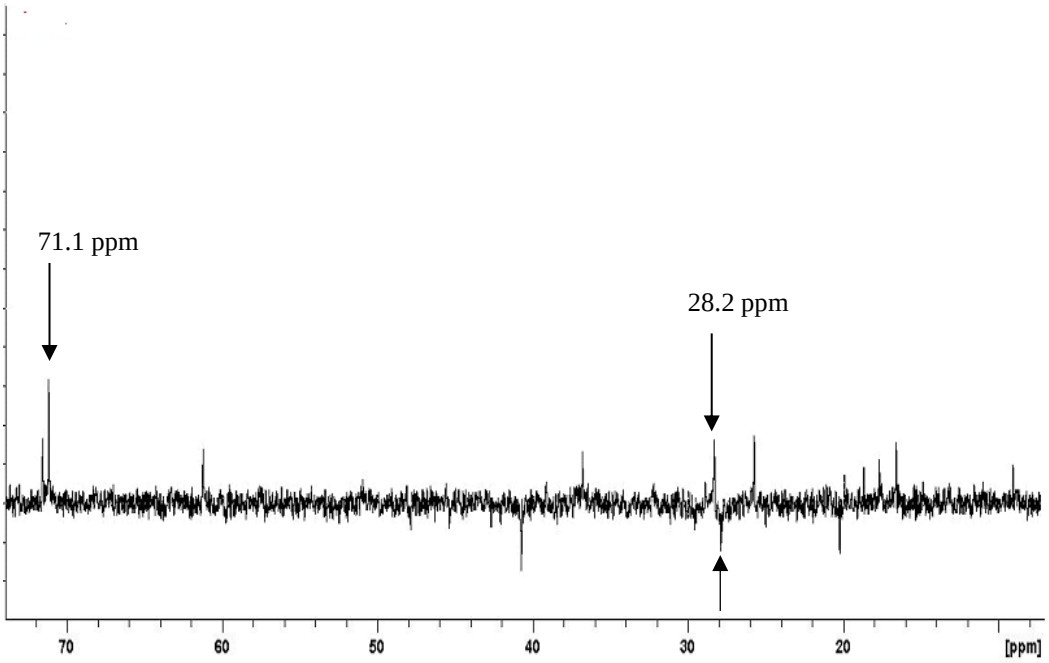

Figure 2.42: A selected region (08.0 – 74.0 ppm) of the DEPT-135 NMR spectrum of compound C (**66**) showing the carbon signals at 71.1 and 28.2 ppm, ($CDCl_3$, 400 MHz).

This proton signal (1.31 ppm) was correlated to the carbon resonances at 71.1 (C-9) (^3J), 16.5 (^3J) and 74.8 ppm (^2J) in the HMBC NMR spectrum (Appendix 12). Hence, one of the 28.2 ppm carbon signals was assigned to one of the two methyl groups attached to the carbon which resonated at 74.8 ppm. These carbon signals

were assigned to 74.8 (C-27), 16.5 (C-28) and 28.2 ppm (C-29) in compound C (**66**), consistent with the hemi-acetal ring in compound A (**64**).

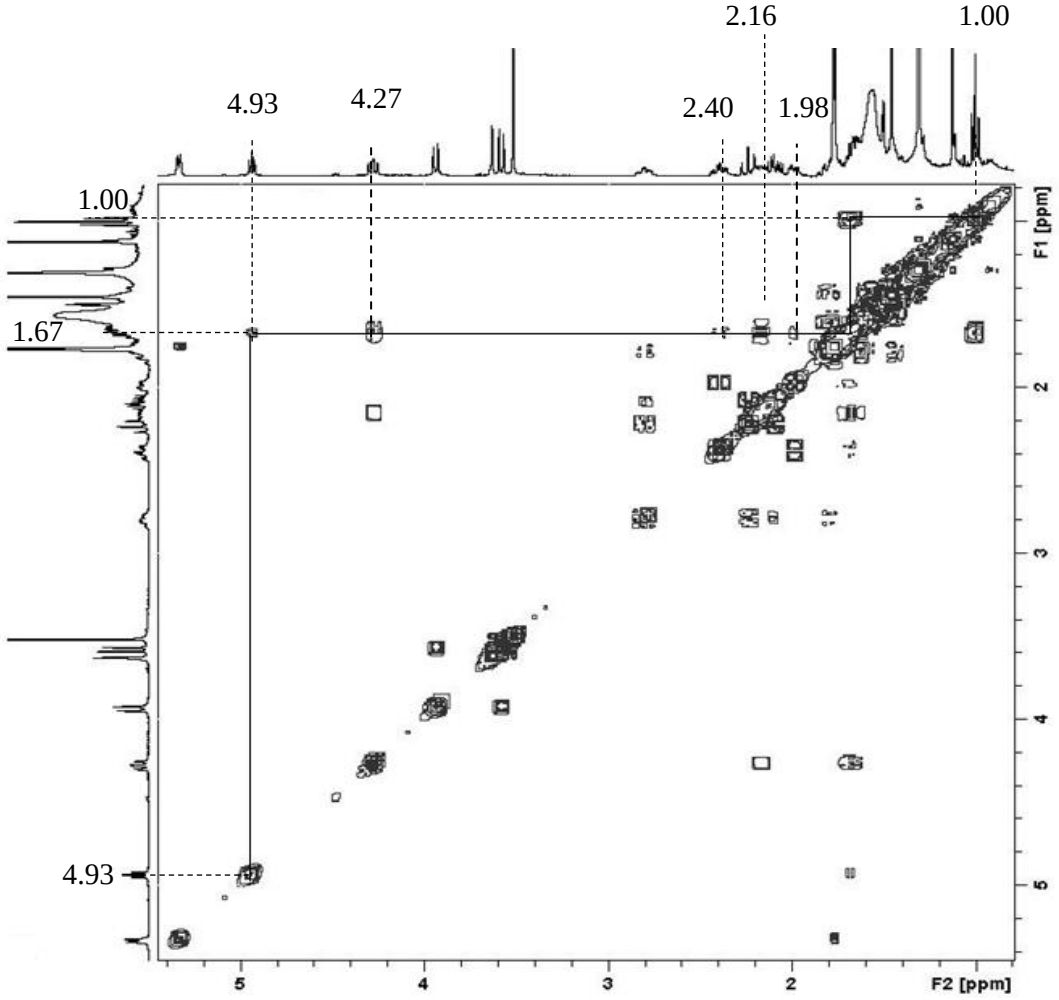

Figure 2.43: Selected region (5.40 – 8.00 ppm) of the COSY spectrum of compound C (**66**) with correlations of the proton signal at 1.67 ppm indicated.

From the COSY NMR spectrum (Figure 2.43), the proton signal at 1.67 ppm was correlated to two different sets of proton signals, thus there could be two coincident proton signals at 1.67 ppm. The first correlation was to the proton signals at 4.93 and 1.00 ppm, which were correlated to carbon signals at 79.7 and 9.00 ppm respectively in the HSQC NMR spectrum (Appendix 10). The other correlation was to the proton signals at 4.27, 2.40, 1.98 and 2.16 ppm. The proton at 4.27 ppm was correlated to a carbon signal at 71.5 ppm, the 2.40 and 1.98 ppm proton signals were correlated to a methylene carbon at 23.8 ppm and the 2.16 ppm proton signal

was one of the methylene protons correlated to the carbon signal at 27.8 ppm. Therefore, the other proton correlated to the carbon which resonated at 27.8 ppm was assigned to the proton signal at 1.67 ppm. In the HMBC NMR spectrum (Appendix 12), the proton signal at 2.40 ppm was correlated to the carbon signal at 42.3 ppm (^2J) while the proton at 1.98 ppm correlated to a carbon signal at 79.1 ppm (^3J). The chemical shifts of these carbon signals matched the C-4 and C-13 resonances of compound A (**64**), hence NMR signals in compound C (**66**) were assigned as 42.3 (C-4), 23.8 (C-5), 23.8 (C-6), 71.5 (C-7), 79.1 (C-13), 2.40 (H-5α), 1.98 (H-5β), 2.16 (H-6α), 1.67 (H-6β) and 4.27 ppm (OH-13).

A proton signal at 3.62 ppm which was correlated to a carbon signal at 61.2 ppm in the HSQC NMR spectrum, was also correlated to carbon signals at 71.5 (C-7) (^3J), 67.6 (^2J) and 71.1 ppm (C-10) (^2J) in the HMBC spectrum (Appendix 12). The chemical shifts of the carbon signals at 61.2 and 67.6 ppm matched C-11 and C-12 of compound A (**64**), confirming that an epoxy group at C-11 and C-12 was also present in compound C (**66**). The proton signal at 2.09 ppm, assigned as H-17β was correlated to C-3 (^2J) and to the carbon signals at 53.7 (^3J) and 212.8 ppm (^3J). The carbon resonances at 53.7 and 212.8 ppm matched those of C-3 and C-37 of compound A (**64**), implying that the right side of compound C (**66**) was very similar to that of compound A (**64**).

On the left side of compound C (**66**), the aromatic proton at 6.99 ppm (H-20) was correlated to proton signals at 7.11 ppm (H-21) and 6.84 ppm (H-22) in the COSY spectrum (Appendix 11) and correlated to carbon signals at 127.9 (C-21) (^2J), 81.1 (C-18) (^3J) and 143.1 ppm (C-24) in the HMBC NMR spectrum (Appendix 12). The 6.84 ppm (H-22) proton signal displayed COSY correlations to proton signals 7.11 (H-21) and 6.72 ppm (H-22) and correlated to carbon signals at 117.0 ppm (C-23) (^2J) and 121.9 ppm (C-19) (^4J) in the HMBC NMR spectrum (Appendix 12). The correlations and the chemical shifts of protons and carbons on this aromatic ring were very similar to those observed for compound A (**64**), hence there was no modification in the benzene ring of compound C (**66**).

A proton signal at 4.93 ppm assigned as H-2, had a COSY correlation to a proton signal at 1.67 ppm. This proton (1.67 ppm) represented the methylene proton

attached to the other carbon signal at 28.2 ppm, which was assigned as C-39. The HMBC NMR spectrum (Appendix 12) indicated that the 4.93 ppm (H-2) proton signal was correlated to the quaternary carbon signal at 81.1 ppm (C-18) (^3J) and a methyl carbon at 9.00 ppm, which had been assigned as C-40. The multiplicity of the proton signal at 1.00 ppm (triplet) indicated that the neighbouring carbon was a methylene, consistent with C-39.

The assignment of carbons at 28.2 (C-39) and 9.00 ppm (C-40) indicated that an ethyl group was attached to C-2 of compound C (**66**) rather than a prenyl epoxy group as in compounds A (**64**) and B (**65**). This difference in C-2 substituents would account for the mass difference of 42 Da, consistent with the difference in the molecular masses of compound A (**64**) (Mr = 635.3458) and compound C (**66**) (Mr = 593.3658).

The ^{1}H NMR spectrum of compound C (**66**) (Figure 2.40) did not display any signal attributable to the NH proton that was expected to be around 4.00 ppm as in compound A (**64**). Furthermore, no correlations were observed in the HMBC NMR spectrum (Appendix 12) from any proton that could be the NH proton to the surrounding carbons such as 79.7 (C-2) and 28.1 ppm (C-39). However, the chemical shifts of carbons at 143.1 ppm (C-24) and 79.7 ppm (C-2) of compound C (**66**) were very similar to those of the carbons 142.3 (C-24) and 76.7 ppm (C-2) of compound A (**64**), thus indicating that an NH proton was present in compound C (**66**). Similarly, an NH proton signal was not reported for terpendoles A (**47**), B (**48**) and D (**50**).[74] The absence of the NH peak in the ^{1}H NMR spectrum of compound C (**66**) could be due to exchange with water molecules (presumably the broad singlet at 1.53 ppm) that could have been in the solvent. A proposed structure of the modified indole region in compound C (**66**) is presented in Figure 2.44.

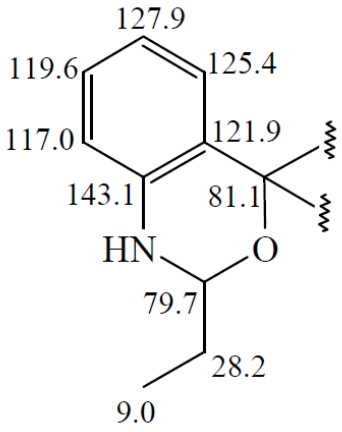

Figure 2.44: ^{13}C NMR chemical shifts (ppm) for the proposed structure of the modified indole region in compound C (**66**), ($CDCl_3$, 400 MHz).

The chemical shifts of the C-2 substituent of compound C (**66**) closely match the predicted ^{13}C NMR spectral data of 1-aminopropanol (Figure 2.45) that were obtained from the ACD Labs software via SciFinder database,[130] hence the assignment of the C-2 substituent is likely correct.

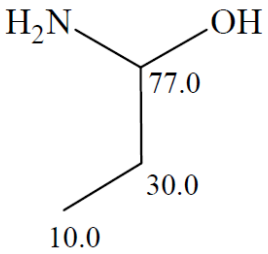

Figure 2.45: The predicted ^{13}C NMR spectral data of 1-aminopropanol.[130]

The COSY and HMBC correlations of some of the proton and carbon signals of compound C (**66**) mentioned in the above discussion are summarised in Figure 2.46 and Table 2.13.

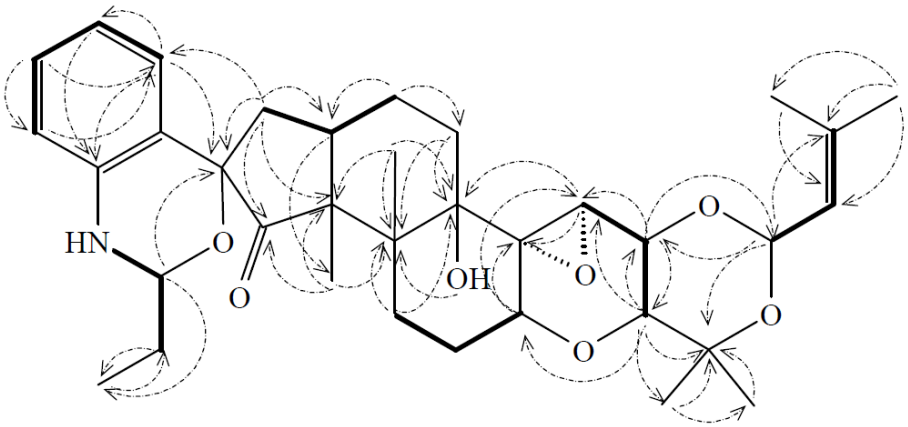

Figure 2.46: The COSY (▬) and ^{1}H - ^{13}C HMBC (-----) correlations observed for compound C (**66**), ($CDCl_3$, 400 MHz).

Table 2.13: COSY and ^{1}H - ^{13}C HMBC correlations observed for compound C (**66**), ($CDCl_3$, 400 MHz).

Atom	**^{13}C (δ ppm)**		**^{1}H (δ ppm)**	**COSY correlation**	**HMBC correlation**
2	79.7		4.93	H-39β	C-18, C-40
5	23.8	Hα	2.40	H-5β, H-6β	C-4
		Hβ	1.98	H-5α, H-6β	C-13
6	27.8	Hα	2.16	H-6β	
		Hβ	1.67	H-6α, H-5α	
7	71.5		4.27	H-6α, H-6β	C-11, C-12
9	71.1		3.57	H-10	C-7, C-10, C-11, C-28
10	71.1		3.94	H-9	C-9, C-31
11	61.2		3.62	H-9	C-7, C-10, C-12, C-13
14	29.5	Hα	1.55		
		Hβ	1.45		C-4, C-13
16	36.7		2.76	H-17α, H-17β, H-15α	
17	40.7	Hα	2.22	H-17β, H-16	C-17, C-20
		Hβ	2.09	H-16	C-3, C-18, C-37
20	125.4		6.99	H-21, H-22	C-18, C-21, C-23
21	127.9		7.11	H-20, H-22, H-23	C-24
22	119.6		6.84	H-20, H-21, H-23	C-20, C-23
23	117.0		6.72	H-20, H-21, H-22	C-20, C-22
25	13.1		1.46		C-3, C-4, C-37
26	17.6		1.12		C-3, C-4, C-5, C-13
28	16.5		1.30	H-29	C-9, C-27, C-29
29	28.2		1.30		C-27
31	92.6		5.56	H-33	C-10, C-34

Atom	^{13}C (δ ppm)		^{1}H (δ ppm)	COSY correlation	HMBC correlation
33	122.0		5.33	H-31	
35	18.6		1.76		C-33, C-34, C-36
36	25.7		1.77		C-33, C-34, C-35
39	28.2	Hα	1.67		C-40
		Hβ	1.67	H-2, H-40	
40	9.0		1.00	H-39β	C-39

The relative stereochemistry of some of the protons was determined using 1D and 2D NOE experiments. Since the NMR data of the right side of compound C (**66**) were similar to that of compound A (**64**), the stereochemistry was likely the same. The similar chemical shifts at C-17, C-18 and C-19 of compounds A (**64**), B (**65**) and C (**66**) indicated that stereochemistry at the spiro centre C-18 was conserved. Therefore, the major difference in structure lies in the modified indole region and the NOE enhancement experiments discussed below mainly concern the C-2 substituent of compound C (**66**).

Irradiation of the 4.93 ppm (H-2) proton signal enhanced the proton signals at 1.67 (H-39) and 1.00 pm (H-40). However, unlike that observed for compounds A (**64**) and B (**65**), irradiation of H-2 did not result in an NOE to H-26, therefore the orientation at H-2 could be different. It is not known whether the C-2 substituents affect the distance between H-2 and H-26 or if the stereochemistry at H-2 differs in compound C (**66**). Since the NH proton signal was not observed in the ^{1}H NMR spectrum (Figure 2.40) of compound C (**66**), no potential correlations to it could be observed. However, the proton coupling constants of H-2 were 6.71 and 2.38 Hz, similar to those of H-2 in compounds A (**64**) and B (**65**), which indicated the likehood that H-2 in all compounds A (**64**), B (**65**) and C (**66**) shared the same stereochemistry. However, further work would be required to determine the complete stereochemistry of compound C (**66**) as was the case for compounds A (**64**) and B (**65**). The spatial correlations of selected protons of compound C (**66**) are indicated in Figure 2.47 and Table 2.14.

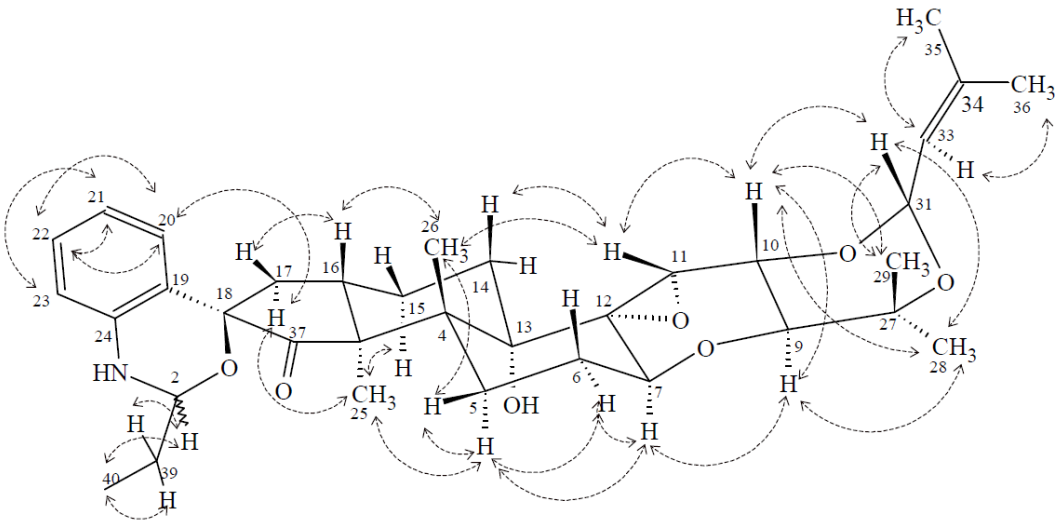

Figure 2.47: NOE correlations of selected protons in compound C (**66**).

Table 2.14: Selected NOE enhancements observed for compound C (**66**), ($CDCl_3$, 400 MHz).

^{1}H (δ ppm)	**NOESY**
4.93 (H-2)	H-40, H-39
1.98 (H-5β)	H-5α
2.16 (H-6α)	H-7
4.27 (H-7)	H-9, H-6α
3.57 (H-9)	H-28, H-7
3.94 (H-10)	H-31, H-28, H-11
3.62 (H-11)	H-14β, H-10
2.22 (H-17α)	H-20, H-17β, H-25
6.99 (H-20)	H-22, H-17α
7.11 (H-21)	H-23
6.84 (H-22)	H-20, H-21
6.72 (H-23)	H-21
1.46 (H-25)	H-5α
1.12 (H-26)	H-11, H-16
1.30 (H-28)	H-31, H-9
1.31 (H-29)	H-31, H-10
5.56 (H-31)	H-33, H-10, H-35, H-28
5.33 (H-33)	H-36, H-33
1.76 (H-35)	H-31, H-33
1.77 (H-36)	H-33, H-31
1.00 (H-40)	H-2, H-39α

The proposed structure of compound C (**66**) is shown below and the NMR assignments are summarised in Figure 2.48 and Table 2.15.

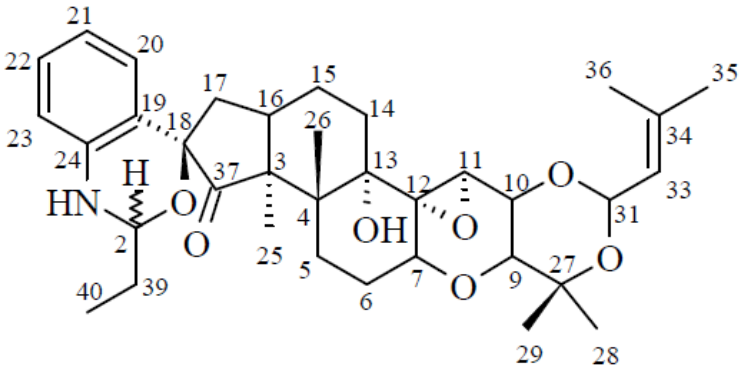

Figure 2.48: The proposed structure of compound C (**66**).

Table 2.15: ^{13}C and ^{1}H NMR assignments for compound C (**66**), ($CDCl_3$, 400 MHz).

Atom	**^{13}C (δ ppm)**		**^{1}H (δ ppm)**	**Multiplicity (*J* Hz)**
NH			nd[a]	
2	79.7		4.93	dt (6.7, 5.3, 1.1)
3	53.5			
4	42.3			
5	23.8	Hα	2.40	td (14.0, 5.0)
		Hβ	1.98	dd (12.3, 5.9)
6	27.8	Hα	2.16	m
		Hβ	1.67	m
7	71.5		4.27	dd (8.1, 10.5)
9	71.1		3.57	d (9.4)
10	71.1		3.94	d (9.1)
11	61.2		3.62	s
12	67.6			
13	79.1			
13-OH			nd	
14	29.5	Hα	1.55	m
		Hβ	1.45	s
15	20.5	Hα	1.81	td (12.7, 3.5)
		Hβ	1.59	m
16	36.7		2.76	tq (12.1, 2.8)
17	40.7	Hα	2.22	t (13.4)
		Hβ	2.09	d (15.6)
18	81.1			
19	121.9			
20	125.4		6.99	dd (8.1, 1.2)
21	127.9		7.11	ddd (8.5, 7.8, 1.4)
22	119.6		6.84	dt (8.9, 7.7, 1.2)
23	117.0		6.72	dd (8.0, 1.0)

Atom	^{13}C (δ ppm)		^{1}H (δ ppm)	Multiplicity (*J* Hz)
24	143.1			
25	13.1		1.46	s
26	17.6		1.12	s
27	74.1			
28	16.5		1.30	s
29	28.2		1.31	s
31	92.6		5.56	d (6.7)
33	122.0		5.33	dt (6.6, 1.9, 1.4)
34	139.0			
35	18.6		1.76	s
36	25.7		1.77	s
37	212.8			
39	28.2	Hα	1.67	s
		Hβ	1.67	
40	9.0		1.00	s

a = not observed

2.4 Identification and structural elucidation of compound D (67).

Compound D (**67**) was isolated as a mixture with terpendole D (**50**) according to the LC-MS and NMR analysis. The known compound, terpendole D (**50**) was also isolated in a pure form in another fraction (Chapter 3). This was the first report of terpendole D (**50**) from this fungal-ryegrass association. The separation of compound D (**67**) and terpendole D (**50**) via semi-preparative HPLC was not successful. Due to the limited amount of compound D (**67**), the sample was subjected to NMR spectroscopy without further purification, in the hope that the data for terpendole D (**50**) could be eliminated via comparison with data acquired during the current research and with literature values.[74] Unfortunately, the sample became contaminated during preparation for NMR analysis with bis(2-ethylhexyl) phthalate (DEHP) (**68**), a plasticiser. However, the NMR signals for terpendole D (**50**) and the plasticiser could be eliminated and a structure for compound D (**67**) was proposed.

2.4.1 UV Spectroscopy

The UV spectrum of compound D (**67**) contained peak maxima at 215, 240 and 295 nm (Figure 2.49) and was similar to those of compounds A (**64**) and B (**65**), hence the compounds contained similar chromophores. In contrast, the UV spectrum of terpendole D (**50**) contained maxima at 230 and 280 nm, consistent with the presence of an indole moiety.

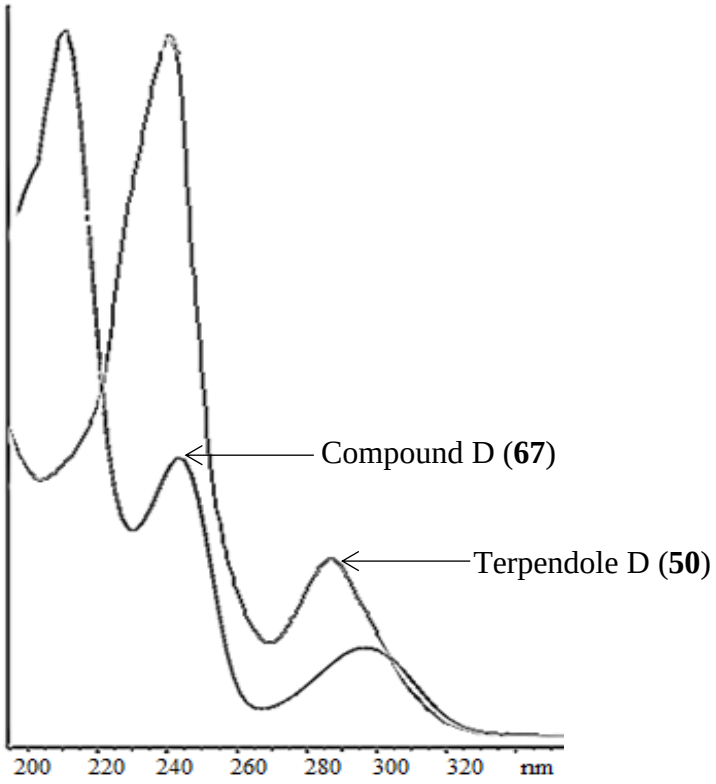

Figure 2.49: The normalised UV absorbance spectra of compound D (**67**) and terpendole D (**50**) obtained from HPLC.

2.4.2 Mass Spectrometry

The chromatogram from the LC-MS analysis (Figure 2.50) indicated that compound D (**67**) and terpendole D (**50**) co-eluted. Compound D (**67**) exhibited a pseudo-molecular ion at *m/z* 636.02 whilst that of terpendole D (**50**) was at *m/z* 506.2.

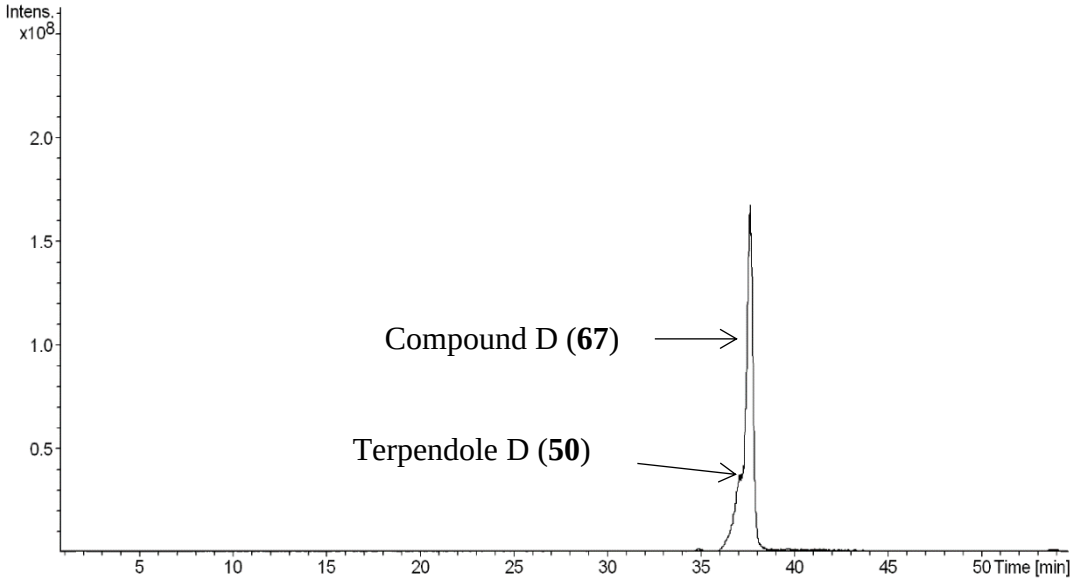

Figure 2.50: The chromatogram of compound D (**67**) co-eluting with terpendole D (**50**) obtained from LC-MS analysis.

The tandem mass spectrum of terpendole D (**50**) produced the characteristic indole diterpenoid fragment ion at *m/z* 182 while the tandem mass spectrum of compound D (**67**) was very similar to that of compound A (**64**), with fragments representing loss of a hydroxyl group in the form of water, indicating the presence of oxygen atom(s) in compound D (**67**). A loss of 100 Da from the parent ion *m/z* 636.02 was also observed, which could be attributed to the loss of the C-2 substituent.

The mixture was later analysed by LC-MS after the NMR analysis and an additional molecular ion at *m/z* 391.2 was detected, due to the plasticiser contaminant.

2.4.3 NMR Spectroscopy

The NMR data of terpendole D (**50**) was first eliminated via comparison with the literature values and with the data acquired in Chapter 3. The NMR data for the plasticiser contaminant were then assigned via COSY and HMBC correlations with reference to literature values. The remaining NMR data were attributable to compound D (**67**).

*Elimination of terpendole D (**50**) peak signals*

The ^{1}H NMR spectra of a sample of pure terpendole D (**50**) and that of the mixture with compound D (**67**) were compared (Figure 2.51 and Figure 2.52). It was clear, from this comparison, that every proton signal of terpendole D (**50**) was also present in the mixture. From the HSQC NMR spectrum (Appendix 14), the NMR spectral data (^{1}H and ^{13}C) of terpendole D (**50**) matched the literature values as in Chapter 3.[74] Seven of the quaternary carbon signals were evident in the ^{13}C NMR spectrum (Appendix 13) leaving the carbon signals at 116.0 (C-18) and 125.0 ppm (C-19) to be determined from HMBC correlations. Hence, the NMR data for terpendole D (**50**) were eliminated from the NMR data of the mixture.

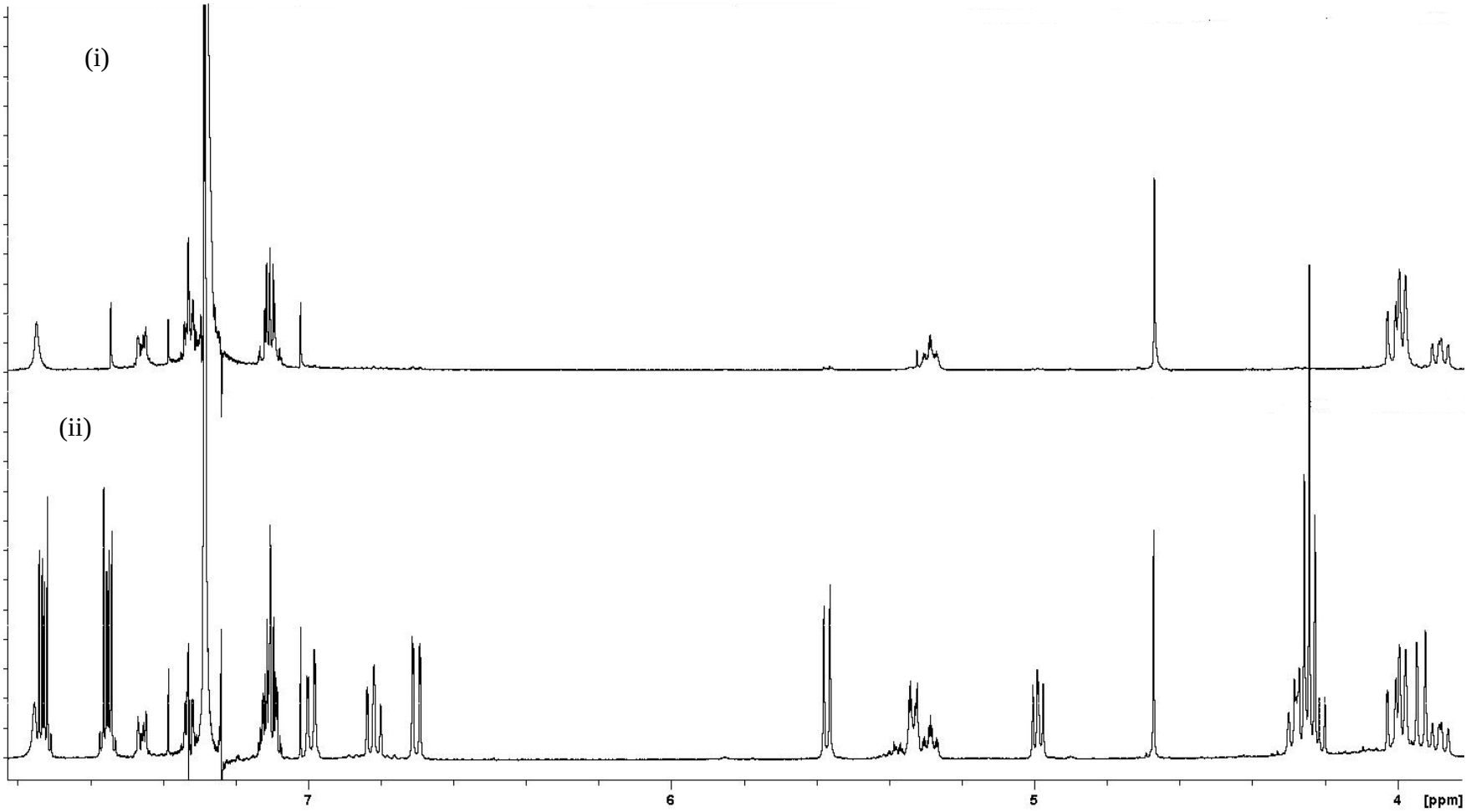

Figure 2.51: The ^{1}H NMR spectra of (i) terpendole D (**50**) and (ii) the mixture of terpendole D (**50**), compound D (**67**) and plasticiser contaminant (chemical shift 3.80 – 8.00 ppm), ($CDCl_3$, 400 MHz).

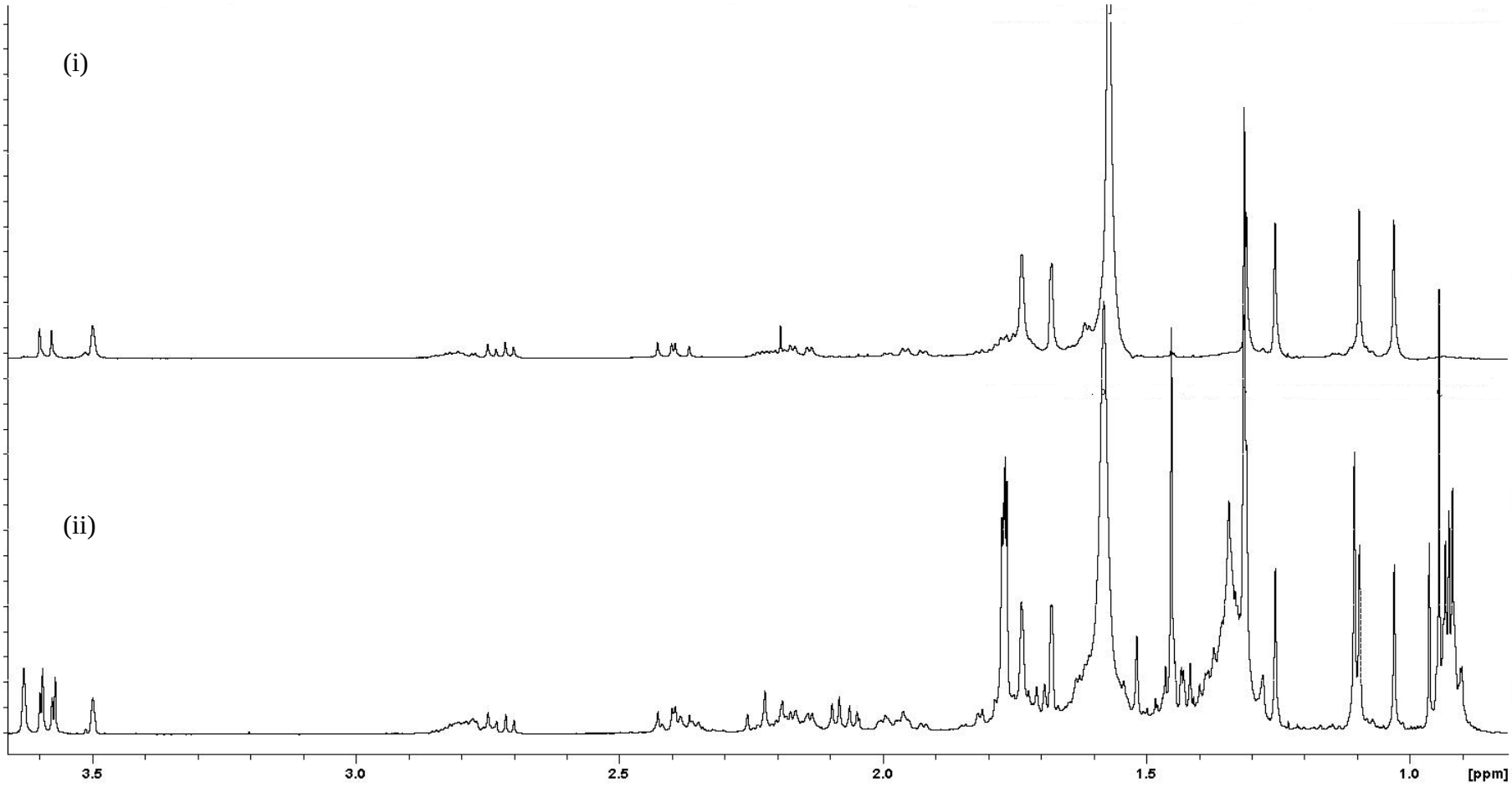

Figure 2.52: The ^{1}H NMR spectra of (i) pure terpendole D (**50**) and (ii) the mixture of terpendole D (**50**), compound D (**67**) and plasticiser contaminant (chemical shift 0.80 - 3.70 ppm), ($CDCl_3$, 400 MHz).

Determination of the contaminant structure.

The ^{1}H NMR peaks associated with the contaminant were of higher intensity compared to those of terpendole D (**50**) and compound D (**67**) (Figure 2.51). These included the aromatic proton signals at 7.55 and 7.73 ppm. Using NMR data from the ^{13}C, HSQC, COSY and HMBC NMR spectra (Appendices 13 - 16), the ^{13}C and ^{1}H assignments (Table 2.16) and the structure of the contaminant were proposed. The contaminant was identified as DEHP (**68**) plasticiser, consistent with the molecular ion at *m/z* 391.2 and closely matching the literature NMR data.[131]

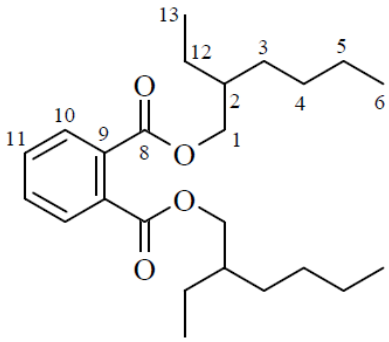

(**68**)

Table 2.16: ^{13}C and ^{1}H NMR assignments for DEHP (**68**).

Atom	**^{13}C (δ ppm)**		**^{1}H (δ ppm)**
1	68.2		4.24
2	38.8		1.70
3	30.4	Hα	1.36
		Hβ	1.34
4	27.2	Hα	2.10
		Hβ	nd[a]
5	22.5	Hα	1.34
		Hβ	nd[a]
6	14.0		1.03
8	167.8		
9	132.4		
10	128.3		7.71
11	130.8		7.54
12	23.8	Hα	2.38
		Hβ	1.97
13	10.9		0.90

a = not observed

This particular plasticiser is found in many plastics and possibly the contamination could have come from the NMR tube cap or from a pipette rubber bulb. The elimination of the signals for DEHP (**68**) and terpendole D (**50**) allowed the NMR data of compound D (**67**) to be analysed and the structure to be determined.

*Determination of compound D (**67**) structure.*

The ^{1}H and ^{13}C NMR signals remaining after elimination of the signals arising from terpendole D (**50**) and DEHP (**68**) indicated that a prenyl moiety was present in compound D (**67**), due to the familiar methine proton signals at 5.33 and 5.56 ppm. These proton signals coupled to each other in the COSY NMR spectrum (Appendix 15) as observed for H-31 and H-33 of compound A (**64**). The HMBC NMR spectrum (Appendix 14) showed that the 5.33 ppm proton signal was correlated to methyl carbon signals at 25.7 and 17.9 ppm. The 5.56 ppm proton signal had correlations to the carbon signal at 139.8 ppm and to two methine resonances at 71.1 ppm, consistent with the correlations observed for the prenyl moiety of compound A (**64**).

In addition, carbon resonances at 71.5, 61.2 and 67.5 ppm were present, similar to those of carbons C-7, C-11 and C-12 of compound A (**64**), indicating that the hemi-acetal and epoxy moieties are also present in compound D (**67**). The presence of the quaternary carbon resonances at 42.2, 53.5, 79.0, 81.8 and 212.8 ppm matched those of carbons C-3, C-4, C-13, C-18 and C-37 of compound A (**64**), hence the right side of compound D (**67**) was identical to that of compound A (**64**), consistent with their similar UV absorptions and molecular formulae. The assignment of the NMR data for compound D (**67**) was carried out by comparison to the equivalent signals in compound A (**64**) (Table 2.17).

This comparison showed that the right side of compound D (**67**) was clearly the same as that of compound A (**64**) (Table 2.17). The chemical shifts were closely aligned, indicating that the stereochemistries of the atoms were also the same. The main difference between the compounds therefore, lies on the left side of the molecule. The aromatic ring evident in compound D (**67**) was similar to that in compound A (**64**), however, the chemical shift at C-2 was further downfield in compound D (**67**) (78.7 ppm) than in compound A (**64**) (76.6 ppm), indicating that

the difference could be at the C-2 substituent. The remaining carbon resonances at 35.2, 31.7, 24.2 and 23.8 ppm would represent the substituent.

Table 2.17: ^{13}C and ^{1}H NMR assignments for compound D (**67**) and compound A (**64**), ($CDCl_3$, 400 MHz).

Atom	Compound D (67)			Compound A (64)		
	^{13}C (δ ppm)		^{1}H (δ ppm)	^{13}C (δ ppm)		^{1}H δ ppm)
NH			nd			4.40
2	78.7		4.99	76.7		4.93
3	53.5			53.7		
4	42.2			42.1		
5	23.8	Hα	2.39	24.0	Hα	2.38
		Hβ	1.97		Hβ	1.94
6	27.8	Hα	2.16	27.8	Hα	2.15
		Hβ	1.68		Hβ	1.64
7	71.5		4.27	71.5		4.27
9	71.1		3.58	71.1		3.58
10	71.1		3.94	71.1		3.94
11	61.2		3.63	61.2		3.63
12	67.6			67.5		
13	79.0			79.0		
13-OH			nd			1.53
14	29.5	Hα	1.55	29.4	Hα	1.58
		Hβ	nd		Hβ	1.42
15	20.5	Hα	1.78	20.1	Hα	1.81
		Hβ	1.60		Hβ	1.63
16	36.7		2.78	36.8		2.75
17	40.7	Hα	2.22	40.3	Hα	2.27
		Hβ	2.18		Hβ	2.12
18	81.7			81.8		
19	121.7			120.5		
20	125.4		6.99	125.3		6.99
21	127.9		7.11	128.2		7.12
22	119.6		7.00	119.5		6.81
23	117.0		6.70	116.6		6.72
24	142.9			142.3		
25	13.1		1.45	12.9		1.46
26	17.4		1.11	17.6		1.09
27	74.7			74.8		
28	16.6		1.32	16.6		1.31
29	28.2		1.32	28.3		1.31
31	92.6		5.57	92.6		5.56
33	122.0		5.33	122.0		5.33

Atom	Compound D (67)		Compound A (64)	
	^{13}C (δ ppm)	^{1}H (δ ppm)	^{13}C (δ ppm)	^{1}H δ ppm)
34	139.6		139.3	
35	18.6	1.77	18.6	1.76
36	25.7	1.78	25.7	1.77
37	212.8		212.2	

The COSY NMR spectrum (Appendix 15) indicated that the proton signal at 4.99 ppm (H-2) was coupled to a proton signal at 1.62 ppm, which was correlated to a methylene signal at 35.2 ppm in the HSQC NMR spectrum (Appendix 14). The signal at 35.2 ppm was assigned as C-39. From the HMBC NMR spectrum (Appendix 16), the proton signal at 4.99 ppm (H-2) was correlated to carbon signals at 81.8 (C-18) (^{3}J) and 24.2 ppm (^{3}J), therefore the carbon resonance at 24.2 ppm was assigned as C-40. The TOCSY NMR spectrum (Figure 2.53) indicated that the proton resonance of H-2 was also correlated to two other proton signals at 1.34 and 0.94 ppm, in addition to the 1.64 ppm proton signal.

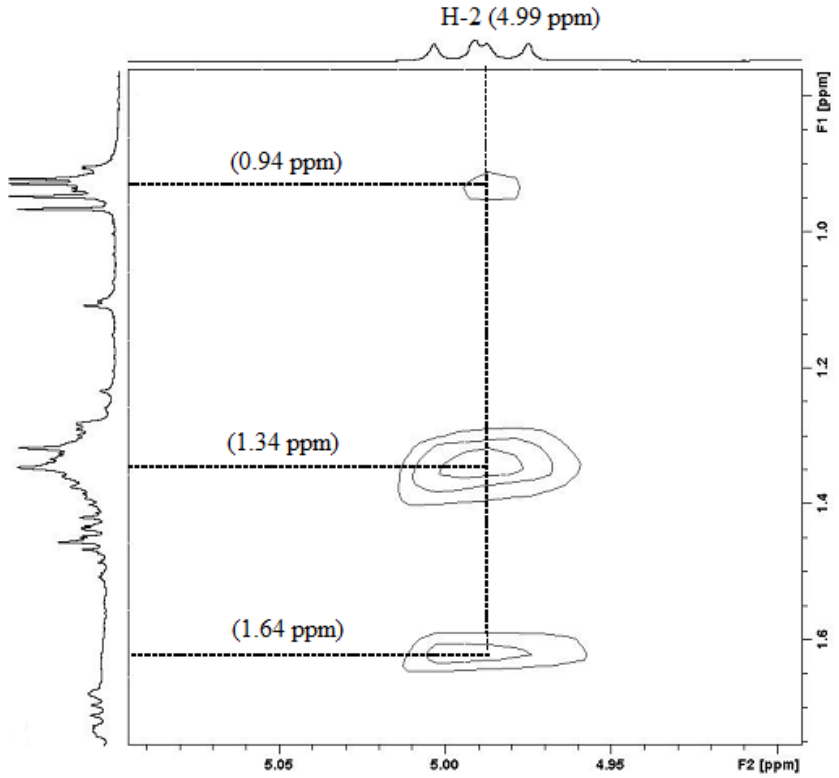

Figure 2.53: A selected region of the TOCSY NMR spectrum of compound D (**67**), ($CDCl_3$, 400 MHz).

The proton signal at 1.34 ppm was correlated to a methylene carbon signal at 31.7 ppm and the proton resonance at 0.94 ppm was correlated to a methyl carbon resonating at 10.9 ppm in the HSQC NMR spectrum (Appendix 15). These correlations implied that a saturated carbon chain could be attached to C-2 (78.7 ppm) of compound D (**67**). However, there were no other clear correlations detected from any of the protons to the methylene carbons mentioned above. Based on the limited information obtained and the molecular mass of the compound, the substituent at C-2 was presumably a pentyl group (Figure 2.54). The ^{13}C and ^{1}H NMR data acquired for the C-2 substituent are listed in Table 2.18.

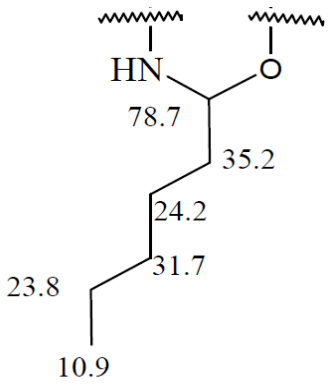

Figure 2.54: The proposed structure of the C-2 substituent in compound D (**67**).

Table 2.18: The NMR assignment of C-39 to C-43 of compound D (**67**).

Atom	**Compound D (67)**	
	^{13}C (δ ppm)	**^{1}H (δ ppm)**
39	35.2	1.62
40	24.2	1.70
41	31.7	1.34
42	23.8	1.97
43	10.9	0.94

The proposed ^{13}C NMR data (Table 2.18) for the C-2 substituent of compound D (**67**) was compared that to predicted for 1-amino-1-hexanol (Figure 2.55)[130] and both closely aligned. This indicated that most likely, pentyl is the C-2 substituent of compound D (**67**), however further work is required to confirm this assumption.

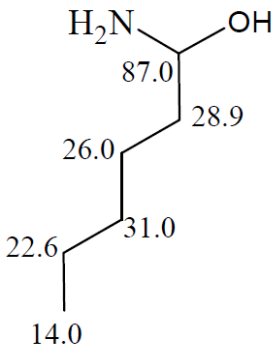

Figure 2.55: The predicted ^{13}C NMR spectral data for 1-amino-1-hexanol.[130]

It was not possible to determine the stereochemistry of the modified indole region. The NH proton signal was not visible in the ^{1}H NMR spectrum (Figure 2.51) but the chemical shifts of 142.9 (C-24) and 78.7 ppm (C-2) indicated the presence of an NH moiety as for compound C (**66**). The structure of compound D (**67**) was then proposed (Figure 2.56).

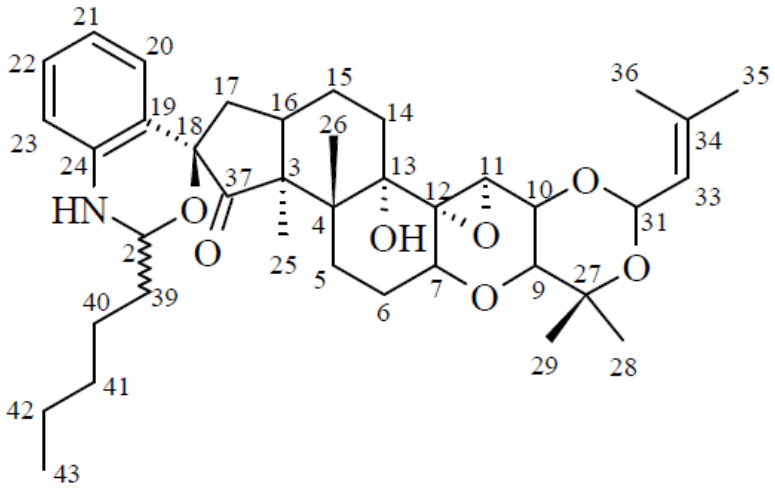

Figure 2.56: The proposed structure of compound D (**67**).

2.5 Discussion

Compounds A – D (**64** – **67**) are novel compounds isolated from the crude extract of perennial ryegrass seed infected with wild-type endophyte. The compounds share the same structure at the right side which is common to some of the known indole diterpenoids including lolitrem B (**3**)[53] and terpendole C (**49**).[67] On the left side, the ring A of lolitrem B (**3**) is not present and the indole region has been modified with a spiro carbon and different substituents at C-2. Therefore, these compounds cannot be classified as indole diterpenoids.

The LC-MS analysis of a fresh extract of perennial ryegrass seed (50 mg) infected with wild-type endophyte performed by Dr Mace (AgResearch, Grasslands) (Section 7.9) found no trace of these compounds. Therefore, it is possible that compounds A – D (**64** – **67**) are artefacts formed during storage of the extract at 5°C for seventeen years or due to the influence of light, heat or other factors. Indole diterpenoid artefacts such as 2,18-dioxopaxilline (**69**)[128] and sulpinine C (**70**),[132] which possess different structural features to compounds A – D (**64** – **67**), have been reported previously.

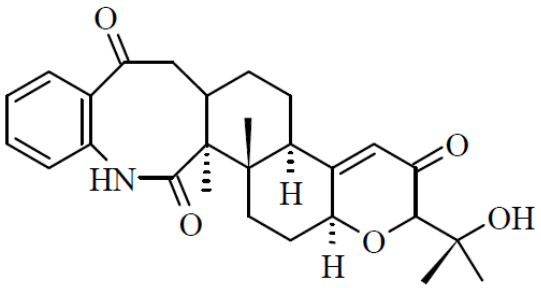

(**69**)

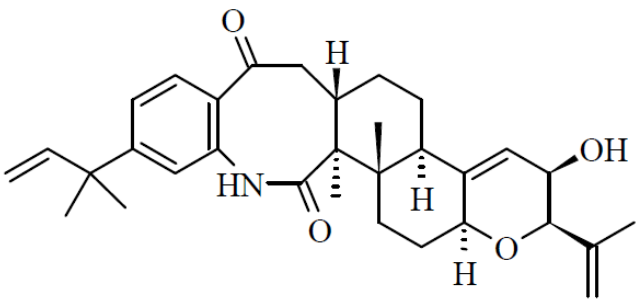

(**70**)

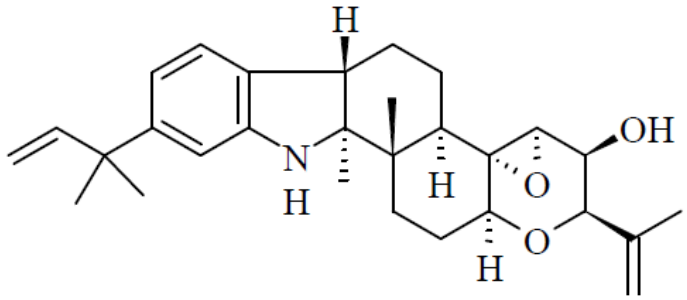

(**71**)

2,18-Dioxopaxilline (**69**) was formed when paxilline (**36**) was treated with thermally inactive sheep bile via a nonenzymatic oxidation process,[128] while sulpinine C (**70**) was presumably formed due to auto-oxidation of sulpinine A (**71**) when stirred in the air.[132] If compounds A – D (**64** – **67**) are produced via similar oxidation processes to those mentioned above, then most probably these compounds would have been formed from oxidation of terpendole C (**49**), followed by further modifications at the indole region and at the C-2 substituents as proposed in Figure 2.57.

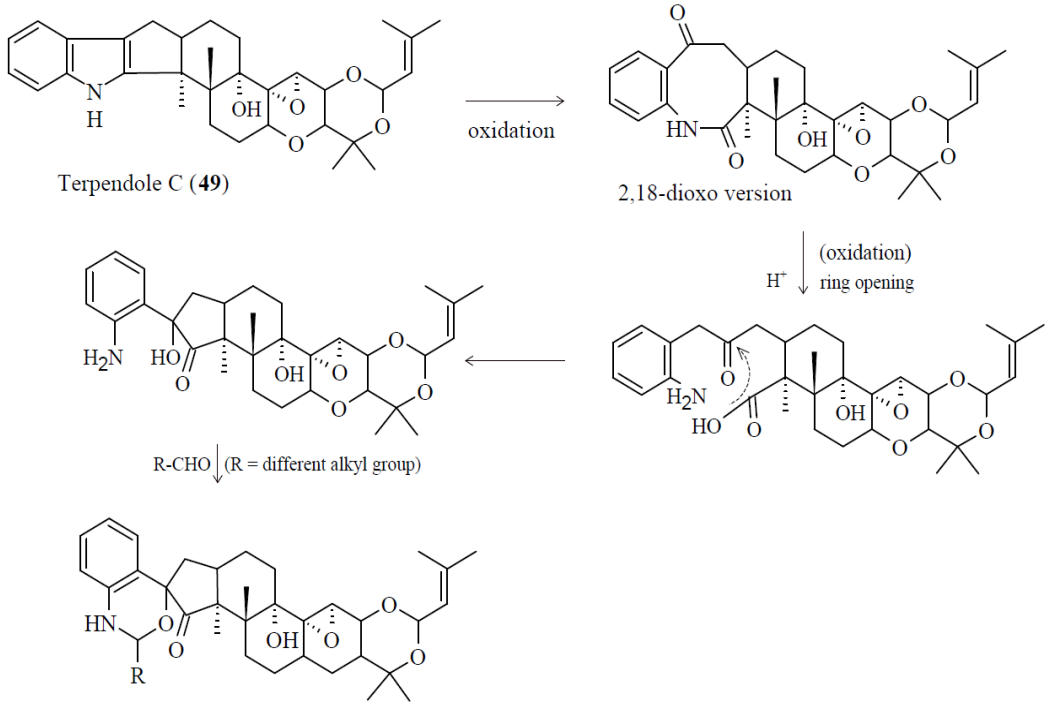

Figure 2.57: The presumed oxidation and modification processes of terpendole C (**49**) that could result in compounds A – D (**64** – **67**).

The possibility of such a modification of an indole diterpenoid to include different alkyl groups (R) at the final stage (Figure 2.57) indicated that compounds A – D (**64** – **67**) could be artefacts of a chemical process. This could explain why terpendole C was not detected in any precursor fraction. However, because of the complexity of the structures of compounds A – D (**64** – **67**), it is possible that these compounds could be formed through different oxidation and modification processes which are not currently understood.

Alternatively, it may be that these compounds are naturally occurring but are present at concentrations below the LC-MS detection limit. Consistent with this hypothesis, is the fact that the pre-lolitrem fraction originated from approximately 300 kg of ryegrass seed and compounds A – D (**64** – **67**) were still only isolated in small quantities. In addition to that, the LC-MS analysis of compound A (**64**) did not show the molecular ion of the 2,18-dioxo version of terpendole C (*m/z* 551) intermediates as proposed in Figure 2.57. The existence of the spiro centre at C-18 of compounds A – D (**64** – **67**) is unique and to date, this is the first report of such structures. In 2002, Li and co-workers isolated two novel antiinsectan indole diterpenoids known as thiersinines A (**72**) and B (**73**) from an extract of *P. theirsii* NRRL 28147.[133]

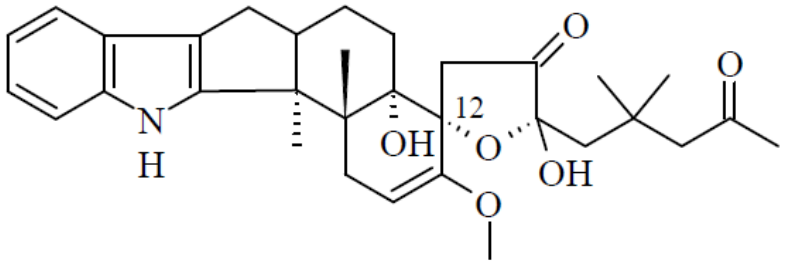

(**72**)

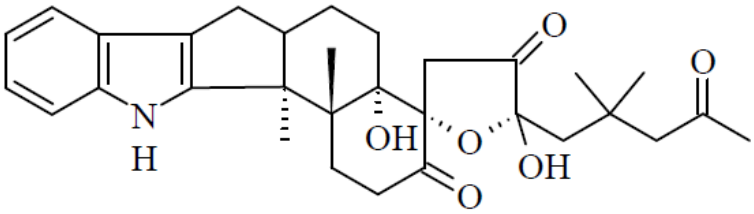

(**73**)

These compounds possessed a unique spirocyclic subunit at C-12 which was unprecedented in the known indole diterpenoids and both exhibited potent activity against fall armyworm.[133] The presence of the spiro centre in these novel compounds indicates that the existence of the spiro carbon in compounds A – D (**64** – **67**) could also possibly be due to natural causes.

Whether compounds A – D (**64** – **67**) are artefacts or not, it is important to understand how they are formed. It is also vital to determine their complete stereochemistry. Hence, recommended future work includes extraction of larger quantities of these compounds and attempting to crystallise them for X-ray analysis. Molecular modelling studies, which could help the stereochemistry determination and predicting the chirality of the compounds, are also required. Optical rotations need to be measured. Since a polarimeter with a microcell is not available at either AgResearch or the University of Waikato, these measurements would need to be conducted elsewhere.

The C-2 substituent of compound D (**67**) also needs to be confirmed which would be possible by NMR analysis of a sample of pure compound D (**67**).

Chapter 3: Identification and structural elucidation of terpendole D (50), 13-desoxypaxilline (37), paspaline (42) and a potential emindole analogue.

The known indole diterpenoid, terpendole D (**50**) was isolated as a white, amorphous powder from the polar layer of a liquid-liquid partition of the crude pre-lolitrem fraction via a series of C18 reversed phase flash columns and semi-preparative HPLC. Previously, terpendole D (**50**) has only been found in the extract of *A. yamanashiensis*[67, 74] and this is the first time it has been reported from *E. festucae* var. *lolii*. The known compounds 13-desoxypaxilline (**37**) and paspaline (**42**) were also isolated in the current research and their deterrent potential against porina larvae was determined. A potential emindole analogue was also detected but due to the amount available, only limited NMR information was obtained.

3.1 Identification and structural elucidation of terpendole D (50).

3.1.1 UV Spectroscopy

Terpendole D (**50**) possesses a similar UV absorbance spectrum (Figure 3.1) to paspaline (**42**), with peak maxima at 231.2 and 280.2 nm.[74]

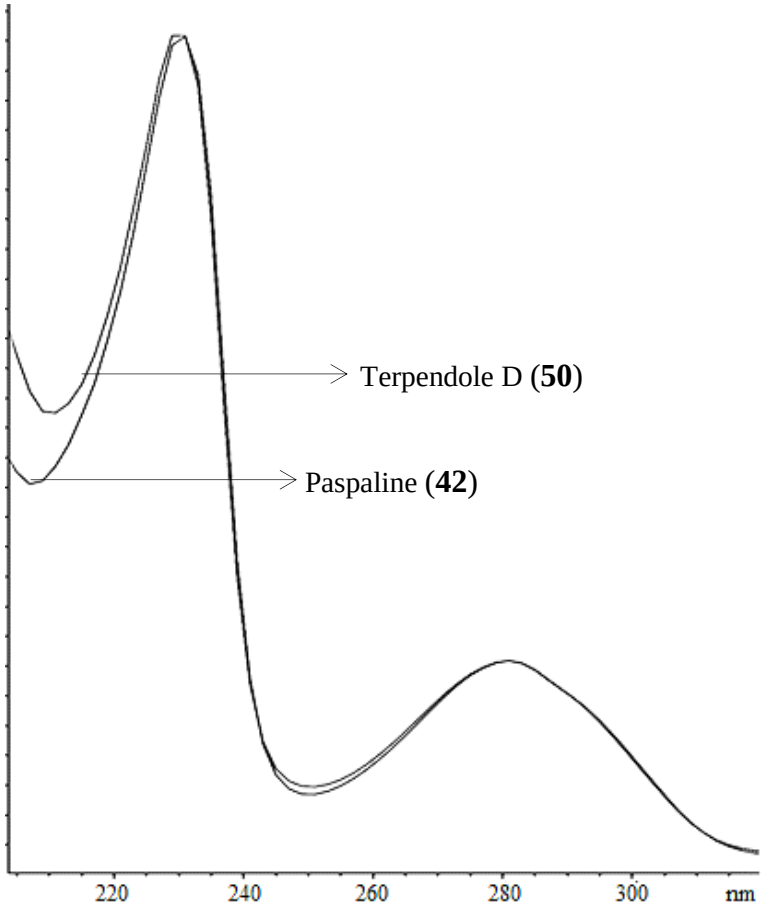

Figure 3.1: The normalised UV absorbance spectra of terpendole D (**50**) and paspaline (**42**) obtained from HPLC.

3.1.2 Mass Spectrometry

The high resolution mass spectrum of terpendole D (**50**) contained a pseudo-molecular ion at *m/z* 506.3224, consistent with a molecular formula of $C_{32}H_{43}NO_4$ (*m/z* 505.3269). Using Electrospray Ionisation Mass Spectrometry (ESI-MS), a parent ion at *m/z* 506.2 was observed.

The tandem mass spectrum of terpendole D (**50**) contained a fragment ion at *m/z* 182.1, attributable to cleavage in ring D across the C-3 – C-4 and C-14 – C-15 bonds (Figure 3.2).

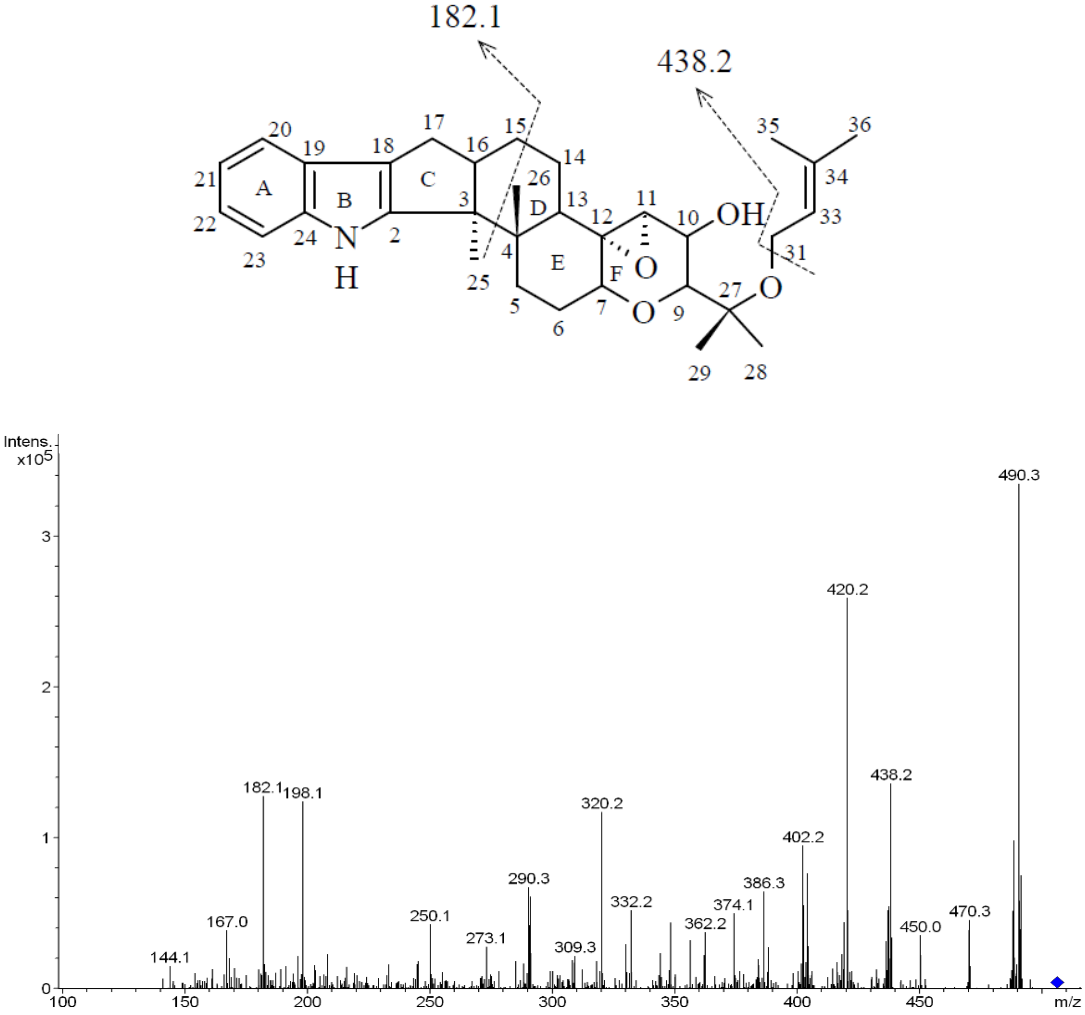

Figure 3.2: The tandem mass spectrum of terpendole D (**50**), *m/z* 506.2 (positive ion mode).

This fragment ion at *m/z* 182.1 [$C_{13}H_{11}N^{+}$] is characteristic for indole diterpenoid compounds such as terpendole and paxilline analogues and indicates that the indole ring is intact.[64] A fragment ion representing a loss of 16 Da from the molecular ion was observed at *m/z* 490.3. This could be the loss of a methyl group at C-25, as suggested by Babu in 2008 when he compared the fragmentations of some indole diterpenoids including terpendole C (**49**) under Atmospheric Pressure Chemical Ionisation (APCI) and ESI in a Liquid Chromatography Ultra Violet Mass

Spectrometry (LC-UV-MS) system.[96] Alternatively, this could be due to the loss of an oxygen atom (potentially at C-10). The fragment ion at *m/z* 438.2 was attributed to the loss of an isoprenyl residue (C_5H_9) from the parent ion *m/z* 506 and loss of C_5H_9O as $C_5H_{11}O$ at C-27 yielded the fragment ion at *m/z* 420.2 Da (Table 3.1).

Table 3.1: The MS^2 fragments of *m/z* 506.2 of terpendole D (**50**), (positive ion mode).

Parent ion (*m/z*)	**Ions loss (Da)**	**Attributable ion loss**	**MS^2 fragment ions (*m/z*)**
506.2	16	CH_2 or O	490.3
	68	C_5H_9	438.2
	86	$C_5H_{10}O$	420.2
	324	$C_{19}H_{32}O_4$	182.1

3.1.3 NMR Spectroscopy

A full range of NMR spectra including ^1H, ^{13}C, DEPT-135, HSQC, HMBC and COSY were acquired to allow the NMR assignment of terpendole D (**50**).

The ^1H NMR spectrum (Figure 3.3) of terpendole D (**50**) contained twenty eight proton signals. These signals consisted of twelve singlets, three doublets, four doublets of doublets, one triplet of doublet and eight multiplets. The four multiplet signals at 7.09, 7.10. 7.32 and 7.45 ppm indicated the presence of an aromatic ring of an indole moiety.

Two singlets at 4.67 and 7.75 ppm in the ^1H NMR spectrum (Figure 3.3) were assigned to the 10-hydroxyl and NH protons as they did not correlate to any carbon signal in the HSQC NMR spectrum (Appendix 21) and each integrated as a single proton and matched the literature values.[74]

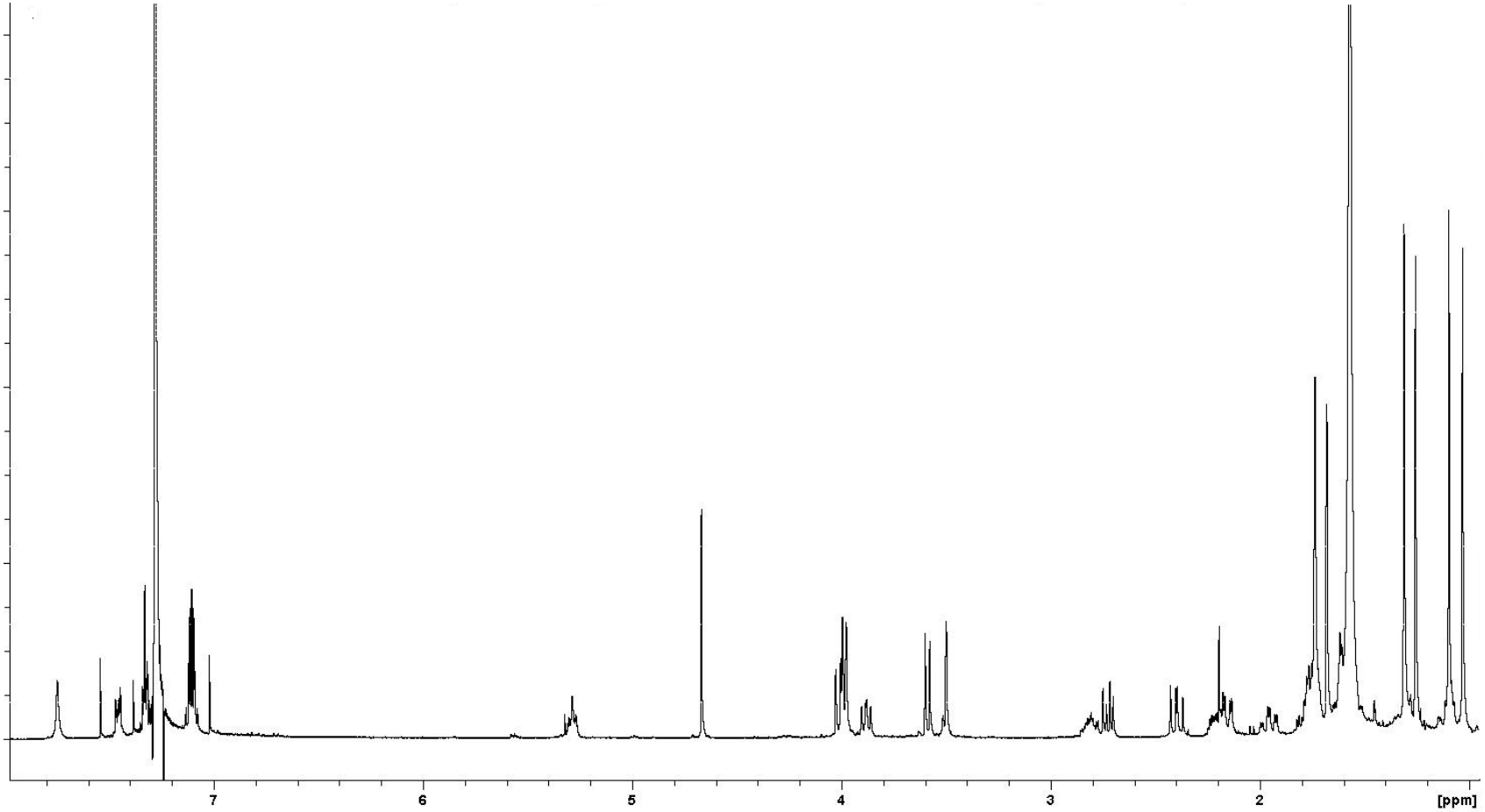

Figure 3.3: The ^{1}H NMR spectrum of terpendole D (**50**), ($CDCl_3$, 400 MHz).

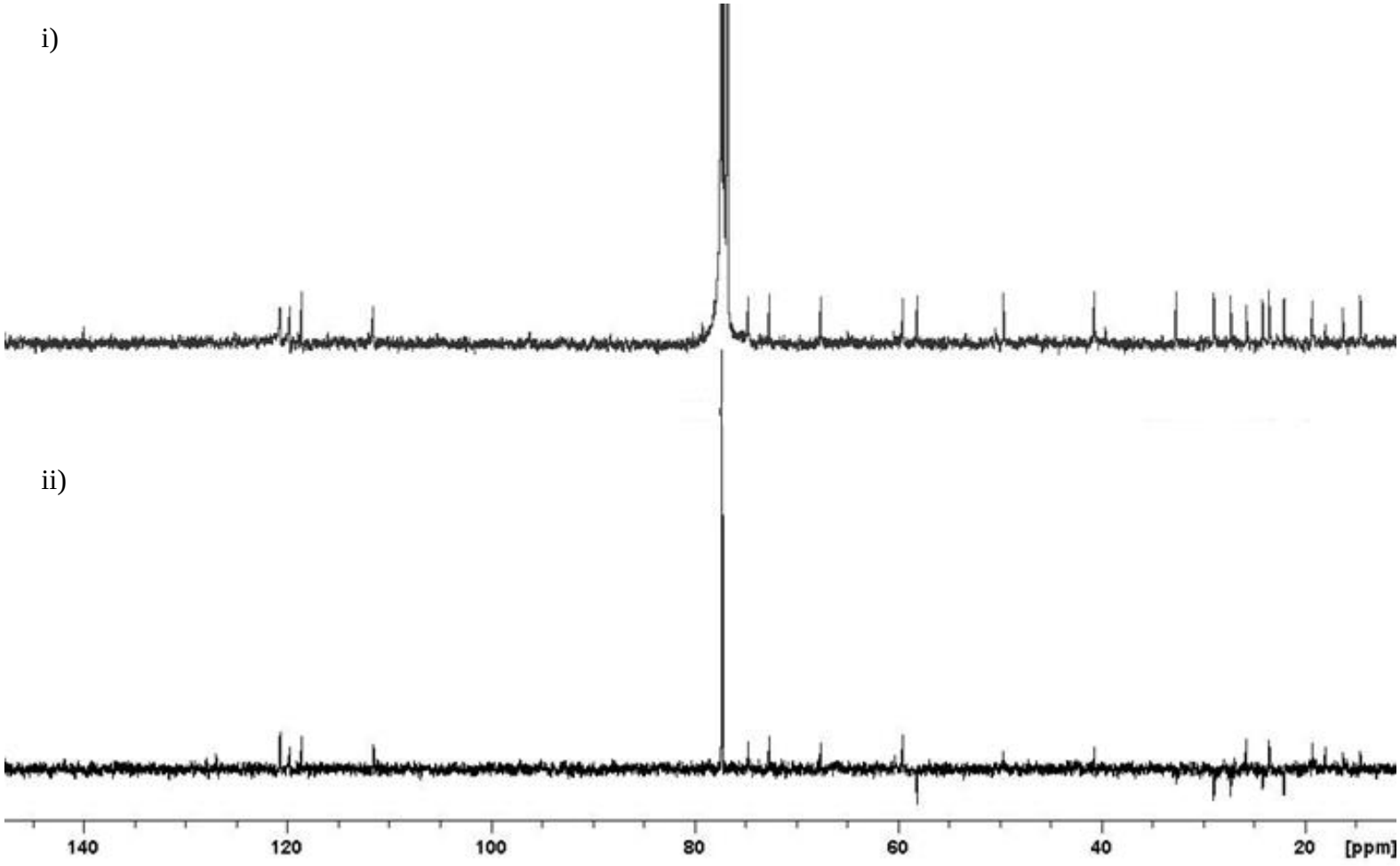

Figure 3.4: (i) ^{13}C and (ii) DEPT-135 NMR spectra of terpendole D (**50**), ($CDCl_3$, 400 MHz).

The ^{13}C NMR spectrum indicated the presence of twenty seven carbons which the DEPT-135 NMR spectrum (Figure 3.4) classified into six methyl, six methylene, eleven methine and four quaternary carbon signals. Five of the thirty two carbon signals suggested by the molecular formula were not visible, hence they were assigned from HMBC correlations and the literature values of terpendole D (**50**).[74]

The connectivity of the carbons was deduced from analysis of the COSY and HMBC correlations as summarised in Table 3.2.

Table 3.2: COSY and ^{1}H - ^{13}C HMBC correlations for terpendole D (**50**), ($CDCl_3$, 400 MHz).

Atom	**^{13}C (δ, ppm)**	**^{1}H (δ, ppm)**	**COSY correlations**	**HMBC correlations**
NH		7.75		C-17
5	32.5 Hα	1.93	H-26	
6	28.9 Hα	2.22	H-15β, H-6β	
7	72.6	3.88	H-6α, H-6β	
9	74.6	3.58	H-11	C-10, C-10, C-27, C-28, C-29
10	67.5	4.01	H-9	C-6, C-11, C-27
10-OH		4.67		C-6, C-10, C-11
11	59.4	3.49	H-9, H-31	C-6, C-12
13	40.6	2.16	H-14α, H-26	C-4, C-12
15	24.1 Hα	1.70		C-13
16	49.5	2.82	H-17α	C-3, C-18
17	27.2 Hα Hβ	2.41 2.71	H-17β	C-18 C-2, C-3, C-18
20	118.5	7.32		C-21
21	119.7	7.09		C-17, C-19, C-23
23	111.4	7.45		C-22
25	14.5	1.03	H-26	C-2, C-3, C-4, C-16
26	16.2	1.10	H-25	C-3, C-4, C-5, C-13
28	19.2	1.25		C-6, C-27, C-29
29	23.5	1.30		C-6, C-27, C-28
31	57.9	3.98		C-33, C-34
33	120.7	5.28	H-31	
35	17.9	1.68		C-33, C-36
36	25.7	1.74		C-33, C-35

Since this is a known indole diterpenoid, only the assignments of the five carbons that were not visible in the ^{13}C NMR spectrum (Figure 3.4) are discussed below.

In the COSY NMR spectrum (Appendix 18), the 1.03 ppm (H-25) proton signal was coupled to the proton signal at 1.10 ppm (H-26) and also to a carbon signal at 149.5 ppm (^{2}J) in the HMBC NMR spectrum (Appendix 22). The 2.71 ppm (H-17β) proton signal was also correlated to the 149.5 ppm (^{3}J) carbon signal which could, therefore, be assigned as C-2. The proton signals H-26 (1.10 ppm) and H-17β (2.71 ppm), as well as the signals at 2.82 ppm (H-16) and 1.03 ppm (H-25), were correlated to a quaternary carbon signal at 50.6 ppm in the HMBC NMR spectrum (Appendix 22) which was then assigned to C-3. The H-26 (1.10) and H-13 (2.15 ppm) signals were correlated to the carbon signal at 39.5 ppm (^{2}J) with a ^{3}J correlation from the H-25 (1.03 ppm) proton, allowing its assignment to C-4 (Figure 3.5).

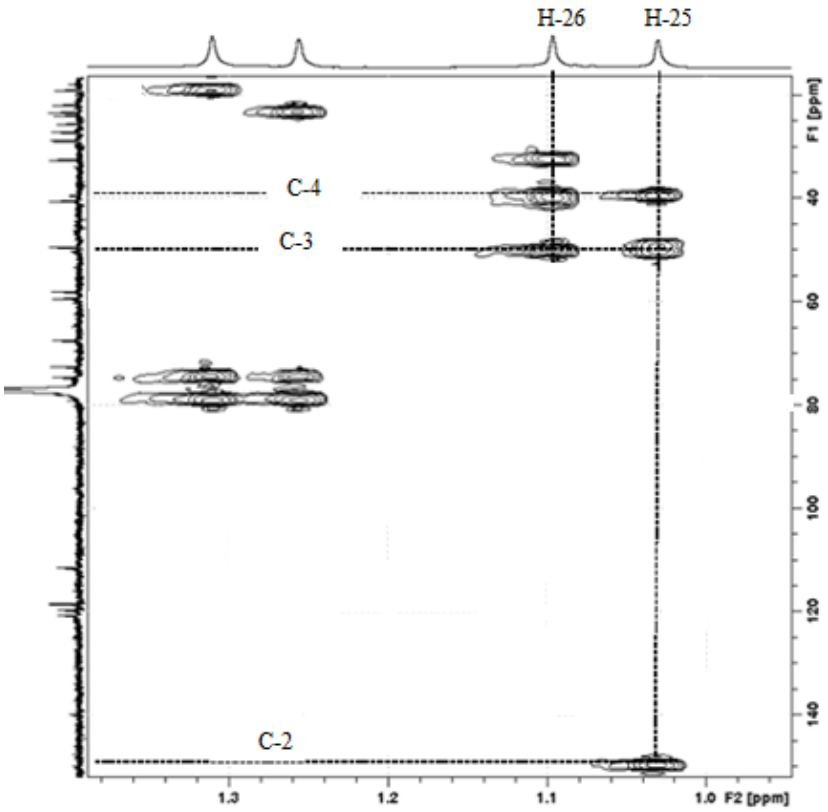

Figure 3.5: An expanded region of the HMBC NMR spectrum of terpendole D (**50**) showing the correlation of protons H-25 and H-26 to carbons C-2, C-3 and C-4.

The H-13 (2.15 ppm) proton correlated to proton signals at 1.70 ppm (H-14α) and 1.10 ppm (H-26) in the COSY NMR spectrum and was correlated to the carbon signal at 65.4 ppm (^2J) in the HMBC NMR spectrum (Appendix 22). Similarly, the proton signal at 3.49 ppm (H-11) with COSY correlations to the proton signals at 3.59 ppm (H-9) and 3.98 ppm (H-31) was also correlated to this carbon (^2J) (Figure 3.6) so could be assigned to C-12.

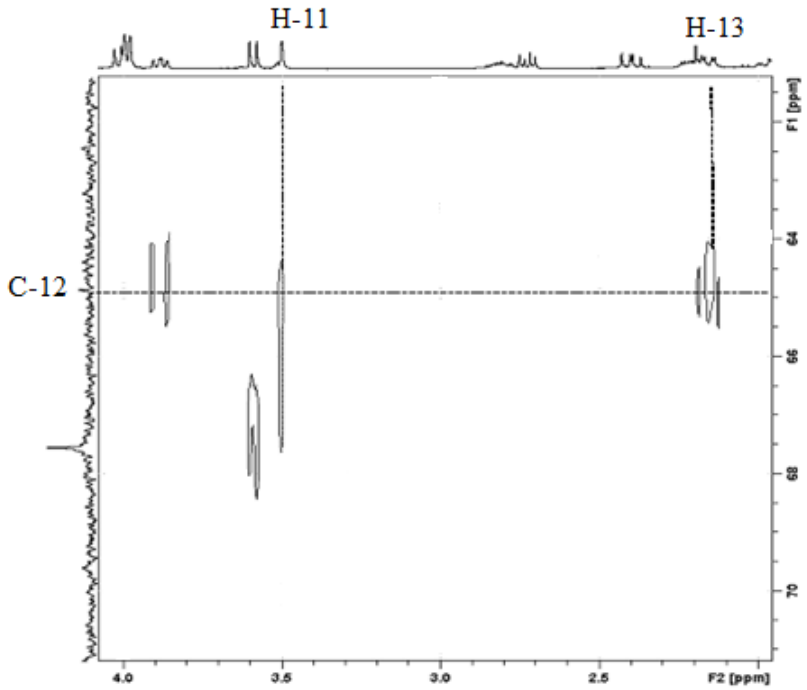

Figure 3.6: A selected region of the HMBC NMR spectrum of terpendole D (**50**) with correlations of H-11 and H-13 protons to carbon C-12. (^{13}C : 60.0 – 75.0 ppm, ^{1}H : 2.0 – 4.0 ppm).

The only carbon signal left to be assigned was that at 137.2 ppm. There were no HMBC correlations observed from any of the protons to this carbon. The NMR data of terpendole D (**50**) reported by Huang and co-workers in 1995[74] was compared with the NMR data of terpendole D (**50**) obtained in this research (Table 3.3), which allowed this carbon resonance to be assigned as C-24. Comparison of the NMR assignment of the isolated terpendole D (**50**) with the literature values, revealed a close match, confirming the identity of terpendole D (**50**). This is the first time this compound has been isolated from the *E. festucae* var. *lolii* - *L. perenne* association.

Table 3.3: ^{1}H and ^{13}C NMR assignments determined for terpendole D (**50**) in comparison to literature values ($CDCl_3$).[74]

Atom	Current Research			Literature values [74]	
	^{13}C (δ, ppm)		^{1}H (δ, ppm)	^{13}C (δ, ppm)	^{1}H (δ, ppm)
NH			7.75		7.85
2	149.5			149.9	
3	50.6			50.3	
4	39.5			39.5	
5	32.5	Hα	1.93	32.5	1.91
		Hβ	1.56		1.58
6	28.9	Hα	2.22	28.9	2.19
		Hβ	1.76		1.72
7	72.6		3.88	72.5	3.86
9	74.6		3.58	74.6	3.58
10	67.5		4.01	67.5	4.00
10-OH			4.67		4.70
11	59.4		3.49	59.4	3.49
12	65.4			64.9	
13	40.6		2.16	40.6	2.13
14	22.0	Hα	1.70	22.0	1.71
		Hβ	nd[a]		1.07
15	24.1	Hα	1.70	24.1	1.72
		Hβ	1.56		1.57
16	49.5		2.82	49.5	2.78
17	27.2	Hα	2.41	27.2	2.37
		Hβ	2.71		2.70
18	118.0			118.4	
19	125.1			125.0	
20	118.5		7.32	118.5	7.44
21	119.7		7.09	119.6	7.09
22	120.6		7.10	120.5	7.09
23	111.4		7.45	111.5	7.31
24	nd[a]			137.2	
25	14.5		1.03	14.5	1.00
26	16.2		1.10	16.2	1.08
27	79.1			79.1	
28	19.2		1.25	19.2	1.24
29	23.5		1.30	23.5	1.29
31	57.9		3.98	58.0	3.96
33	120.7		5.28	120.6	5.26
34	139.9			139.9	
35	17.9		1.68	17.9	1.66
36	25.7		1.74	25.7	1.71

a: not observed

Hence, the full NMR assignment of terpendole D (**50**) (Figure 3.7) was determined as in Table 3.4.

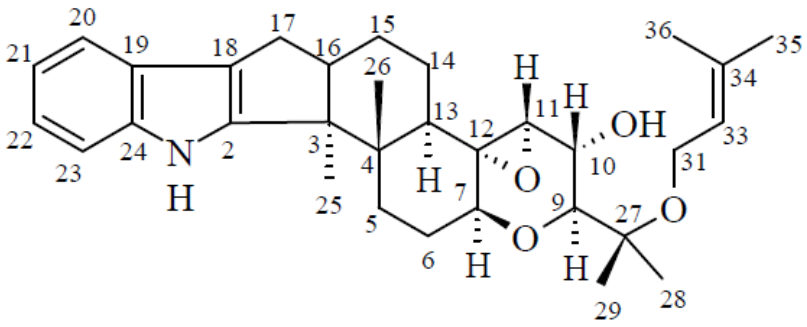

Figure 3.7: The structure of terpendole D (**50**).

Table 3.4: ^{13}C and ^{1}H NMR assignments for terpendole D (**50**) determined in the current research, ($CDCl_3$, 400 MHz).

Atom	**^{13}C (δ, ppm)**		**^{1}H (δ, ppm)**	**Multiplicity (*J* Hz)**
NH			7.75	s
2	149.5[a]			
3	50.6[a]			
4	39.5[a]			
5	32.5	Hα	1.93	td (26.8, 13.5, 4.3)
		Hβ	1.56	s
6	28.9	Hα	2.22	m
		Hβ	1.76	m
7	72.6		3.88	dd (9.8, 7.3)
9	74.6		3.58	d (9.2)
10	67.5		4.01	d (9.5)
10-OH			4.67	s
11	59.4		3.49	s
12	65.4[a]			
13	40.6		2.16	dd (12.6, 3.8)
14	22.0	Hα	1.70	s
		Hβ[b]	1.07	
15	24.1	Hα	1.70	s
		Hβ	1.56	s
16	49.5		2.82	m
17	27.2	Hα	2.41	dd (14.4, 10.8)
		Hβ	2.71	dd (13.1, 6.4)

Atom	^{13}C (δ, ppm)	^{1}H (δ, ppm)	Multiplicity (*J* Hz)
18	116.0		
19	125.1		
20	118.5	7.32	m
21	119.7	7.09	m
22	120.6	7.10	m
23	111.4	7.45	m
24	137.2[b]		
25	14.5	1.03	s
26	16.2	1.10	s
27	79.1		
28	19.2	1.25	s
29	23.5	1.30	s
31	57.9	3.98	d (7.0)
33	120.7	5.28	m
34	139.9		
35	17.9	1.68	s
36	25.7	1.74	s

a: determined by HMBC experiment, b: determined from reference 74.

The HSQC spectrum (Appendix 21) indicated that the chemical shifts of protons H-20 (7.32 ppm) and H-23 (7.45 ppm) in this report are similar to those of H-23 (7.31 ppm) and H-20 (7.44 ppm) respectively in the literature review.[74] The chemical shift of H-20 in this report aligned with that of H-23 in the literature; therefore, it is possible that these protons are misassigned the literature.

Terpendole D (**50**) is the second terpendole compound to be isolated from perennial ryegrass infected with wild-type endophyte. Based on LC-MS analysis, other terpendole-like compounds are also present in this association but are yet to be isolated. Terpendole D (**50**) was tested on porina larvae as part of the current study (Chapter 5).

3.2 Identification and structural elucidation of 13-desoxypaxilline (37).

13-Desoxypaxilline (**37**) was previously isolated from this association by Gatenby and co-workers.[46] It was isolated in this research and its bioactivity against porina larvae determined, therefore the structural information is discussed briefly.

3.2.1 UV Spectroscopy

The UV spectra of 13-desoxypaxilline (**37**) and paspaline (**42**) were similar to that of paxilline (**36**), with peak maxima at 231 nm and 280 nm and a minimum at 253 nm (Figure 3.8), consistent with literature data.[46] An authentic sample of paxilline (**36**) was available from Dr Finch at AgResearch for comparison.

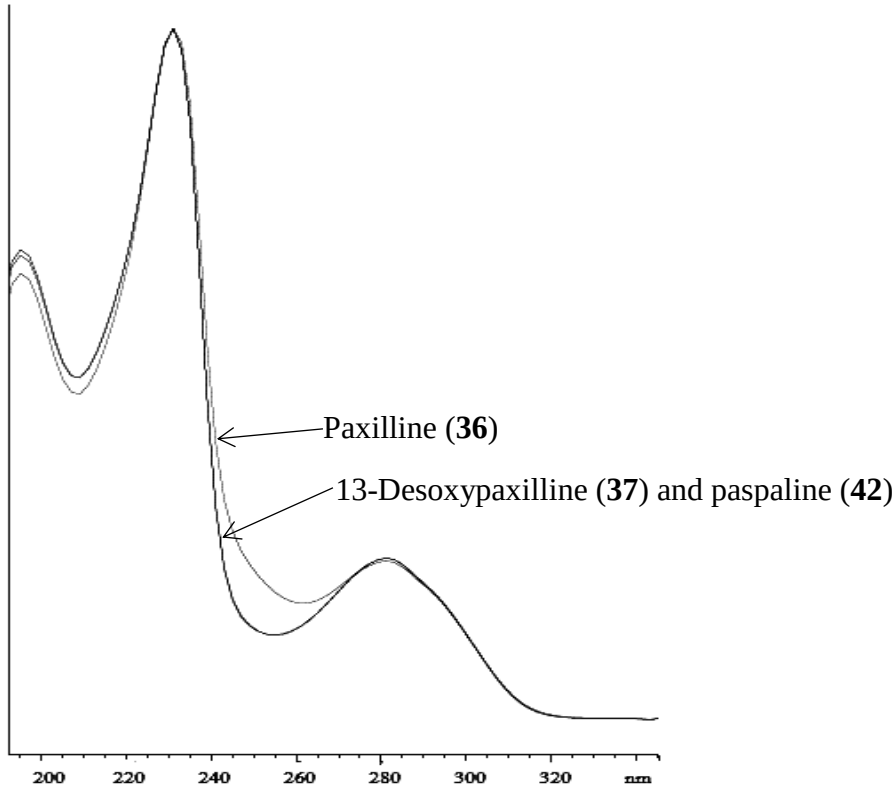

Figure 3.8: The normalised UV absorbance spectra of 13-desoxypaxilline (**37**) and paspaline (**42**) compared to that of paxilline (**36**) obtained from HPLC.

3.2.2 Mass Spectrometry

The high resolution mass spectrum of 13-desoxypaxilline (**37**) exhibited a pseudo-molecular ion of *m/z* 420.2468, consistent with the molecular formula of $C_{27}H_{33}NO_3$ (*m/z* 419.2460). The tandem mass spectrum of 13-desoxypaxilline (**37**) in positive ion mode (Figure 3.9) contained the characteristic fragment ions for indole diterpenoids at *m/z* 182 and 130. Fragment ions of *m/z* 402.2 and 362.2 were produced by loss of the hydroxyl group as water (18 Da) and C_3H_5OH (58 Da) respectively.

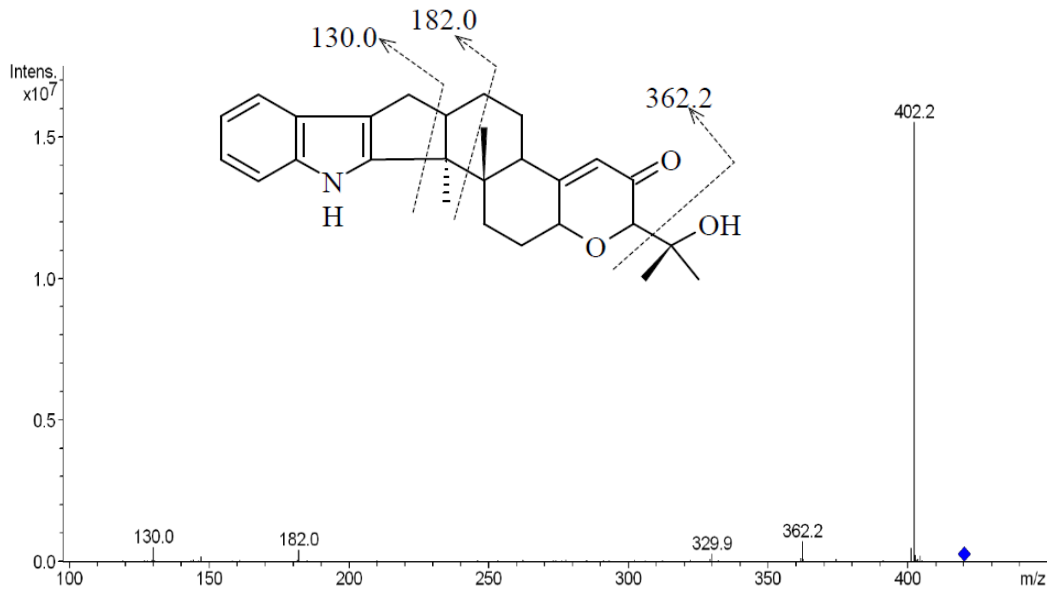

Figure 3.9: The tandem mass spectrum of 13-desoxypaxilline (**37**), *m/z* 420.2 (positive ion mode).

3.2.3 NMR Spectroscopy.

Structural elucidation of 13-desoxypaxilline (**37**) was determined with data acquired from 1D and 2D NMR experiments including ^{1}H, ^{13}C, DEPT-135, HSQC and HMBC experiments (Appendices 23 – 28). The NMR data were compared with the NMR data in the literature [46] which showed good consistency (Figure 3.10 and Table 3.5).

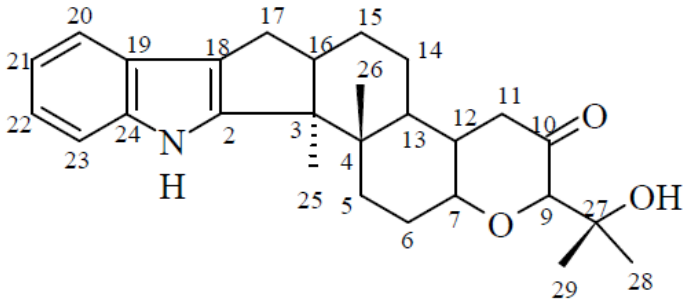

Figure 3.10: The structure of 13-desoxypaxilline (**37**).

Table 3.5: ^{13}C and ^{1}H NMR assignments for 13-desoxypaxilline (**37**) isolated in the current research compared with the literature values.[46]

Atom	In this research ($CDCl_3$, 400 MHz) ^{13}C (δ ppm)		^{1}H(δ ppm)	Literature values[46] ($CDCl_3$, 300 MHz) ^{13}C (δ ppm)	^{1}H (δ ppm)
NH			7.78	-	7.76
2	149.2		-	149.2	-
3	50.5		-	50.5	-
4	42.4		-	42.4	-
5	32.8	Hα Hβ	2.16 1.75	32.9	2.13 1.71
6	29.9	Hα Hβ	2.33 1.95	30.0	2.31 1.95
7	74.7		4.31	74.8	4.28
9	82.6		3.76	82.6	3.73
10	198.2		-	198.3	-
11	121.8		5.90	121.9	5.88
12	168.5		-	168.2	-
13	42.5		2.47	42.6	2.45
14	25.5	Hα Hβ	1.73 1.56	25.5	1.74 1.55
15	24.1	Hα Hβ	1.74 1.85	24.1	1.70 1.87
16	48.9		2.85	48.9	2.81
17	27.3	Hα Hβ	2.44 2.76	27.3	2.41 2.74
18	118.6			118.6	-
19	124.9		-	125.0	-
20	118.6		7.46	118.6	7.43
21	119.9		7.12	119.9	7.09
22	120.9		7.14	120.9	7.09
23	111.5		7.33	111.6	7.31

Atom	In this research ($CDCl_3$, 400 MHz) ^{13}C (δ ppm)	^{1}H(δ ppm)	Literature values[46] ($CDCl_3$, 300 MHz) ^{13}C (δ ppm)	^{1}H (δ ppm)
24	140.0	-	140.0	-
25	14.6	1.10	14.6	1.08
26	16.3	1.03	16.3	1.00
27	72.4	-	72.4	-
27-OH				4.22
28	26.7	1.32	26.7	1.30
29	24.1	1.30	24.2	1.28

3.3 Identification and structural elucidation of paspaline (42).

Paspaline (**42**) was also previously isolated from this association by Gatenby and co-workers.[46] It was isolated in this research and the bioactivity against porina larvae determined.

3.3.1 Mass Spectrometry

The high resolution mass spectrum of paspaline (**42**) exhibited a pseudo-molecular ion at *m/z* 422.2985, consistent with the molecular formula of $C_{28}H_{39}NO_2$ (*m/z* 421.2981). The tandem mass spectrum of paspaline (**42**) in positive ion mode (Figure 3.11) contained the characteristic fragment ions of an indole diterpenoid (*m/z* 182 and 130) and an ion at *m/z* 406.2 resulting from loss of water.

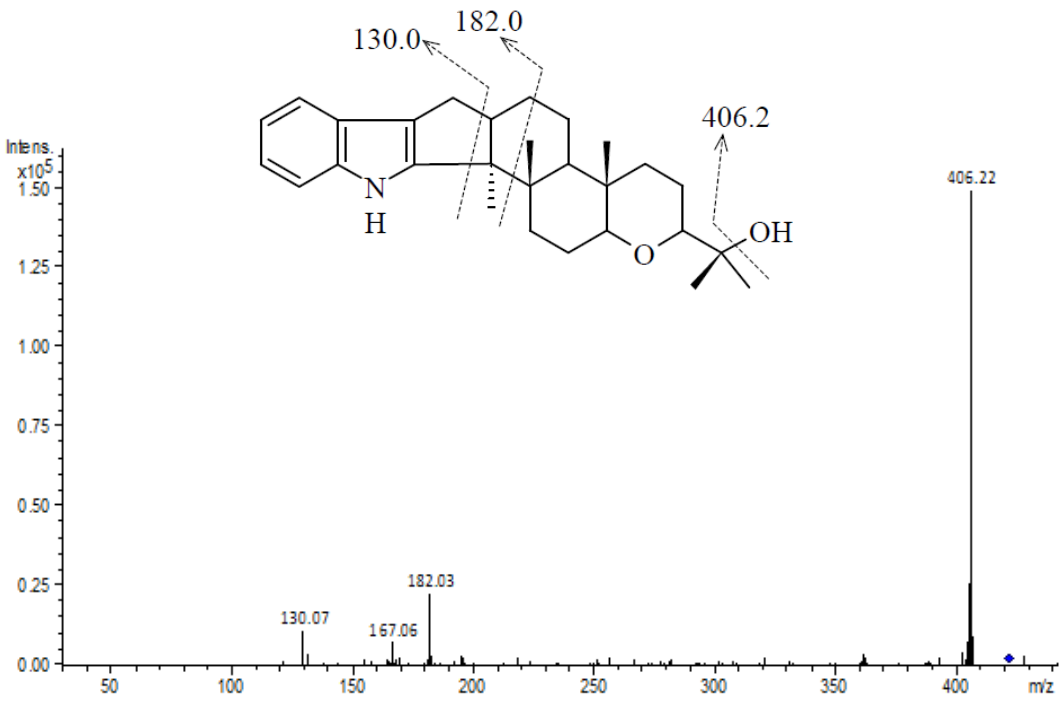

Figure 3.11: The tandem mass spectrum of paspaline (**42**), *m/z* 422.2 (positive ion mode).

3.3.2 NMR Spectroscopy

The NMR data of paspaline (**42**) were acquired with both 1D and 2D NMR experiments such as ^{1}H, ^{13}C, DEPT-135, HSQC and HMBC experiments (Appendices 29 – 34). The NMR assignment was compared with that of Gatenby and co-workers[46] and was found to match very closely (Figure 3.12 and Table 3.6).

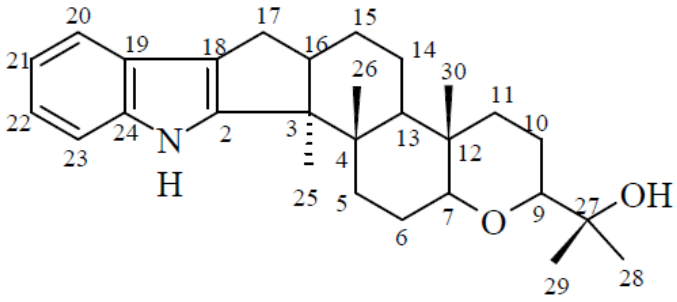

Figure 3.12: The structure of paspaline (**42**).

Table 3.6: ^{13}C and ^{1}H NMR assignments of paspaline (**42**) isolated in the current research compared with literature values.[63]

Atom	In this research (CDCl$_3$, 400 MHz)			Literature values[63] (CDCl$_3$, 300 MHz)	
	^{13}C (δ ppm)		^{1}H (δ ppm)	^{13}C (δ ppm)	^{1}H (δppm)
NH			7.74		7.81
2	150.8			150.9	-
3	53.0			53.8	-
4	40.0			40.1	-
5	33.9	Hα	1.99	34.0	1.96
		Hβ	1.64		1.63
6	24.6	Hα	1.73	24.7	1.72
		Hβ	1.81		1.82
7	85.7		3.04	85.8	3.04
9	84.7		3.23	84.8	3.23
10	22.0	Hα	1.48	22.0	1.45
		Hβ	1.69		1.66
11	37.6	Hα	1.14	37.7	1.14
		Hβ	1.84		1.85
12	36.5		-	36.6	-
13	46.5		1.49	46.5	1.50
14	21.9	Hα	1.48	22.0	1.46
		Hβ	1.69		1.69
15	25.3	Hα	1.63	25.3	1.61

Atom	In this research ($CDCl_3$, 400 MHz)		Literature values[63] ($CDCl_3$, 300 MHz)	
	^{13}C (δ ppm)	^{1}H (δ ppm)	^{13}C (δ ppm)	^{1}H (δppm)
	Hβ	1.78		1.79
16	48.7	2.78	48.8	2.76
17	27.5	2.35	27.6	2.34
		2.67		2.68
18	118.3		118.3	-
19	125.1		125.2	-
20	118.4	7.44	118.4	7.43
21	119.5	7.10	119.4	7.08
22	120.4	7.08	120.5	7.08
23	111.4	7.29	111.5	7.30
24	139.9	-	140.0	-
25	14.6	1.05	14.6	1.03
26	19.9	1.16	20.0	1.14
27	71.9	-	72.0	-
28	23.7	1.20	23.8	1.19
29	26.1	1.22	26.1	1.21
30	12.7	0.91	12.7	0.88

3.4 Identification and structural elucidation of a potential emindole analogue.

During the semi-preparative HPLC of terpendole D (**50**), an earlier eluting fraction was collected. LC-MS indicated that this early eluting fraction contained a compound with parent ion of *m/z* 406.2, consistent with that of an emindole analogue.

Emindoles are the smallest known indole diterpenoids. Four known analogues of emindole with a molecular mass of 405 are emindole SB (**46**),[66] emeniveol (**74**)[134] emindole DA (**75**)[135] and emindole SA (**76**).[136]

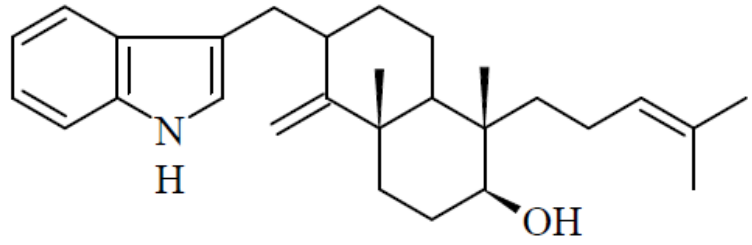

(**74**)

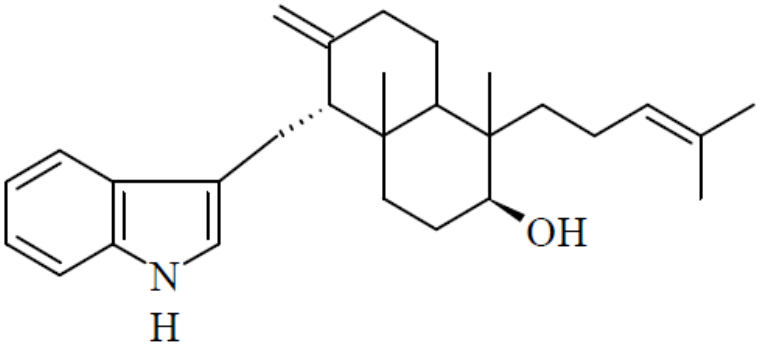

(**75**)

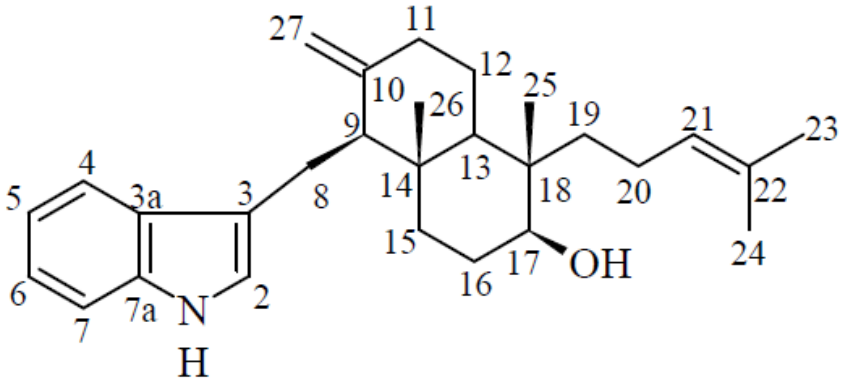

(**76**)

Emindole SB (**46**) has been previously isolated from the mycelium of *C. paspali*,[66] *E. striata*,[62] *A. yamanashiensis*[67] and *P. paxilli*[137] and it is a precursor to paspaline (**42**) in the biosynthetic pathway. Analogues of emindole have never been reported from the wild-type endophyte and the detection of such a compound would be consistent with the proposed biosynthetic pathway.

3.4.1 Mass Spectrometry

Low resolution ESI-MS of the possible emindole analogue showed a parent ion of *m/z* 406.2, consistent with a molecular formula of $C_{28}H_{39}NO$.

The tandem mass spectrum contained the characteristic fragment ion $[C_9H_8N^+]$ at *m/z* 130, indicating the presence of the indole moiety. The fragment ion at *m/z* 144 could represent an extra methylene attached to $[C_9H_8N^+]$ (Figure 3.13). The loss of a hydroxyl group as water (18 Da) resulting in a fragment ion *m/z* at 388.3, indicated that there was only one hydroxyl group in the compound.

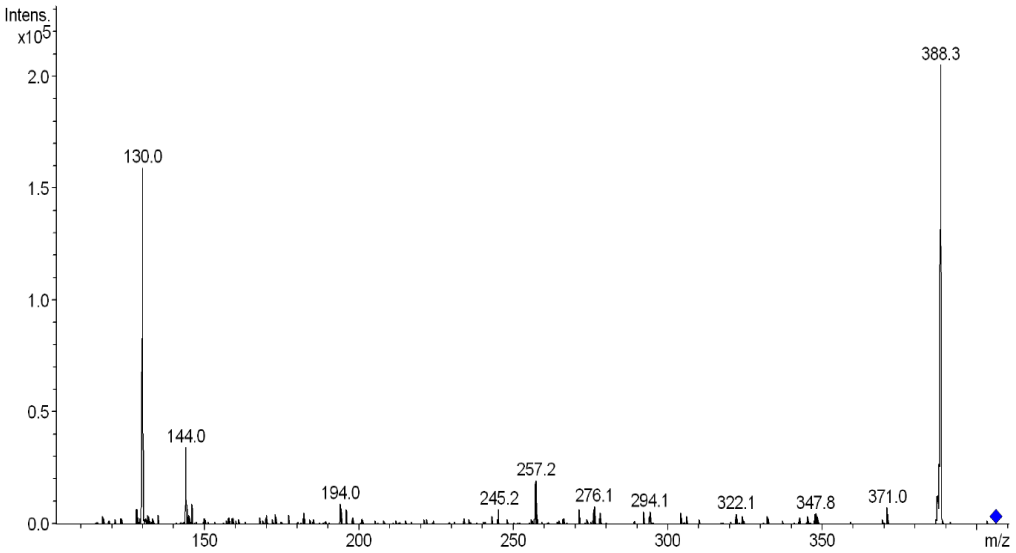

Figure 3.13: The tandem mass spectrum of the emindole analogue *m/z* 406.2, (positive ion mode).

3.4.2 NMR Spectroscopy

The compound was subjected to NMR analysis but due to the limited amount of compound isolated, only a ^{1}H NMR spectrum (Appendix 35) was acquired.

The presence of an indole moiety was indicated by aromatic proton signals as doublets at 7.59 and 7.35 ppm, triplets at 7.13 and 7.12 ppm and an NH proton at 7.96 ppm in the ^{1}H NMR spectrum (Appendix 35). Another aromatic proton signal at 6.99 ppm could also be part of the indole moiety. A triplet proton signal at 5.07 ppm could be a methine proton of a prenyl moiety and singlets at 4.77 and 4.76 ppm indicated that the compound could contain methylene and/or oxygenated protons. These proton signals were not present in the literature data of emindole SB (**46**),[66] hence this potential emindole could have a different structure. The four strong singlet signals at 1.67, 1.52, 1.13 and 0.81 ppm could represent four methyl groups in the compound and the other upfield proton signals (0.80 – 3.00 ppm) could represent methylene and methine protons in the potential emindole analogue. Since there was no other NMR data available, these upfield proton signals cannot specifically be assigned. In order to assist the determination of some of the structural features of the potential emindole analogue, the acquired ^{1}H NMR data were compared to the literature NMR data of emeniveol (**74**)[134] and emindoles DA (**75**)[135] and SA (**76**)[136] (Table 3.7). The numbering systems used for the known emindole analogues were not consistent, therefore the system used in Table 3.7 was that used for the ^{1}H NMR data of emindole SA (**76**).[136]

The comparison of the ^{1}H NMR data of the analogues (Table 3.7) enabled the proposed allocation of chemical shifts for some of the protons of the potential emindole analogue isolated in this report. The compound contained an indole-3-methyl group. The proton signal at 6.99 ppm was allocated as H-2 as it closely matches the H-2 proton signals of emeniveol (**74**)[134], emindoles DA (**75**)[135] and SA (**76**).[136] This was not reported in emindole SB (**46**),[66] hence C-2 of the potential emindole analogue is not a quaternary carbon.

Table 3.7: The proposed ^{1}H NMR assignments of the potential emindole analogue compared to the literature values of emeniveol (**74**), emindoles DA (**75**) and SA (**76**).[134-136]

Atom		**^{1}H (δ, ppm)**			
		Emeniveol (74)[134]	**Emindole DA (75)[135]**	**Emindole SA (76)[136]**	**Potential emindole analogue**
NH		7.98	7.87	7.88	7.96
2		6.93	6.89	6.89	6.99
4		7.56	7.56	7.62	7.59
5		7.10	7.08	7.11	7.12
6		7.18	7.16	7.17	7.13
7		7.33	7.33	7.31	7.35
8	Hα	3.11	3.13	2.98	3.15
	Hβ	2.56	2.70	2.82	2.58
9		2.58	2.06	2.19	2.60
10	Hα	0.91			
	Hβ	1.77			
11	Hα	1.48	2.28	1.98	2.19
	Hβ	1.48	2.18	2.39	2.38
12	Hα	1.12	1.42	1.59 – 1.66	1.30 – 1.70
	Hβ	1.12	1.58 – 1.65	1.36 – 1.47	1.30 – 1.70
13			1.73 – 1.76	1.35	1.30 – 1.70
15	Hα	1.65	1.32	2.05	1.30 – 2.07
	Hβ	1.65	1.94 – 2.02	1.35 – 1.43	1.30 – 2.07
16	Hα	1.60	1.73 – 1.80	1.63 – 1.79	1.60 – 1.80
	Hβ	1.77	1.73 – 1.80	1.63 – 1.79	1.60 – 1.80
17		3.52	3.62	3.59	3.56
19	Hα	1.22	1.34 – 1.40	1.24 – 1.33	1.30 – 1.60
	Hβ	1.45	1.51 – 1.59	1.47 – 1.56	1.30 – 1.60
20	Hα	1.80	1.96 – 2.06	1.80 – 1.95	1.80 – 2.06
	Hβ	1.80	1.96 – 2.06	1.80 – 1.95	1.80 – 2.06
21		5.04	5.16	5.09	5.07
23		1.57	1.67	1.61	1.57
24		1.65	1.71	1.68	1.67
25		0.78	0.83	0.81	0.81
26		1.10	0.98	0.87	1.11
27		4.73	4.51	4.84	4.76
		4.75	4.16	4.72	4.77

An exocyclic methylene group was also determined to be in the compound. The proton signals at 4.77 and 4.76 ppm were closely aligned with those of the H-27 methylene protons of emeniveol (**74**), emindoles DA (**75**) and SA (**76**).[134-136] It was not clear whether this exocyclic methylene group is attached to C-10 as in emindole

SA (**76**) or C-14 as in emeniveol (**74**). The chemical shifts of the H-11 protons of emindole SA (**76**)[136] and DA (**75**)[135] were similar to the proton signals at 2.19 and 2.38 ppm of the potential analogue. These signals were not present in emeniveol (**74**),[134] indicating that the exocyclic methylene could be at C-10 of the compound.

The proton signal at 3.56 ppm closely matches those of H-17 of emeniveol (**74**), emindoles SA (**76**) and DA (**75**) (Table 3.7), indicating that a hydroxyl group is attached to C-17 of the compound, which is consistent with the loss of a hydroxyl group as water in the tandem mass spectrum (Figure 3.13). The proton signal at 5.07 ppm of the compound was assigned as H-21 because it aligns with the chemical shift of this proton in the literature. This proton signal was a triplet, indicating that the neighbouring carbon is likely a methylene. In addition, the proposed methyl proton signals at 1.57 and 1.67 ppm were similar to the proton signals of the aliphatic methyl groups H-23 and H-24 of the known compounds as reported in the literature, therefore indicating that the unknown compound could also contain a prenyl moiety. Based on the limited information, the structure of the unknown compound could be very similar to that of emindoles SA (**76**) and DA (**75**) and on account of the variations in the chemical shifts, it could be an isomer of either SA (**76**) or DA (**75**).

However, in the ^{1}H NMR spectrum (Appendix 35), there were proton signals at 3.85 – 4.40 ppm which did not match the literature values of any of the known compounds. These signals indicated than an electron-withdrawing group could be around these protons but due to the limited NMR information, it was not clear whether these signals belong to the unknown compound or are due to a contaminant. Contamination peaks from the NMR solvent such as those at 7.02, 7.35 and 7.55 ppm were also observed.

3.5 Discussion

The isolation of terpendole D (**50**), is only the second terpendole to be reported from this association, indicating that the wild-type endophyte has the capacity to produce more terpendole compounds. The diversity of biosynthetic intermediates produced by this endophyte is supported by the isolation of the known paspaline (**42**) and 13-desoxypaxilline (**37**) as well as the potential emindole analogue mentioned above and further indole diterpenoid intermediates indicated by LC-MS analysis (Chapter 4). Some of these compounds were easily detectable by LC-MS but were not present in sufficient quantities to be isolated as pure compounds. Some were isolated in trace quantities only, providing insufficient material to produce any NMR data.

The isolated terpendole D (**50**), paspaline (**42**) and 13-desoxypaxilline (**37**) were used in experiments on porina larvae to identify any bioactivity against this pasture pest (Chapter 5).

The NMR analysis of the potential emindole analogue requires future work. The isolation of a pure sample is needed so that the complete structure can be determined, which will yield useful information in terms of the biosynthetic pathway and bioactivity.

In 1988, Nozawa and co-workers[136] proposed possible biosynthetic pathways for emindoles and paxilline (**36**). These pathways involved cyclisation processes in the early stages of the biosynthesis, which could explain the diversity of indole diterpenoid intermediates. A better understanding of the pathways, especially at the early stages of the biosynthetic process could also explain the structural complexity of compounds A – D (**64** – **67**) in Chapter 2. Could it be possible that oxidation and other biosynthetic processes involved in the formation of compounds A – D (**64** – **67**) occurred during the early biosynthetic pathway? It is currently unknown and requires more work in the future.

Chapter 4: LC-MS analysis of crude extract.

LC-MS is an analytical chemistry technique involving a physical separation via Liquid Chromatography (LC) and mass analysis by using Mass Spectrometry (MS). Often components in a mixture are first ionised (ESI-MS for example) to generate a mixture of ions. Precursor or parent ions of a specific mass-to-charge ratio (*m/z)* are selected (MS^1) and then further fragmented to generate product ions (MS/MS or MS^2) in tandem mass spectrometry. Sometimes, selected product ions are further fragmented to produce another set of product ions (MS^3). The pattern of fragmentation ions yields structural information as to the substructures present in the compound.

The early pathway indole diterpenoids are characterised by fragment ions at *m/z* 182.0 [$C_{13}H_{12}N^+$] and 130.0 [$C_9H_8N^+$] in tandem mass spectrometry as in Figure 4.1. These fragment ions indicate the presence of the indole moiety. Compounds were selected based on these characteristic fragment ions and molecular masses and retention times were noted as indicators of potential indole diterpenoids.

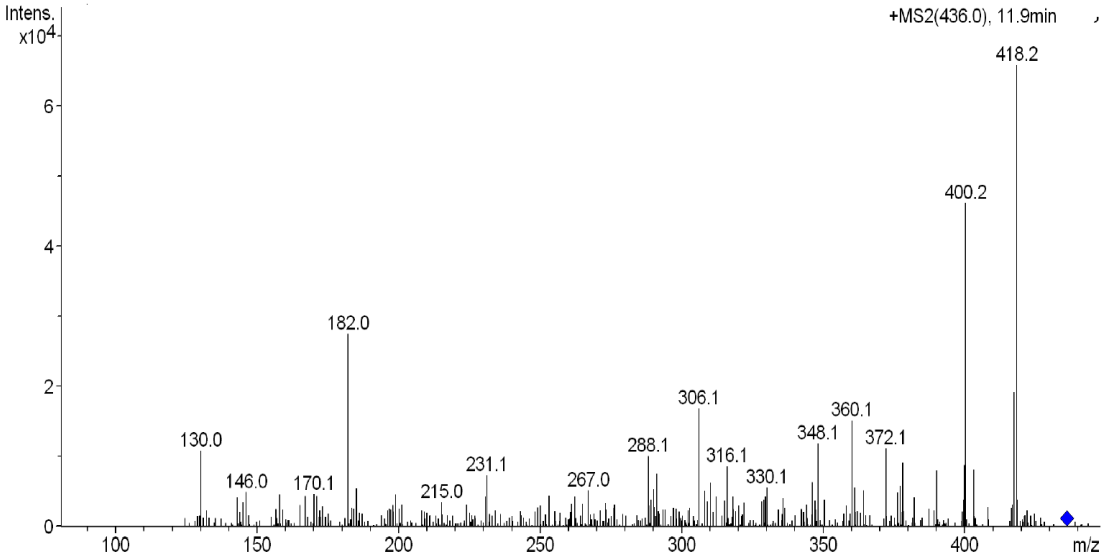

Figure 4.1: Tandem mass spectrum of a potential indole diterpenoid, retention time 11.9 min, *m/z* = 436.0 (positive ion mode).

Compounds A – D (**64** – **67**) did not possess the above indole diterpenoid characteristic ions but were structurally related to terpendole C (**49**) and lolitrem B (**3**). Based on the similar fragmentation patterns, further potential analogues were observed in the crude extract.

4.1 Indole diterpenoid alkaloids.

The LC-MS analysis of the pre-lolitrem crude extract using the protocol in Section 7.4, indicated the presence of potential indole diterpenoid alkaloids within the mass region 400 - 650 Da (positive ion mode). Some of these compounds possessed the same molecular masses but had different retention times (Figure 4.2), hence could be isomers.

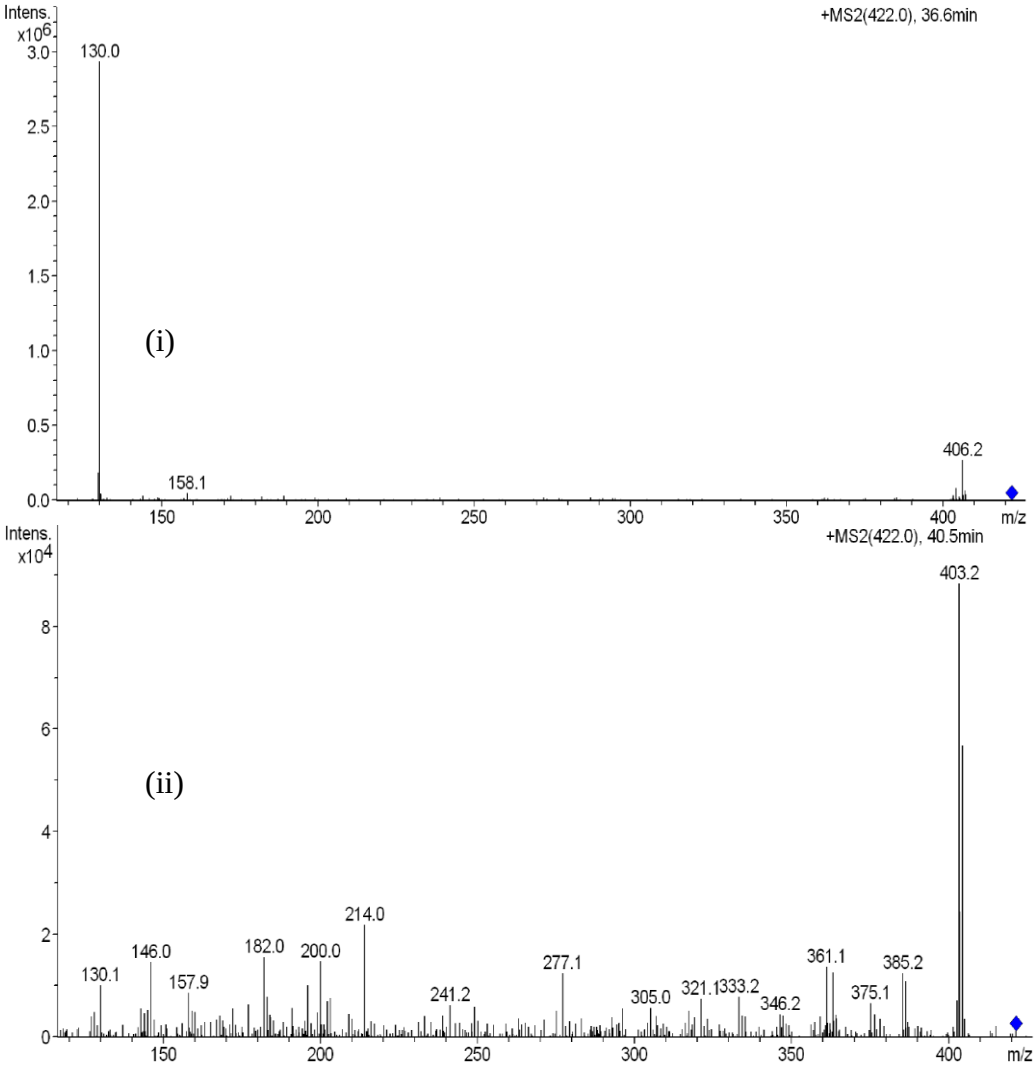

Figure 4.2: Tandem mass spectra of indole diterpenoids *m/z* 422.0, retention time (i) 36.6 and (ii) 40.5 minutes (positive ion mode).

The presence of the characteristic fragment ions *m/z* 182 and/or 130 in the tandem mass spectrum implied that the compounds were potential indole diterpenoids expressed in perennial ryegrass when infected with wild-type endophyte. These potential indole diterpenoids are listed in Table 4.1 with selected MS^2 product ions.

Table 4.1: The potential indole diterpenoid alkaloids and selected tandem mass fragmentation ions from LC-MS analysis of the crude extract.

Parent ions $[M+H]^+$	**Relative signal intensity (%)**	**Retention time (min)**	**Selected MS^2 product ions**
[a]406.0	85.6	34.4	388.3, 257.2, 144.0, 130.0
406.0	56.9	35.9	388.2, 280.1, 182.0, 144.0, 130.0
[b]420.0	100	25.1	402.2, 182.0, 130.0
[c]422.0	100	36.6	406.2, 130.0
422.0	94.2	40.5	403.2, 385.0, 182.0, 146.0, 130.0
436.0	100	9.8	417.2, 400.1, 378.1, 360.1, 182.0, 146.0, 130.0
[d]436.0	100	19.5	418.2, 400.1, 378.1, 360.1, 182.0, 146.0, 130.0
436.0	68.6	23.5	418.2, 400.1, 378.1, 360.1, 182.0, 146.0, 130.0
436.0	31.7	31.7	417.1, 400.1, 378.1, 360.1, 182.0, 146.0, 130.0
454.0	100	11.8	436.2, 418.2, 400.2, 318.1, 182.0, 130.0
[e]506.0	90.4	36.5	490.3, 470.3, 438.2, 420.2, 402.2, 320.2, 198.1, 182.1
522.0	100	33.6	504.3, 454.2, 436.2, 418.2, 400.2, 382.1, 182.0
522.0	46.7	40.7	504.3, 486.2, 454.2, 436.2, 418.2, 400.2, 382.2, 318.1, 182.1
536.0	71.8	27.5	518.2, 500.2, 452.2, 434.2, 416.2, 182.0
536.0	42.4	42.4	518.2, 500.2, 452.2, 434.2, 416.2, 398.1, 182.0
554.0	30.2	34.6	536.2, 517.3, 489.3, 469.1, 451.1, 433.1, 415.1

a= potential emindole analogue in Section 3.4, b = 13-desoxypaxilline (**37**), c = paspaline (**42**), d = paxilline (**36**), e = terpendole D (**50**).

Some of the selected MS^2 ions were present in many other potential indole diterpenoids and knowing the common structural features of these ions will assist the structural elucidation of these compounds.

Two potential emindole compounds with *m/z* 406.0 were noted in the analysis. Based on the observed MS^2 fragment ions, these compounds likely differ in structure. Each could contain a single oxygen atom due to the formation of a fragment ion at *m/z* 388.3, which could result from the loss of a hydroxyl group as water (18 Da). Both compounds yielded the characteristic ion at *m/z* 130 and in addition, gave an *m/z* 144 [$C_9H_8N^+ + CH_2$] ion, which could be formed from an extra methylene group added to the *m/z* 130 ion (Figure 4.3).

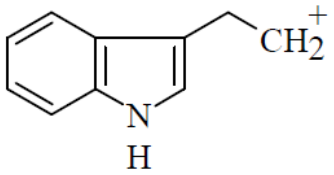

Figure 4.3: The structure of the fragment ion at *m/z* 144.0 from the tandem mass spectrum of the emindole analogue (positive ion mode).

The fragment ion at *m/z* 182 appeared in the tandem mass spectrum of the compound which eluted after 35.9 minutes but not the compound which eluted earlier (*m/z* $[M+H]^+$ = 406.0 at 34.4 minutes). The absence of the *m/z* 182 ion indicated that this emindole analogue could contain C-2 as a methine with a similar structure to that of emindole SA (**76**) (Section 3.4). In contrast, the other potential analogue with the *m/z* 182 ion could contain a quaternary C-2 as in emindole SB (**46**).

A compound with a similar molecular mass to that of paspaline (**42**) (*m/z* 422.0) eluted after 40.5 minutes. The tandem mass spectrum contained a fragment ion at *m/z* 403.2 which represents a loss of 19 Da. This could be due to the loss of a hydroxyl group as water plus another hydrogen atom [H_2O + H]. Another water molecule was lost and yielded an *m/z* 385 ion. This indicated that this compound could contain at least two oxygen atoms. The occurrence of alkaloids with a similar

molecular mass to paxilline (**36**) (*m/z* 436.0) indicated that these compounds could be isomers with different stereochemistry around some centres. However, paxilline (**36**) and paspaline B (**43**) shared the same molecular masses but differed in the substituents at C-9 and C-12. Paspaline B (**43**) has not been reported from wild-type endophyte and could be one of these compounds but was not confirmed in this analysis. An unidentified ion of *m/z* 436 reported by Saikia and co-worker in 2012,[83] may be consistent with the observation in this analysis. To propose potential structures for some of the common fragment ions seen in the MS^2 tandem mass spectra of the potential indole diterpenoids, the structure of paxilline (**36**) was used (Figure 4.4).

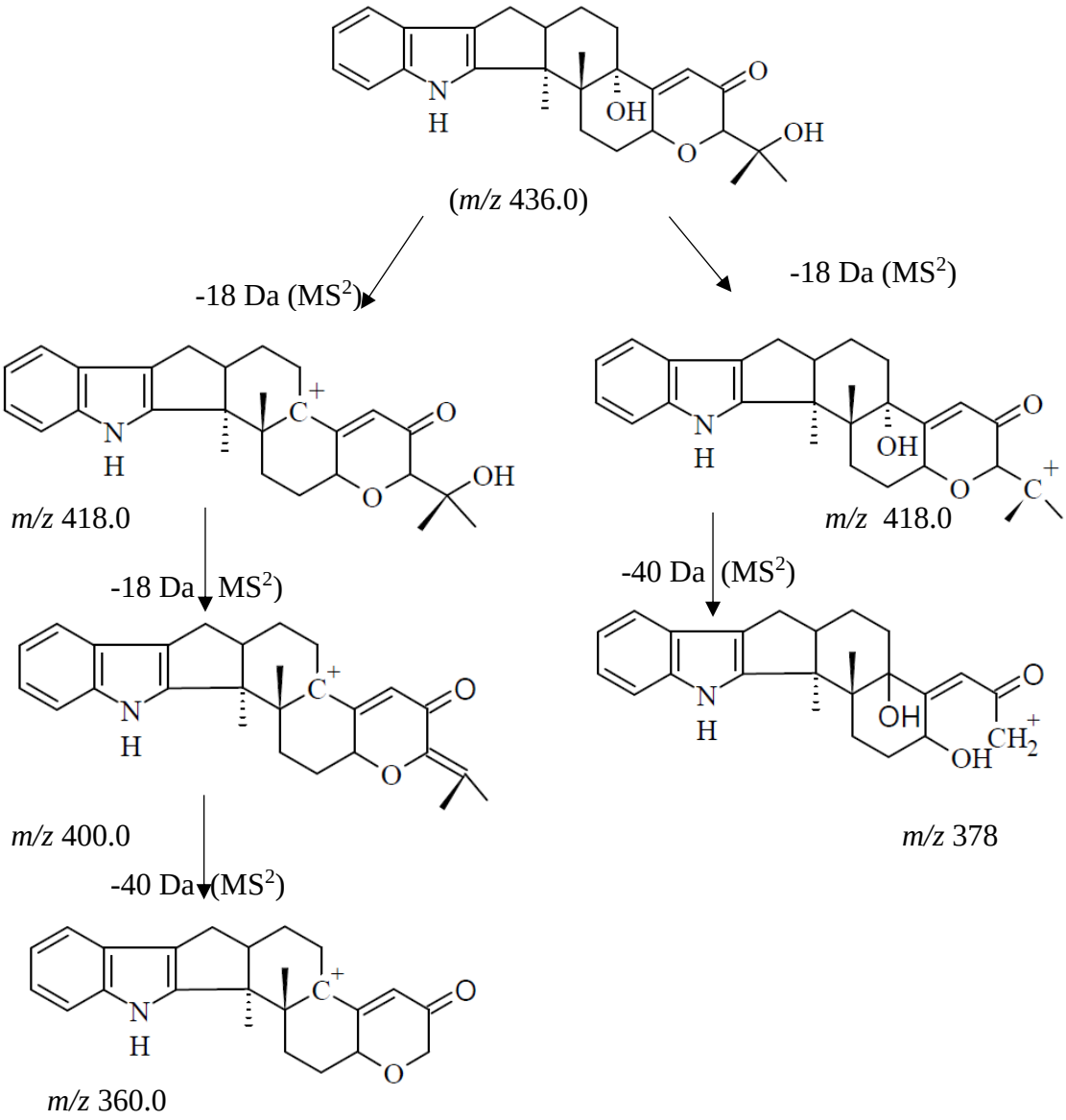

Figure 4.4: The potential structures of selected MS^2 fragment ions observed for paxilline (**36**) (positive ion mode).

The presence of the parent ions at *m/z* 454, 522 and 536 could indicate the presence of terpendoles I (**55**)[75], J (**53**)[75] and M (**59**)[46] respectively. This could not be confirmed but did indicate that further terpendole analogues could be expressed by wild-type endophyte in addition to terpendoles M (**59**)[46] and D (**50**).

4.2 Analogue of compounds A – D (64 – 67).

The LC-MS analysis indicated that a further analogue of compounds A – D (**64** – **67**) could be in the extract. The base peak chromatogram of the parent ions resulting from these compounds (*m/z* 636) often shows two strong peaks of about 100 Da difference (Figure 4.5). The 100 Da difference could be attributed to the loss of the C-2 substituent in the compounds

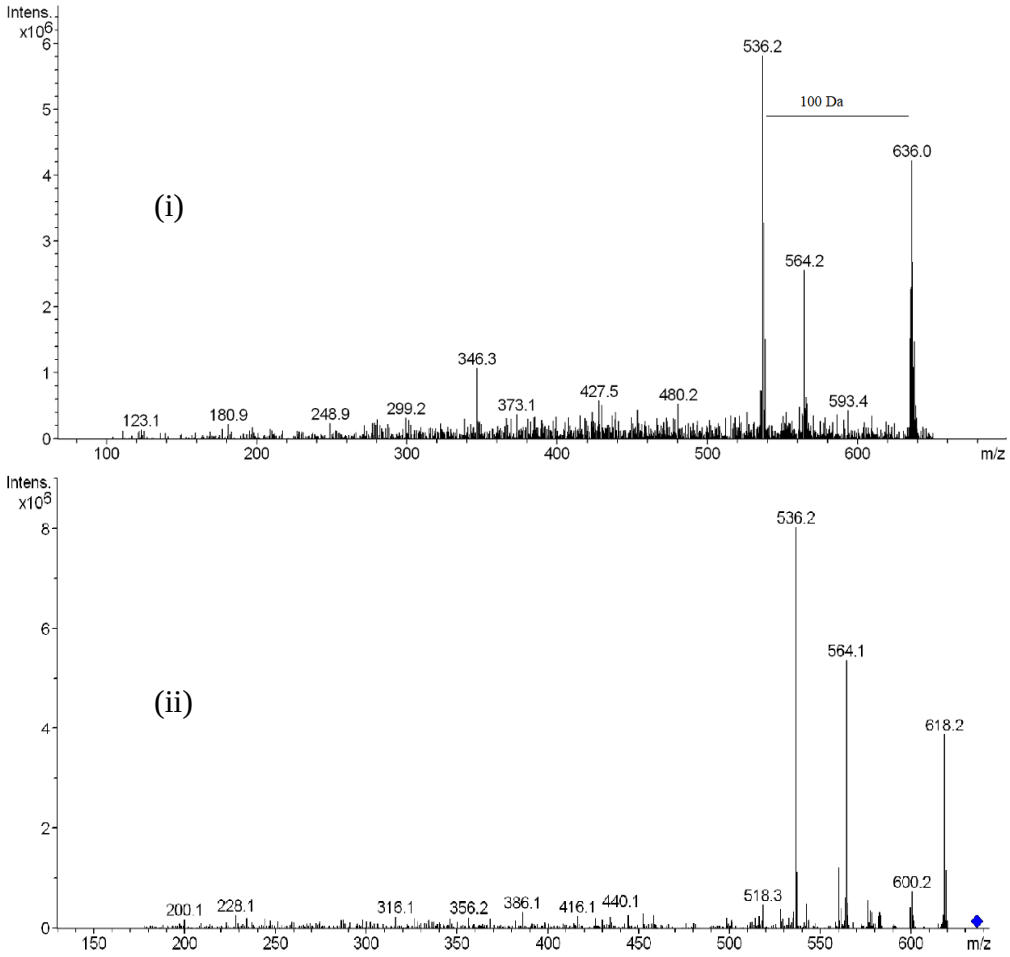

Figure 4.5: The common (i) base peak LC-MS chromatogram of *m/z* 636 and (ii) resulting tandem mass spectrum (positive ion mode) of compound A (**64**).

Under tandem mass spectrometry, typical indole diterpenoid fragment ion(s) such as *m/z* 130 and 182 were not observed, indicating the absence of the indole moiety in these compounds. Most of the fragment ions resulted from losing hydroxyl as water. Based on a similar fragmentation pattern to compound A (**64**), another potentially related compound was detected with a molecular ion at *m/z* 652.0 (Table 4.2).

Table 4.2: Analogues of compound A (**64**) detected via LC-MS analysis.

Parent ions $[M+H]^+$	**Relative signal intensity (%)**	**Retention time (min)**	**Selected MS^2 product ions**
[a]594.0	92.3	35.0	494.2, 536.3, 558.4, 576.4
[b]636.0	89.4	28.6	618.4, 600.3, 576.4, 564.3, 536.3
[c]636.0	82.0	29.2	618.4, 600.3, 576.4, 564.3, 536.3
[d]636.0	98.5	37.8	618.2, 600.2, 564.1, 536.2
652.0	90.2	24.7	634.4, 616.4, 576.5, 552.3

a = compound C (**66**), b = compound B (**65**), c = compound A (**64**), d = compound D (**67**).

The fragmentations of compounds A – D (**64** – **67**) are discussed in Chapter 2 and the structural features of the resulting fragment ions for compound A (**64**) were proposed (Figure 4.6). The proposed substructure of the fragmentation ions of compound A (**64**) could be used to predict the possible structural features of the analogue.

The tandem mass spectrum of the unknown analogue ion at *m/z* 652 indicated that at least two oxygen atoms are present in the compound. The loss of a hydroxyl group as water (18 Da) resulted in the formation of a fragment ion *m/z* 634.4 and loss of another water molecule (18 Da) resulted in the *m/z* 616.4 ion. The fragment ion at *m/z* 576.5 resulted from a 76 Da loss from the molecular ion. A similar fragment ion was observed in the tandem mass spectra of compounds A (**64**) and B (**65**) which may indicate a common structural feature of this analogue with compounds A (**64**) and B (**65**). A loss of 100 Da from the parent ion (*m/z* 652.0) resulted in the daughter fragment ion at *m/z* 552.3, similar to the loss of the 100 Da from parent ions observed in the tandem mass spectra of compounds A (**64**) and B (**65**).

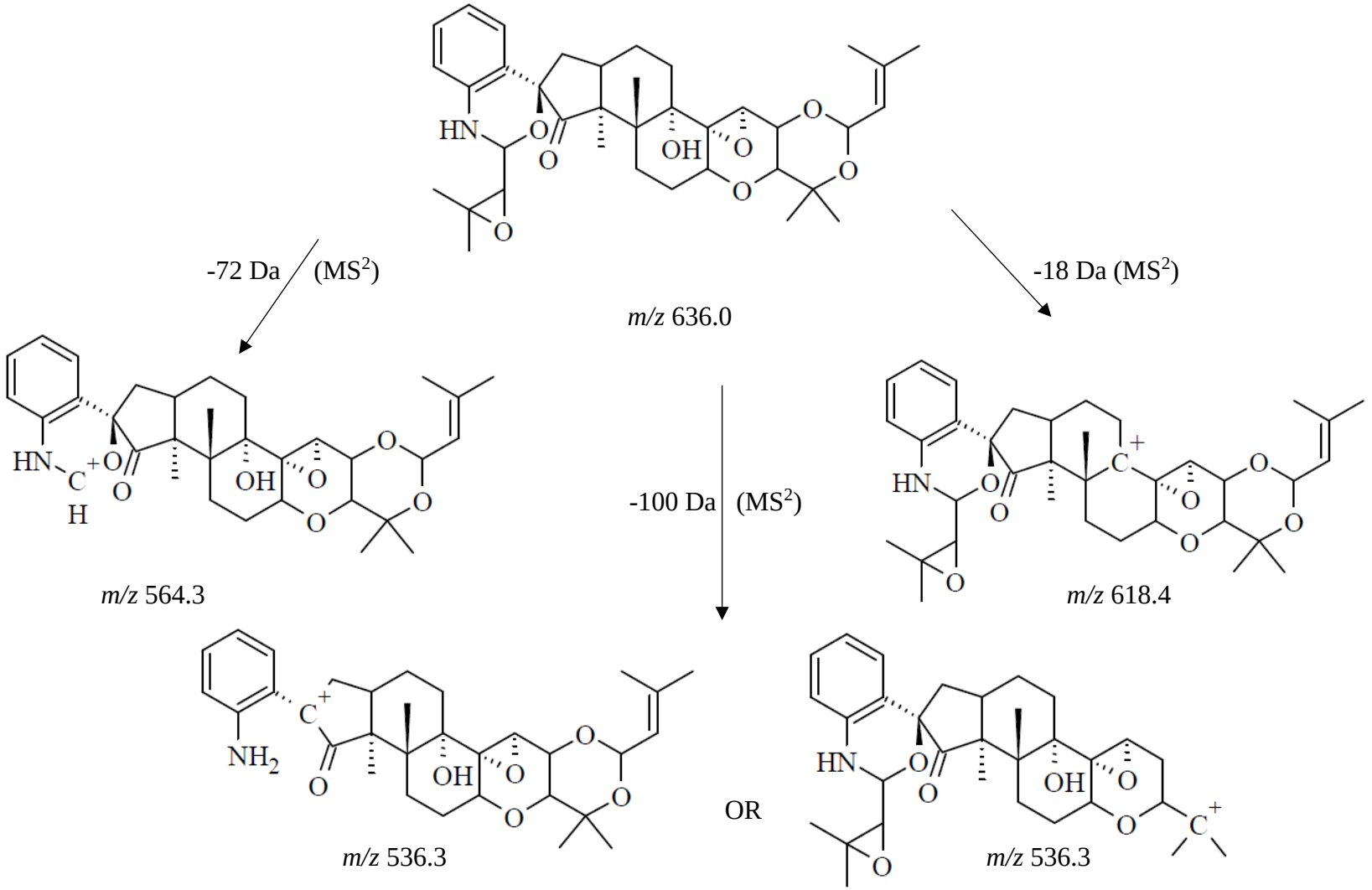

Figure 4.6: The structures of selected MS^2 fragment ions of compound A (**64**), (positive ion mode).

4.3 Discussion

The LC-MS analysis indicated that there are more potential indole diterpenoids which are yet to be isolated. This reflects the diversity of indole diterpenoid intermediates that the wild-type endophyte is capable of expressing in perennial ryegrass. Some of these compounds were present in very small amounts in the crude sample, making it impossible to purify a reasonable amount for structural analysis. Quantitative analysis of a fresh extract of perennial ryegrass seed infected with wild-type endophyte is required so that the actual proportion of these potential indole diterpenoid intermediates expressed can be determined. This analysis would also confirm whether compounds A – D (**64** – **67**) and their potential analogues are artefacts or a new group of natural products. These compounds are not classified as indole diterpenoids because the indole moiety is not present.

Detection of another potential analogue of compound A (**64**) via LC-MS analysis implying that more such compounds could be present in the crude extract. The similar fragmentation pattern of this compound and compounds A (**64**) and B (**65**) indicating that the unknown compound could be a modified version of terpendole J (**56**), similar to the proposed modification of terpendole C (**49**) to form compounds A (**65**) and B (**65**).

The molecular ion of terpendole J (**56**) is *m/z* 522 and the addition of 100 Da and opening up of the indole region would result in a compound of molecular ion at *m/z* 622.0. However, further work is required to confirm this.

Chapter 5: Bioactivities of selected indole diterpenoids and related compounds against porina larvae.

The majority of the strains of *E. festucae* var. *lolii* that infect perennial ryegrass produce the alkaloids peramine (**1**), ergot alkaloids and indole diterpenoids that vary in their bioactivities.[79, 138] Ergot alkaloids and some of the indole diterpenoids have neurotoxic effects on grazing livestock while peramine (**1**) and some of the indole diterpenoids are active against invertebrates, with little or no effects on grazing livestock.[1, 79, 139, 140] Some of the ergot alkaloids have also shown insecticidal activity.[141]

The wild-type endophyte provides its host, perennial ryegrass, with strong resistance to Argentine stem weevil adults and larvae and black beetle adults due to the production of peramine (**1**) and ergovaline (**2**) respectively.[89, 140] However, ergovaline (**2**) is toxic to grazing livestock, causing vaso-constriction that causes heat stress and reduces live-weight gain. The endophyte is also detrimental to grazing livestock due to the production of lolitrem B (**3**), the major cause of ryegrass staggers. The search for endophyte strains that do not produce either lolitrem B (**3**) or ergovaline (**2**) resulted in the commercial availability of novel endophytes including AR1 and AR37.[20] AR1 expresses peramine (**1**) as the major product[142] while AR37 expresses epoxy-janthitrems, the only alkaloids known to be produced by this endophyte and which affect a broad spectrum of insect pests including porina larvae.[110] AR37 can cause ryegrass staggers but episodes tend to be less severe and more transient than the staggers caused by the wild-type endophyte.[91] Epoxy-janthitrem I (**4**) at 14 mg/kg and 8 mg/kg caused a similarly prolonged tremor effect in mice compared to that of lolitrem B (**3**) at 2 mg/kg.[78]

Research is continuing in the search for an endophyte in ryegrass that can potentially deter a spectrum of insect pests without any detrimental effects on grazing livestock. Loline alkaloids (such as loline (**77**)), are effective insect deterrent compounds but they are only produced by *Epichloë* endophytes infecting tall fescue and meadow fescue.[79]

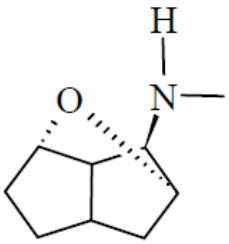

(**77**)

When the loline-producing tall-fescue endophyte, AR525, was artificially inoculated into perennial ryegrass, only one of three common loline derivatives, *N*-formyl loline (**78**) was expressed in the plant and only at a much lower concentration than in the original host.[143]

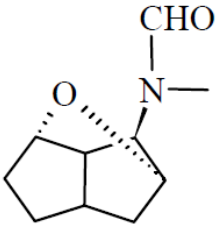

(**78**)

Some *E. festucae* var. *lolii* endophytes do not produce lolitrem B (**3**) or epoxy-janthitrems but can express compounds produced earlier in the biosynthetic pathway.[30] AR1 for example produces low concentrations of paxilline (**36**) and paspaline (**42**) and high concentrations of 13-desoxypaxilline (**37**) plus other unknown indole diterpenoids.[144] Other endophyte strains such as Frc7 from *E. festucae* and Lp1 from *E. festucae* var. *lolii* also express indole diterpenoids other than lolitrem B (**3**).[144] Since paxilline (**36**) is known to have some anti-insect effects,[61] it is possible that other early-pathway indole diterpenoids could also be bioactive towards insects. Currently, how insect pests respond to the early indole diterpenoid biosynthetic pathway metabolites is a huge gap in our understanding. It is crucial to have this information so that endophyte strains can be screened for desirable bioactive alkaloids and then selected for inoculation into commercial cultivars and further testing. To narrow the gap in our knowledge, the compounds isolated in this research (paspaline (**42**), 13-desoxypaxilline (**37**), terpendole D (**50**), compounds A (**64**) and B (**65**)) with other available indole diterpenoids (paxilline (**36**) and lolitrem B (**3**)), were tested against porina larvae.

5.1 Porina

5.1.1 Classification of porina

Porina, the common name for *Wiseana* spp. (Lepidoptera: Hepialidae), are a group of related moths endemic to New Zealand (Table 5.1). The caterpillars (Figure 5.1) of this genus are significant pests of pastures in New Zealand, especially in the South Island and the central and lower North Island.

Figure 5.1: Porina caterpillars**.** (Adapted from reference 146).

Table 5.1: Scientific classification of porina (*Wiseana* spp).

Kingdom	**Animalia**
Phylum	Arthropoda
Class	Insecta
Order	Lepidoptera
Family	Hepialidae
Genus	*Wiseana*

Adapted from reference 146.

There are seven species of *Wiseana* present in New Zealand which are currently described as *W. cervinata, W. copularis, W. fuliginea, W. jocosa, W. mimica, W. umbraculata* and *W. signata*. Three of these (*W. cervinata, W. copularis* and *W. signata*) have two haplotypes each (Northern and Southern). The identification of these species as moths initially relied on morphological characteristics and phylogenetic analysis.[145, 146] The male moths were differentiated by the wing scale

shape and antennal segment shape, while females were classified from dissection and examination of genitalia.[145] These identification methods worked well for moths but could not be used to differentiate the larvae. Richards and co-workers recently developed non-sequencing DNA based methods that allow rapid identification of moths and larvae to species and haplotypes.[147]

W. cervinata and *W. copularis* were traditionally thought to be the major dominant species that damaged pasture in New Zealand based on time of flight. However, molecular identification methods now suggest that *W. copularis* (which has northern and southern haplotypes) may be the most widespread and the more significant of the two.[145, 147] *W. copularis* Southern haplotype is found in parts of the South Island while *W. copularis* Northern haplotype occurs in the South, North and Chatham Islands. Up to four species have been found to co-exist in a single pasture; for example larvae of *W. mimica, W. jocosa, W. copularis* and *W. fuliginea* were found in one pasture near Te Anau.[147] *W. cervinata* Northern and *W. signata* Northern occur in the North Island while *W. cervinata* Southern and *W. signata* Southern have been observed in the South Island and on Chatham Island.[147] The distribution of *W. fuliginea* appears to be limited to wet lowland.

The most significant difference between these species is the time of the moth flight, which thus affects the time over which the caterpillar develops for each species (Figure 5.2). *W. copularis* moths emerge in the South Island in January and late in February to early March in the central and lower North Island. *W. cervinata* moths emerge to lay eggs in spring and are not seen after December. The development of larvae from early flying moths may be three months ahead of those from the late flights. This significantly affects the timing of applications of diflubenzuron, an insect growth regulator that is used to control porina and which is most effective against early larval stages.

Moths do not feed, live only for a few days and fly when the temperature is above 8.3º C. Each female moth is capable of laying up to 3000 eggs during the dispersal flight and can fly up to a distance of 300 m. They are strongly attracted to light.

Figure 5.2: The life cycle of *Wiseana cervinata.* (Adapted from reference 150).

The eggs hatch in 10 – 21 days and initially, the young caterpillars form silk tunnels on the soil surface, which they live in. At around 4 - 15 weeks, the caterpillars burrow underground, forming 10 - 12 mm tunnels. The eggs and caterpillars are vulnerable to dry weather and trampling by stock until they have burrowed.[148]

Caterpillars emerge at night, feed on the aerial parts of a range of plants including ryegrass, the major component of pasture in New Zealand and the host for endophytes. Larvae tend to feed while partially remaining in their burrow but can move to a fresh part of the pasture to construct a new burrow when needed. They often remove grass and clover and take it down into their burrows for several days in cold weather. Depending on the adult flight time, their damage is most noticeable from April – September.

5.1.2 Control of porina.

Porina larvae can occur in very high densities, causing severe and widespread pasture damage in late autumn and throughout winter as plant growth slows.[104] To reduce porina damage, a few control methods are available to farmers.

a. Insecticides.

The control of porina larvae using insecticides is common. Diflubenzuron, an insecticide that inhibits moulting of larvae, is very effective against young larvae if potentially damaging populations are detected early enough before damage is visible.[149] Organophosphate insecticides such as diazinon and chlorpyrifos can also be used when large larval populations are observed, and pasture damage is clearly visible. In recent years, a novel bacterium *Yersinia* n. sp. (MH96) cf. *entomophaga* (EN65 strain), has been identified which is pathogenic to *Wiseana* spp larvae, causing significant mortality of larvae and reducing their feeding damage on white clover.[150] This bacterium is being considered for development as a biopesticide.

b. Grazing, mob stocking and rolling

The alternative, low-cost methods to control porina larvae have been regular grazing, mob stocking and rolling. Due to desiccation and physical injury from grazing, short pasture reduces the survival of eggs and the young larvae before they burrow. In South Otago, this has been shown to reduce porina densities by up to 69%.[31]

c. Novel endophyte AR37

The AR37-infected ryegrass, expressing epoxy-janthitrems, is the only endophyte known to be effective against porina. Jensen & Popay in 2004[151] found that growth, development, weight gain and survival of larvae were reduced by AR37 compared to endophyte-free ryegrass in two no-choice pot trials. In a short-term, no-choice bioassay, consumption by larvae of both AR37-infected and endophyte-free ryegrass was similar but larvae showed a preference for endophyte-free ryegrass in a choice assay.[151] In a field investigation in 2012, Popay and co-workers[29] observed significantly lower densities of porina and less damage on plots of perennial ryegrass infected with AR37 compared with ryegrass infected with AR1 and

endophyte-free grass. The effects in the field reflected the strong deterrent and/or toxic effects of AR37 on porina, seen in the pot experiment.[151] The field experiment also indicated that diploid, AR37-infected cultivars may be more resistant to larvae compared to AR37-infected tetraploid cultivars.

Subsequently, epoxy-janthitrem I (**4**), the major compound of AR37, was shown to reduce feeding and growth of porina larvae in a semi-synthetic diet bioassay. In 2010, Finch and co-workers showed in a seven day bioassay that pure epoxy-janthitrem I (**4**) had a dose-dependent effect on feeding and weight gain of porina larvae.[78] Larvae were fed with semi-synthetic diets containing 0, 1, 2.5, 5 and 10 µg/g pure epoxy-janthitrem I (**4**) and the diet consumption and weight gain were significantly reduced when exposed to levels of 2.5 µg/g and higher. The survival rate was 99% during this short trial, indicating that the compound was deterrent rather than toxic.[78] In 2015,[97] Hennessy conducted a porina larval bioassay with a synthetic diet containing epoxy-janthitrem I (**4**) at concentrations of 0, 1, 2.5 and 5 µg/g for three weeks. The results were consistent with those of Finch,[78] showing that epoxy-janthitrem I (**4**) had a strong deterrent effect on porina larvae that increased with increasing concentrations. The concentration of epoxy-janthitrem I (**4**) in ryegrass decreases at low temperatures and it is possible thatthis compound may be toxic to the larvae as well as a deterrent but further research is required to confirm this. The concentration of epoxy-janthitrems in ryegrass is significantly affected by the plant species.[97,152]

5.2 Effect of paxilline (36), paspaline (42), 13-desoxypaxilline (37), lolitrem B (3), terpendole D (50), compound A (64) and compound B (65) on porina larvae.

To determine if indole diterpenoid and related compounds are bioactive against porina larvae, the deterrent effects of paxilline (**36**), paspaline (**42**), 13-desoxypaxilline (**37**), lolitrem B (**3**), terpendole D (**50**) and the novel compounds A (**64**) and B (**65**) were investigated in three different experiments during the summer seasons of 2015, 2016 and 2017.

Each treatment was fed to porina larvae via a semi-synthetic diet twice weekly and fresh diet was prepared weekly. The compounds were added into the semi-synthetic diet as a DMSO solution (400 µL) and a solvent control (DMSO) was used in each experiment. The effects of the tested alkaloid were determined by the change in diet weight for each feeding period (= consumption), the weight change and survival of the larvae during the experiment.

The stability of the tested alkaloid in the 10 µg/g treatments was determined by analysing diets twice a week by HPLC using paxilline (**36**) as a standard (2 mg/25 mL MeOH). All of the tested alkaloids were stable in the diet.

The first experiment was conducted in 2015 to investigate the effect of different concentrations of paxilline (**36**) on porina larvae. The treatments consisted of five concentrations of paxilline (**36**) (0, 1, 2.5, 5, 10 µg/g). Each treatment had fifteen replicates of 122-day old larvae weighing between 68 and 287 mg (Section 7.10.3). The experiment was conducted over four weeks from the 28th April to 26th May 2015.

In experiment II, conducted in 2016, the effects of lolitrem B (**3**), paspaline (**42**) and 13-desoxypaxilline (**37**) on porina were compared, with the effect of paxilline (**36**) used as a positive control. Two concentrations (5 and 10 µg/g) of each of the compounds and a solvent control (0 µg/g) were tested against larvae to give nine treatments in total. The lower concentrations of 1.0 and 2.5 µg/g were not included in this experiment. Despite the mild effect of 2.5 µg/g paxilline (**36**) on consumption

and weight gain of porina, the effect was lower than those at higher concentrations in the first experiment testing paxilline (**36**) only. Since the compounds were pure, only one solvent or DMSO standard control was required for all the different indole diterpenoids because the matrices for each treatment were the same. There were fifteen replicate porina larvae used per treatment. The larvae were 93 days old, weighing between 54 and 202 mg. The experiment was conducted over three weeks from 22nd February to 14th March 2016.

The last experiment was conducted in 2017 to identify the effect of terpendole D (**50**), compound A (**64**) and compound B (**65**) on porina larvae. Concentrations of 5 and 10 µg/g of each compound plus paxilline (**36**) and one solvent control were used as the treatments. The duration was intended to be three weeks, but the experiment was terminated after two weeks (4th – 18th April 2017) when no effect of the test compounds had been observed. There were fifteen replicates of 63 day old larvae per treatment with a weight range of 57 to 113 mg.

5.2.1 Effect of paxilline (36) on porina larvae.

5.2.1.1 Mean diet consumption and weight change of porina larvae.

The total mean diet consumption by porina larvae was significantly reduced by paxilline (**36**) at concentrations of 2.5 µg/g and above. The total mean consumption (± SEM) at 0, 1, 2.5, 5 and 10 µg/g was 299 (21.7), 237 (19.8), 158 (16.7), 86 (8.4) and 53 (2.0) mg respectively; ($P < 0.001$) (Figure 5.3). The feeding was also significantly less at concentrations of 5 and 10 µg/g than at 2.5 µg/g.

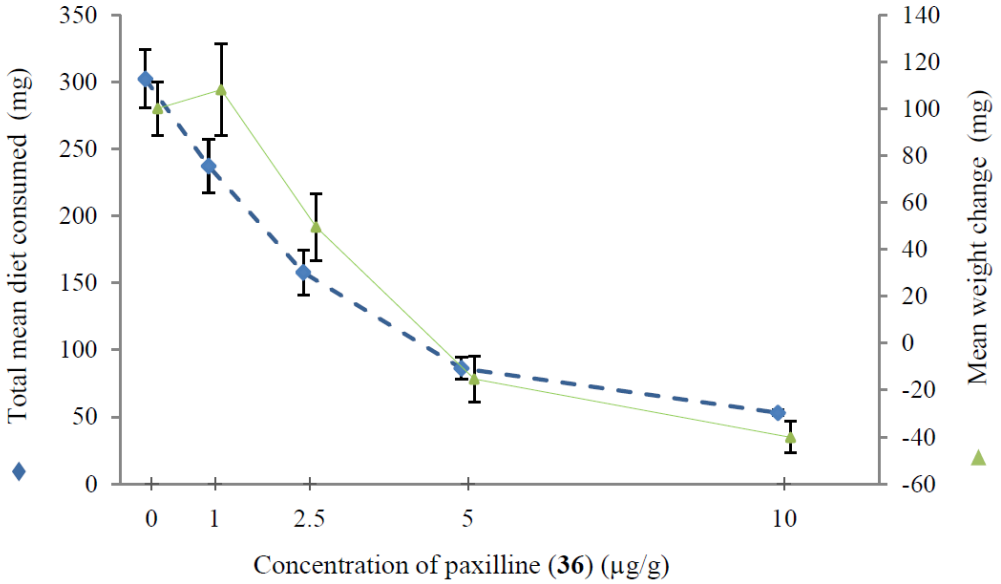

Figure 5.3: Total mean diet consumption and mean weight change (± SEM) of porina larvae fed diet containing paxilline (**36**) at concentrations of 0, 1.0, 2.5, 5.0 and 10.0 µg/g.

All differences in feeding were reflected in the weight change of the porina larvae (total mean weight change (± SEM) at 0, 1, 2.5, 5, 10 µg/g was 100 (11.5), 109 (19.4), 49 (14.2), -18 (9.8) and - 46 (6.7) mg respectively ($P < 0.001$).

The initial weight of larvae did not differ significantly between treatments. Larvae fed diets containing 2.5 µg/g paxilline (**36**) gained significantly less weight than those fed diets with 0 and 1 µg/g, but significantly more than the larvae on diets containing 5 and 10 µg/g (Figure 5.3). There was no significant difference between

the weight gain of larvae fed on 0 µg/g and 1 µg/g. Results showed that paxilline (**36**) gave a dose-dependent effect on both food consumption and larval weight. This compound may contribute to the effect of endophytes observed in the field. AR1 expresses a low concentration of paxilline (**36**) but does not affect porina larvae, which is consistent with the effect observed. [124] The concentration of paxilline (**36**) produced in other associations is currently unknown.

5.2.1.2 The survival rate of porina larvae.

The survival of the larvae was unexpectedly low in the solvent control (66.7 %) and at the lowest paxilline (**36**) concentration of 1.0 µg/g (80.0 %), although differences were not significant. A similar result was observed in a trial conducted on the effect of epoxy-janthitrems on porina larvae this year. The high mortality that occurred in the DMSO solvent control in that experiment was attributed to the high amount of feeding on this treatment that resulted in the DMSO becoming toxic to the larvae.[153] This did not occur in the other treatments due to a reduced consumption. All larvae at the 2.5 µg/g paxilline (**36**) dose survived the four week experiment while at the higher concentrations (5 and 10 µg/g), the survival rate dropped (Table 5.2). Further investigation is required to confirm if the solvent caused high mortality including calculation of the DMSO consumed in each diet treatment.

Table 5.2: Survival rate of porina larvae (n = 15 larvae/treatment) after four weeks.

Concentration (µg/g) of paxilline (36)	**Number of surviving larvae**	**Survival rate (%)**
0.0	10	66.7
1.0	12	80.0
2.5	15	100.0
5.0	13	86.7
10.0	10	66.7

5.2.1.3 Stability of paxilline (36) in the larval diet.

The semi-synthetic diets were analysed for paxilline (**36**) twice a week (Table 5.3). The results showed that the paxilline (**36**) content in the diet was about 8 µg/g throughout the four week experiment which indicated that it was stable in the diet. Therefore, porina larvae were exposed to consistent concentrations of paxilline (**36**) during the trial.

Table 5.3: The paxilline (**36**) concentrations from extracts of fresh (F), replacement (R) and remaining (O_1, O_2) diets used in 10 µg/g larval treatment diet over 4 weeks.

Diet 10 µg/g	Date	Paxilline (36) concentration (µg/g)	Mean paxilline (36) concentration (µg/g)
[a]F	28/04/15	9.6	8.4
	05/05/15	7.6	
	12/05/15	8.5	
	19/05/15	7.7	
[b]R	01/05/15	8.1	7.94
	08/05/15	8.3	
	15/05/15	7.7	
	22/05/15	7.6	
[c]O_1	01/05/15	8.1	8.3
	08/05/15	8.5	
	15/05/15	8.6	
	22/05/15	7.8	
[d]O_2	05/05/15	8.0	8.3
	12/05/15	8.2	
	19/05/15	8.3	
	26/05/15	8.6	

a = Fresh (F) prepared diet, *b* = Replacement (R) diet stored in the fridge for the next feeding session, *c* = Diet (O_1) recovered after 3 days feeding on fresh diet, *d* = Diet (O_2) recovered after four days feeding with O_1 diet.

5.2.2 Effect of lolitrem B (3), paspaline (42) and 13-desoxypaxilline (37) on porina larvae

5.2.2.1 Mean diet consumption by porina larvae

Over three weeks, mean consumption by porina larvae fed on diet containing 5 µg/g (132.7 mg) and 10 µg/g (76.8 mg) paxilline (**36**) and 5 µg/g (119.9 mg) and 10 µg/g (85.3 mg) lolitrem B (**3**) was significantly less than the mean diet consumed by the solvent control (283.1 mg), ($P < 0.001$; SED ± 20.7) (Figure 5.4).

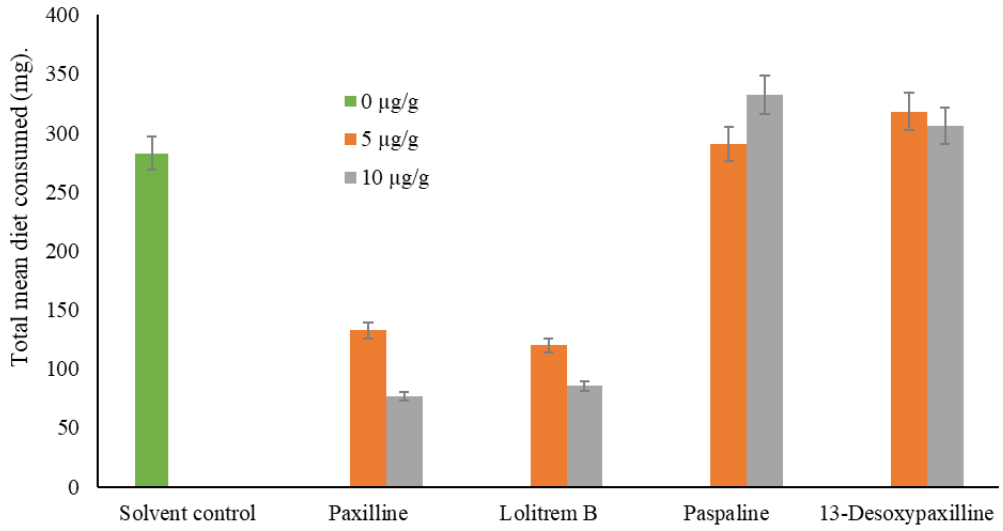

Figure 5.4: The total mean weight of diet (mg) consumed by porina larvae of a solvent control (0 µg/g), paxilline (**36**), lolitrem B (**3**), paspaline (**42**) and 13-desoxypaxilline (**37**) treatments (5 µg/g and 10 µg/g) ± SED over the three weeks.

There was no significant difference in the mean diet consumed over the six feeding periods containing 5 µg/g (290.7 mg) and 10 µg/g (332.3 mg) paspaline (**42**) or 5 µg/g (317.8 mg) and 10 µg/g (306.0 mg) 13-desoxypaxilline (**37**) compared to the solvent control treatment. This showed that paspaline (**42**) and 13-desoxypaxilline (**37**) had no deterrent activity against the porina larvae.

5.2.2.2 Mean weight change of porina larvae.

The initial weight of larvae did not differ significantly between treatments. By the end of the experiment, the mean weight change of surviving larvae on both paxilline (**36**) and lolitrem B (**3**) treatments (5 µg/g and 10 µg/g) was significantly lower than for the solvent control (0 µg/g) ($P < 0.001$) (Figure 5.5). However, the mean weight change of larvae fed diets containing paspaline (**42**) (10 µg/g) and 13-desoxypaxilline (**37**) (5 µg/g and 10 µg/g) was significantly higher than the solvent control. There was no difference between the solvent control and 5 µg/g paspaline (**42**) (Figure 5.5). The total mean weight changes of larvae fed on diet with solvent control (0 µg/g) was 80.0 mg and of those fed on 5 µg/g paxilline (**36**), lolitrem B (**3**), paspaline (**42**) and 13-desoxypaxilline (**37**), -6.5, -10.1, 86.5 and 117.8 mg respectively. The mean weight changes of larvae fed on diet with 10 µg/g paxilline (**36**), lolitrem B (**3**), paspaline (**42**)) and 13-desoxypaxilline (**37**) were -31.3, -27.8, 114.8, and 110.1 mg respectively (SED ± 16.8; $P < 0.001$).

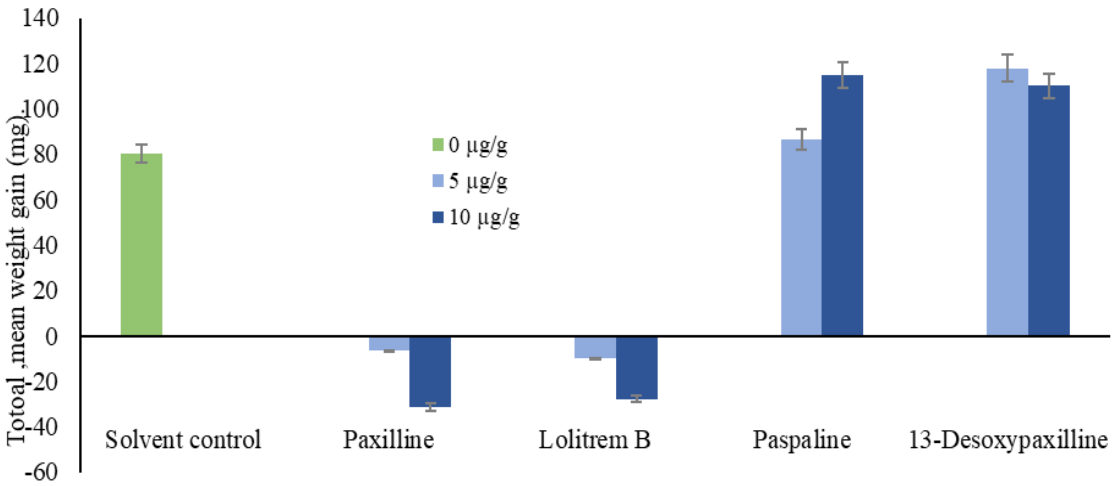

Figure 5.5: The mean weight change (mg) of porina larvae when fed a solvent control, paxilline (**36**), lolitrem B (**3**), paspaline (**42**) and 13-desoxypaxilline (**37**) over three weeks ± SED.

5.2.2.3 The survival rate of porina larvae.

The survival rate of larvae fed a diet with 5 and 10 µg/g paxilline (**36**) and lolitrem B (**3**) was significantly less than for those in the solvent control, paspaline (**36**) and 13-desoxypaxilline (**37**) treatments ($P < 0.001$). Larvae exposed to a diet containing

10 µg/g paxilline (**36**) had a significantly lower survival than those at 10 µg/g lolitrem B (**3**), indicating that paxilline (**36**) may be more deterrent or toxic to porina than lolitrem B (**3**). The number of larvae that survived at 5 µg/g paxilline (**36**) and lolitrem B (**3**) diet was not significantly different. When larvae were fed a diet containing paspaline (**42**), 13-desoxypaxilline (**37**) or solvent control, survival rates were similar (Table 5.4).

Table 5.4: Percentage of porina larvae surviving after three weeks exposure to two concentrations of paxilline (**36**), lolitrem B (**3**), paspaline (**42**) and 13-desoxypaxilline (**37**) compared to a solvent control.

Treatment	**Concentration (µg/g)**	**Number of surviving larvae**	**Survival rate of larvae (%)**
Solvent control	0	13	86.7
Paxilline **(36**)	5	7	46.7
	10	1	6.7
Lolitrem B **(3**)	5	6	40.0
	10	4	26.7
Paspaline **(42**)	5	13	86.7
	10	15	100.0
13-desoxypaxilline **(37**)	5	15	100.0
	10	15	100.0
P-value < 0.001			

5.2.2.4 Stability of lolitrem B (3), 13-desoxypaxilline (37) and paspaline (42) in the larval diet.

The analysis of the diet showed that none of the compounds degraded during the experiment (Table 5.5), although the concentration recovered was less than the theoretical value of 10.0 µg/g.

Table 5.5: The concentrations (µg/g) of paxilline (**36**), lolitrem B (**3**), paspaline (**42**) and 13-desoxypaxilline (**37**) in fresh (F), replacement (R) and recovered (O_1, O_2) diets prepared with concentrations at 10 µg/g over three weeks.

Diet (10 µg/g)	Date	Concentration (µg/g)							
		Paxilline (36)		Lolitrem B (3)		Paspaline (42)		13-Desoxypaxilline (37)	
		Individual	Mean	Individual	Mean	Individual	Mean	Individual	Mean
[a]**F**	22/02/16	8.7		9.2		8.1		9.2	
	29/02/16	9.2	8.7	9.0	9.1	8.5	8.5	8.6	6.8
	07/03/16	8.2		9.3		8.6		8.7	
[b]**R**	25/02/16	8.7		8.9		9.1		9.0	
	03/03/16	8.6	8.5	9.2	9.1	8.4	8.4	9.1	8.8
	10/03/16	8.3		9.1		8.4		8.5	
[c]**O_1**	25/02/16	8.5		8.8		9.4		8.8	
	03/03/16	8.9	8.6	8.5	8.9	9.1	9.0	9.2	9.2
	10/03/16	8.3		9.4		8.9		9.3	
[d]**O_2**	29/02/16	8.9		8.5		9.0		8.8	
	07/03/16	8.4	8.5	9.2	8.8	9.1	9.1	8.6	8.7
	14/03/16	8.4		8.9		9.0		9.2	

a = Fresh (F) prepared diet, *b* = Replacement (R) diet stored in the fridge for the next feeding session, *c* = Diet (O_1) recovered from the larva after three days feeding, *d* = Diet (O_2) recovered after four days feeding with O_1 diet.

5.2.3 Effect of terpendole D (50), compound A (64) and compound B (65) on porina larvae.

5.2.3.1 Mean diet consumption

The diet consumption of porina larvae on compound A (**64**), compound B (**65**) and terpendole D (**50**) treatments at 5 µg/g and 10 µg/g, was not significantly different from the total mean diet consumption on the solvent control. However, diet consumption on paxilline (**36**) at both concentrations was significantly different. The total mean diet consumption on 5 µg/g paxilline (**36**), compound A (**64**), compound B (**65**) and terpendole D (**50**) was 101.5, 267.4, 256.3 and 280.3 mg respectively. Total mean diet consumption of larvae when fed diets with 10 µg/g paxilline (**36**), compound A (**64**), compound B (**65**) and terpendole D (**50**) was 48.1, 288.2, 258.7 and 267.9 mg respectively in comparison to the total mean diet consumption on the solvent control as 234.8 mg; ($P < 0.001$) (Figure 5.6).

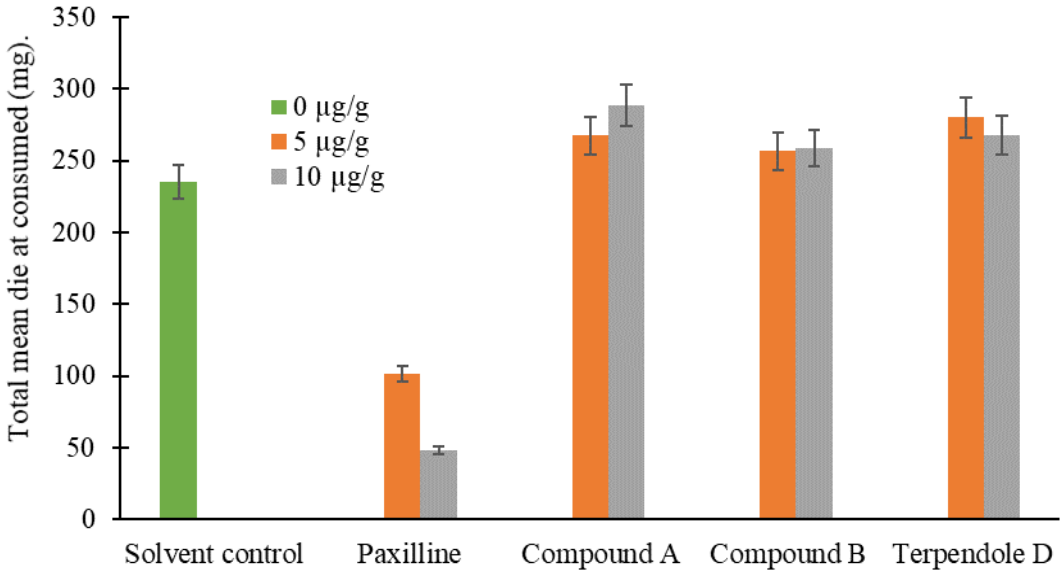

Figure 5.6: The average amount (mg) of diet consumed by porina larvae with 0 µg/g solvent control and 5 µg/g and 10 µg/g paxilline (**36**), compound A (**64**), compound B (**65**) and terpendole D (**50**) over a two week experiment ± SED.

Since none of the compounds, other than the paxilline used as the positive control, showed any biological activity against porina larvae after two weeks, the experiment was ceased at this point.

5.2.3.2 Mean weight change of porina larvae

As with the feeding, the weight gain of porina larvae was not significantly affected when larvae were fed on 5 µg/g or 10 µg/g of compound A (**64**), compound B (**65**) or terpendole D (**50**) compared to the solvent control. However, the weight change of larvae exposed to 5 µg/g and 10 µg/g paxilline (**36**) diet was significantly less than those exposed to all the other treatments (Figure 5.7) ($P < 0.001$: SEM ± 3.6).

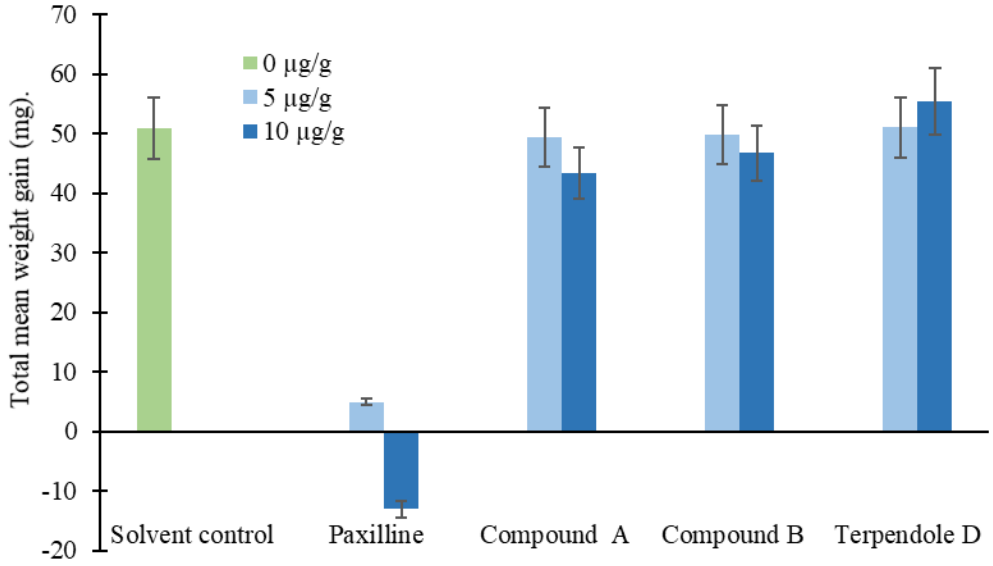

Figure 5.7: The mean weight gain of porina larvae fed a diet with a solvent control 0 µg/g, 5 µg/g and 10 µg/g paxilline (**36**), compound A (**64**), compound B (**65**) and terpendole D (**50**) over two weeks ± SEM.

The weight changes of larvae on 5 µg/g paxilline (**36**), compound A (**64**), compound B (**65**) and terpendole D (**50**) were 4.9, 49.3, 49.8 and 51.0 mg respectively. Similarly, the total weight changes of porina larvae on 10 µg/g paxilline (**36**), compound A (**64**), compound B (**65**) and terpendole D (**50**) were -13.1, 43.3, 46.7 and 55.4 mg respectively. The total weight change of larvae on the solvent control was 50.9 mg. As observed in previous experiments, paxilline significantly reduced the weight change of porina ($P < 0.001$) compared with the solvent control and the other treatments.

5.2.3.3 The survival rate of porina larvae.

After two weeks, the survival rate of the porina larvae did not differ between treatments (P > 0.05) (Table 5.6). Three larvae died, one from the solvent control and one at each concentration of terpendole D (**50**).

Table 5.6: The survival rate of porina larvae after two weeks feeding on diets containing paxilline (**36**), compound A (**64**), compound B (**65**) and terpendole D (**50**) at 5 and 10 µg/g and a solvent control.

Compound	**Concentration (µg/g)**	**Number of surviving larvae**	**Larval survival rate (%)**
Solvent control	0	14	93.3
Paxilline (**36**)	5	15	100.0
	10	15	100.0
Compound A (**64**)	5	15	100.0
	10	15	100.0
Compound B (**65**)	5	15	100.0
	10	15	100.0
Terpendole D (**50**)	5	14	93.3
	10	14	93.3
P-value > 0.05			

5.2.3.4 Stability of compound A (64), compound B (65) and terpendole D (50) in the larval diet.

All of the compounds were stable over the experimental period, although the concentrations were less than 10 µg/g (Table 5.7).

Table 5.7: The concentration of compound A (**64**), compound B (**65**), terpendole D (**50**) and paxilline (**36**) from extracts of fresh (F), replacement (R) and remaining (O_1, O_2) diets prepared with 10 µg/g of each test compound fed to porina over two weeks.

Diet (10µg/g)	Date	Concentration (µg/g)							
		Paxilline (36)		Compound A (64)		Compound B (65)		Terpendole D (50)	
		Individual	Mean	Individual	Mean	Individual	Mean	Individual	Mean
[a]F	04/04/17	8.5	8.2	7.4	8.0	8.5	8.2	7.8	7.7
	11/04/17	7.9		8.5		7.9		7.6	
[b]R	07/04/17	8.3	8.2	8.2	7.9	8.6	8.9	8.2	8.0
	14/04/17	8.1		7.6		9.1		7.8	
[c]O_1	07/04/17	8.9	9.0	8.1	8.2	8.2	8.8	8.6	8.6
	14/04/17	9.1		8.3		9.4		8.7	
[d]O_2	11/04/17	8.1	8.3	9.4	8.8	8.5	8.7	9.1	8.6
	18/04/17	8.5		8.1		8.8		8.1	

a = Fresh (F) prepared diet, *b* = Replacement (R) diet stored in the fridge for the next feeding session, *c* = Diet (O_1) recovered from the larva feeding after 3 days, *d* = Diet (O_2) recovered after four days feeding with O_1 diet.

5.3 Discussion

Paxilline (**36**) and lolitrem B (**3**) are potent feeding deterrents to porina larvae, whereas paspaline (**42**), 13-desoxypaxilline (**37**), compound A (**64**), compound B (**65**) and terpendole D (**50**) had no bioactivity toward porina larvae.

Paxilline (**36**) expressed biological activity against porina larvae in the first experiment (Section 5.2.1) therefore was used as a positive control in latter experiments. The reduced consumption of diet containing 5 and 10 µg/g paxilline was consistent with the weight change of larvae. Diet consumption was significantly less when the larvae were fed a diet with 5 and 10 µg/g compared to those of larvae fed with lower concentrations. This effect of paxilline (**36**) on weight change was consistent over the three experiments. In addition, the first experiment showed that there was a significant effect of paxilline (**36**) on larvae consumption at 2.5 µg/g compared to the solvent control. However, the survival rate of larvae exposed to 5 µg/g and 10 µg/g paxilline (**36**) in the three experiments (Table 5.8) showed some variability.

Table 5.8: Summary of the survival rate of porina larvae at 5 and 10 µg/g paxilline (**36**) in the three experiments.

Experiment	Duration (weeks)	The survival rate (%) of porina larvae when exposed to paxilline (36).	
		5 µg/g	10 µg/g
I	4	86.7	66.7
II	3	46.7	6.7
III	2	100.0	100.0

Clearly, the survival rate of the larvae was highest in the last experiment and lowest in the second experiment. The high survival rate in the third experiment could be explained by the short duration of the experiment but this does not explain the difference in survival rate between the first and second experiments. The concentration of paxilline (**36**) in the diets during all three experiments was similar, so this cannot explain the difference in survival rate. The reason for the high

survival of larvae in experiment 1 compared to experiment II may be related to the size of the larvae and their age at the start of the trial. In the first experiment, larvae were older and heavier than those in the other experiments (Table 5.9).

Table 5.9: The ages and initial mean weight (mg) of the porina larvae exposed to 5 µg/g and 10 µg/g paxilline (**36**) at the beginning of the three experiments.

Experiment	Larval age (days)	Initial larval mean weight (mg) exposed to paxilline (36)	
		5 µg/g	10 µg/g
I	122	180.4	177.9
II	93	117.4	118.1
III	63	81.2	78.7

The initial mean weight of the larvae exposed to the 5 and 10 µg/g paxilline (**36**) treatment in experiment I were 180.4 and 177.9 mg respectively compared to 117.4 and 118.1 mg for experiment II. Larvae used in the first experiment were much heavier and older than those used in the other experiments, suggesting that bigger larvae are more resistant and less affected by paxilline (**36**). Younger larvae were involved in experiment III and were all survived, however the exposure to paxilline (**36**) was only for two weeks. The mortality at 10 µg/g in experiment II occurred in the third week, indicating that more than two weeks exposure to paxilline (**36**) was needed for larvae to die as a result of either starvation or toxicity. Thus, age and size of the porina larvae, as well as the duration of the experiment, likely affected the survival rate. Further experiments would be required to investigate how these factors affect the feeding deterrence and/or toxicity of paxilline (**36**).

From the current results, both paxilline (**36**) and lolitrem B (**3**) deterred feeding by porina larvae by a similar amount at 5 µg/g. Both caused a high mortality of larvae, suggesting they may be toxic as well as deterrent. Larval survival on diet containing paxilline (**36**) at 10 µg/g was higher than for lolitrem B (**3**) at the same concentration indicating that paxilline (**36**) is the more potent of the two compounds. Paxilline (**36**) also reduced consumption and weight gain of porina relative to the

solvent control at 2.5 µg/g but lolitrem B (**3**) was not tested at this concentration. These two indole diterpenoids, together with epoxy-janthitrem I (**4**),[78] are now known to be active against porina larvae whereas paspaline (**42**), 13-desoxypaxilline (**37**), terpendole D (**50**), compounds A (**64**) and compound B (**65**) are not.

Compounds A (**64**) and B (**65**) contain a 13-hydroxyl group as found in paxilline (**36**) and lolitrem B (**3**). This structural feature is therefore not solely responsible for the deterrent effects of paxilline (**36**) and lolitrem B (**3**). It is possible that the opening up of the indole moiety in compounds A (**64**) and B (**65**) affect their ability to deter porina feeding. Paspaline (**42**), 13-desoxypaxilline (**37**) and terpendole D (**50**) all contain the indole moiety but lack the 13-hydroxyl group and are not effective against porina larvae. The only difference in the structure of 13-desoxypaxilline (**37**) and paxilline (**36**) is the 13-hydroxyl group. Paxilline (**36**) is effective against porina larvae while 13-desoxypaxilline (**37**) is not.

The three indole diterpenoids paxilline (**36**), lolitrem B (**3**) and epoxy-janthitrem I (**4**) that affect porina larvae cause tremors in mice.[1, 55, 78] Do insects such as porina larvae also experience neurological effects after feeding on them? Could this be the reason for the deterrent effect of these alkaloids? The root aphid, *A. lentisci* has been observed to suffer tremors when feeding on ryegrass infected with AR37, suggesting that a neurotoxic effect is also possible in insects, although we cannot be sure if epoxy-janthitrems were responsible for that.[116] Paspaline (**42**), 13-desoxypaxilline (**37**) and terpendole D (**50**) are non-tremorgenic to mice and are not bioactive against porina larvae. Further research is required to identify whether insect pests such as porina also experience neurological effects and whether those effects cause the anti-feedant response to the indole diterpenoid. Lolitrems A (**12**), C (**13**), F (**15**) and other indole diterpenoid intermediates that cause tremors in mice should also be tested on porina larvae and if all are active, the mechanisms behind those effects are likely to be similar. There may also be some similarities in the mechanism behind the mouse and insect responses. This is an area that has not previously been explored in plant fungal interactions.

Peramine (**1**) and lolines are not indole diterpenoids and as such do not contain similar structural features or cause tremors in livestock, yet they are active against certain insect pests.[28, 154] These compounds are small molecules with two rings, both containing an N-methyl group. This group may also be important for the effects on insects.

The deterrent effect of paxilline (**36**) on porina larvae broadens the list of insect pests which are affected by paxilline (**36**) and which includes Argentine stem weevil, fruit beetle, corn earworm and fall armyworm.[61, 101, 102] The ability of paxilline (**36**) to deter these insect pests may contribute to the effect of endophytes in the field, however with low detrimental effects compared to lolitrem B (**3**) on livestock.[56] An endophyte strain expressing paxilline (**36**) without lolitrem B (**3**) could therefore, be useful for the protection of ryegrass from porina larvae.

Chapter 6: Future Recommendations

The stereochemistries of compounds A – C (**64** – **66**) were not fully determined. Therefore, future work could be undertaken to confirm the stereochemistry of these compounds. This would involve extraction of more of these compounds and attempting to crystallise them for X-ray analysis. In addition, computational chemistry to calculate parameters such as electronic circular dichroism (ECD) curves and chemical shifts to compare them to the experimental values could be undertaken. This would assist in the assignment of the stereochemistry.

The structure of compound D (**67**) has not yet been completed. Further isolation of compound D (**67**) would allow the C-2 substituent to be confirmed and once that is confirmed, the stereochemistry can be determined.

The determination of whether compounds A – D (**64** – **67**) are naturally occurring or artefacts is also important. Even though the LC-MS analysis did not detect any of these compounds in the fresh extract of perennial ryegrass seed infected with wild-type endophyte, it is possible that the amounts of these compounds were below the detectable limit in this extract. If they are naturally occurring, then a new group of alkaloids has been discovered. To confirm this, a detailed quantitative investigation of a fresh extract of wild-type endophyte-infected seed is required.
However, if they are artefacts, then it is likely that they are formed from modification of the indole moiety of terpendole C (**49**). This indicates that terpendole C (**49**) could also be expressed by wild-type endophyte. The condition for the storage of the seed extracts was also important to consider in order to avoid any possibility of auto-oxidation processes during the storage period. Investigation of auto-oxidation of terpendoles and lolitrem analogues would clarify the formation of these analogues.

Due to the complexity of the structures and the fact that this is the first report of such structures, they were referred to as compounds A – D (**64** – **67**) in this study. The nomenclature of the compounds requires completion in the future.

Spectroscopic analysis of the potential emindole analogue isolated in Section 3.4 also needs to be completed. This will confirm the actual structure of this compound and will help to close some gaps in the biosynthetic pathway of indole diterpenoids expressed by wild-type endophyte. The LC-MS analysis of the crude extract showed traces of additional potential indole diterpenoids, which require future isolation and purification. It is also important to apply a quantitative analysis of fresh herbage infected by wild-type endophyte to determine the quantities which animal and insects would be exposed to in the field.

Although porina larvae were affected when exposed to paxilline (**36**) and lolitrem B (**3**), they were not affected by paspaline (**42**), 13-desoxypaxilline (**37**), terpendole D (**50**), compound A (**64**) or compound B (**65**). Paxilline (**36**) and lolitrem B (**3**) cause tremors in mice so it is important to determine whether the tremorgenic and insect effects are correlated by broadening the range of compounds tested.

The age and size of porina larvae could also contribute to the survival rate of the larvae when exposed to paxilline (**36**), therefore, it is important to determine how these factors affect the deterrence and/or toxicity of paxilline (**36**).

Chapter 7: Experimental.

7.1 Commonly used laboratory techniques.

Freeze-Drying

Samples were freeze-dried using a Flexi-Dry MP freeze-drier.

Centrifugation

Samples were centrifuged for 2 minutes at 12000 rpm (Eppendorf Centrifuge 5418).

Sonication

To aid dissolution, samples were sonicated in an ultrasonic bath (Cole-Parmer or Aquawave, Barnstead International).

7.2 Commonly used solvents and chemicals.

Solvent	**Source**
Acetonitrile (ACN)	Fisher Scientific HPLC grade
Deuterated Chloroform ($CDCl_3$)	Aldrich (1 mL ampoule) BDH Chemicals Ltd (25 mL Bottle)
Ethyl acetate	HiPerSolv
Dichloromethane (DCM)	Fisher Scientific. HPLC grade
Distilled water	Millipore Milli-Q grade
Methanol (MeOH)	Fisher Scientific. HPLC grade
Petroleum Spirit	Fisher Scientific. HPLC grade

Chemical	**Source**
Silica gel (Merck grade 9385, 230-400 mesh, 60A)	Sigma-Aldrich
YMC-gel ODS-A, YMC	YMC Co. Ltd

7.3 Commonly used fractionation techniques.

All eluting fractions were collected in conical flasks or test tubes. Fractions were combined on the basis of a suitable analysis and concentrated using a rotary evaporator.

7.3.1 Normal phase flash chromatography.

Normal phase flash column chromatography was conducted using silica gel (Merck grade 9385, 230-400 mesh, 60Å). The sample was dissolved in a minimum volume of DCM and loaded onto the column head. The sample vial was rinsed with DCM. Details of the eluting solvents are given for each purification step later in this chapter.

7.3.2 Reversed phase C18 chromatography.

Reversed phase column chromatography was conducted using C18 material (YMC-gel ODS-A, YMC). Samples were prepared for chromatography by dissolving them in the minimum volume of DCM and loading onto the column head. The sample vial was rinsed with DCM and then with MeOH if any insoluble residue remained. Elution was achieved under pressure of nitrogen gas. Details of the eluting solvents are given for each purification step later in this chapter.

7.3.3 Size exclusion chromatography.

A Sephadex LH-20 column (150 g) packed in MeOH was available from Associate Professor Prinsep. The sample was dissolved in MeOH (1 mL) and loaded onto the column head. The column was then eluted with MeOH.

7.3.4 Semi-preparative HPLC chromatography.

The sample was purified using an HPLC reversed phase column (4.6 mm x 250 mm, 5µ) Phenomenex, PRODIGY (3) C18 ODS) at 1.8 mL/min. Eluting compounds were detected with a Hewlett-Packard 1040m diode array UV detector at wavelengths of 230 nm and 280 nm and an Agilent 1100 Series HPLC

Fluorescence detector connected in series. The details of each semi-preparative process are outlined later in the isolation section.

7.3.4.1 Preparation of sample for HPLC analysis.

The selected fractions were dried under nitrogen and dissolved in MeOH (1 mL). When fractions were not fully soluble in MeOH, a few drops of DCM were added to the sample. A subsample (5 µL) was injected into the HPLC for analysis.

7.4 Commonly used characterisation techniques.

7.4.1 Liquid Chromatography Mass Spectrometry.

Samples were analysed using an HPLC system (Ultimate 3000; Dionex) directly coupled to an electrospray ionisation (ESI)-ion trap mass spectrometer (AMAZon X; Bruker Daltonics). Hystar (Bruker Daltonics) was used to control the dual systems. Samples (10 µL) were separated on a C18 column (Altima C18, 5µ; 150 x 2.1 mm) using the gradient outlined in Table 7.1 at 200 µL/min. The *m/z* of the eluting compounds was assessed with 4.5 kV capillary voltage for positive ions, nebuliser pressure at 1.5 bar and desolvation at 225 ºC with a nitrogen flow of 8 L/min. Tandem mass spectra were produced using the protonated ion of a compound and collision-induced dissociation (CID) to induce fragmentation of the parent ion. Chromatograms and spectra were annotated in DataAnalysis (Bruker Daltonics).

Table 7.1: HPLC gradient for general LC-MS analysis.

Time (min)	**Mobile phase A** [a]**ACN:H_2O (2:3) + 0.1%** [b]**AA**	**Mobile phase B ACN+ 0.1% AA**
0	80	20
20	50	50
40	0	100
50	0	100
55	80	20
60	80	20

a = acetonitrile, *b* = acetic acid.

7.4.2 Preparation of sample for LC-MS analysis.

Samples for LC-MS analysis were dissolved in methanol (1 mL), 5 µL transferred into an LC-vial and then 995 µL methanol – water (4:1) added. Where the sample was not fully dissolved in MeOH, a few drops of DCM was added to aid dissolution.

7.4.3 High Resolution Mass Spectrometry.

Semi-pure and pure compounds were analysed using an ESI-TOF mass spectrometer (MicroTOF; Bruker Daltonics) operated with MicroTOF Control (Bruker Daltonics). Samples (≤ 0.1 mg/mL) were resuspended in HPLC-grade MeOH and introduced into the mass spectrometer via a syringe pump (3 µL/min). The positive ions were assessed using a capillary voltage of 4.5 kV and nebuliser pressure of 0.5 bar. Desolvation was carried out with a nitrogen flow of 4 L/min at 180 ºC. The machine was calibrated with a solution of sodium formate (2 mM).

7.4.4 Nuclear Magnetic Resonance Spectroscopy

Nuclear magnetic resonance spectra were recorded on a Bruker AVIII-400 NMR spectrometer. The chemical shifts were determined at 300 K and referenced to residual chloroform in $CDCl_3$ (^{1}H 7.26 ppm, ^{13}C 77. 1 ppm). Samples were dissolved in $CDCl_3$ (800 µL) before the 1D and 2D NMR spectra were acquired.

7.5 Isolation of compounds A (64) and B (65), paspaline (42) and 13-desoxypaxilline (37).

The isolation of compounds A (**64**) and B (**65**), 13-desoxypaxilline (**37**) and paspaline (**42**) is summarised in Figure 7.1. The fractions resulting from each step were analysed by LC-MS (Section 7.4.1) and/or HPLC to allow the pooling of appropriate fractions.

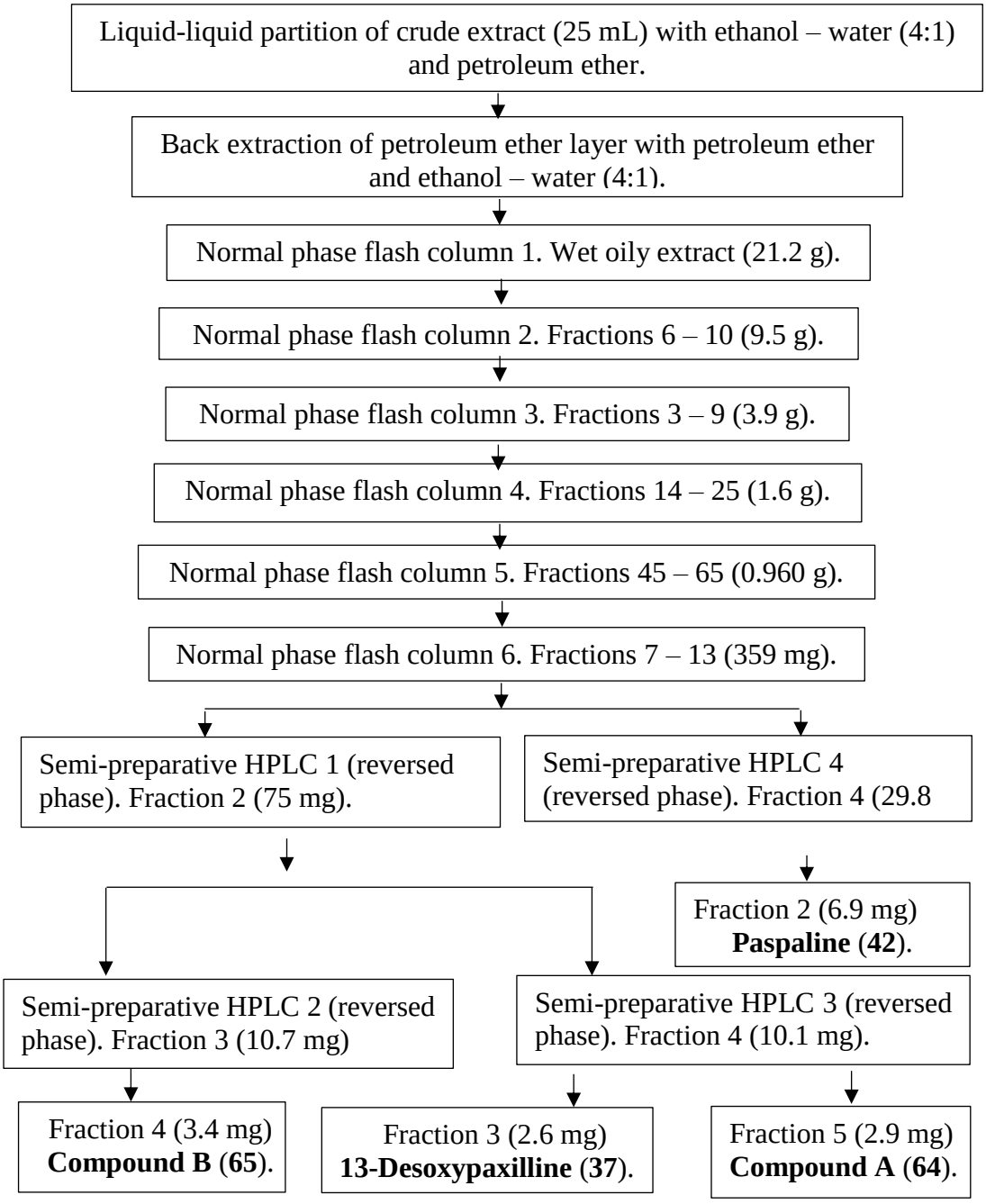

Figure 7.1: Flowchart of the isolation of compound A (**64**), compound B (**65**), 13-desoxypaxilline (**37**) and paspaline (**42**).

7.5.1 Liquid-liquid partition

The crude sample (200 mL) was the pre-lolitrem fraction remaining from Dr Finch's PhD research.[55] It had been stored in a sealed round bottomed flask as an oily mixture at 5°C since 1997. Crude black extract (5 mL) was defatted using a liquid-liquid partition between ethanol – water (4:1) (250 mL) and petroleum ether (250 mL). The non-polar layer was collected and rinsed three times with ethanol – water (4:1) (250 mL) and dried down by rotary evaporation. The liquid-liquid partitioning of the crude sample (5 mL) was repeated to partition 25 mL crude sample in total. Both layers were dried down by rotary evaporation to yield petroleum ether soluble material (oily, wet) (33.9 g) and ethanol – water soluble material (dark, orange-brown, oily) (6.5 g). The petroleum ether soluble layer was subjected to back-extraction in order to recover more material.

7.5.2 Back extraction

A subsample of the petroleum ether soluble layer (10 mL) was diluted with further petroleum ether (100 mL) and transferred into a 500 mL separating funnel. Ethanol – water (4:1) (100 mL) was added and the solution was shaken to mix well and left to settle for 15 minutes. The petroleum ether, interface and ethanol – water were collected into conical flasks. The petroleum ether layer was re-extracted with 3 volumes of ethanol – water (4:1) (100 mL). The back extraction was repeated in 10 mL aliquots until the entire sample was processed. The fractions were dried to yield an ethanol – water layer (9.8 g), an interface layer (1.9 g) and a petroleum ether layer (21.2 g) (all wet weight). LC-MS / HPLC analysis indicated that the resulting ethanol – water and petroleum ether layers contained indole diterpenoid compounds. The petroleum ether layer was therefore further fractionated whilst the ethanol – water layer was put aside for further investigation.

7.5.3 Normal phase flash column 1

The target fraction from the petroleum ether layer resulting from the liquid-liquid partition (21.2 g) was dissolved in a minimum amount of DCM and loaded onto a normal phase flash column (2.5 x 7 cm) which had been previously primed with petroleum ether (PE). The column was then eluted as below.

1 x 750 mL PE	(fraction 1)
2 x 500 mL PE – DCM (1:1)	(fractions 2, 3)
3 x 500 mL DCM	(fractions 4 – 6)
3 x 500 mL DCM – ACN (9:1)	(fractions 7 – 9)
2 x 500 mL DCM –ACN (4:1)	(fractions 10, 11)
1 x 500 mL DCM –ACN (1:1)	(fractions 12)
1 x 500 mL ACN	(fractions 13)
1 x 500 mL ACN – MeOH (1:1)	(fractions 14)
1 x 500 mL MeOH	(fractions 15)

HPLC analysis indicated that the target compounds eluted in the DCM to DCM – ACN (4:1) fractions (fractions 6 – 10). These fractions were pooled and dried down to yield oily material (9.5 g).

7.5.4 Normal phase flash column 2

The target fraction resulting from normal phase flash column 1 (Section 7.5.3) (9.5 g) was dissolved in a minimum amount of DCM and loaded onto a normal phase flash column (2.5 x 7 cm) which had been previously primed with DCM. Fractions of 100 mL were collected when the column was eluted as below.

5 x 100 mL DCM	(fractions 1 – 5)
4 x 100 mL DCM – ACN (49:1)	(fractions 6 – 9)
4 x 100 mL DCM – ACN (19:1)	(fractions 10 – 13)
3 x 100 mL DCM – ACN (9:1)	(fractions 14 – 16)
3 x 100 mL DCM – ACN (4:1)	(fractions 17 – 19)

HPLC analysis indicated that the target compounds eluted in fractions 3 – 9. These fractions were combined and dried down to yield 3.9 g material.

7.5.5 Normal phase flash column 3

The target fraction resulting from normal phase flash column 2 (Section 7.5.4) (3.9 g) was dissolved in DCM and loaded onto a normal phase column (15 x 1.5 cm)

which had been primed with DCM. Fractions of 20 mL were collected and the column was eluted as below.

400 mL DCM	(fractions 1 – 20)
160 mL DCM – MeOH (19:1)	(fractions 21 – 28)
100 mL DCM – MeOH (9:1)	(fractions 29 – 33)
100 mL DCM – MeOH (4:1)	(fractions 34 – 38)

HPLC analysis indicated that the target compounds eluted in fractions 14 – 25. These fractions were pooled and dried down to yield 1.6 g material.

7.5.6 Normal phase flash column 4

The target fraction resulting from the normal phase flash column 3 (Section 7.5.5) (1.6 g) was dissolved in a minimum amount of DCM and loaded onto a normal phase flash column (1.5 x 15 cm). The column had been previously primed with ethyl acetate (EtOAc) – petroleum ether (PE) (1:9). Fractions of 10 mL were collected when the column was eluted as below.

500 mL EtOAc – PE (1:9)	(fractions 1 – 50)
250 mL EtOAc – PE (1:4)	(fractions 51 – 75)
150 mL EtOAc – PE (1:1)	(fractions 76 – 90)

HPLC analysis indicated that the target compounds eluted in fractions 45 – 65. These fractions were combined and dried down to yield 0.96 g material.

7.5.7 Normal phase flash column 5

The target fraction resulting from the normal phase flash column 4 (Section 7.5.6) (0.96 g) was dissolved in a minimum amount of DCM and loaded onto a normal phase flash column (1.5 x 13 cm) which had been previously primed with ACN – DCM (1:19). Fractions of 20 mL were collected when the column was eluted as below.

400 mL ACN – DCM (1:19)	(fractions 1 – 20)
200 mL ACN – DCM (1:4)	(fractions 21 – 30)
100 mL ACN – DCM (1:1)	(fractions 31 – 35)

Selected fractions were analysed by HPLC which indicated that the target compounds had eluted in fractions 7 – 13. These fractions were pooled and dried via rotary evaporation to yield 359 mg material.

7.5.8 Normal phase flash column 6

The target fraction resulting from the normal phase flash column 5 (Section 7.5.7) (359 mg) was loaded in a minimal amount of DCM onto a normal phase flash column (1.5 x 13 cm) which has been previously primed with ACN – DCM (1:19). Fractions of 10 mL were collected and the column eluted with 450 mL ACN – DCM (1:19). Selected fractions were analysed via HPLC and based on that, they were pooled as below

001 – 100 mL	(fraction 1)
100 – 210 mL	(fraction 2)
210 – 250 mL	(fraction 3)
250 – 320 mL	(fraction 4)
320 – 450 mL	(fraction 5)

HPLC analysis of the pooled fractions indicated that the target compounds eluted in fraction 2 (75.0 mg) and fraction 4 (29.8 mg).

7.5.9 Semi-preparative HPLC 1

The target fraction resulting from normal phase flash column 6 (Section 7.5.8) (75.0 mg) was dissolved in MeOH (600 µL) and subsamples applied to the column (25 µL). The subsample was eluted with ACN – water (4:1) at a flow rate of 1.8 mL/min for 15 minutes. Five fractions were collected as listed below.

Fraction number	Elution time (minutes)
1	0.0 – 4.1
2	4.1 – 4.7
3	4.7 – 5.5
4	5.5 – 6.0
5	6.0 – 15.0

HPLC analysis indicated that the target compounds were eluted in fractions 3 and 4. Each was dried down separately to yield cream powders of 10.7 and 10.1 mg respectively.

7.5.10 Semi-preparative HPLC 2

The resulting fraction 3 from semi-preparative HPLC 1 (Section 7.5.9) (10.7 mg) was resuspended in MeOH (200 µL). Subsamples (15 µL) were applied to the column and eluted with ACN – water (7:3) at a flow rate of 1.8 mL/min for 20 minutes. Five fractions were collected as listed below.

Fraction number	Elution time (minutes)
1	0.0 – 10.4
2	10.4 – 11.3
3	11.3 – 12.8
4	12.8 – 14.0
5	14.0 – 20.0

The target compound was in fraction 4, which was dried down to yield a white amorphous powder (3.4 mg). LC-MS analysis identified this as pure compound B (**65**) which was then subjected to structural elucidation with mass spectrometry and NMR spectroscopy.

Compound B (65): White amorphous solid (2.9 mg); ^{1}H and ^{13}C NMR data at 400 MHz ($CDCl_3$) see Table 2.11; HRESIMS *m/z* 635.5683 (calculated for $C_{37}H_{49}NO_8$, 635.5686, Δ -0.3 ppm); MS^2 (positive ion) see Table 2.6; UV (MeOH) λ_{max} 215,

240, 295 nm, accurate measurement of UV absorbance spectrum remains to be determined.

7.5.11 Semi-preparative HPLC 3

The resulting fraction 4 from semi-preparative HPLC 1 (Section 7.5.9) (10.1 mg) was further separated using the protocol in Section 7.5.10. Each run was 15 minutes and six fractions were collected as listed below.

Fraction number	Elution time (minutes)
1	0.0 – 9.5
2	9.5 – 10.5
3	10.5 – 11.4
4	11.4 – 12.9
5	12.9 – 13.6
6	13.6 – 15.0

HPLC analysis showed the target compounds to be present in fractions 3 and 5 which were dried down to yield white amorphous powders of 2.6 mg and 2.9 mg respectively. LC-MS analysis identified these to be 13-desoxypaxilline (**37**) and pure compound A (**64**) respectively. The compounds were subjected to structural elucidation with mass spectrometry and NMR spectroscopy.

Compound A (64): White amorphous solid (3.4 mg); ^{1}H and ^{13}C NMR data at 400 MHz ($CDCl_3$) see Table 2.5; HRESIMS *m/z* 635.3453 (calculated for $C_{37}H_{49}NO_8$, 635.3458, Δ -0.5 ppm); MS^2 (positive ion) see Table 2.1; UV (MeOH) λ_{max} 215, 240, 295 nm, accurate measurement of UV absorbance spectrum remains to be determined.

7.5.12 Semi-preparative HPLC 4

The resulting fraction 4 from normal phase flash column 6 (Section 7.5.8) (29.8 mg) was further purified by semi-preparative HPLC. The sample was dissolved in MeOH (400 µL) and subsamples (15 µL) were injected onto the column with an eluent of ACN – water (4:1) at a flow rate of 1.8 mL/min. Each run required 15 minutes and three fractions were collected as listed below.

Fraction number	Elution time (minutes)
1	0.0 – 7.3
2	7.3 – 8.0
3	8.0 – 15.0

LC-MS analysis showed the target compound was in fraction 2, which was dried down to yield a cream amorphous powder (6.9 mg) which was identified as paspaline (**42**).

7.6 Isolation of compound C (66).

Compound C (**66**) was isolated from the non-polar layer of the liquid-liquid partition of crude extract (20 mL). The partitioning used was the same as that detailed in section 7.5.1 and the isolation process is summarised in Figure 7.2. The samples were analysed by LC-MS with the protocol detailed in Section 7.4.1.

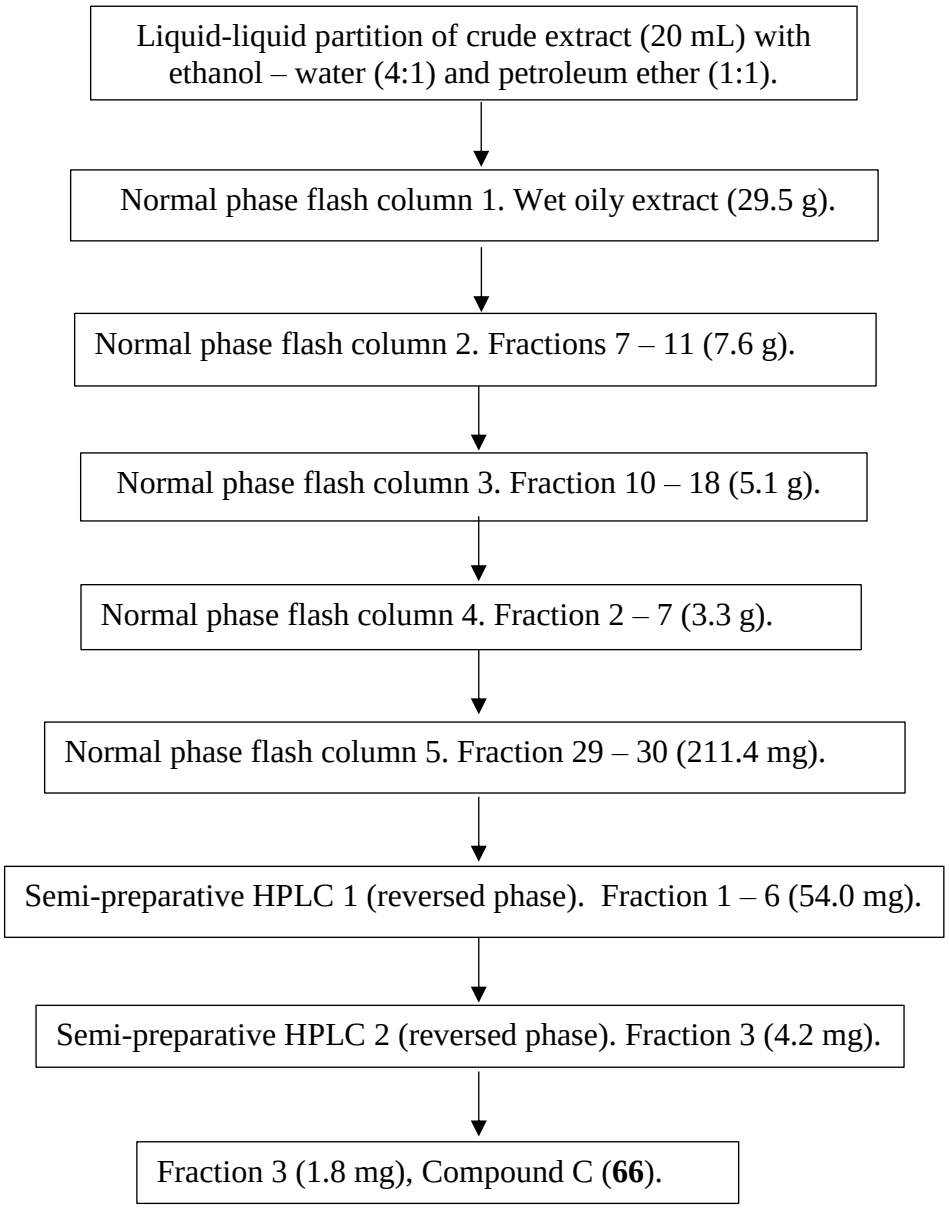

Figure 7.2: Flowchart of the isolation of compound C (**66**).

7.6.1 Liquid-liquid partition

An aliquot of the crude sample (20 mL) was subjected to liquid-liquid partitioning using the protocol in Section 7.5.1 to yield a petroleum ether layer (29.5 g) and a methanol – water layer (4.3 g). The petroleum ether layer was further fractionated.

7.6.2 Normal phase flash column 1

The non-polar layer resulting from the liquid-liquid partition (Section 7.6.1) (29.5 g) was dissolved in a minimum amount of DCM and loaded onto a normal phase flash column (2.5 x 13 cm) which had been previously primed with petroleum ether (PE). The column was then eluted as below

4 x 150 mL PE	(fractions 1 – 4)
3 x 150 mL PE – DCM (1:1)	(fractions 5 – 7)
4 x 150 mL DCM	(fractions 8 – 11)
5 x 150 mL DCM – ACN (9:1)	(fractions 12 – 16)
1 x 300 mL DCM –ACN (4:1)	(fractions 17)
2 x 150 mL DCM –ACN (1:1)	(fractions 18, 19)
2 x 150 mL DCM –ACN (1:4)	(fractions 20, 21)
1 x 150 mL ACN – MeOH (1:1)	(fractions 22)
1 x 300 mL MeOH	(fractions 23)

Fractions were analysed by LC-MS, which showed fractions 7 – 11 contained the target compound. These fractions were pooled and dried down to yield oily material (7.6 g).

7.6.3 Normal phase flash column 2

The target fraction resulting from normal phase flash column 1 (Section 7.6.2) (7.6 g) was dissolved in a minimum amount of DCM and loaded onto a normal phase flash column (2.5 x 13 cm) which had been previously primed with DCM. The column was then eluted as below

1 x 200 mL DCM	(fraction 1)
8 x 50 mL DCM	(fractions 2 – 9)
6 x 50 mL DCM – ACN (19:1)	(fractions 10 – 15)
6 x 50 mL DCM – ACN (9:1)	(fractions 16 – 21)
1 x 150 mL DCM – ACN (4:1)	(fractions 22)
1 x 300 mL MeOH	(fractions 23)

Fractions were analysed by LC-MS which showed fractions 10 – 18 to contain the target compound. These fractions were pooled and dried down to yield oily material (3.6 g). Other similar fractions (from previous columns) were combined with this fraction to yield 5.1 g material.

7.6.4 Normal phase flash column 3

The target fraction resulting from normal phase flash column 2 (Section 7.6.3) (5.1 g) was dissolved in a minimum amount of DCM and loaded onto a normal phase flash column (2.5 x 18 cm) which had been previously primed with PE. The column was then eluted as below:

1 x 100 mL PE	(fraction 1)
1 x 50 mL EtOAc – PE (1:3)	(fraction 2)
10 x 40 mL EtOAc – PE (1:3)	(fractions 3 – 12)
1 x 300 mL EtOAc – PE (3:1)	(fractions 13)

Fractions were analysed by LC-MS and fractions 2 – 7 were found to contain the target compound. These fractions were pooled and dried down to yield oily material (3.3 g).

7.6.5 Normal phase flash column 4

The target fraction resulting from normal phase flash column 3 (Section 7.6.4) (3.3 g) was dissolved in a minimum amount of DCM and loaded onto a normal phase flash column (2.5 x 18 cm) which had been previously primed with PE. The column was then eluted as below:

1 x 100 mL PE	(fraction 1)
1 x 80 mL EtOAc – PE (1:9)	(fraction 2)
16 x 20 mL EtOAc – PE (1:9)	(fractions 3 – 18)
13 x 20 mL EtOAc – PE (1:4)	(fractions 19 – 31)
13 x 20 mL EtOAc – PE (2:3)	(fractions 32 – 44)
1 x 200 mL EtOAc – PE (2:3)	(fraction 45)

Fractions were analysed by LC-MS and the target compound found to be contained in fractions 29 – 30, which were pooled and dried down to yield dark green material (211.4 mg).

7.6.6 Normal phase flash column 5

The target fraction resulting from normal phase flash column 4 (Section 7.6.5) (211.4 mg) was dissolved in a minimum amount of DCM and loaded onto a normal phase flash column (1.5 x 22 cm) which had been previously primed with ACN – DCM (1:19). The column was then eluted as below:

1 x 25 mL ACN – DCM (1:19)	(fraction 1)
11 x 5 mL ACN – DCM (1:19)	(fractions 2 – 12)
4 x 10 mL ACN – DCM (1:19)	(fractions 13 – 16)
1 x 50 mL ACN – DCM (2:4)	(fraction 17)

Fractions were analysed by LC-MS and the target compound found to be contained in fractions 1 – 6, which were pooled and dried down to yield dark green material (54.0 mg).

7.6.7 Semi-preparative HPLC 1

The target fraction resulting from normal phase flash column 5 (Section 7.6.6) (54.0 mg) was dissolved in MeOH (800 µL) with five drops of DCM to aid dissolution. This was subjected to semi-preparative HPLC as described in Section 7.2. Subsamples (15 µL) were injected onto the column and eluted with ACN –

water (4:1) at 1.8 mL/min. Each run was 30 minutes long and seven fractions collected as listed below:

Fraction number	Elution time (minutes)
1	0.0 – 5.4
2	5.4 – 7.7
3	7.7 – 9.3
4	9.3 – 12.2
5	12.2 – 16.5
6	16.5 – 22.5
7	22.5 – 30.0

The fractions were analysed by LC-MS which showed the target compound to be contained in fraction 3. It was dried down to yield a cream material (4.2 mg).

7.6.8 Semi-preparative HPLC 2

The target fraction resulting from semi-preparative HPLC 1 (Section 7.6.7) (4.2 mg) was further purified. The sample was dissolved in MeOH (200 µL) and subsamples (15 µL) injected onto the HPLC using the same protocol as in Section 7.6.7. Each run required 15 minutes and four fractions were collected as listed below:

Fraction number	Elution time (minutes)
1	0.0 – 6.3
2	6.3 – 7.2
3	7.2 – 8.4
4	8.4 – 15.0

The fractions were analysed by LC-MS and the fraction attributed to compound C (**66**) was found to elute at 7.8 minutes (fraction 3). This fraction was dried to yield a cream powder (1.8 mg).

Compound C (66): White amorphous solid (1.8 mg); ^{1}H and ^{13}C NMR data at 400 MHz ($CDCl_3$) see Table 2.15; HRESIMS *m/z* 593.3686 (calculated for $C_{35}H_{47}NO_7$, 593.3658, Δ -2.7 ppm); MS^2 (positive ion) see Table 2.12; UV (MeOH) λ_{max} 215, 240, 292 nm, accurate measurement of UV absorbance spectrum remains to be determined.

7.7 Isolation of compound D (67).

The isolation of compound D (**67**) involved further fractionation of the polar layer (6.4 g) resulting from the liquid-liquid partition in Section 7.5.1 and a series of reversed phase columns. Collected fraction(s) were analysed by LC-MS and/or HPLC with UV. Compound D (**67**) coeluted with terpendole D (**50**) and was isolated as a mixture as summarised below (Figure 7.3).

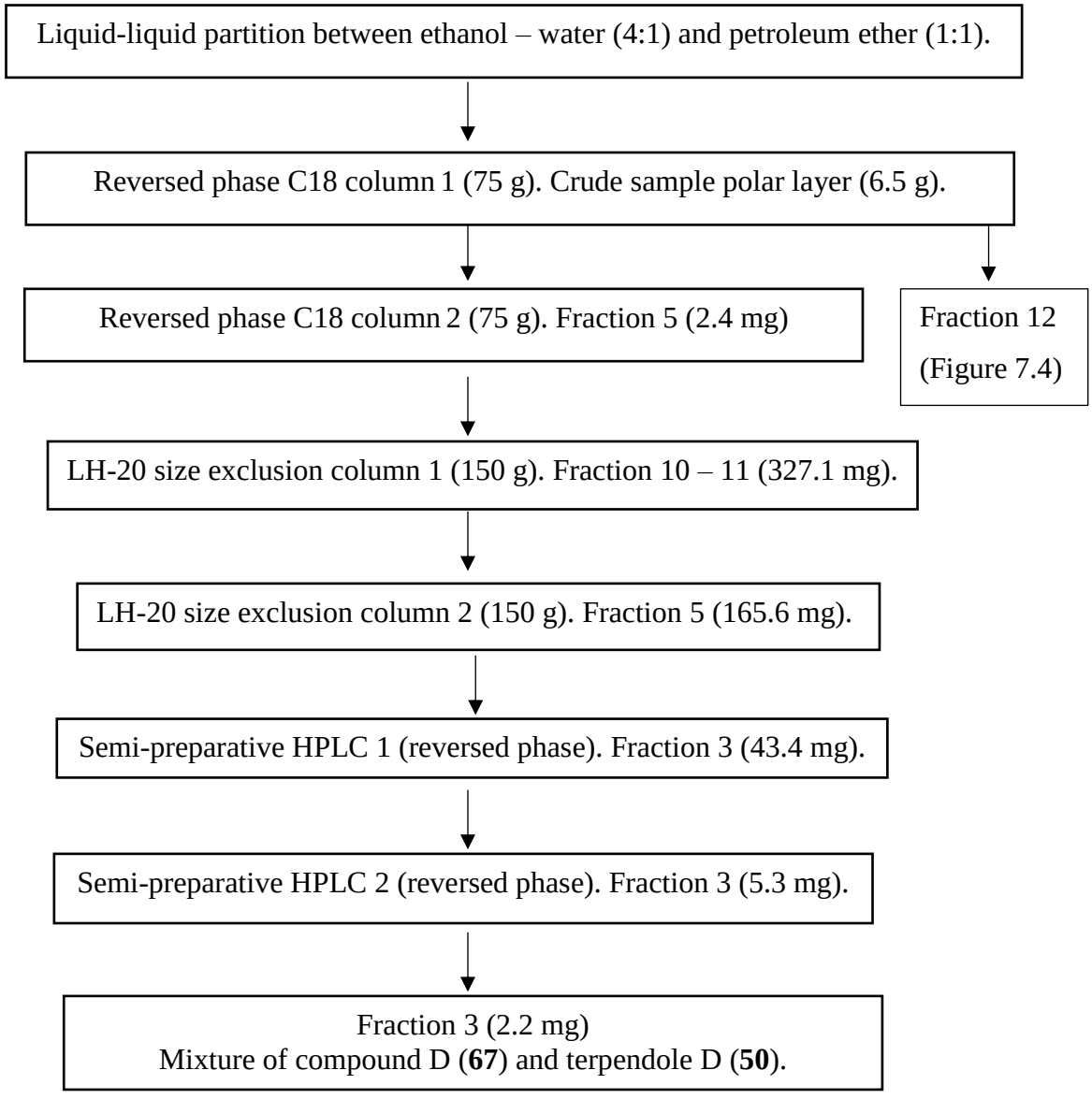

Figure 7.3: Flowchart of the isolation of compound D (**67**) which coeluted with terpendole D (**50**).

7.7.1 Liquid-liquid partition

The liquid-liquid partition was performed as described in Section 7.5.1. The dark, orange-brown, oily ethanol – water soluble material (6.5 g) was further fractionated.

7.7.2 Reversed Phase C18 Column 1

The resulting target fraction from the liquid-liquid partition (Section 7.7.1) (6.5 g) was dissolved in a minimum amount of DCM and loaded onto a reversed phase C18 column (75 g). Elution of the sample utilised the stepwise gradient system given below. All fractions collected were 150 mL except for fraction 13 (200 mL) and were dried down by rotary evaporation prior to analysis.

1 x	H_2O	(fraction 1)
1 x	H_2O – MeOH	(fraction 2)
1 x	H_2O – MeOH (1:1)	(fraction 3)
1 x	H_2O – MeOH (3:7)	(fraction 4)
1 x	H_2O – MeOH (1:9)	(fraction 5)
2 x	MeOH	(fractions 6, 7)
2 x	MeOH – DCM (9:1)	(fractions 8, 9)
1 x	DCM	(fraction 10)
1 x	MeOH	(fraction 11)
1 x	MeOH – H_2O (1:1)	(fraction 12)
1 x	H_2O	(fraction 13)

The LC-MS (protocol as in Section 7.4.1) analysis indicated that fraction 5 contained the majority of the target compounds and this fraction was dried down to yield 2.4 g of material.

7.7.3 Reversed Phase C18 Column 2

The target fraction resulting from reversed phase C18 column 1 (2.4 g) was dissolved in a minimum amount of DCM and loaded onto the same reversed phase column (75 g) (Section 7.7.2). The sample was eluted with the stepwise gradient

system below. All fractions were 150 mL and were dried down by rotary evaporation prior to analysis.

1 x H_2O	(fraction 1)
1 x H_2O – MeOH (1:1)	(fraction 2)
3 x H_2O – MeOH (3:7)	(fractions 3 – 5)
4 x H_2O – MeOH (1:4)	(fractions 6 – 9)
2 x H_2O – MeOH (1:9)	(fractions 10, 11)
2 x MeOH	(fractions 12, 13)
1 x MeOH – DCM (1:1)	(fraction 14)
1 x DCM	(fraction 15)
1 x MeOH	(fraction 16)
1 x MeOH – H_2O (1:1)	(fraction 17)
1 x H_2O	(fraction 18)

The LC-MS analysis indicated that the target compounds were mostly in fractions 10 and 11 which were combined and dried down to yield 327.1 mg material.

7.7.4 Size Exclusion Column 1

The target fraction resulting from reversed phase C18 column 2 (Section 7.7.3) (327.1 mg) was dissolved in a minimal amount of MeOH and loaded onto a size exclusion column (Section 7.3.3). The sample vial was rinsed with a minimum amount of MeOH and the rinsings were added to the column. The column was then eluted with 200 mL of MeOH followed by twelve fractions of 50 mL. Each fraction was dried down by rotary evaporation and analysed by LC-MS. Fraction 5 contained the target compounds. This fraction was dried down to yield 165.6 mg of material.

7.7.5 Size Exclusion Column 2

The target fraction resulting from size exclusion column 1 (Section 7.7.4) (165.6 mg) was dissolved in a minimum amount of MeOH and loaded onto the same column used in Section 7.7.4. The column was then eluted first with 200 mL

MeOH and then with 100 mL of MeOH followed by twenty fractions of 10 mL each. Each fraction was dried down and analysed by LC-MS. Fractions 6 – 8 contained the target compounds, so were combined and dried to yield 43.4 mg of material.

7.7.6 Semi-preparative HPLC 1

Prior to semi-preparative HPLC, a quick isocratic analysis on LC-MS was performed to determine the best eluents for the HPLC system. It was found that ACN – H_2O, (9:1) produced the best resolution and separation of peaks.

The target fraction resulting from size exclusion column 2 (Section 7.7.5) (43.4 mg) was further separated via reversed phase, semi-preparative HPLC (Section 7.3.4). The sample was dissolved in MeOH (400 µL) and subsamples (20 µL) were injected. Four fractions were collected as below:

Fraction number	Elution time (minutes)
1	0.0 – 5.0
2	5.0 – 8.0
3	8.0 – 13.0
4	13.0 – 20.0

LC-MS analysis indicated that the target compounds were contained in fraction 3 which was dried down to yield 5.3 mg of material.

7.7.7 Semi-preparative HPLC 2

The target fraction resulting from semi-preparative HPLC 1 (Section 7.7.6) (5.3 mg) was further purified. The sample was dissolved in MeOH (200 µL) and subsamples (15 µL) injected onto the HPLC using the same protocol as in Section 7.7.6. Each run required 15 minutes and four fractions were collected as listed below:

Fraction number	Elution time (minutes)
1	0.0 – 7.5
2	7.5 – 8.0
3	8.0 – 8.5
4	8.5 – 15.0

The fractions were analysed by LC-MS and the fraction containing compound D (**67**) was found to coelute with terpendole D (**50**) at 8.3 minutes (fraction 3). This fraction was dried to yield a cream powder (2.2 mg) which was subjected to NMR analysis.

Compound D (66) mixture with terpendole D (**50**): Cream amorphous solid (2.2 mg); ^{1}H and ^{13}C NMR data at 400 MHz ($CDCl_3$) see Table 2.17; ESIMS *m/z* 635.02; MS^2 (positive ion) 618.2, 600.2, 564.1, 536.2; UV (MeOH) λ_{max} 215, 240, 295 nm, accurate measurement of UV absorbance spectrum and HRESIMS remains to be determined

7.8 Isolation of terpendole D (50)

The isolation of terpendole D (**50**) involved further fractionations of fraction 12 (151.8 mg) resulting from the reversed phase C18 column 2 in Figure 7.4. A series of reversed phase columns were run (Figure 7.4) and collected fraction(s) were analysed by LC-MS and/or HPLC. Paspaline (**42**) and a potential emindole analogue were also isolated as summarised below.

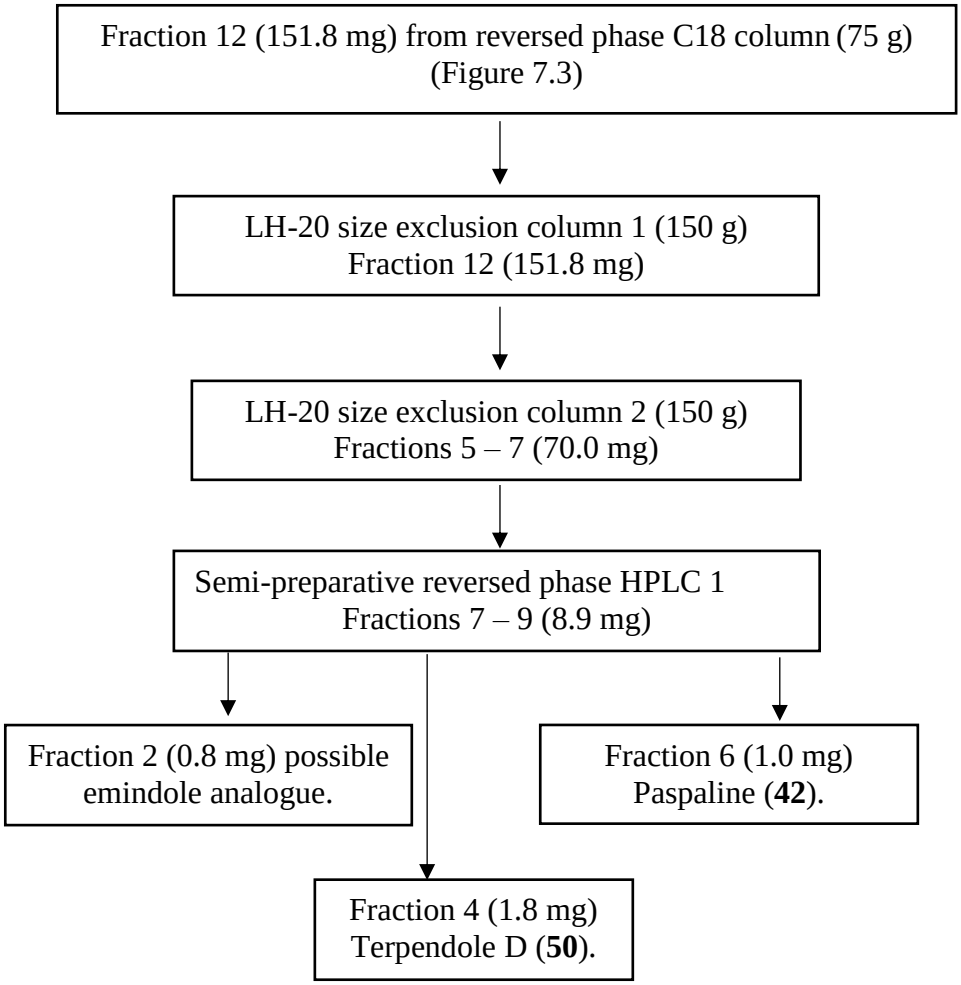

Figure 7.4: Flowchart of the isolation of terpendole D (**50**) together with paspaline (**42**) and a potential emindole analogue.

7.8.1 Size Exclusion Column 1

The target fraction 12 resulting from reversed phase C18 column 2 (Section 7.7.3) (151.8 mg) was dissolved in a minimal amount of MeOH and loaded onto a size exclusion column (Section 7.3.3). The sample vial was rinsed with a minimum

amount of MeOH and the rinsings were added to the column. The column was then eluted with 200 mL of MeOH followed by twelve fractions of 50 mL each. Fractions were dried down by rotary evaporation and analysed by LC-MS. Fractions 5 – 7 contained the target compounds. They were combined and dried down to yield 70.0 mg material.

7.8.2 Size Exclusion Column 2

The target fraction resulting from size exclusion column 1 (Section 7.8.1) (70.0 mg) was dissolved in a minimum amount of MeOH and loaded onto the same column used in Section 7.8.1. Thirteen fractions (20 mL each) were collected, dried down and analysed by LC-MS. Fractions 7 – 9 contained the target compounds and were combined and dried to yield 8.9 mg material.

7.8.3 Semi-preparative HPLC 1

The target fraction resulting from size exclusion column 2 (Section 7.8.2) (8.9 mg) was further separated via reversed phase, semi-preparative HPLC (Section 7.3.4). The sample was dissolved in MeOH (400 µL) and subsamples (20 µL) were injected. Seven fractions were collected as below:

Fraction number	Elution time (minutes)
1	0.0 – 6.9
2	6.9 – 7.3
3	7.3 – 9.2
4	9.2 – 9.8
5	9.8 – 10.7
6	10.7 – 11.5
7	11.5 – 15.0

LC-MS analysis indicated that the target compounds were contained in fractions 2, 4 and 6 which were dried down to yield emindole analogue (0.8 mg), terpendole D (**50**) (1.8 mg) and paspaline (**42**) (1.0 mg), respectively.

7.9 LC-MS analysis of fresh crude extract.

The LC-MS analysis of the fresh extract of perennial ryegrass seed (50 mg) infected with wild-type endophyte was conducted by Dr Mace (AgResearch, Grasslands). The seed was grounded then 50 mg was extracted with isopropanol (1 mL) by rotating using an over-over mixer in a 2 mL vial for 1 hour followed by centrifugation for 5 minutes. The supernantant was transferred into a 1 mL HPLC vial and 5 µL was analysed via LC-MS analysis using a previously reported gradient and protocol.[155]

7.10 Porina experiments

7.10.1 Aliquots for porina larvae treatment.

Aliquots for addition to the porina diet were prepared prior to the beginning of the experiment. The quantity required per test compound was calculated based on 25 g of semi-synthetic diet per treatment per week.

7.10.1.1 Experiment One

The effect of paxilline on porina larvae was determined in a four week experiment. Paxilline (**36**) as an acetonitrile solvate was available from Dr Finch (AgResearch).[55] A stock solution of paxilline (**36**) (2.01 mg) in MeOH (2.5 mL) was prepared. The quantities of paxilline (**36**) required for the different treatments (0, 1, 2.5, 5, 10 µg/g) were equivalent to 0, 33.83, 84.45, 169.03, 337.19 µL aliquots of the stock solution. The aliquots for each treatment were transferred into labelled 1 mL LC vials using a 250 µL positive displacement pipette and dried under a flow of nitrogen. They were stored at 5º C prior to use.

7.10.1.2 Experiment Two

The effects of lolitrem B (**3**), 13-desoxypaxilline (**37**) and paspaline (**42**) on porina larvae were determined in a three week experiment. Lolitrem B (**3**) was available from Dr Finch while 13-desoxypaxilline (**37**) and paspaline (**42**) were isolated during the current research. Paxilline (**36**) was also included as a positive control.

Aliquots equivalent for two concentrations (5 and 10 µg/g) per compound were prepared plus a 0 µg/g solvent control (DMSO). The amount of each compound required to make the weekly diets was calculated and a stock solution of each was made by dissolving the required amount in MeOH (2.5 mL) (Table 7.2). Aliquots were dried down under nitrogen and stored at 5º C until required.

Table 7.2: The equivalent amount of aliquots (µL) for the required concentration (µg/g) of paxilline (**36**), lolitrem B (**3**), paspaline (**42**) and 13-desoxypaxilline (**37**).

Compound stock solution	**Treatment Concentration (µg/g)**	**Equivalent aliquot of stock solution (µL)**
Solvent control	0	0.0
Paxilline (**36**)	5	278.5
(1.22 mg / 2.5 mL MeOH)	10	555.5
Lolitrem B **(3**)	5	276.5
(1.13 mg/ 2.5 mL MeOH)	10	555.1
Paspaline (**42**)	5	195.3
(1.60 mg/ 2.5 mL MeOH)	10	390.6
13-desoxypaxilline (**37**)	5	91.9
(3.40 mg/ 2.5 mL MeOH)	10	183.8

7.10.1.3 Experiment Three

The effects of the newly isolated compound A (**64**), compound B (**65**) and terpendole D (**50**) on porina larvae were investigated in this experiment. Paxilline (**36**) was again included as a positive control. Aliquots equivalent for two concentrations (5 and 10 µg/g) per compound plus a solvent control were prepared as detailed previously. A stock solution of each compound was prepared and aliquots were taken as in Table 7.3. The aliquots were dried down under nitrogen gas and stored at 5º C until required.

Table 7.3: The equivalent amount of aliquots (µL) for the required concentrations (µg/g) of paxilline (**36**), compound A (**64**), compound B (**65**) and terpendole D (**50**).

Compound stock solution	Treatment Concentration (µg/g)	Equivalent aliquot from stock solution. (µL)
Solvent control	0	0.0
Paxilline (**36**)	5	278.5
(1.22 mg / 2.5 mL MeOH)	10	555.5
Compound A (**64**)	5	115.7
(2.70 mg / 2.5 mL MeOH)	10	231.5
Compound B (**65**)	5	91.9
(3.40 mg / 2.5 mL MeOH)	10	183.8
Terpendole D (**50**)	5	223.2
(1.40 mg / 2.5 mL MeOH)	10	446.4

7.10.2 Semi-synthetic diet and treatments

The semi-synthetic diet for the porina larvae was prepared based on the method outlined by Popay.[84] Fresh carrot (100 g) was combined with 100 mL deionised water and blended (Waring commercial blender, model HGB2WTG4) with fresh clover (100 g, harvested from potted plants kept in an AgResearch screen house). The mixture was finely blended and Brewer's yeast (16 g) was mixed in before it was transferred into a 500 mL beaker. In a 1 L beaker, agar (12 g) and deionised water (300 mL) were mixed, heated in the microwave with occasional stirring until boiling and then cooled down to 70 ºC. While the agar was cooling down, the carrot mixture was warmed in the microwave for 2 x 1 minute on medium power with thorough stirring after every minute. The carrot mixture was mixed with the agar and stirred thoroughly to ensure that the entire agar was included. The diet was split between two beakers (500 mL) so that one could be used and the other kept warm in a water bath to prevent setting of the agar. Aliquots of diet mixture (25 g) were weighed into beakers (50 mL) and the test compounds, (dissolved in 400 µL DMSO) were added immediately. (The solvent control semi-synthetic diet contained only 400 µL DMSO). The diet mixture was stirred thoroughly and quickly to ensure it was homogeneous and did not set before it was transferred into

a 90 mm plastic Petri dish to cool down. The diet was stored in a small chilly bin to keep it cool and reduce exposure to light before it was fed to the porina larvae.

7.10.3 Collection and rearing of porina (moths and larvae)

7.10.3.1 Collection of adult porina moths.

Porina moths were collected by Colin Ferguson (AgResearch) at Allanton (45.91S, 170.26E), Otago. They were attracted to a light source (Compact Fluorescent Light) between 10.00 pm and 11:45 pm and caught by hand. Each individual female moth was held in a 60 mL specimen vial at room temperature to allow them to lay their eggs. The moths for the first experiment were collected on the 6th and 7th of December 2014, on the 6th November 2015 for the second experiment and those for the third experiment were collected on the 31st December 2016.

After oviposition, the eggs were separated from the moths. The eggs from individual moths were kept in separate containers and moths were stored individually in vials at -20°C until identified. The eggs were sent to the Ruakura Campus overnight or otherwise were stored at 4 °C for 2 – 3 days before sending to avoid transport over weekends. The eggs were received at the Ruakura campus on the 11th Dec 2014, the 11th November 2015 and the 9th January 2017 for the first, second and third experiments respectively.

7.10.3.2 Identification of female Porina moths.

Female moths were identified by Colin Ferguson by examination of their bursa copulatrix according to Dugdale (1994).[145] Thirty eight *W. cervinata* female moths were collected in 2014, forty *W. copularis* in 2015 and thirty nine *W. copularis* in 2016. Previous work has shown that the two species do not differ in their response to epoxy-janthitrems (A.J. Popay unpublished).

7.10.3.3 Porina egg sterilisation

Once the porina eggs arrived at the Ruakura Campus, they were sterilised to remove any micro-organisms that could affect egg development and the porina larvae when hatching. Eggs were surface sterilised using the methods outlined by Carpenter

(1983)[156] with copper oxychloride solution (0.5 mg) in deionised water (500 mL). A piece of fine nylon cloth was placed on top of a 250 mL glass beaker and eggs from a single moth were poured onto the mesh. The copper oxychloride solution (10 mL) was sprayed onto the eggs with a pipette. After two minutes, the eggs were washed carefully with deionised water (20 mL). The sterilised eggs were then placed on a moist piece of filter paper (LabServ qualitative filter paper, 9 cm) in a 9 cm Petri dish and sealed with parafilm. The Petri dishes were kept in a plastic container in a controlled environment room at 15 °C until the eggs hatched.

7.10.3.4 Porina larvae hatching

Porina eggs hatched within 10 - 21 days. After 10 days incubation, the Petri dishes were checked daily for any sign of hatching and once eggs started to hatch, the larvae were transferred into a labelled plastic container (quarter filled with Yates bloom Décor fine bark chips). The remaining eggs were checked and after 24 hours, the eggs that did not hatch were then discarded. The eggs started to hatch on the 28th December 2014, the 22nd November 2015 and the 31st January 2017 for the first, second and third experiments respectively. Approximately 40 larvae from a single moth were allocated to each container and about 15 - 20 small chunks of control semi-synthetic diet were evenly distributed over the bark. They were kept in a 15°C controlled environment room using a 16:8 light:dark regime, with weekly changes of diet.

7.10.3.5 Rearing porina larvae

Porina larvae were fed once a week with fresh control semi-synthetic diet (Section 7.10.2) and were kept in the controlled room until they were at least 8 weeks old. For the first few weeks, the diet fed previously to the larvae was carefully observed to make sure that none of the tiny larvae had stuck to it, before it was replaced with a new diet.

7.10.3.6 Porina larvae weighing and replicate allocation.

Prior to the day of the experiment, the larvae were removed from their storage container. Individual larvae were checked carefully with a soft dusting brush to

avoid any injury. Those that were at least 2 cm long were considered mature enough and were transferred into individually labelled plastic containers (30 mL). Fifteen larvae were required for each treatment. The containers were stacked in a polystyrene box and covered with damp paper towels to maintain humidity without food. An extra twenty larvae were selected in case of unresponsive larvae or if any selected larvae were outside the suitable weight range. They were stored in the controlled environment room overnight.

On the day of the experiment, each individual larva was weighed (Metler Toledo analytical balance XS204, readability 0.1 mg) and allocated to a treatment group of fifteen replicates. Each replicate group had larvae of a similar size, with the lightest larvae assigned to replicate 1 and the heaviest larvae to replicate 15. Within each replicate group, the larvae were randomly assigned to the different treatments and transferred into individually labelled polystyrene specimen containers (70 mL) two-thirds filled with moist Yates bloom Décor fine bark chips.

7.10.3.7 Porina larvae Bioassay

A fresh diet was made once a week and plugs were fed to the larvae on the same day. The diet plugs for each treatment were cut with a 10 mm core-borer and each individual plug was weighed and added to the container with the porina larvae. The leftover diet was stored in the fridge and used for the replacement of the larval diet 4 days later. On the diet replacement day, the remaining diet from each larva was gently brushed to remove as much dirt as possible before weighing. A new diet plug was weighed and fed to the larvae. If diet had not been touched, the porina larva was checked for mortality. The weight of a larva was recorded if dead but not included in the analysis of data as the time of death was unknown. Samples of the freshly prepared, refrigerated and remaining uneaten diet (10 µg/g) were analysed by HPLC to determine the stability of the test compounds. At the completion of each experiment, porina larvae were reweighed and their final weight recorded.

7.10.4 HPLC analysis of diet extract.

7.10.4.1 HPLC protocol

Aliquots of 10 µg/g diet extract (10 µL) were analysed using a Zorbax column (SIL 4.6mm x 250mm, 5µm) eluted with acetonitrile – dichloromethane (1:4) and a flow rate of 1.8 mL/min. The extract peak was detected with a Hewlett-Packard 1040M diode array UV detector at 230 nm and 280 nm since paxilline (**36**) is not fluorescent.

7.10.4.2 Standard solution

A standard solution of paxilline (**36**) (2 mg) in MeOH (25 mL) was used as an internal standard for all of the analytes. This was because the available amounts of isolated compounds were not enough to make up their own individual standard solutions.

On injection of 10 µL (the equivalent of 0.8 µg) paxilline (**36**) standard solution, a peak eluted at about 4.6 minutes with an area of 1349 square units. This means that theoretically, 10 µL of porina diet containing 10 µg/g paxilline (**36**) would produce a peak area of 126 square units (the equivalent of 0.075 µg paxilline (**36**)).

7.10.4.3 Porina larvae diet extraction

The samples from the 10 µg/g treatments were extracted and analysed to determine their stability. The diet samples (100 ± 2 mg) were transferred into Eppendorf safe-lock tubes (2 mL) on the day of larval diet feeding. The samples were extracted with dichloromethane – methanol (2:1) (1 mL) on a rotating wheel at 20 rpm (Labnet international, inc. mini labroller^{TM}) for one hour. Samples were centrifuged for 2 minutes at 12000 rpm (Eppendorf Centrifuge 5418) and the supernatant (750 µL) was transferred into a LC-vial (1 mL), dried under nitrogen and then freeze-dried to remove any residual solvent. The extract was then redissolved in DCM (100 µL) and an aliquot (10 µL) was injected for HPLC analysis. When the HPLC analysis could not be completed on the same day, the extract was stored in the fridge overnight and analysed the following day.

7.10.4.4 Mean diet consumption

Consumption was determined from the weight change in diets for each live larva during each feeding period.

Experiment I

The analysis of mean consumption (per measurement time) was carried out with a restricted maximum likelihood (REML) linear mixed model. The variation in consumption differed between treatments and REML allowed for those differences.

Experiment II

The mean diet consumption was analysed with repeated measures ANOVA as there was no evidence of time by treatment interactions; therefore, the overall treatment means for each larva were used.

Experiment III

The mean diet consumption was analysed using one-way ANOVA with initial porina weight as a covariate. Contrast analysis was used to compare the means of the treatment to the Nil and to 5 µg/g and 10 µg/g. Values were log-transformed prior to analysis to stabilise the variance. Back-transformed means with approximate error were used for plotting the graph of the total mean diet consumption.

7.10.5 Statistical analysis

Statistical analysis of the mean diet consumption, weight gain and mortality of porina larvae was conducted using Microsoft Excel 2010 and GenStat 16th edition by Dr Vanessa Cave (Statistician at AgResearch, Ruakura).

7.10.5.1 Mean weight change

The data for the weight change between the beginning and the end of the experiment were obtained for the surviving larvae.

Experiment I

The variations in data differed between treatments thus mean weight change data was analysed using REML to allow for these variances.

Experiment II

The mean weight change was analysed with one-way ANOVA as there was no evidence of time by treatment interactions.

Experiment III

The mean weight change was analysed using one-way ANOVA. Contrast analysis was used to compare the means of the treatments for the Nil, 5 and 10 µg/g treatments.

7.10.5.2 Mortality rate

The survival rate was obtained from the number of porina alive at the end of the experiment. Survival curves per treatment were compared using the Kaplan-Meier estimate for all the experiments.

Appendices

8.1 List of Appendices

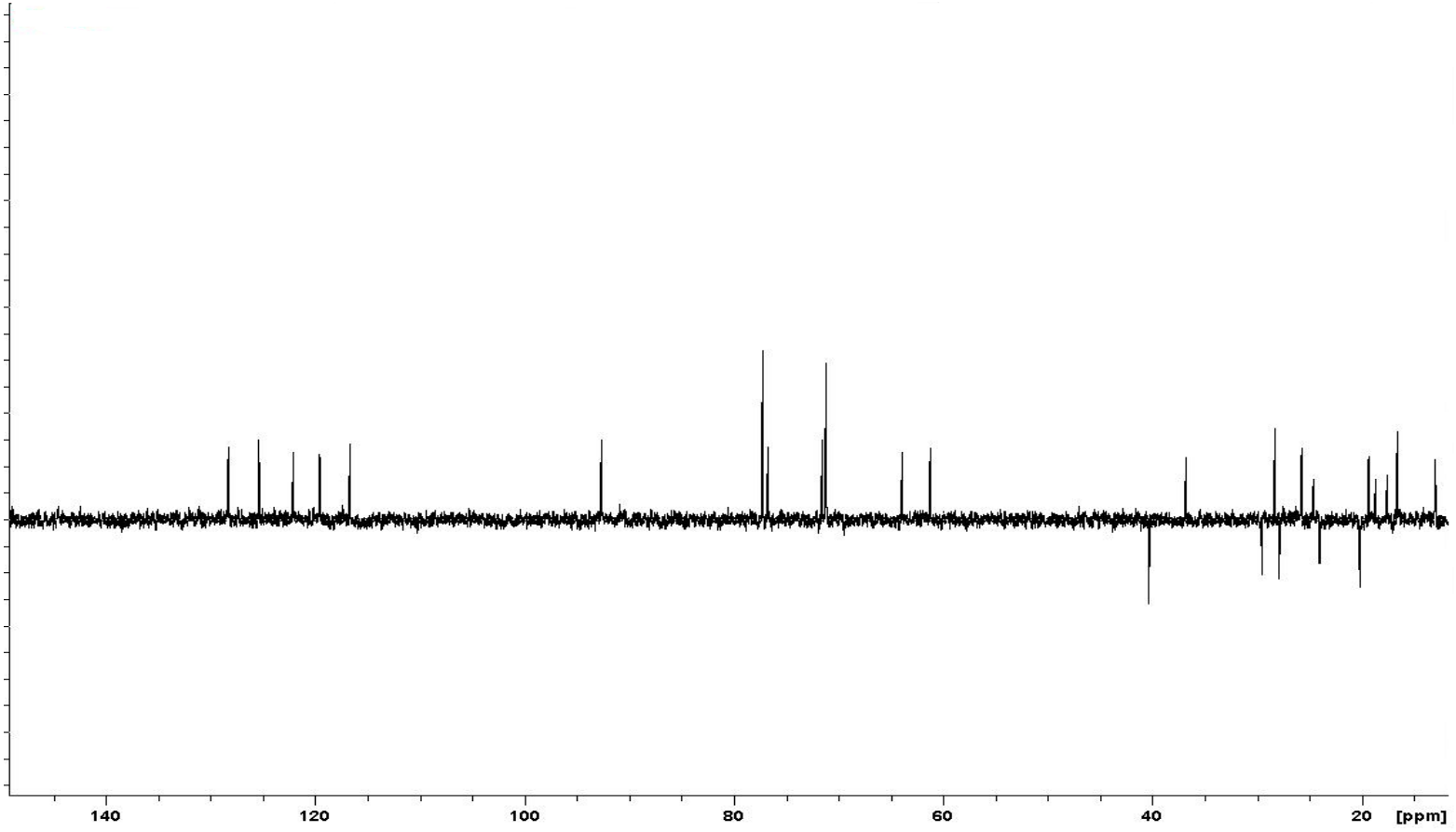

Appendix 1: The DEPT-135 NMR spectrum of compound A (**64**), ($CDCl_3$, 400 MHz).

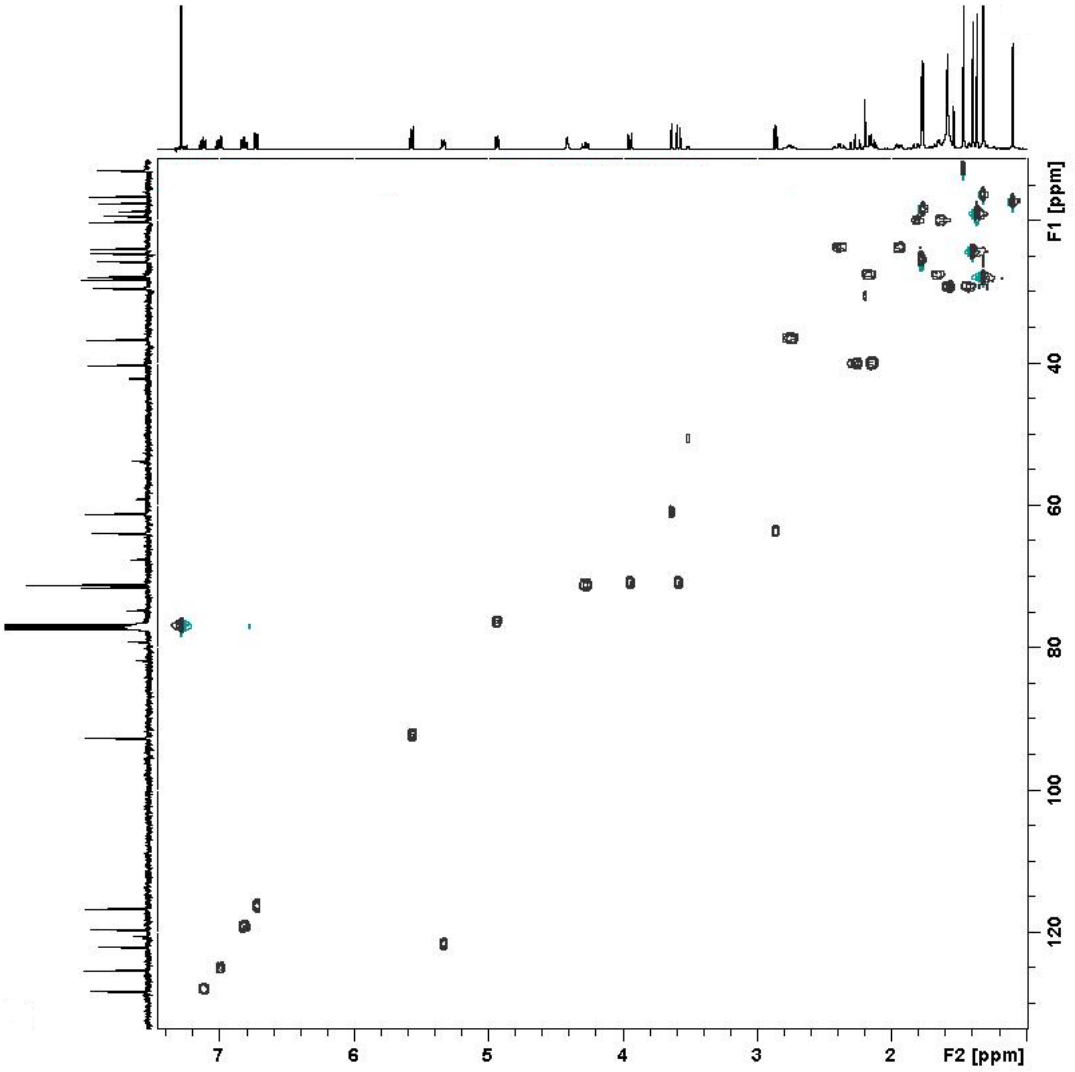

Appendix 2: The HSQC NMR spectrum of compound A (**64**), ($CDCl_3$, 400 MHz).

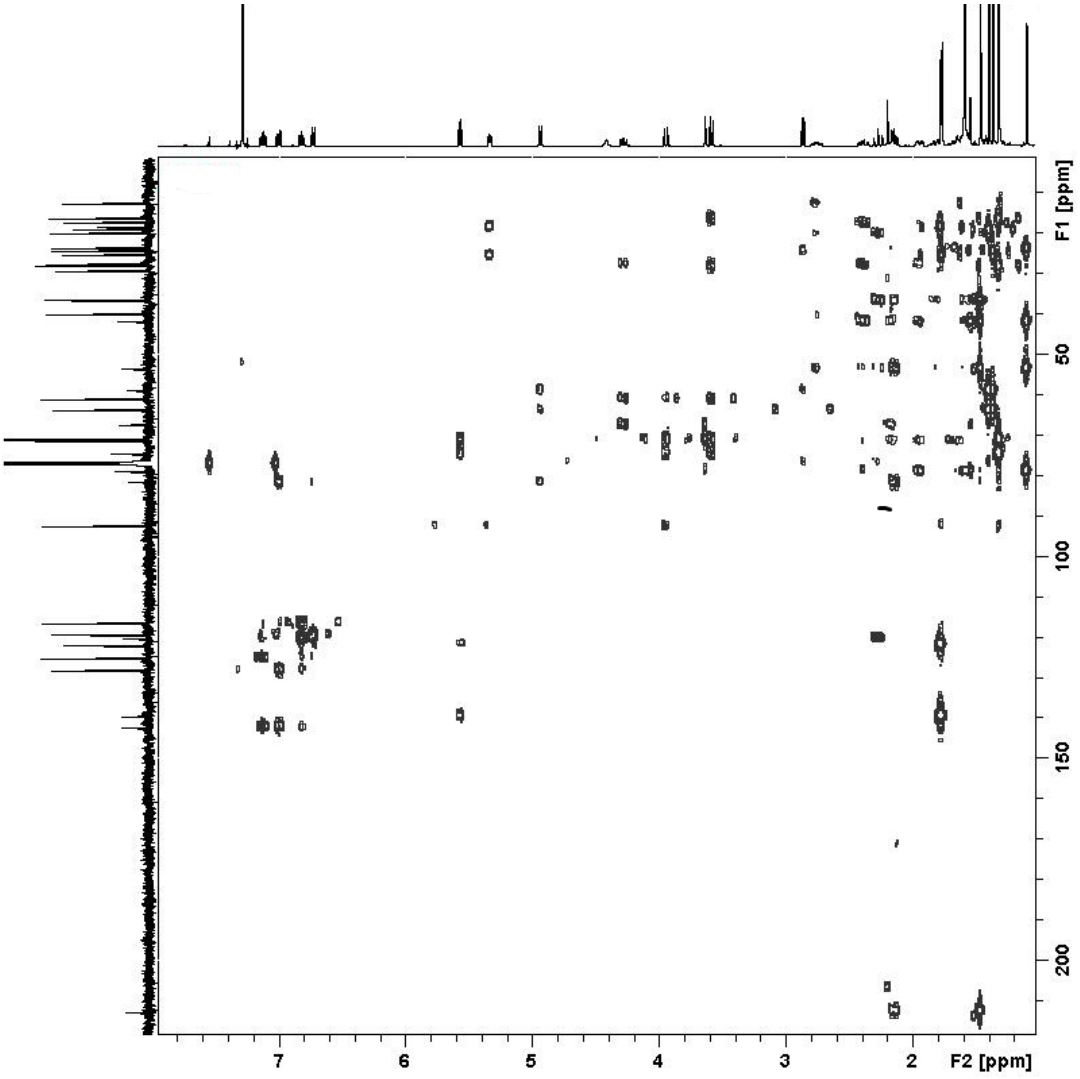

Appendix 3: The HMBC NMR spectrum of compound A (**64**), ($CDCl_3$, 400 MHz).

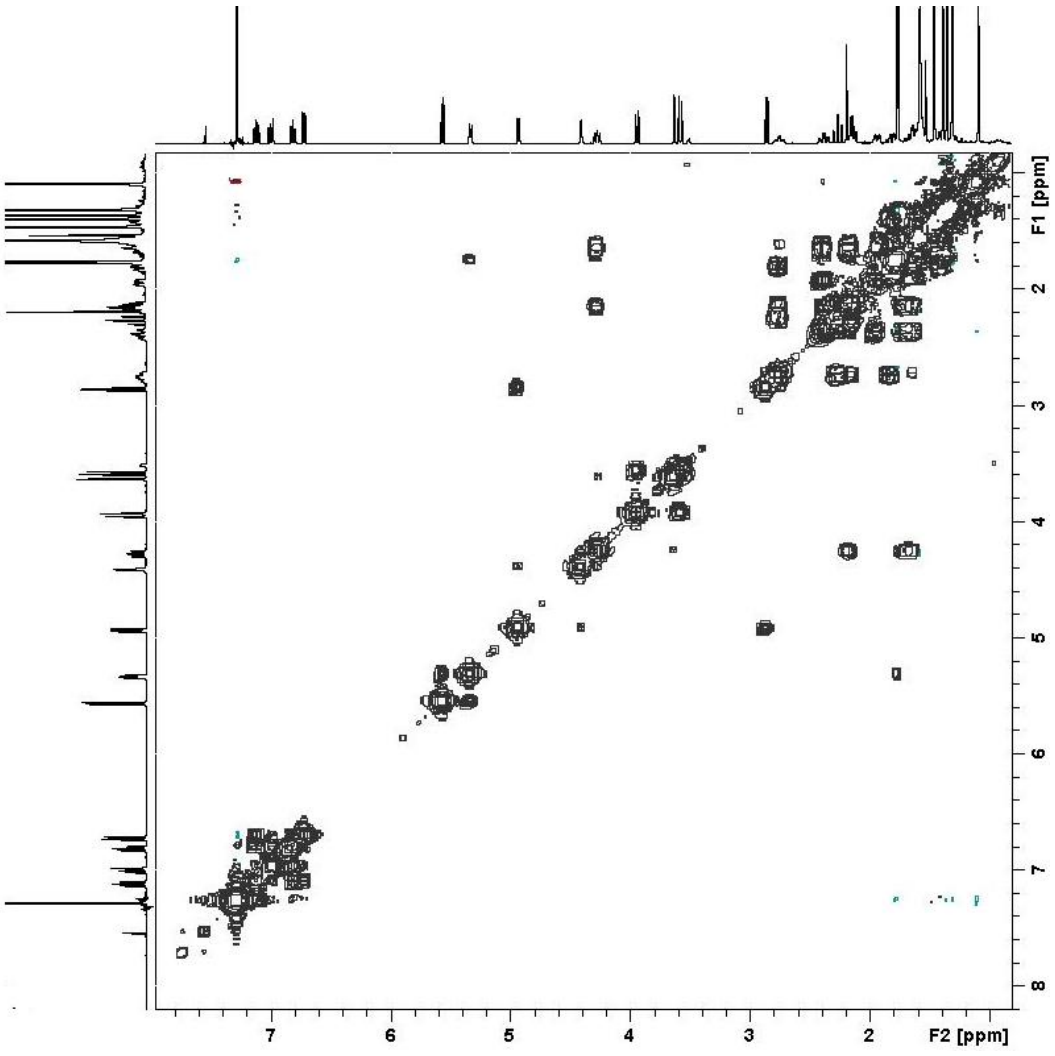

Appendix 4: The COSY NMR spectrum of compound A (**64**), ($CDCl_3$, 400 MHz).

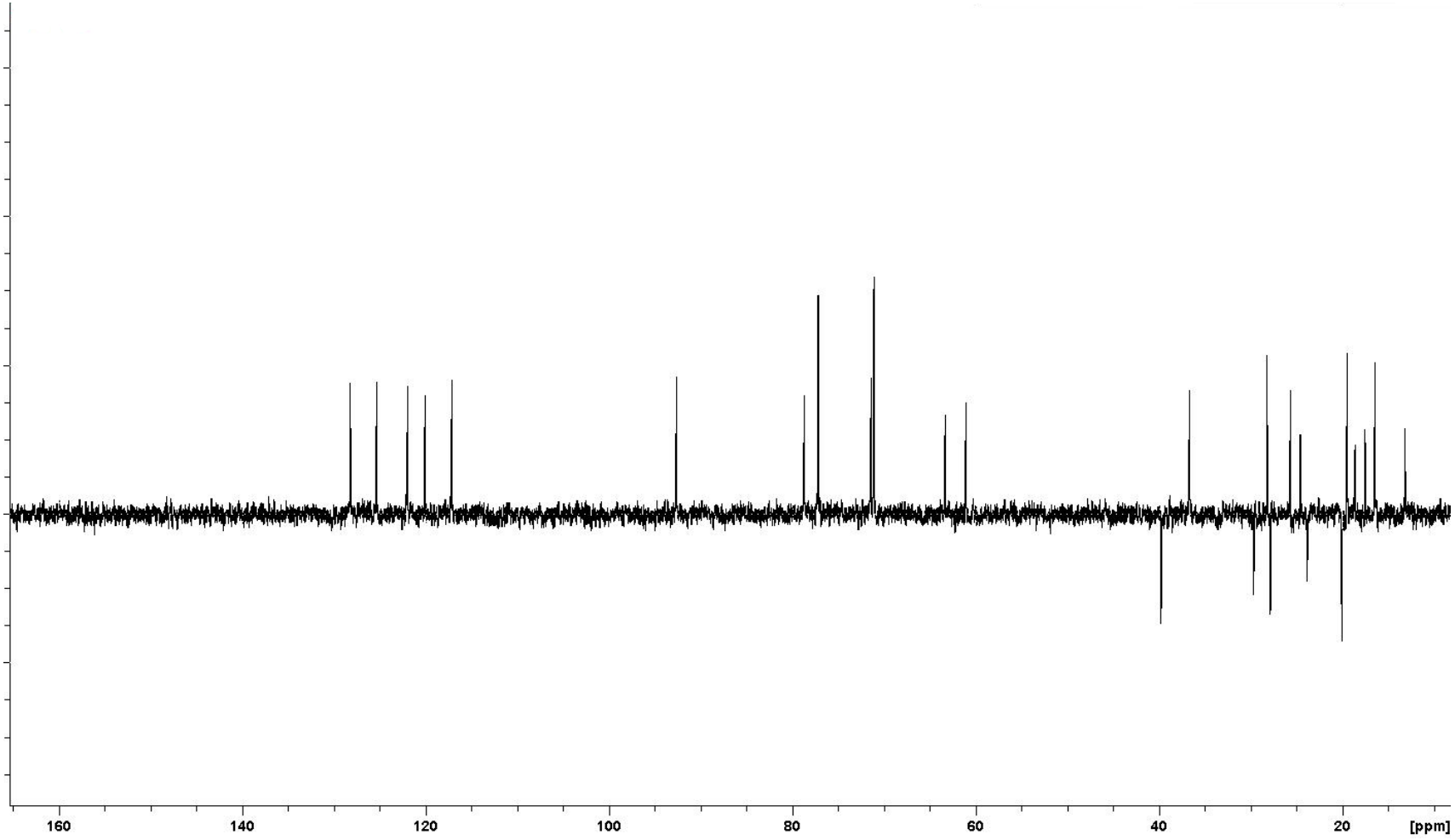

Appendix 5: The DEPT-135 NMR spectrum of compound B (**65**), ($CDCl_3$, 400 MHz).

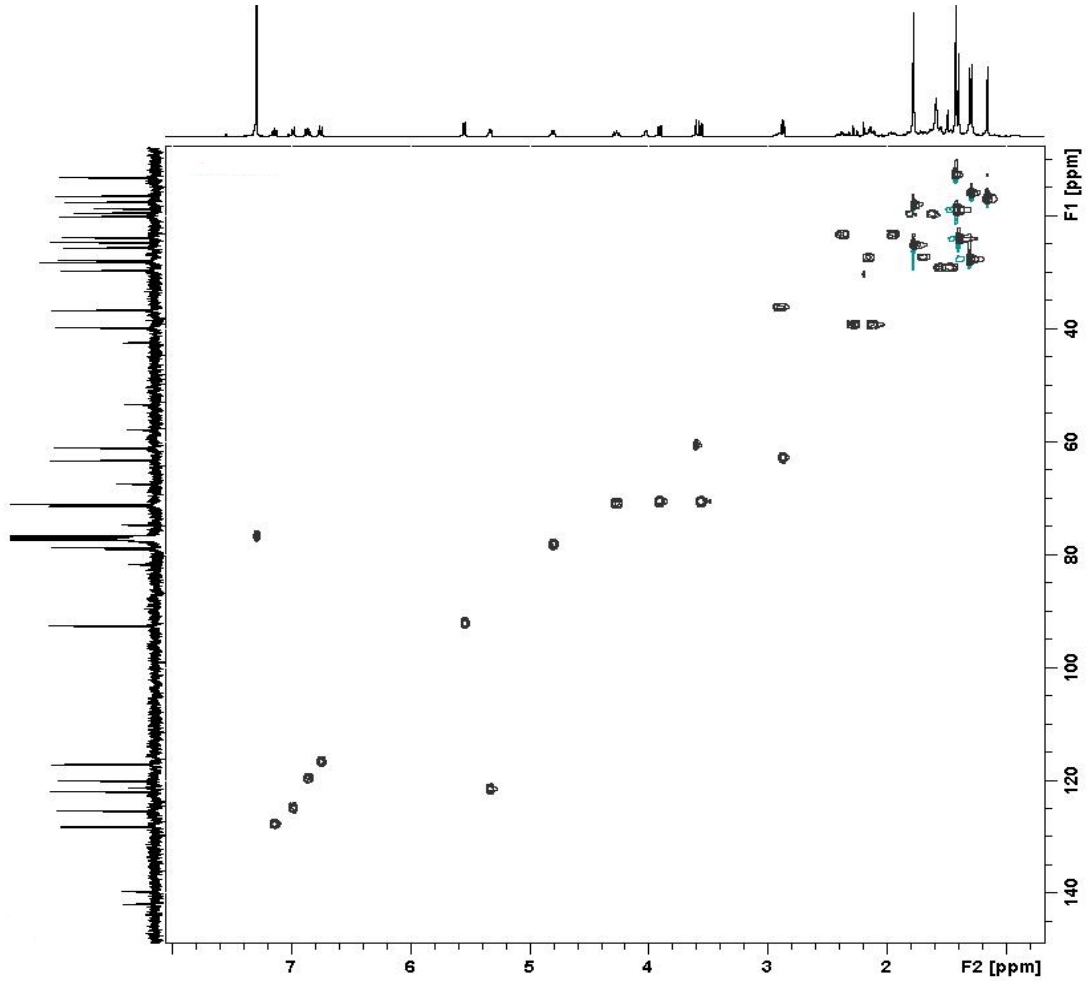

Appendix 6: The HSQC NMR spectrum of compound B (**65**), ($CDCl_3$, 400 MHz).

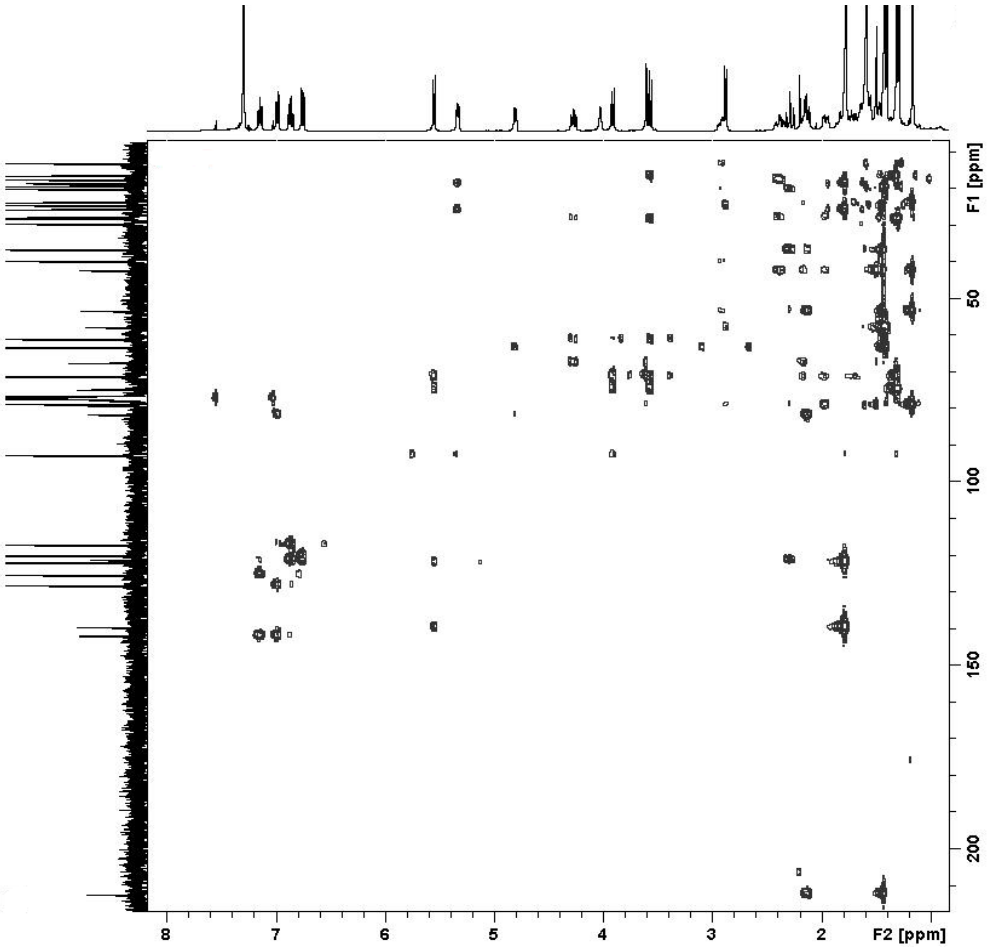

Appendix 7: The HMBC NMR spectrum of compound B (**65**), ($CDCl_3$, 400 MHz).

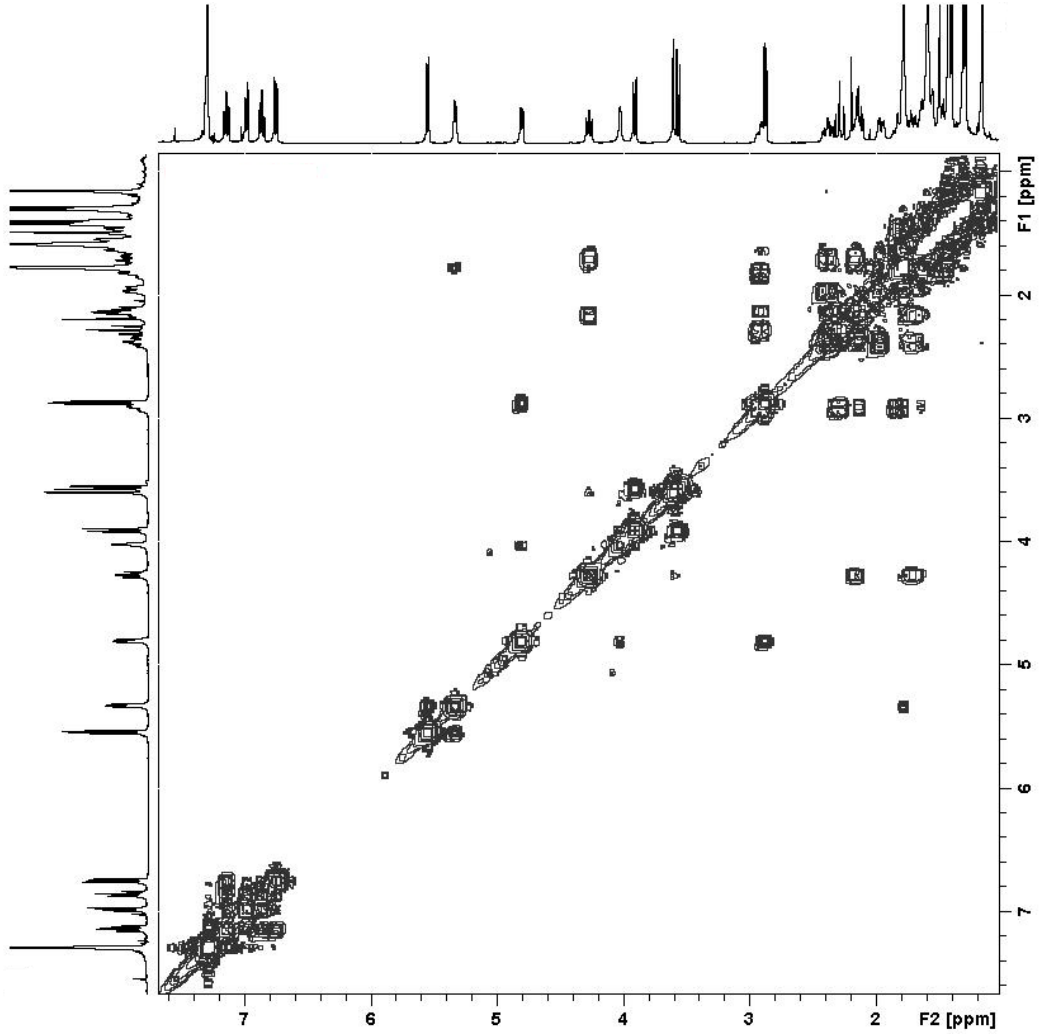

Appendix 8: The COSY NMR spectrum of compound B (**65**), ($CDCl_3$, 400 MHz).

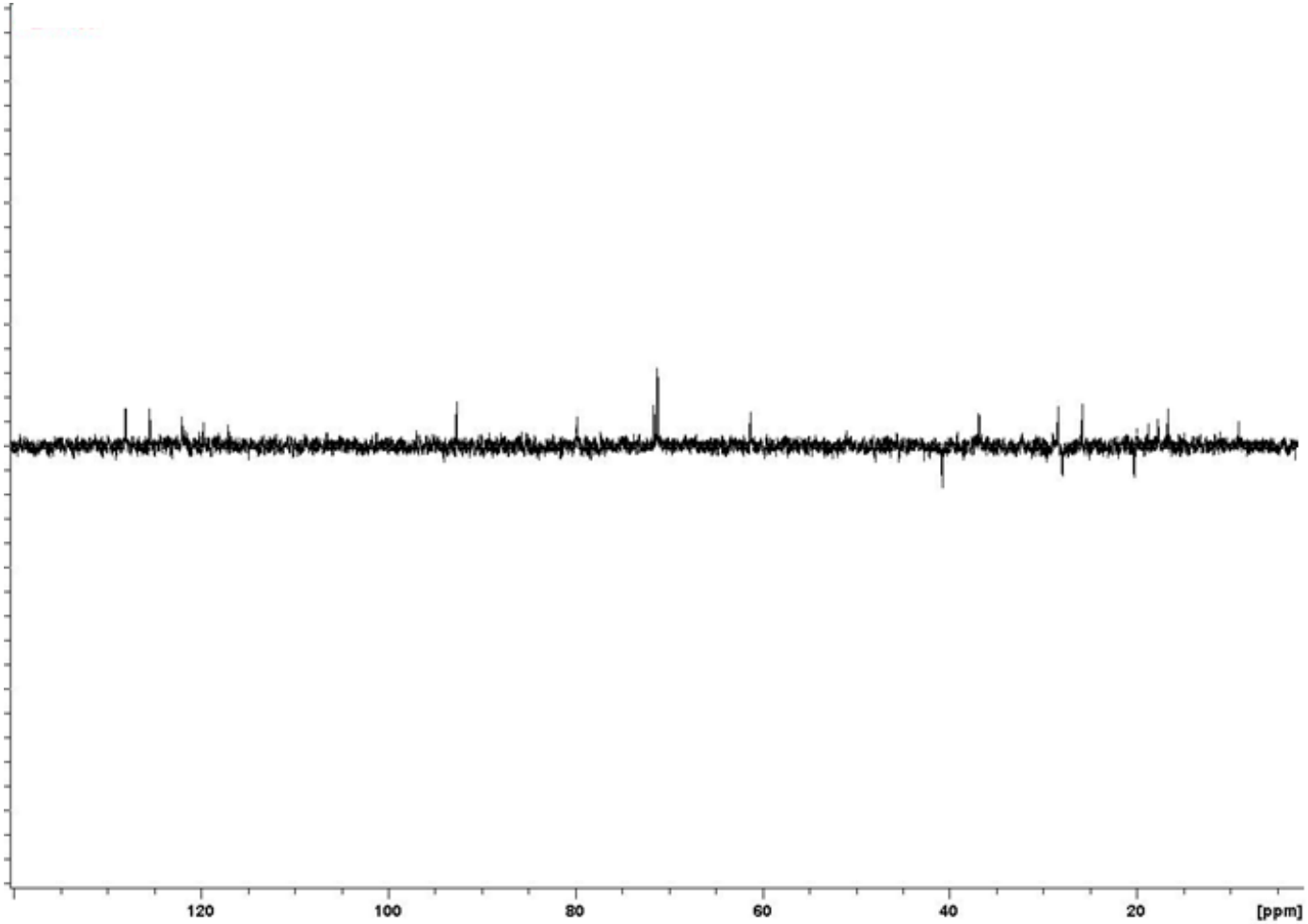

Appendix 9: The DEPT-135 NMR spectrum of compound C (**66**), ($CDCl_3$, 400 MHz).

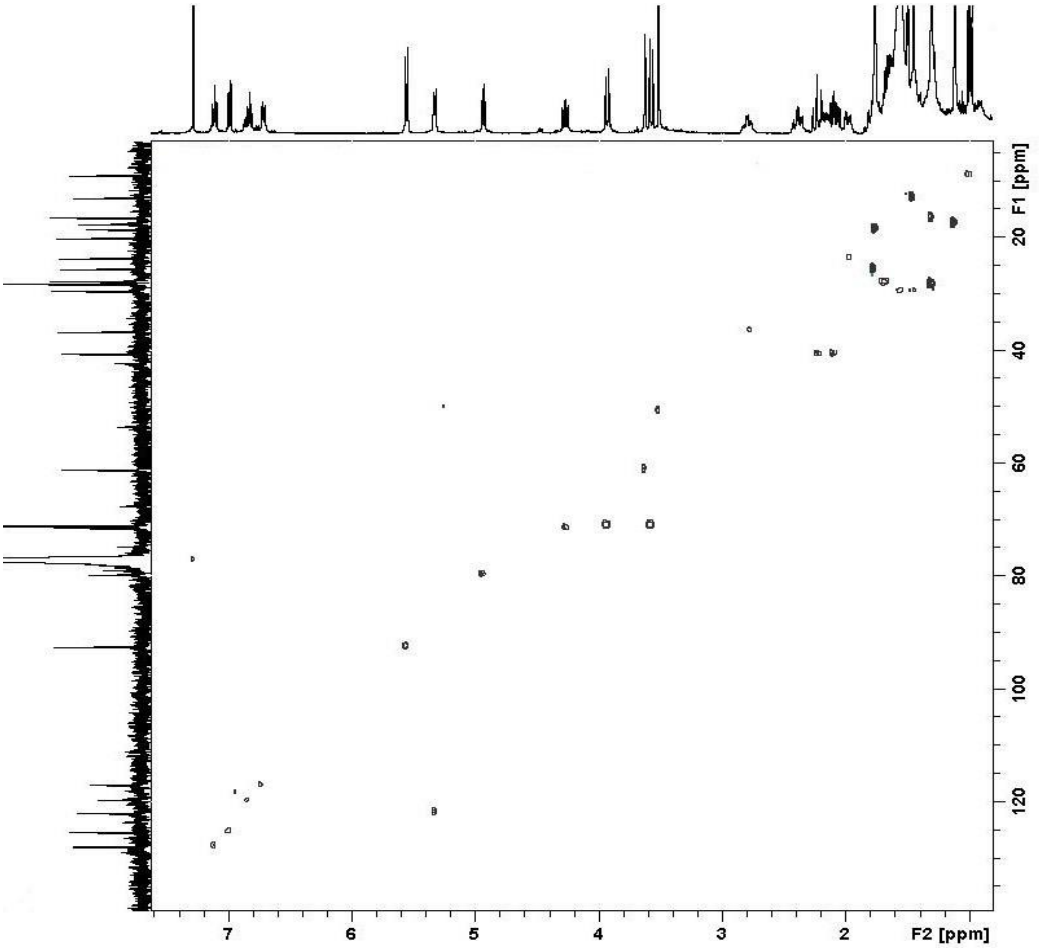

Appendix 10: The HSQC NMR spectrum of compound C (**66**), ($CDCl_3$, 400 MHz).

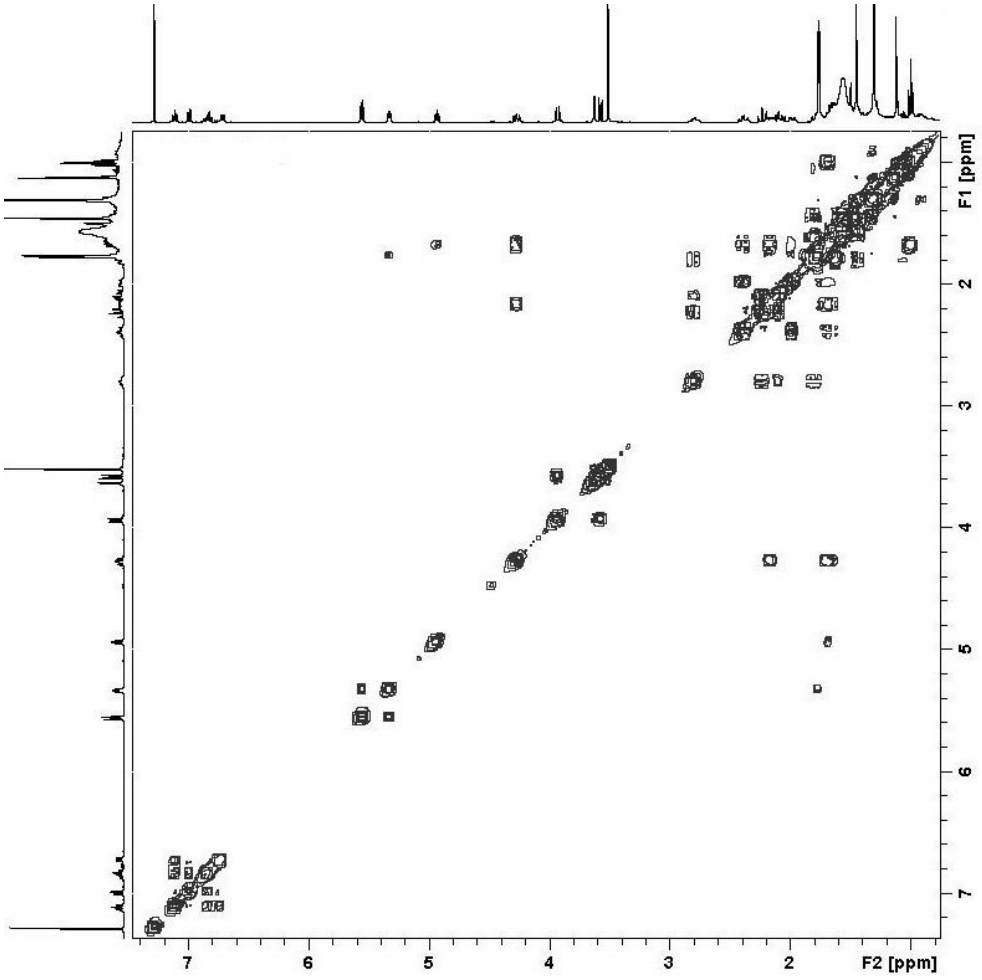

Appendix 11: The COSY NMR spectrum of compound C (**66**), ($CDCl_3$, 400 MHz).

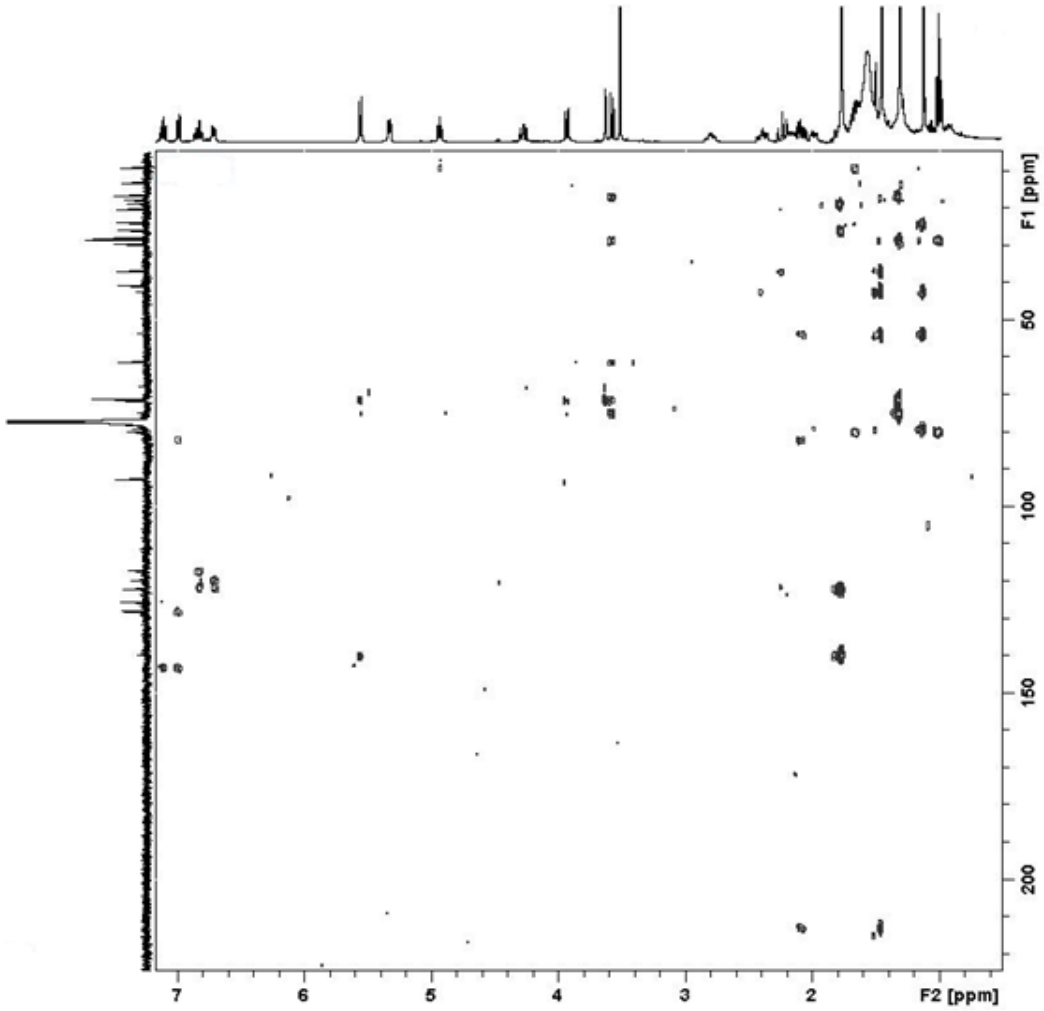

Appendix 12: The HMBC NMR spectrum of compound C (**66**), ($CDCl_3$, 400 MHz).

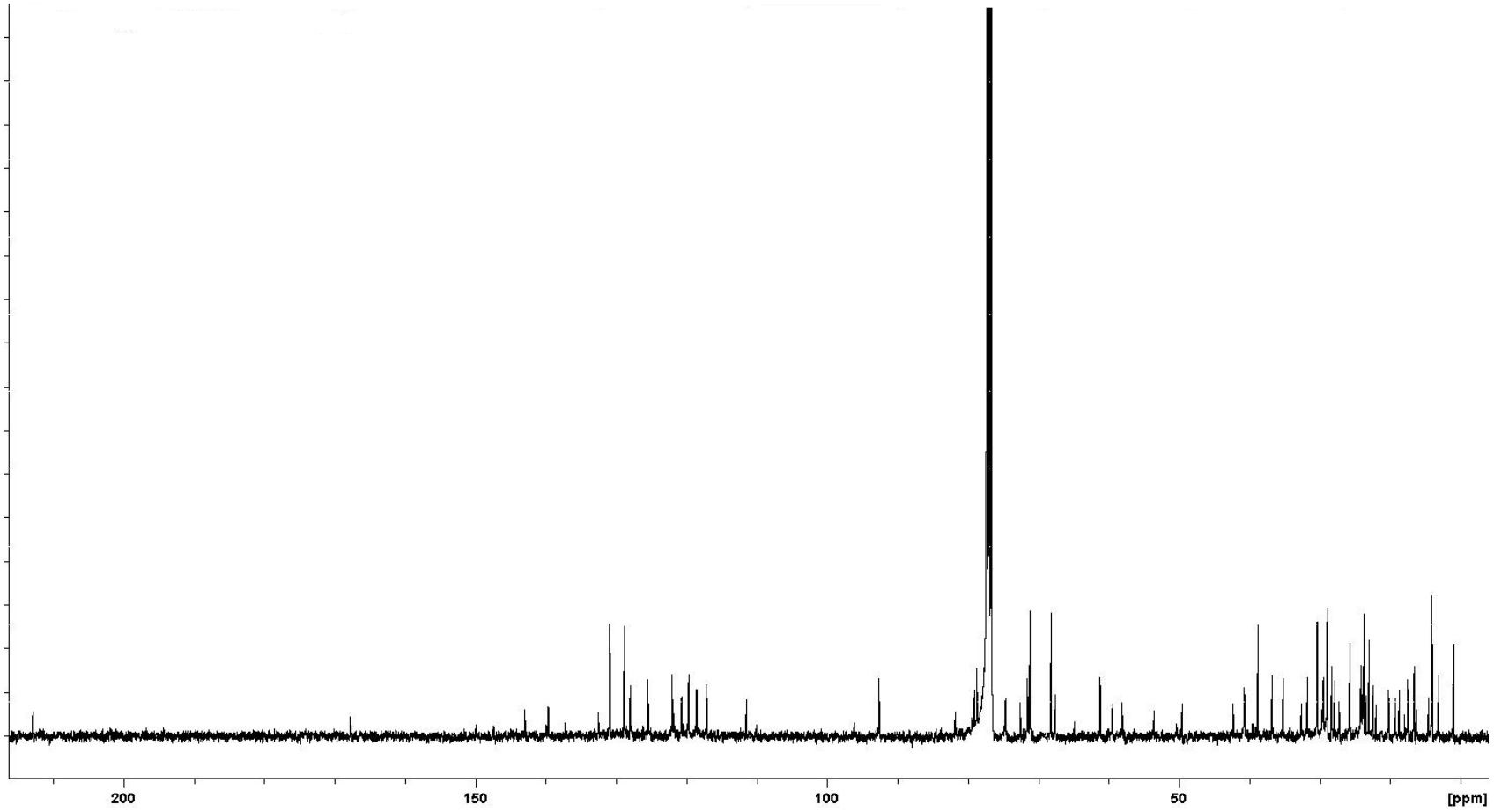

Appendix 13: The ^{13}C NMR spectrum of compound D (**67**), ($CDCl_3$, 400 MHz).

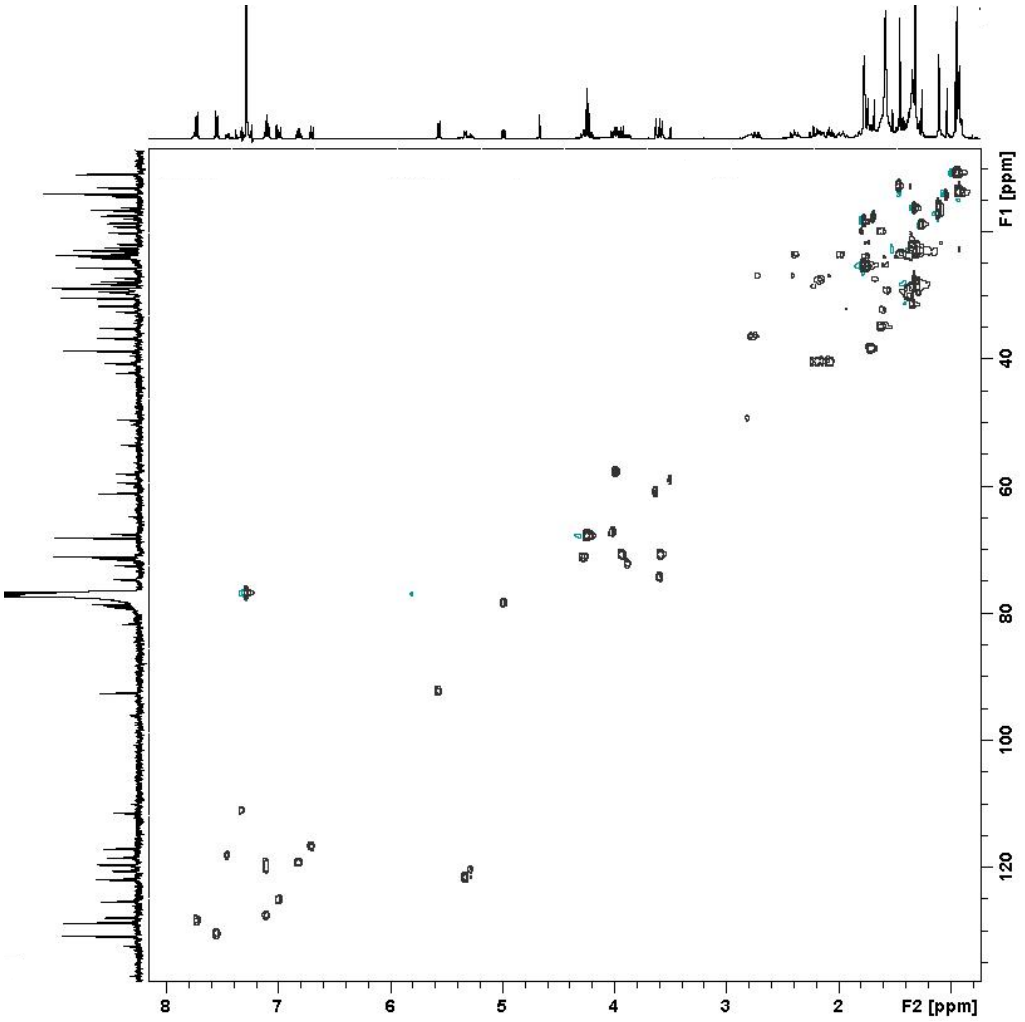

Appendix 14: The HSQC NMR spectrum of compound D (**67**), ($CDCl_3$, 400 MHz).

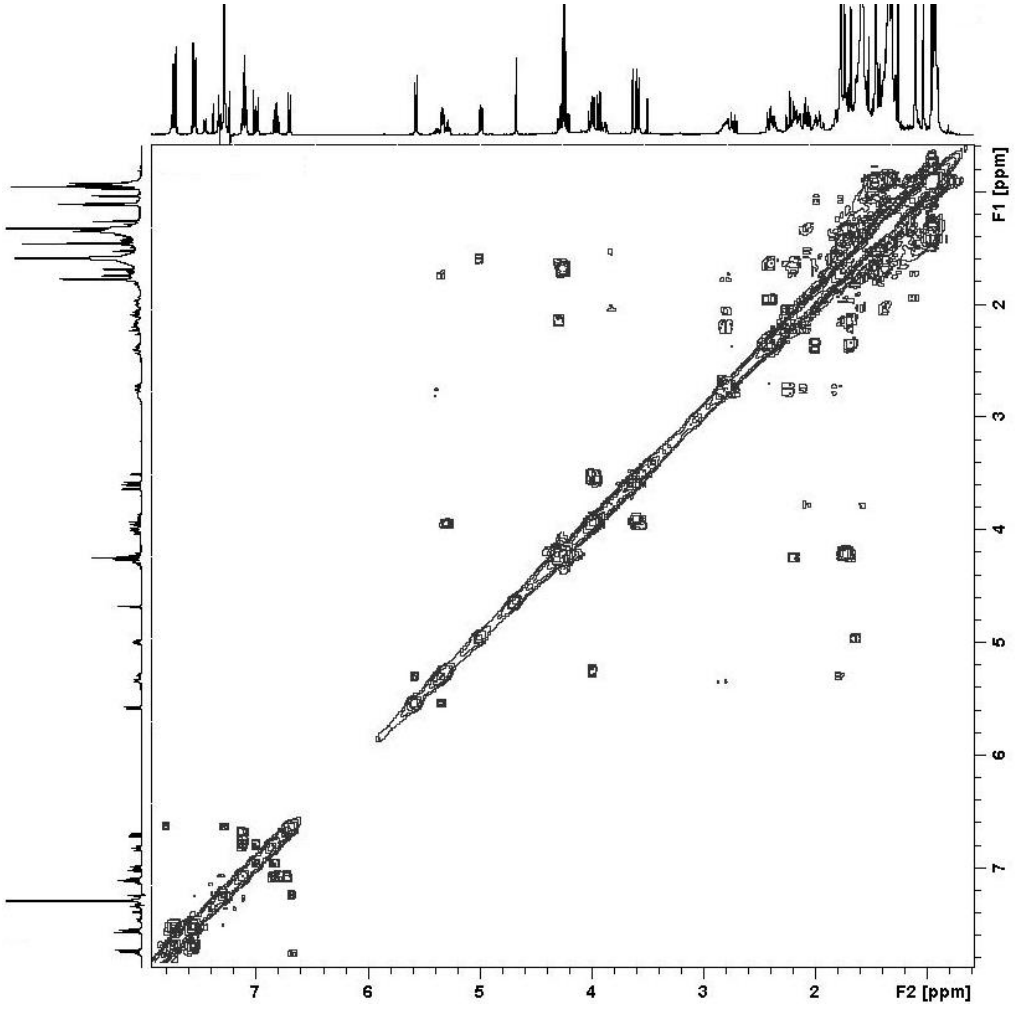

Appendix 15: The COSY NMR spectrum of compound D (**67**), ($CDCl_3$, 400 MHz).

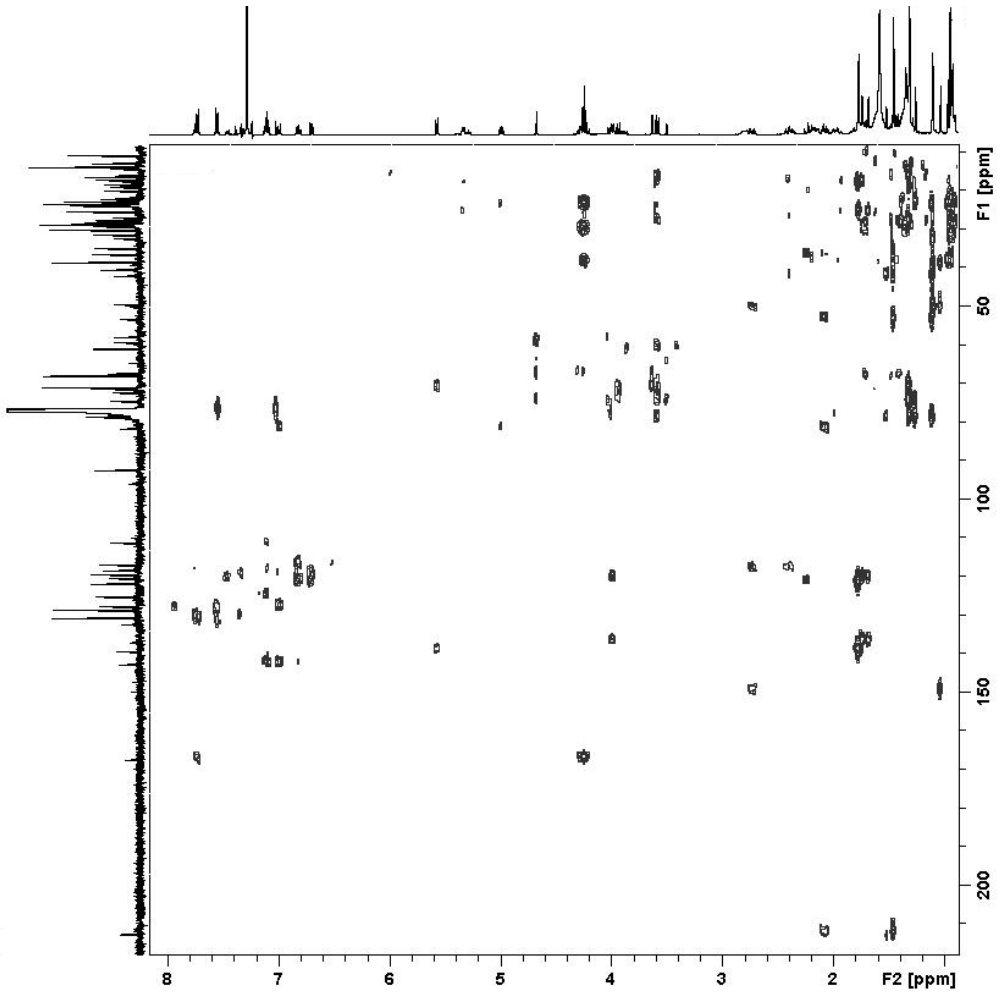

Appendix 16: The HMBC NMR spectrum of compound D (**67**), ($CDCl_3$, 400 MHz).

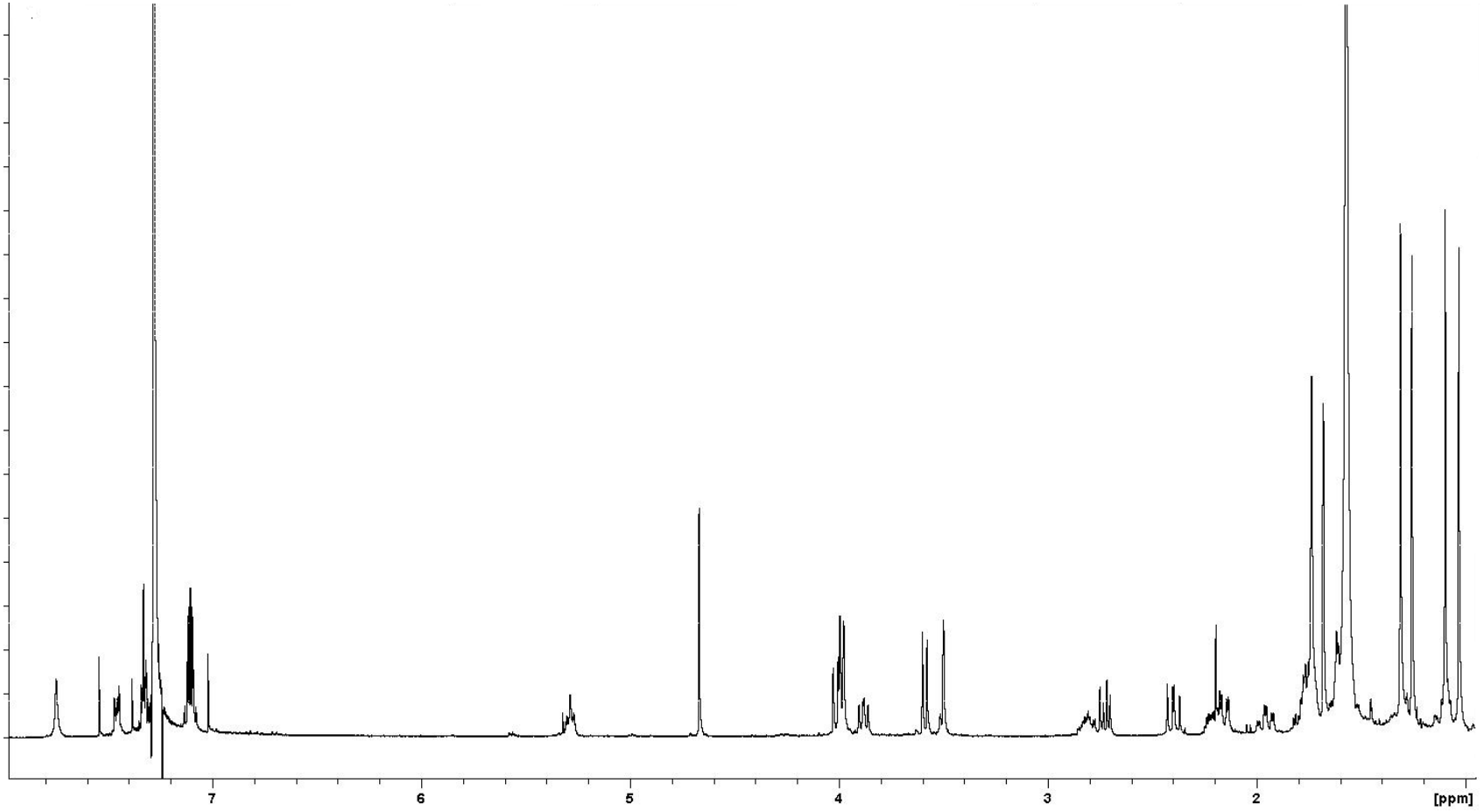

Appendix 17: The ^{1}H NMR spectrum of terpendole D (**50**), ($CDCl_3$, 400 MHz).

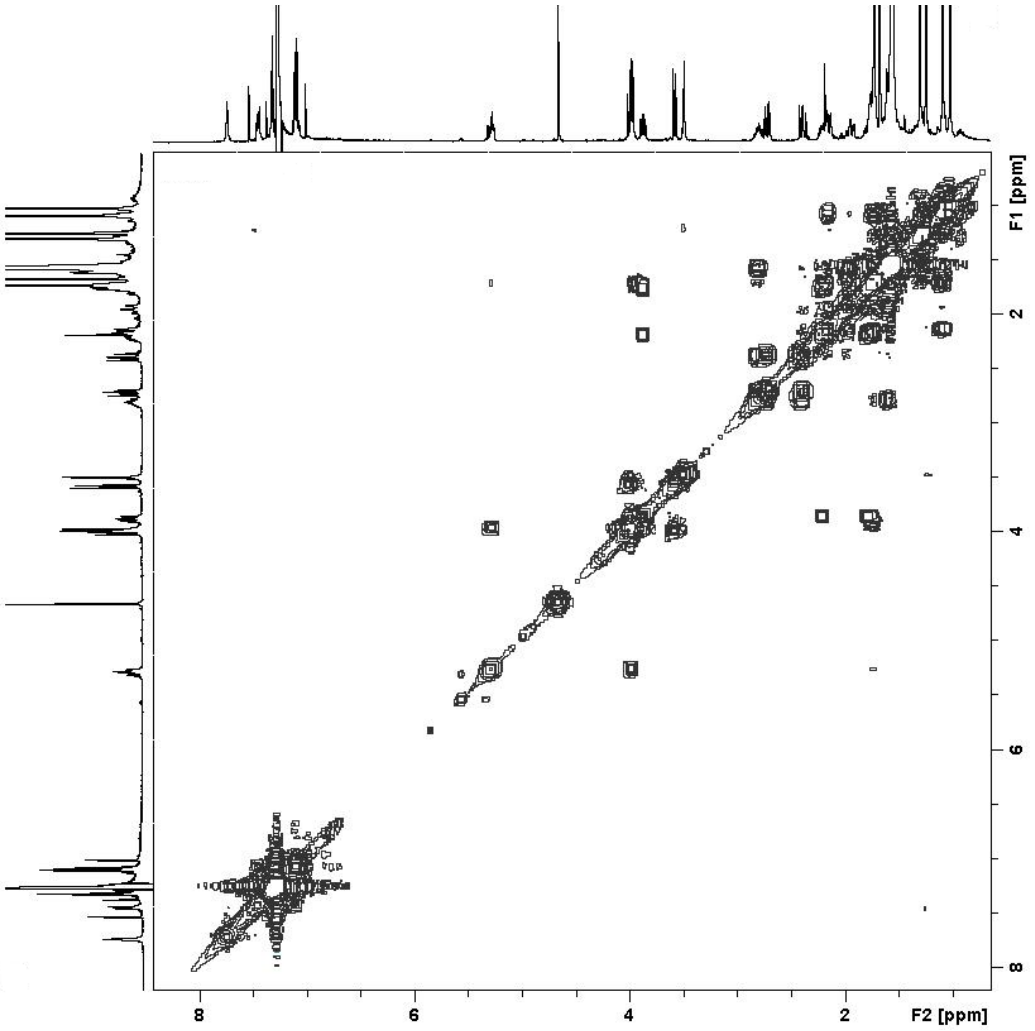

Appendix 18: The COSY NMR spectrum of terpendole D (**50**), ($CDCl_3$, 400 MHz).

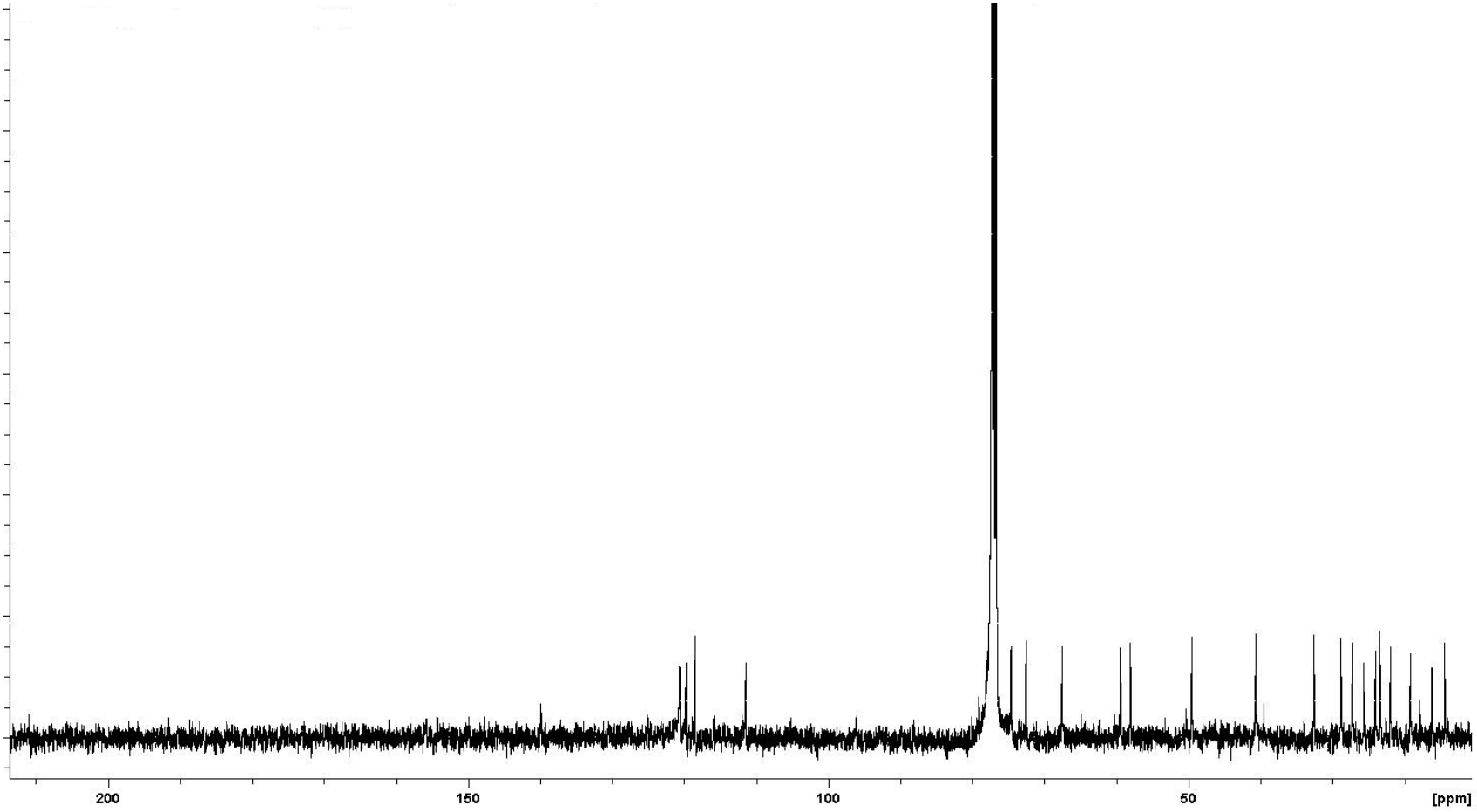

Appendix 19: The ^{13}C NMR spectrum of terpendole D (**50**), ($CDCl_3$, 400 MHz).

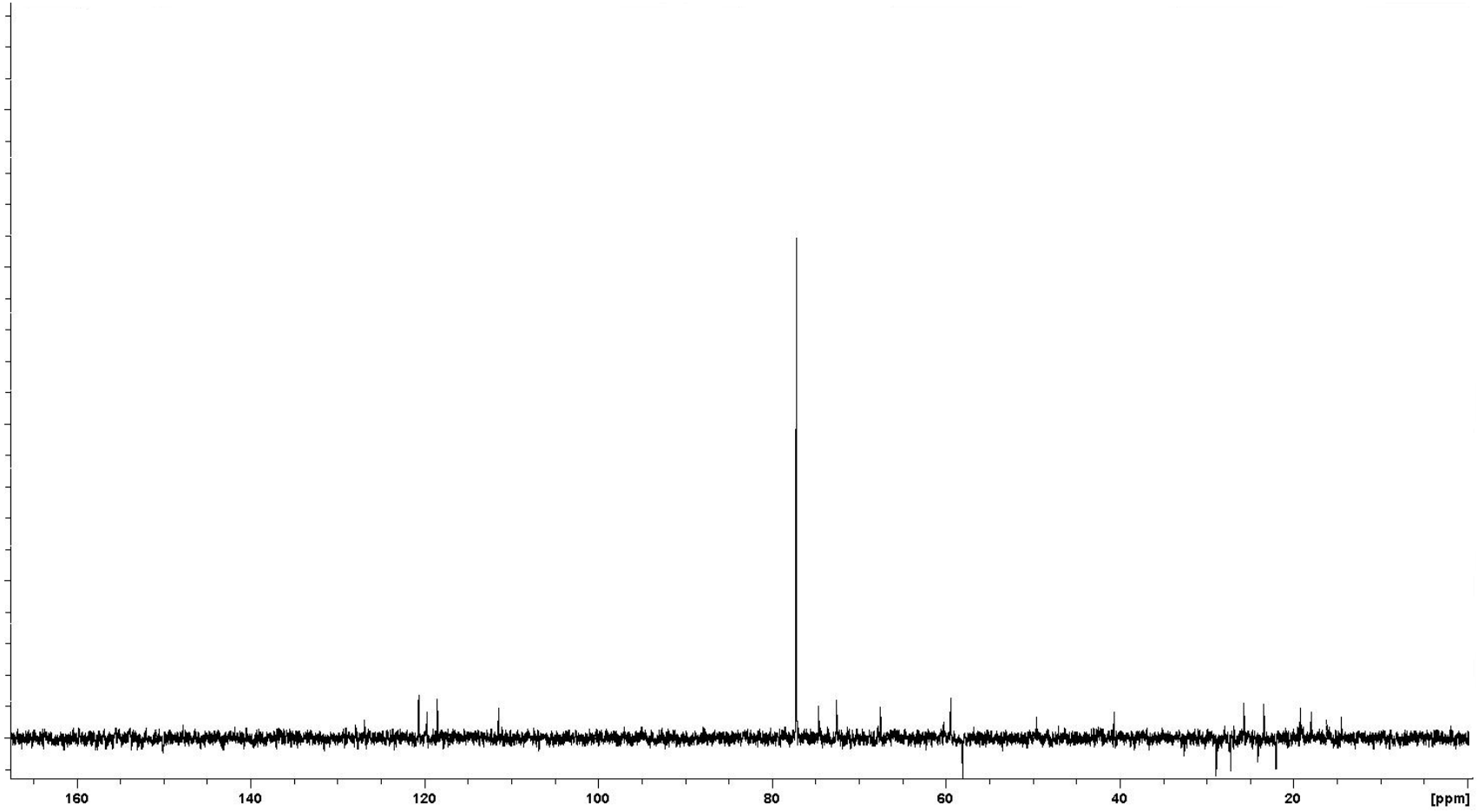

Appendix 20: The DEPT-135 NMR spectrum of terpendole D (**50**), ($CDCl_3$, 400 MHz).

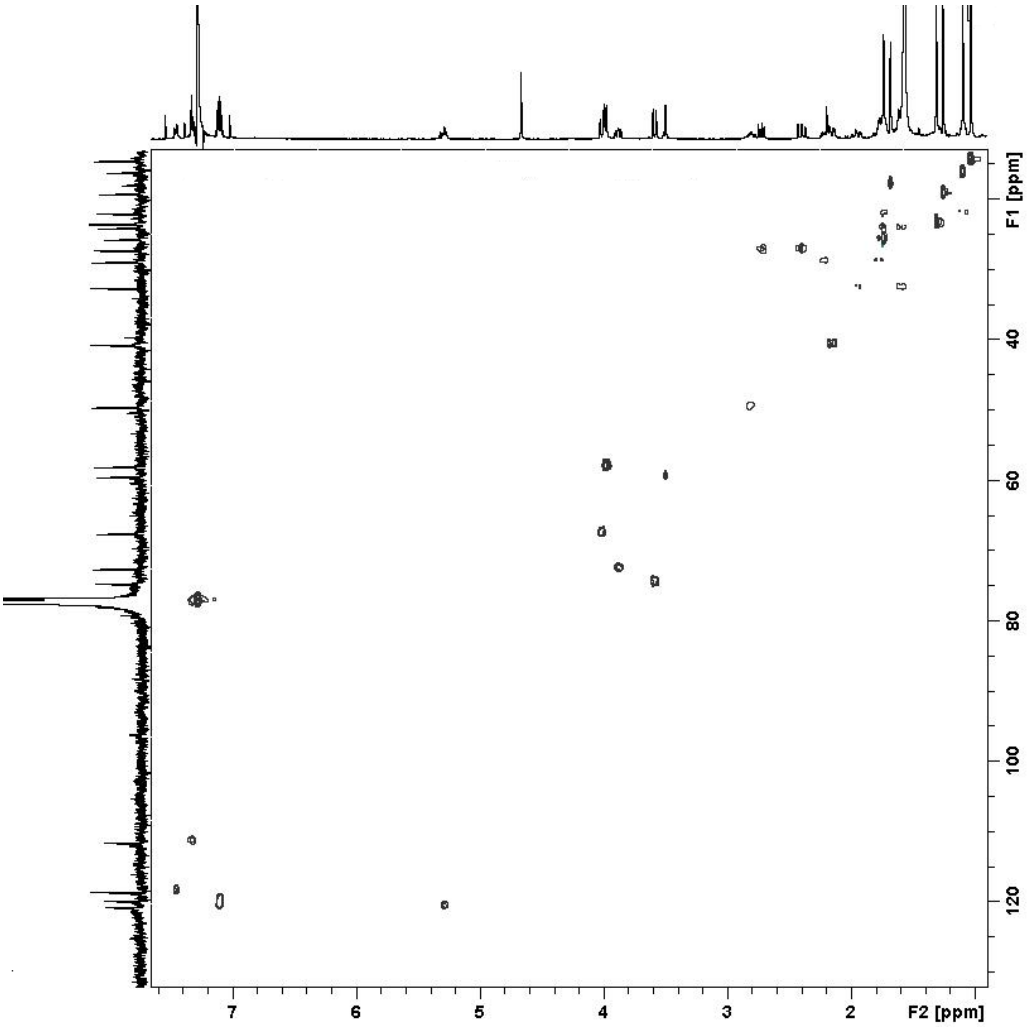

Appendix 21: The HSQC NMR spectrum of terpendole D (**50**), ($CDCl_3$, 400 MHz).

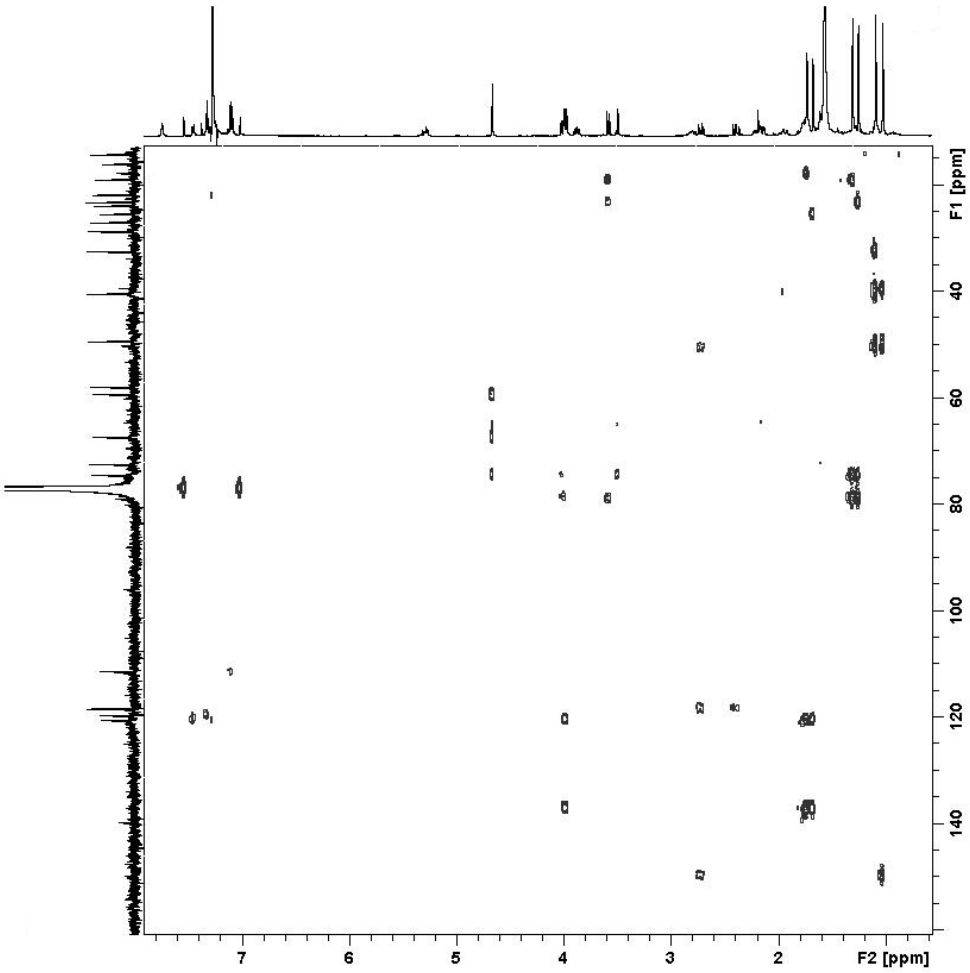

Appendix 22: The HMBC NMR spectrum of terpendole D (**50**), ($CDCl_3$, 400 MHz).

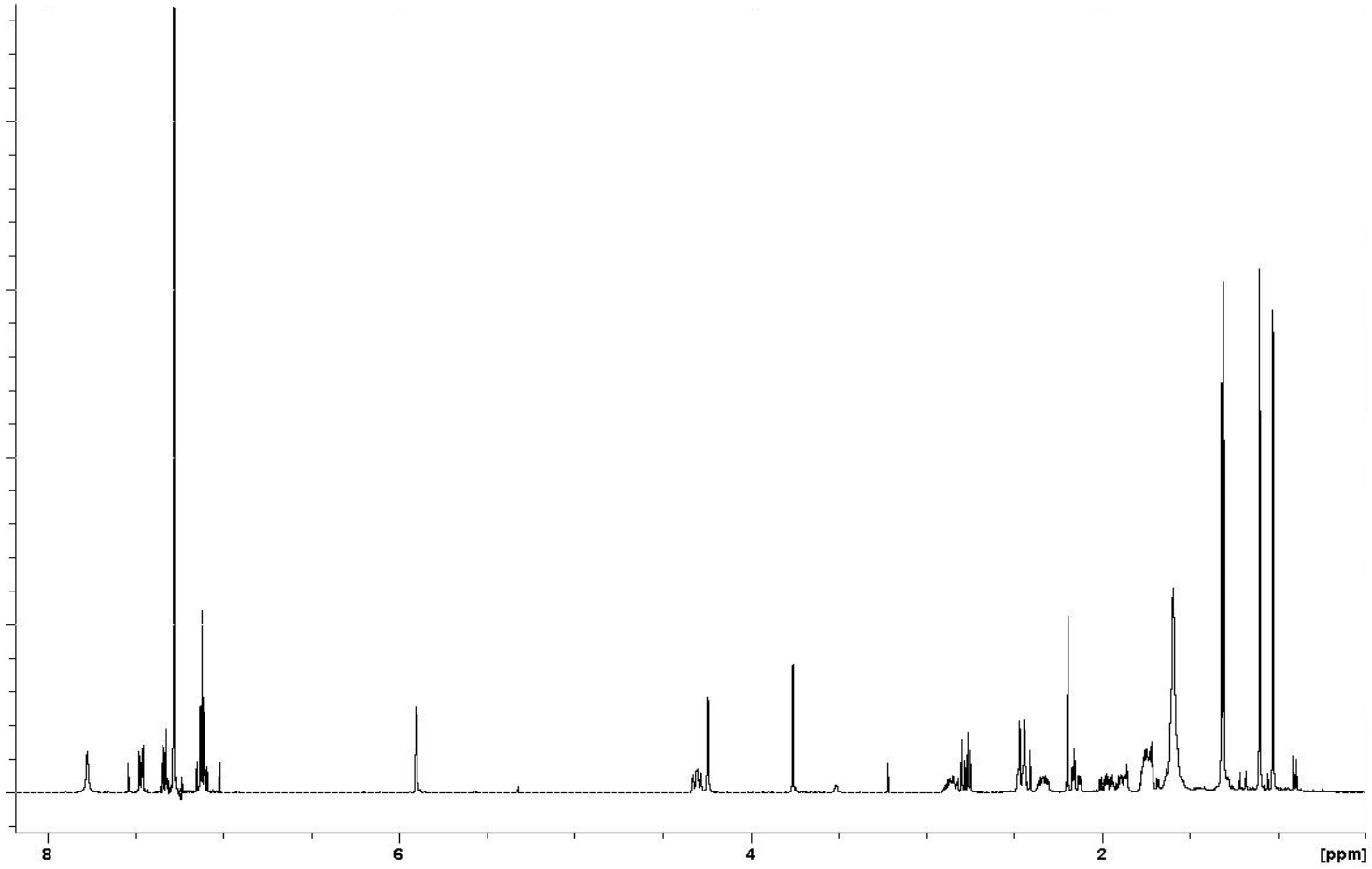

Appendix 23: The ^{1}H NMR spectrum of 13-desoxypaxilline (**37**), ($CDCl_3$, 400 MHz).

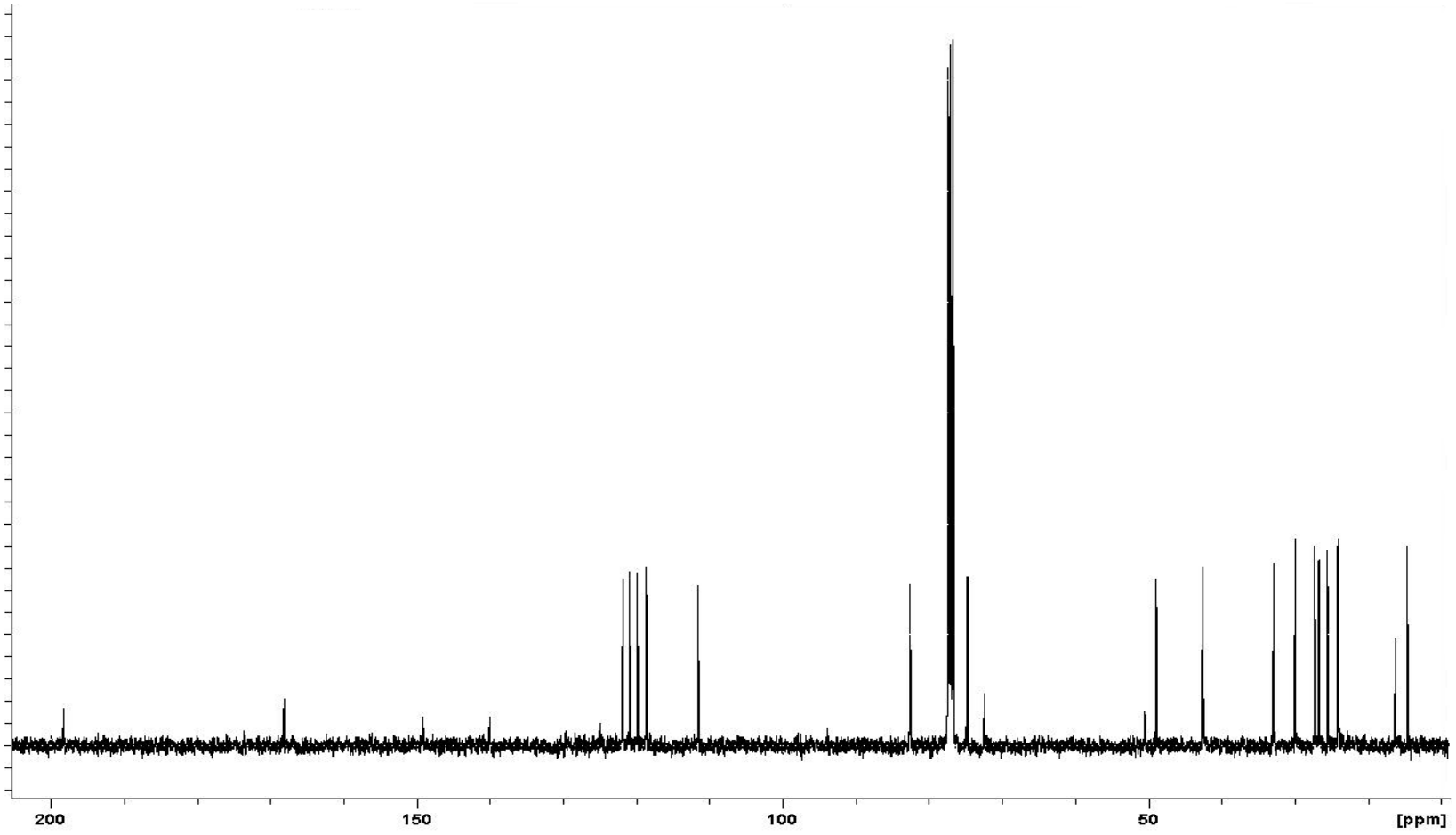

Appendix 24: The ^{13}C NMR spectrum of 13-desoxypaxilline (**37**), ($CDCl_3$, 400 MHz).

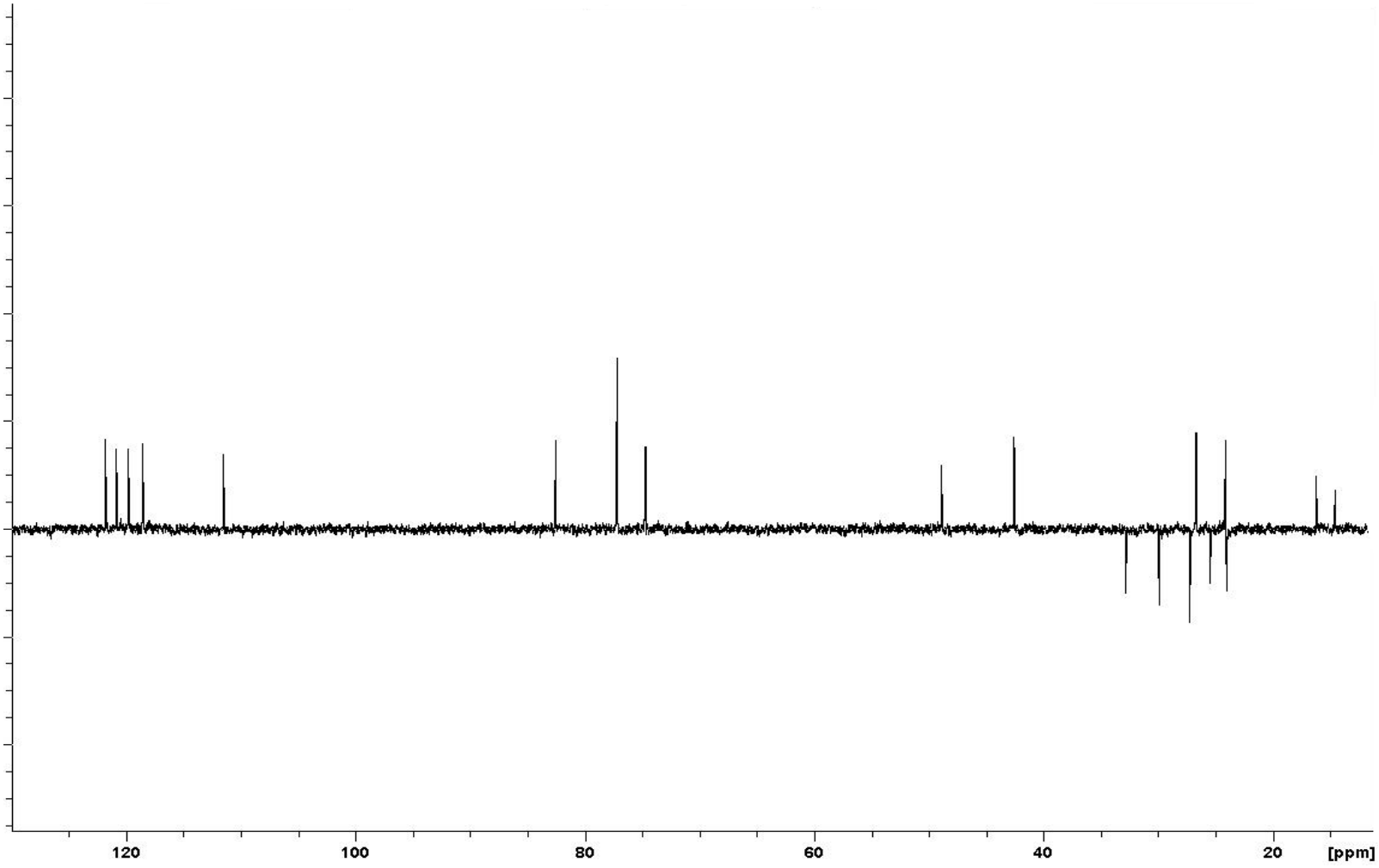

Appendix 25: The DEPT-135 NMR spectrum of 13-desoxypaxilline (**37**), ($CDCl_3$, 400 MHz).

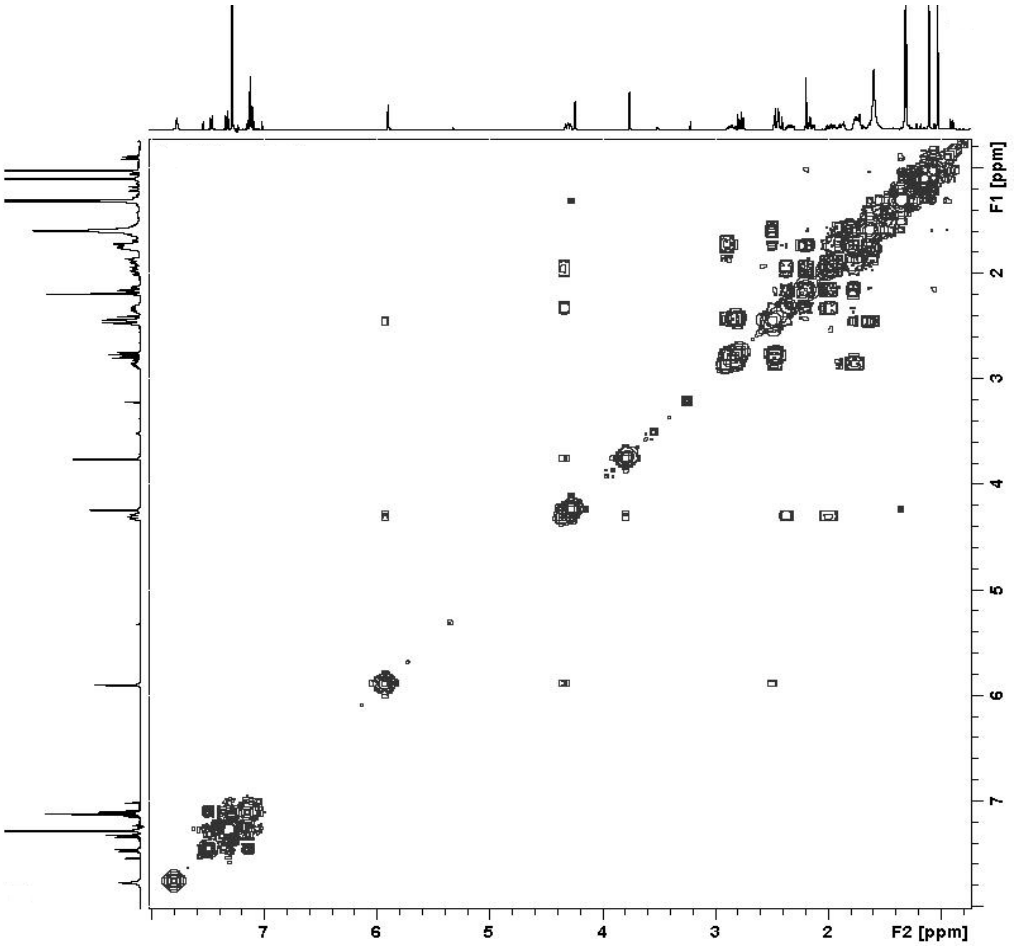

Appendix 26: The COSY NMR spectrum of 13-desoxypaxilline (**37**), ($CDCl_3$, 400 MHz).

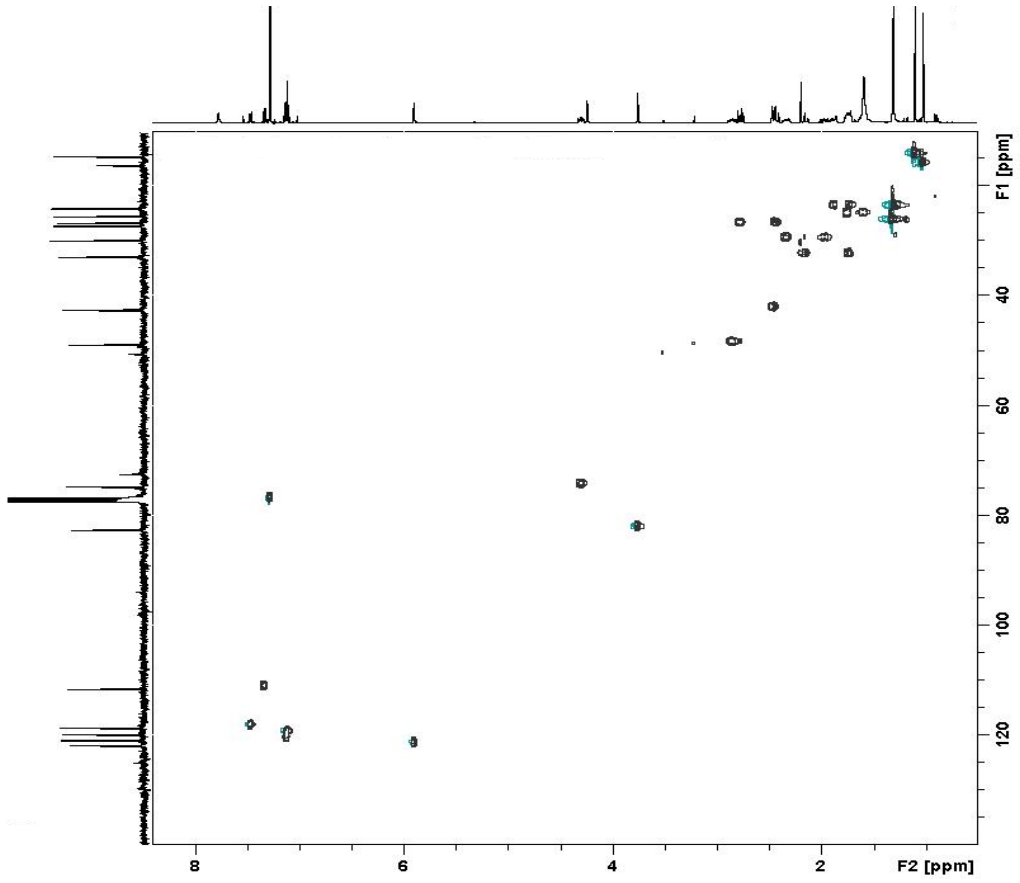

Appendix 27: The HSQC NMR spectrum of 13-desoxypaxilline (**37**), ($CDCl_3$, 400 MHz).

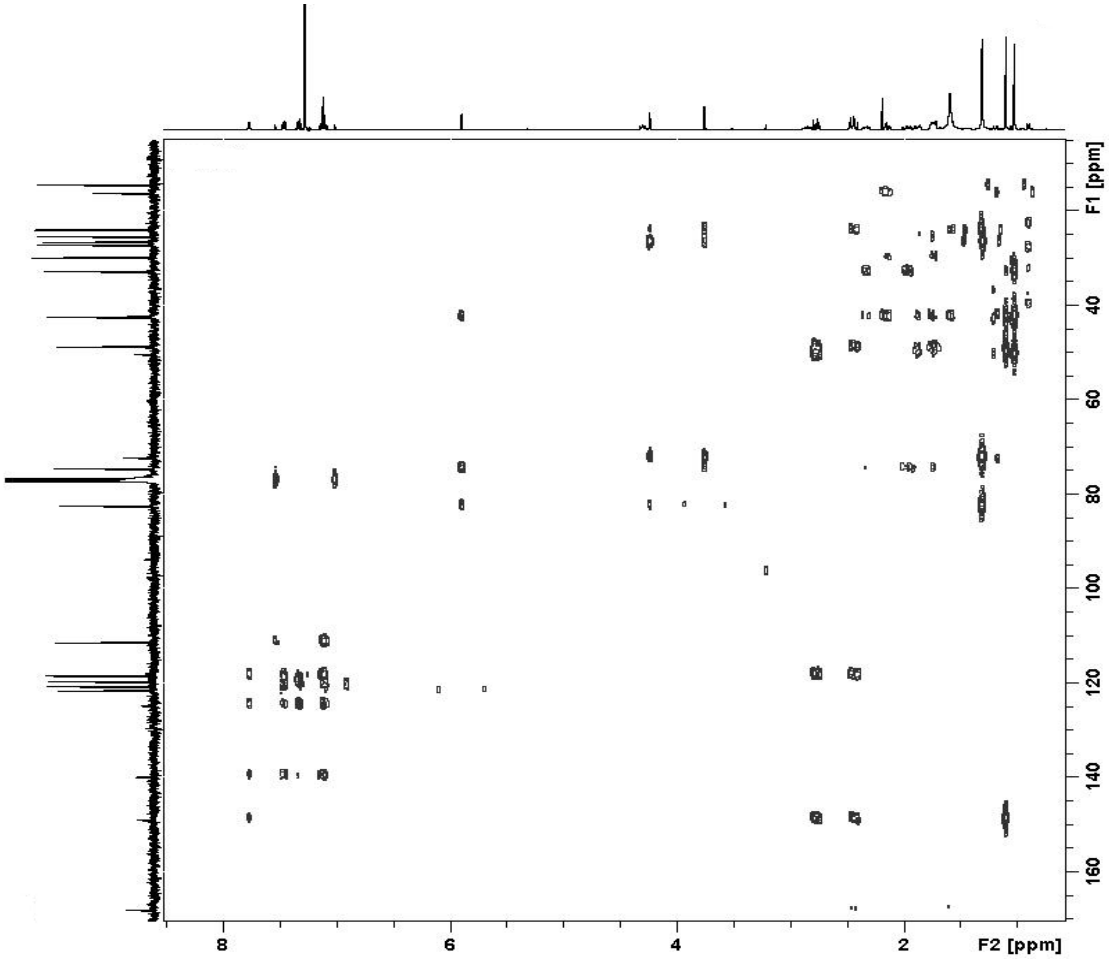

Appendix 28: The HMBC NMR spectrum of 13-desoxypaxilline (**37**), ($CDCl_3$, 400 MHz).

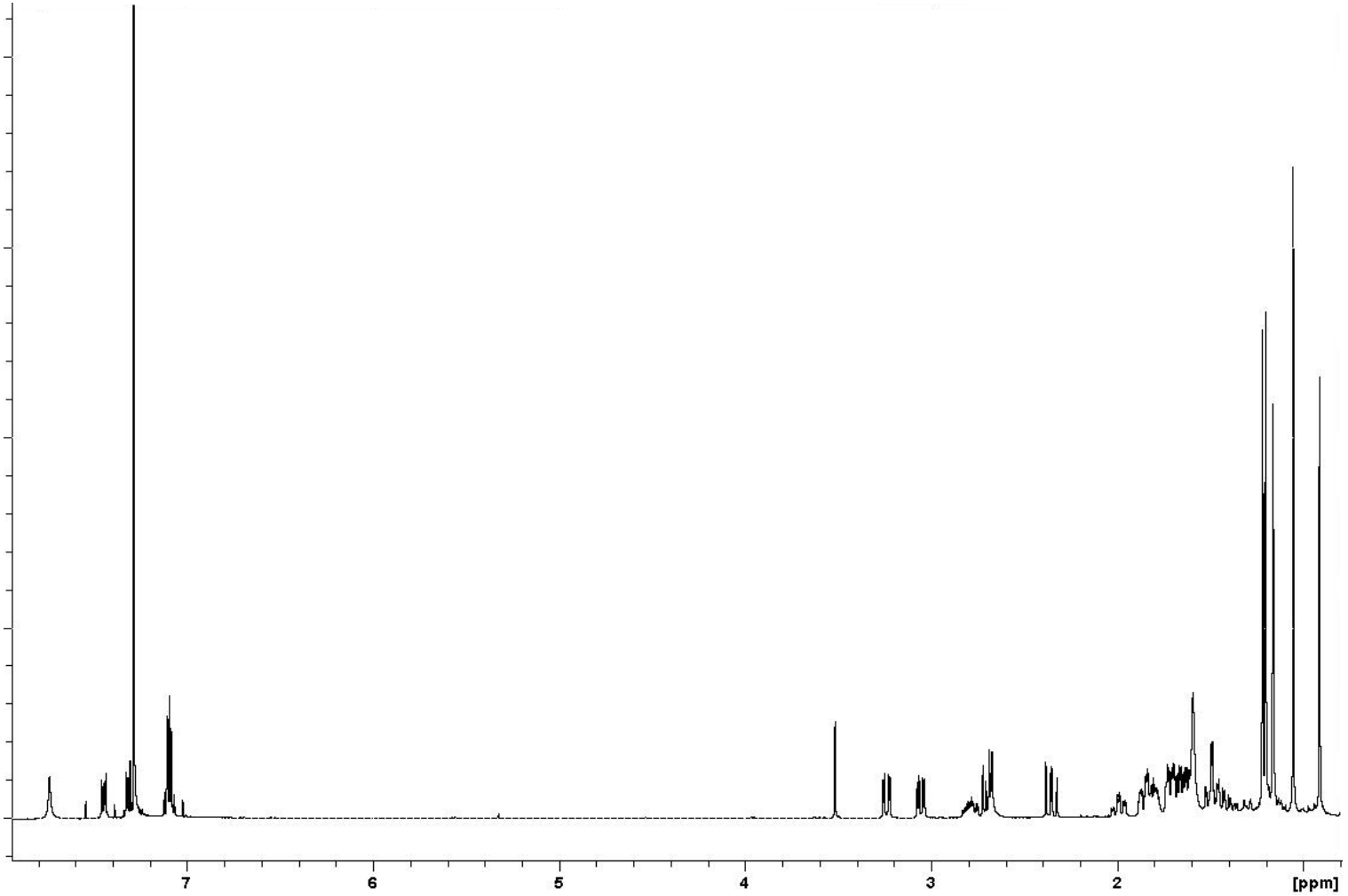

Appendix 29: The ^{1}H NMR spectrum of paspaline (**42**), ($CDCl_3$, 400 MHz).

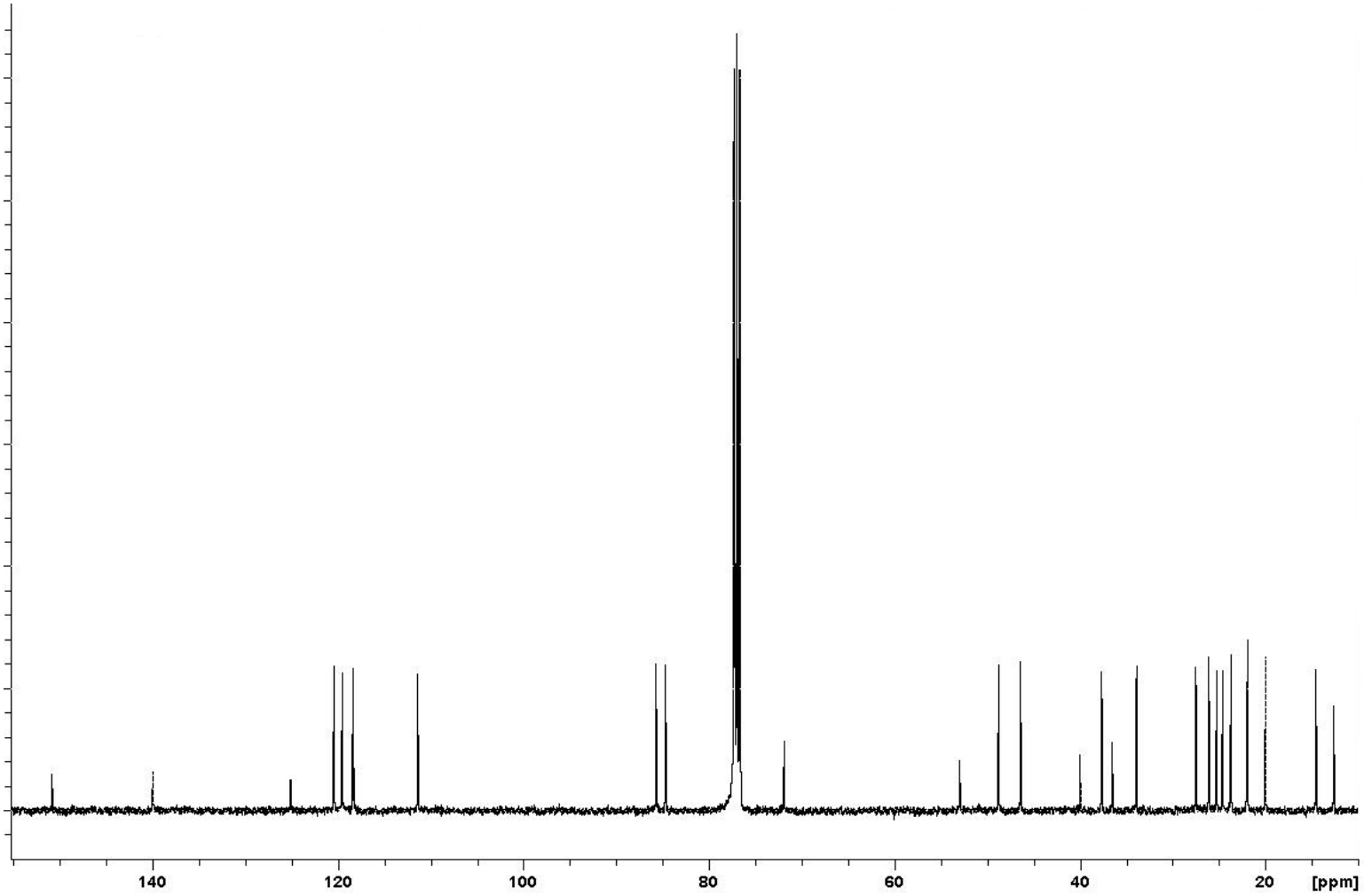

Appendix 30: The ^{13}C NMR spectrum of paspaline (**42**), ($CDCl_3$, 400 MHz).

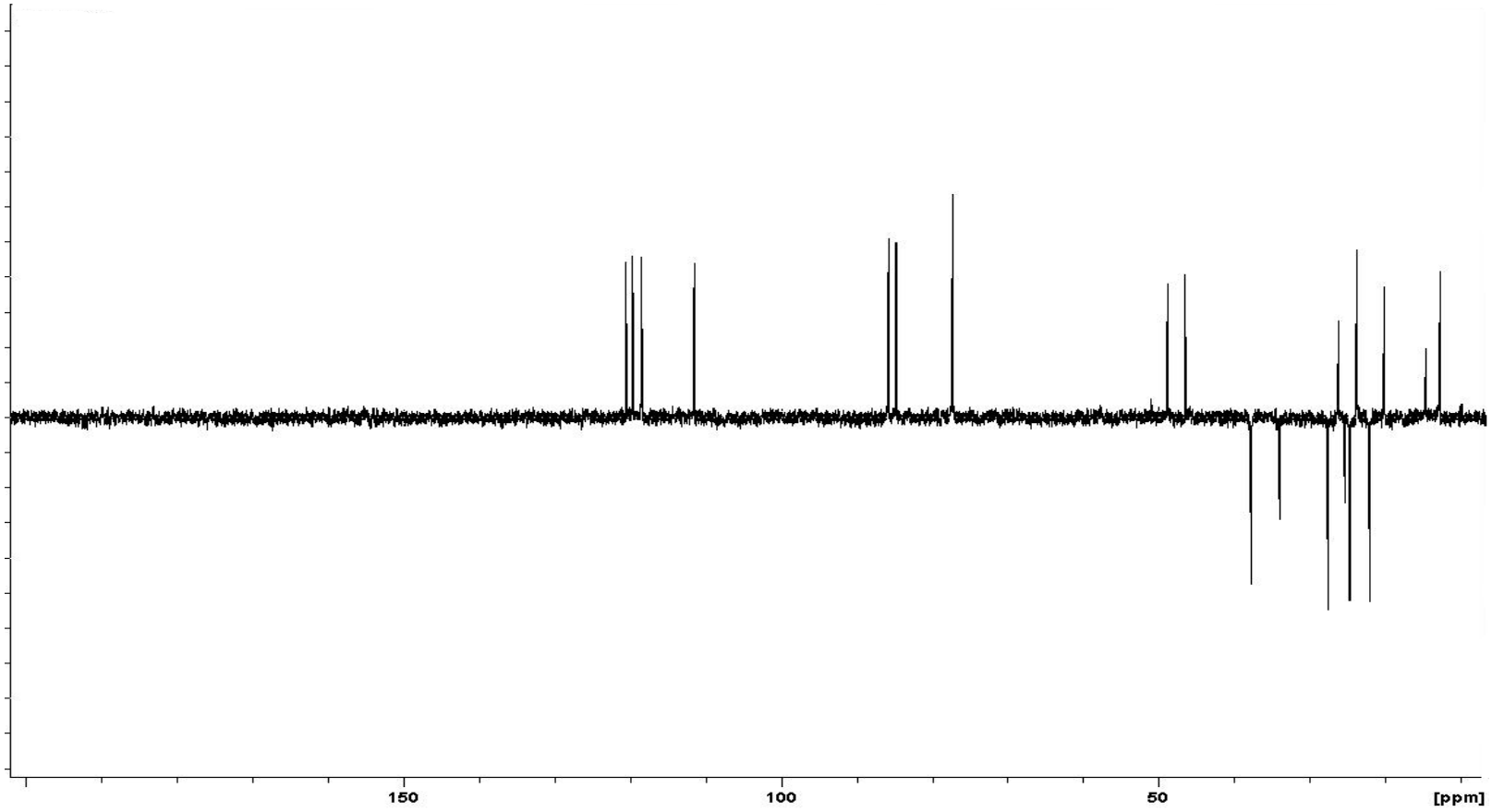

Appendix 31: The DEPT-135 NMR spectrum of paspaline (**42**), ($CDCl_3$, 400 MHz).

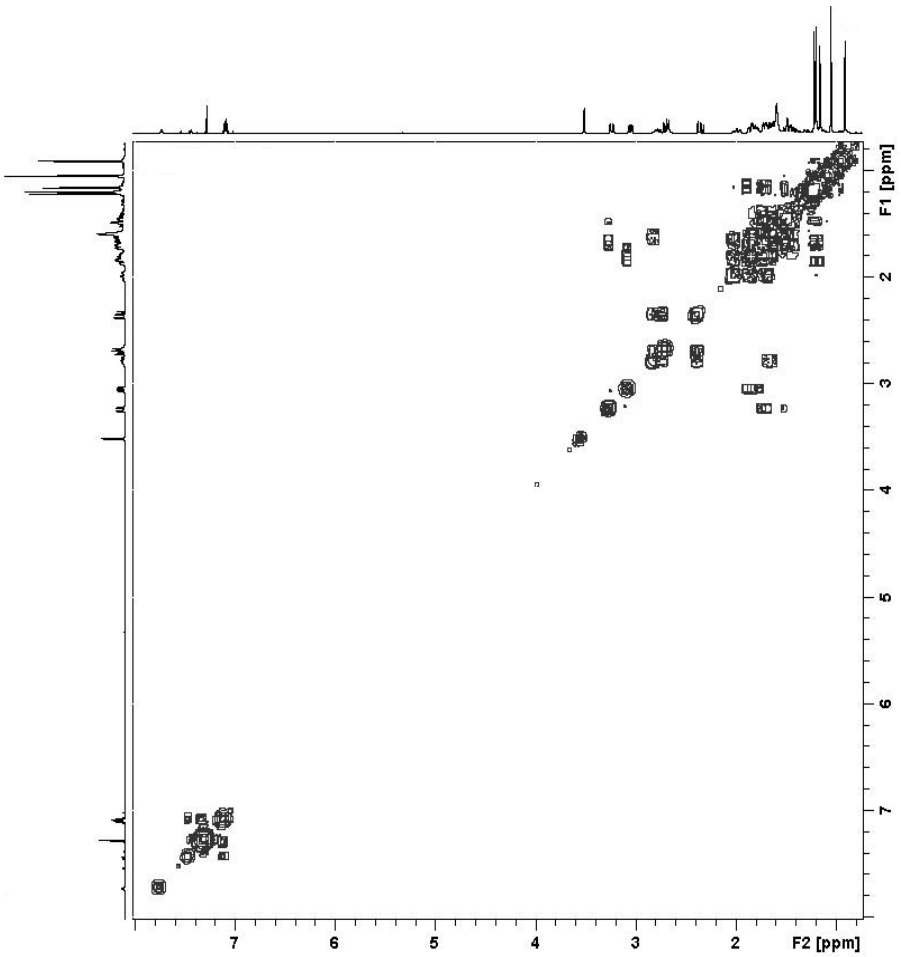

Appendix 32: The COSY NMR spectrum of paspaline (**42**), ($CDCl_3$, 400 MHz).

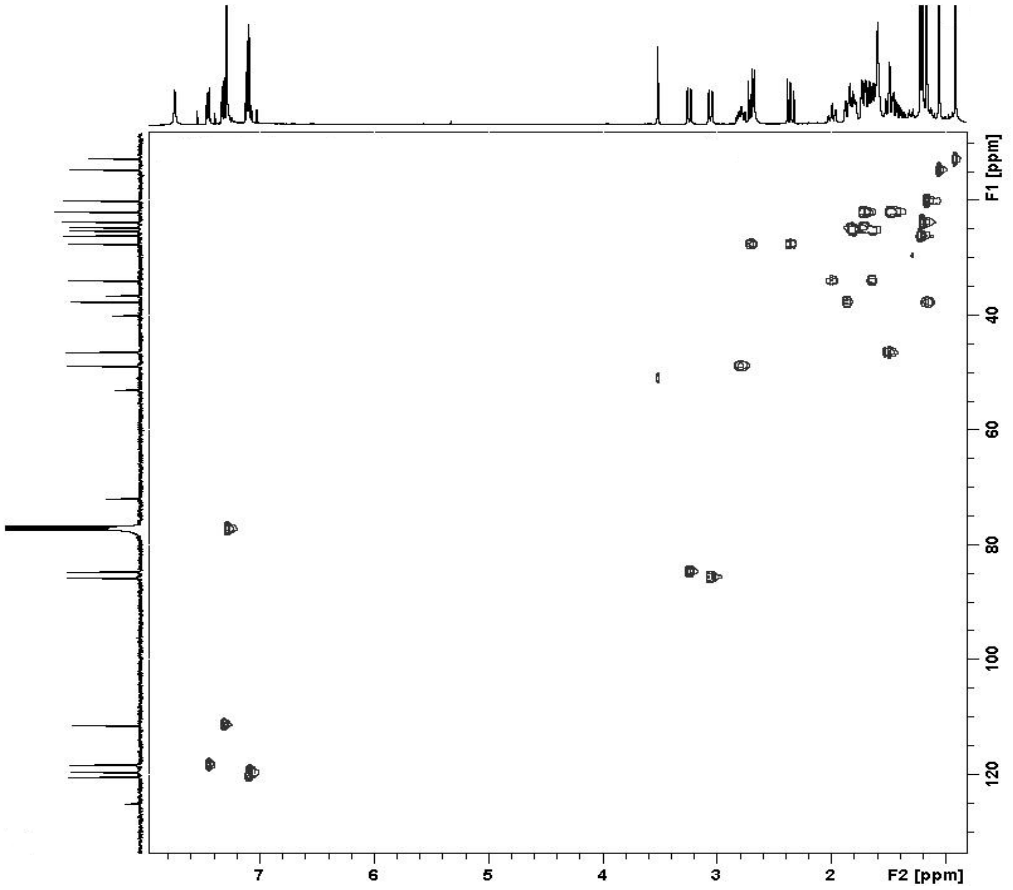

Appendix 33: The HSQC NMR spectrum of paspaline (**42**), ($CDCl_3$, 400 MHz).

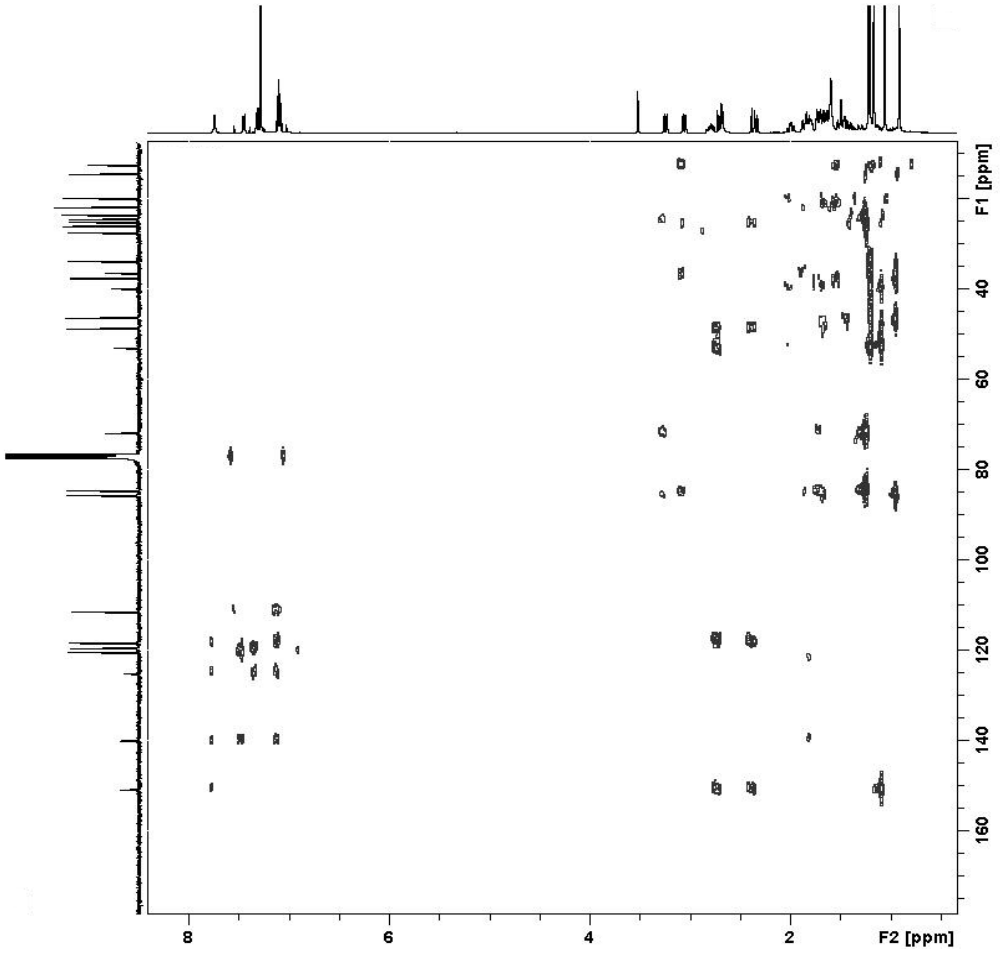

Appendix 34: The HMBC NMR spectrum of paspaline (**42**), ($CDCl_3$, 400 MHz).

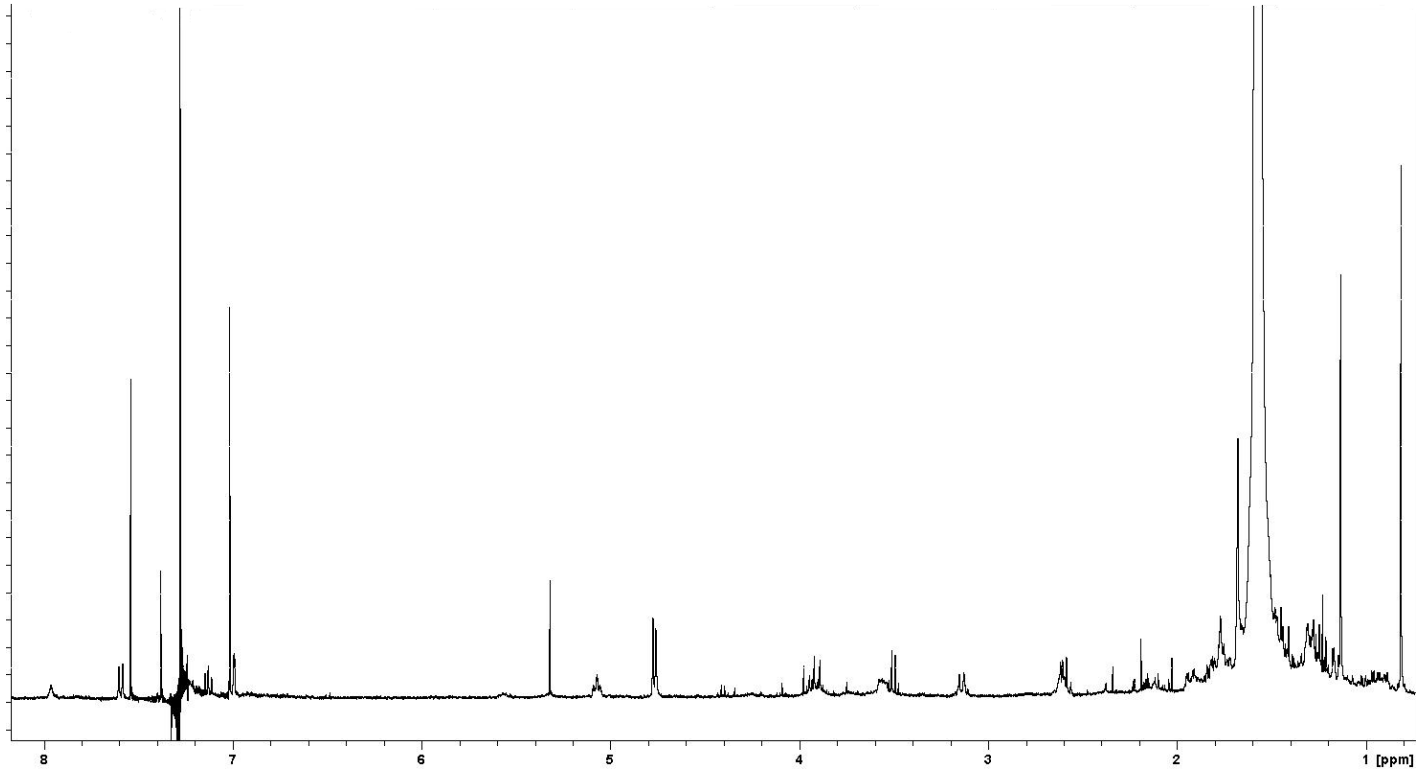

Appendix 35: The ^{1}H NMR spectrum of the potential emidole analogue, ($CDCl_3$, 400 MHz).

References

1. Gallagher, R. T.; White, E. P.; Mortimer, P. H. *N. Z. Vet. J.* **1981**, *29*, 189-190.
2. Young, A.; Hume, D. E.; McCulley, R. L. *J. Anim. Sci.* **2013**, *91*, 2379-2394.
3. Johnson, L. J.; De Bonth, A. C. M.; Briggs, L. R.; Caradus, J. R.; Finch, S. C.; Fleetwood, D. J.; Fletcher, L. R.; Hume, D. E.; Johnson, R. D.; Popay, A. J.; Tapper, B. A.; Simpson, W. R.; Voisey, C. R.; Card, S. D. *Fungal Diver.* **2013**, *60*, 171-188.
4. 2018 Pickering Medal: Making the grass 'greener' by commercialising a novel grass-fungi partnership. https://royalsociety.org.nz/what-we-do/medals-and-awards/medals-and-awards-news/2018-pickering-medal-making-the-grass-greener-by-commercialising-a-novel-grass-fungi-partnership/ (accessed November 2018).
5. Leuchtmann, A.; Bacon, C. W.; Schardl, C. L.; White Jr, J. F.; Tadych, M. *Mycologia* **2014**, *106*, 202-215.
6. Glenn, A. F.; Bacon, C. W.; Price, R.; Hanlin, R. T. *J. Microbiol. Methods* **1996**, *1*, 148-155.
7. Latch, G. C. M.; Potter, L. R.; Tyler, B. F. *Ann. Appl. Biol.* **1987**, *111*, 59-64.
8. Latch, G. C. M.; Christensen, M. J.; Samuels, G. J. *Mycotaxon* **1984**, *20*, 535-550.
9. Schardl, C. L.; Leuchtmann, A.; Tsai, H. F.; Collett, M. A.; Watt, D. M.; Scott, D. B. *Genetics* **1994**, *136*, 1307-1317.
10. Hopkirk, C. S. M. *N. Z. J. Agric. Res.* **1935**, *52*, 18-21.
11. Cunningham, I. J.; Hartley, W. J. *N. Z. Vet. J.* **1959**, *7*, 1-7.
12. Neill, J. C. *N. Z. J. Sci. Technol.* **1940**, *21*, 280-291.
13. Sampson, K. *Trans. Br. Mycol. Soc.* **1935**, *19*, 337-343.
14. di Menna, M. E.; Finch, S. C.; Popay, A. J.; Smith, B. L. *N. Z. Vet. J.* **2012**, *60*, 315-328.

15. Gilruth, J. A. Meningo-encephalitis (stomach staggers) in horses, cattle and sheep. In *Annual Report of the New Zealand Department of Agriculture.*, 1906; Vol. 14, pp 293-297.
16. Thornton, R. H. *N. Z. Vet. J.* **1964**, *12*, 13-16.
17. Fletcher, L. R.; Harvey, I. C. *N. Z. Vet. J.* **1981**, *29*, 185-186.
18. Gaynor, D. L.; Rowan, D. D.; Latch, G. C. M.; Pilkington, S. *Proc. N. Z. Weed Pest Control Conf.* **1983**, *36*, 220-224.
19. Pfeifer, M.; Martis, M.; Asp, T.; Mayer, K. F. X.; Lübberstedt, T.; Byrne, S.; Frei, U.; Studer, B. *Plant Physiol.* **2013**, *161*, 571-582.
20. Charlton, J. F. L.; Stewart, A. V. *Proc. N. Z. Grassl. Assoc.* **1999**, *61*, 147-166.
21. Clay, K.; Schardl, C. *Am. Nat.* **2002**, *160*, 99-127.
22. Koulman, A.; Lane, G. A.; Christensen, M. J.; Fraser, K.; Tapper, B. A. *Phytochem.* **2007**, *68*, 355-360.
23. AgResearch AgPest : Porina. http://agpest.co.nz/?pesttypes=porina (accessed August 2016).
24. Schardl, C. L. *Fungal Genet. Biol.* **2001**, *33*, 69-82.
25. Spiering, M. J.; Greer, D. H.; Schmid, J. *Ann. Bot.* **2006**, *98*, 379-387.
26. Panaccione, D. G.; Beaulieu, W. T.; Cook, D. *Fungal Ecol.* **2014**, *28*, 299-314.
27. Rowan, D. D.; Gaynor, D. L. *J. Chem. Ecol.* **1986**, *12*, 647-658.
28. Rowan, D. D.; Hunt, M. B.; Gaynor, D. L. *J. Chem. Soc.* **1986**, *12*, 935-936.
29. Ball, O. J. P.; Barker, G. M.; Prestidge, R. A.; Lauren, D. R. *J. Chem. Ecol.* **1997**, *23*, 1419-1434.
30. Schardl, C. L.; Young, C. A.; Faulkner, J. R.; Florea, S.; Pan, J. *Fungal Ecol.* **2012**, *5*, 331-344.
31. Floss, H. G. *Tetrahedron* **1976**, *32*, 873-912.
32. Brunner, R.; Stuetz, P. L.; Tscherter, H.; Stadler, P. A. *Can. J. Chem.* **1979**, *57*, 1638-1641.
33. Ma, Y.; Meyer, K. G.; Afzal, D.; Agena, E. A. *J. Chromatogr. A* **1993**, *652*, 535-538.
34. Oliveira, J. A.; Rottinghaus, G. E.; Gonzalez, E. *N. Z. J. Agric. Res.* **2003**, *46*, 117-122.

35. Ball, O. J. P.; Miles, C. O.; Prestidge, R. A. *J. Econ. Entomol.* **1997**, *90*, 1382-1391.

36. Lane, G. A.; Tapper, B. A.; Davies, E. Ergot alkaloids additional to ergovaline in endophyte-infected perennial ryegrass and tall fescue in New Zealand. Ryegrass endophyte: An essential New Zealand symbiosis. In *Grassland Research and Practise Series*, 1999; Vol. *7*, pp 95-100.

37. Diana Di Mavungu, J.; Malysheva, S. V.; Sanders, M.; Larionova, D.; Robbens, J.; Dubruel, P.; Van Peteghem, C.; De Saeger, S. *Food Chem.* **2012**, *135*, 292-303.

38. Shelby, R. A.; Olsovska, J.; Havlicek, V.; Flieger, M. *J. Agric. Food Chem.* **1997**, *45* (12), 4674-4679.

39. Lehner, A. F.; Craig, M.; Fannin, N.; Bush, L.; Tobin, T. *J. Mass Spectrom.* **2005**, *40*, 1484-1502.

40. Mohamed, R.; Gremaud, E.; Richoz-Payot, J.; Tabet, J.-C.; Guy, P. A. *J. Chromatogr. A.* **2006**, *1114*, 62-72.

41. Rowan, D. D.; Shaw, G. J. *N. Z. Vet. J.* **1987**, *35*, 197-198.

42. Lehner, A. F.; Duringer, J. M.; Estill, C. T.; Tobin, T.; Craig, A. M. *Toxicol. Mech. Methods* **2011**, *21*, 606-621.

43. Saikia, S.; Parker, E. J.; Koulman, A.; Scott, B. *FEBS Lett.* **2006**, *580*, 1625-1630.

44. Munday-Finch, S. C.; Wilkins, A. L.; Miles, C. O.; Tomoda, H.; Omura, S. *J. Agric. Food Chem.* **1997**, *45*, 199-204.

45. Weedon, C. M.; Mantle, P. G. *Phytochem.* **1987**, *26*, 969-971.

46. Gatenby, W. A.; Munday-Finch, S. C.; Wilkins, A. L.; Miles, C. O. *J. Agric. Food Chem.* **1999**, *47*, 1092-1097.

47. Munday-Finch, S. C.; Wilkins, A. L.; Miles, C. O. *J. Agric. Food Chem.* **1998**, *46*, 590-598.

48. Tapper, B. A.; Lane, G. A. Janthitrems found in a *Neotyphodium* endophyte of perennial ryegrass. In *5th International Symposium on Neotyphodium/Grass Interactions*, 2004; Vol. 301.

49. Gallagher, R. T.; Campbell, A. G.; Hawkes, A. D.; Holland, P. T.; McGaveston, D. A.; Pansier, E. A. *N. Z. Vet. J.* **1982**, *30*, 183-184.

50. Munday-Finch, S. C.; Miles, C. O.; Wilkins, A. L.; Hawkes, A. D. *J. Agric. Food Chem.* **1995**, *43*, 1283-1288.

51. Miles, C. O.; Munday, S. C.; Wilkins, A. L.; Ede, R. M.; Towers, N. R. *J. Agric. Food Chem.* **1994**, *42*, 1488-1492.
52. Munday-Finch, S. C.; Wilkins, A. L.; Miles, C. O.; Ede, R. M.; Thomson, R. A. *J. Agric. Food Chem.* **1996**, *44*, 2782-2788.
53. Gallagher, R. T.; Hawkes, A. D.; Steyn, P. S.; Vleggaar, R. *J. Chem. Soc., Chem. Commun.* **1984**, 614-616.
54. Ede, R. M.; Miles, C. O.; Meagher, L. P.; Munday, S. C.; Wilkins, A. L. *J. Agric. Food Chem.* **1994**, *42*, 231-233.
55. Munday-Finch, S. C. Aspects of the chemistry and toxicology of indole-diterpenoid mycotoxins involved in tremorganic disorder of livestock. PhD Thesis, University of Waikato, 1997.
56. Miles, C. O.; Wilkins, A. L.; Gallagher, R. T.; Hawkes, A. D.; Munday, S. C.; Towers, N. R. *J. Agric. Food Chem.* **1992**, *40*, 234-238.
57. Gallagher, R. T.; Hawkes, A. D.; Stewart, J. M. *J. Chromatogr.* **1985**, *321*, 217-226.
58. England, D. B.; Magolan, J.; Kerr, M. A. *Org. Lett.* **2006**, *8*, 2209-2212.
59. Selala, M. I.; Musuku, A.; Schepens, P. J. C. *Anal. Chim. Acta.* **1991**, *244*, 1-8.
60. Kawai, K.; Nozawa, K. *Bioact. Mol.* **1989**, *10*, 205-212.
61. Belofsky, G. N.; Gloer, J. B.; Wicklow, D. T.; Dowd, P. F. *Tetrahedron* **1995**, *51*, 3959-3968.
62. Nozawa, K.; Nakajima, S.; Kawai, K. I.; Udagawa, S. I. *J. Chem. Soc., Chem. Commun.* **1988**, *9*, 2607-2610.
63. Munday-Finch, S. C.; Wilkins, A. L.; Miles, C. O. *Phytochem.* **1996**, *41*, 327-332.
64. Mantle, P. G.; Weedon, C. M. *Phytochem.* **1994**, *36*, 1209-1217.
65. Nozawa, K.; Horie, Y.; Udagawa, S.; Kawai, K.; Yamazaki, M. *Chem. Pharm. Bull.* **1989**, *37*, 1387-1389.
66. Fehr, T.; Acklin, W. *Helv. Chim. Acta* **1966**, *49*, 1907-1910.
67. Huang, X. H.; Tomoda, H.; Nishida, H.; Masuma, R.; Omura, S. *J. Antibiot.* **1995**, *48*, 1-4.
68. TePaske, M. R.; Gloer, J. B.; Wicklow, D. T.; Dowd, P. F. *J. Nat. Prod.* **1992**, *55*, 1080-1086.

69. Laakso, J. A.; Narske, E. D.; Gloer, J. B.; Wicklow, D. T.; Dowd, P. F. *J. Nat. Prod.* **1994**, *57*, 128-133.
70. Springer, J. P.; Clardy, J. *Tetrahedron Lett.* **1980**, *21*, 231-234.
71. Cole, R. J.; Dorner, J. W.; Lansden, J. A.; Cox, R. H.; Pape, C.; Cunfer, B.; Nicholson, S. S.; Bedell, D. M. *J. Agric. Food Chem.* **1977**, *25*, 1197-1201.
72. Gallagher, R. T.; Finer, J.; Clardy, J.; Leutwiler, A.; Weibel, F.; Acklin, W.; Arigoni, D. *Tetrahedron Lett.* **1980**, *21*, 235-238.
73. Cole, R. J.; Dorner, J. W.; Springer, J. P.; Cox, R. H. *J. Agric. Food Chem.* **1981**, *29*, 293-295.
74. Huang, X.-H.; Nishida, H.; Tomoda, H.; Tabata, N.; Shiomi, K.; Yang, D.-J.; Takayanagi, H.; Omura, S. *J. Antibiot.* **1995**, *48*, 5-11.
75. Tomoda, H.; Tabata, N.; Yang, D.; Takayanagi, H.; Omura, S. *J. Antibiot.* **1995**, *48*, 793-804.
76. Gallagher, R. T.; Latch, G. C. M.; Keogh, R. G. *Appl. Environ. Microbiol.* **1980**, *39*, 272-273.
77. Kawahara, T.; Nagai, A.; Takagi, M.; Shin-ya, K. *J. Antibiot.* **2012**, *65*, 535-538.
78. Finch, S. C.; Wilkins, A. L.; Popay, A. J.; Babu, J. V.; Tapper, B. A.; Lane, G. A. The Isolation and Bioactivity of Epoxy-janthitrems from AR37 Endophyte-infected Perennial Ryegrass. Poster 80. In *Proceedings of the 7th International Symposium of Fungal Endophytes of Grasses*, 2010.
79. Bush, L. P.; Wilkinson, H. H.; Schardl, C. L. *Plant Physiol.* **1997**, *114*, 1-7.
80. Schardl, C. L.; Florea, S.; Pan, J.; Nagabhyru, P.; Bec, S.; Calie, P. J. *Curr. Opin. Plant Biol.* **2013**, *16*, 480-488.
81. Schardl , C. L.; Young, C. A.; Hesse, U.; Amyotte, S. G.; Andreeva, K.; Calie, P. J.; Fleetwood, D. J.; Haws, D. C.; Moore, N.; Oeser, B.; Panaccione, D. G.; Schweri, K. K.; Voisey, C. R.; Farman, M. L.; Jaromczyk, J. W.; Roe, B. A.; O'Sullivan, D. M.; Scott, B.; Tudzynski, P.; An, Z.; Arnaoudova, E. G.; Bullock, C. T.; Charlton, N. D.; Chen, L.; Cox, M.; Dinkins, R. D.; Florea, S.; Glenn, A. E.; Gordon, A.; Güldener, U.; Harris, D. R.; Hollin, W.; Jaromczyk, J.; Johnson, R. D.; Khan, A. K.; Leistner, E.; Leuchtmann, A.; Li, C.; Liu, J.; Liu, J.; Liu, M.; Mace, W.; Machado, C.; Nagabhyru, P.; Pan, J.; Schmid, J.; Sugawara, K.; Steiner, U.; Takach, J. E.; Tanaka, E.; Webb, J. S.; Wilson, E. V.; Wiseman, J. L.;

Yoshida, R.; Zeng, Z. *PLoS Genetics* **2013**, *9*, https://doi.org/10.1371/journal.pgen.1003323.

82. Young, C. A.; Felitti, S.; Shields, K.; Spangenberg, G.; Johnson, R. D.; Bryan, G. T.; Saikia, S.; Scott, B. *Fungal Genet. Biol.* **2006**, *43*, 679-693.
83. Saikia, S.; Takemoto, D.; Tapper, B. A.; Lane, G. A.; Fraser, K.; Scott, B. *FEBS Letters* **2012**, *586*, 2563-2569.
84. Popay, A. J. *N. Z. Plant Prot.* **2001**, *54*, 251.
85. Gallagher, R. T.; Hawkes, A. D. *Experientia* **1986**, *42*, 823-825.
86. Mortimer, P. H.; Fletcher, L. R.; Di Menna, M. E.; Harvey, I. C.; Smith, G. S.; Barker, G. M.; Gallagher, R. T.; White, E. P. *Proc. Ruakura Farmers' Conf.* **1982**, *34*, 71-74.
87. Prestidge, R. A.; Pottinger, R. P.; Barker, G. M. *Proc. N. Z. Weed Pest Control Conf.* **1982**, *35*, 119-122.
88. Barker, G. M.; Pottinger, R. P.; Addison, P. J.; Prestidge, R. A. *N. Z. J. Agric. Res.* **1984**, *27*, 271-277.
89. Dymock, J. J.; Rowan, D. D.; McGee, I. R. *Proc. Australas. Conf. Grassl. Invertebr. Ecol., 5th* **1988**, *5*, 35-43.
90. Fletcher, L. R.; Markham, L. J.; White, S. R. *Proc. N. Z. Grassl. Assoc.* **1994**, *56*, 265-270.
91. Fletcher, L. R.; Finch, S. C.; Sutherland, B. L.; deNicolo, G.; Mace, W. J.; van Koten, C.; Hume, D. E. *N. Z. Vet. J.* **2017**, *65*, 232-241.
92. McLeay, L. M.; Smith, B. L.; Munday-Finch, S. C. *Res. Vet. Sci.* **1999**, *66*, 119-127.
93. McMillan, L. K.; Carr, R. L.; Young, C. A.; Astin, J. W.; Lowe, R. G. T.; Parker, E. J.; Jameson, G. B.; Finch, S. C.; Miles, C. O.; McManus, O. B.; Schmalhofer, W. A.; Garcia, M. L.; Kaczorowski, G. J.; Goetz, M.; Tkacz, J. S.; Scott, B. *Mol. Genet. Genomics* **2003**, *270*, 9-23.
94. Popay, A. J.; Wyatt, R. T. *Proc. N. Z. Plant Prot. Conf.* **1995**, *48*, 229-36.
95. Popay, A. J.; Thom, E. R. *Proc. N. Z. Grassl. Assoc.* **2009**, *71*, 121-126.
96. Babu, J. Bioactive chemicals of importance in endophyte-infected grasses. PhD Thesis, University of Waikato, New Zealand, 2009.
97. Hennessy, L. Epoxy-janthitrems, effects of temperature on *in planta* expression and their bioactivity against porina larvae. MSc Thesis, University of Waikato, Hamilton, New Zealand, 2015.

98. Bluett, S. J.; Thom, E. R.; Clark, D. A.; Macdonald, K. A.; Minneé, E. M. K. *N. Z. J. Agric. Res.* **2005a**, *48*, 197-212.
99. Prestidge, R. A.; Gallagher, R. T. *Proc. N. Z. Weed Pest Control Conf.* **1985**, *38*, 38-40.
100. Dymock, J. J.; Prestidge, R. A.; Rowan, D. D. *Proc. N. Z. Weed Pest Control Conf.* **1989**, *42*.
101. Dowd, P. F.; Cole, R. J.; Vesonder, R. F. *J. Antibiot.* **1988**, *41*, 1868-1872.
102. Prestidge, R. A.; Ball, O. J. P. The role of endophytes in alleviating plant biotic stress in New Zealand. In *Proceedings of the Second International Symposium of Acremonium/Grass Interactions*, 1993; pp 141-151.
103. Barker, G. M. *Ann. Appl. Biol.* **2008**, *153*, 381-393.
104. Ferguson, C. M.; Barratt, B. I. P.; Bell, N.; Goldson, S. L.; Hardwick, S.; Jackson, M.; Jackson, T. A.; Phillips, C. B.; Popay, A. J.; Rennie, G.; Sinclair, S.; Townsend, R.; Wilson, M. *N. Z. J. Agric. Res.* **2018**.
105. Popay, A. J.; Hume, D. E. Endophytes improve ryegrass persistence by controlling insects. In *Pasture Persistence* 2011; pp 149-156.
106. Popay, A., J; Goldson, S. L.; McCulley, R. L.; Ferguson, C. M. *N. Z. Plant Prot.* **2011**, *64*, 55-62.
107. Ferguson, C. M.; Shand, J. A.; Evans, A. A.; Barratt, B. I. P. *Proc. N. Z. Plant Prot. Conf.* **1994**, *47*, 279-281.
108. Spiller, D.; Turbott, E. G. *Rec. Auck. Inst.* **1994**, *3*, 79-83.
109. Piddock, G., Black beetles could damage Waikato pastures in summer. *Waikato Times* 26 Aug 2014, 2014.
110. Hume, D. E.; Ryan, D. L.; Cooper, B. M.; Popay, A. J. *Proc. N. Z. Grassl. Assoc.* **2007**, *69*, 201-205.
111. East, R.; King, P. D.; Watson, R. N. *N. Z. J. Ecol.* **1981**, *4*, 56-64.
112. Pearson, W. D. *Proc. Australas. Conf. Grassl. Invertebr. Ecol., 5nd* **1988**, *5*, 297-303.
113. Thom, E. R.; Popay, A. J.; Hume, D. E.; Fletcher, L. R. *Crop Pasture Sci.* **2012**, *63*, 927-943.
114. AR37 for persistent dairy pastures. Root aphid - fact sheets. http://www.ar37.com.au/ (accessed September 2014).
115. Popay, A.; Gerard, P. J. *N. Z. Plant Prot.* **2007**, *60*, 223-227.
116. Popay, A. J.; Cox, N. R. *Front. Plant Sci.* **2016**, *7*, 1395.

117. Jensen, J. G.; Popay, A. J. Reductions in root aphid populations by non-toxic endophyte strains in tall fescue. In *Grasslands Research and Practice. 'Proceedings of the 6th International Symposium on Fungal Endophytes of Grasses'*, New Zealand Grassland Association: Dunedin, 2007; Vol. 13, pp 341-344.

118. Lefort, M. C.; Boyer, S.; Vereijssen, J.; Sprague, R.; Glare, T. R.; Worner, S. P. *PeerJ.* **2015**, *3*, 1454.

119. Milne, G. Can pasture persistence be improved through the use of non-ryegrass species? In *Grassland Research and Practice Series*, 2011; Vol. 15, pp 157-162.

120. Latch, G. C. M.; Tapper, B. A. *Proc. Jap. Assoc. Mycotoxicology Suppl.* **1988**, *1*, 220-223.

121. Latch, G. C. M.; Christensen, M. J. *Ann. Appl. Biol.* **1985**, *107*, 17-24.

122. Popay, A. J.; Latch, G. C. M. *Proc. Australas. Conf. Grassl. Invertebr. Ecol., 6th* **1993**, *6*, 129-155.

123. Easton, H. S.; Christensen, M. J.; Eerens, J. P. J.; Fletcher, L. R.; Hume, D. E.; Keogh, R. G.; Lane, G. A.; Latch, G. C. M.; Pennell, C. G. L.; Popay, A. J.; Rolston, M. P.; Sutherland, B. L.; Tapper, B. A. *Proc. N. Z. Grassl. Assoc.* **2001**, *63*, 37-46.

124. Popay, A. J.; Hume, D. E.; Baltus, J. G.; Latch, G. C. M.; Tapper, B. A.; Lyons, T. B.; Cooper, B. M.; Pennell, C. G.; Eerens, J. P. J.; Marshall, S. L. In *Field performance of perennial ryegrass (Lolium perenne) infected with toxin-free fungal endophytes (Neotyphodium spp.)*, Grassland Research and Practice Series, 1999; pp 113-122.

125. Popay, A. J.; Silvester, W. B.; Gerard, P. J. New endophyte isolate suppresses root aphid, *Aploneura lentisci*, in perennial ryegrass. In *5th International Symposium on Neotyphodium/Grass Interactions*, 2004; p 317.

126. Stewart, A. V.; Charlton, J.; Association, N. Z. G. *Pasture and forage plants for New Zealand*. New Zealand Grassland Association, New Zealand Grassland Trust: 2006.

127. Lane, G. A. *Ryegrass endophyte: An essential New Zealand symbiosis* **1999**, 85-94.

128. Mantle, P. G.; Burt, S. J.; Macgeorge, K. M.; Bilton, J. N.; Sheppard, R. N. *Xenobiotica* **1990**, *20*, 809-821.
129. Advanced Chemistry Development, Inc. (ACD/Labs) Software V14.01 (© 1994-2013 ACD/Labs Release 2012), accessed via Chemsketch 3D (Freeware) 2012, (accessed October 2018).
130. Advanced Chemistry Development, Inc. (ACD/Labs) Software V11.01 (© 1994-2018 ACD/Labs), accessed via SciFinder database, (accessed September 2018).
131. Nair, J. J.; Ndhlala, A. R.; Chukwujekwu, J. C.; Van Staden, J. *J. S. Afr. Bot.* **2012**, *80*, 21-24.
132. Laakso, J. A.; Gloer, J. B.; Wicklow, D. T.; Dowd, P. F. *J. Org. Chem.* **1992**, *57*, 2066-2071.
133. Li, C.; Gloer, J. B.; Wicklow, D. T.; Dowd, P. F. *Org. Lett.* **2002**, *4*, 3095-3098.
134. Kimura, Y.; Nishibe, M.; Nakajima, H.; Hamasaki, T.; Shigemitsu, N.; Sugawara, F.; Stout, T. J.; Clardy, J. *Tetrahedron Lett.* **1992**, *33*, 6987-6990.
135. Kawai, K.; Nozawa, K. *Mycotoxin and Phytcotoxins* **1988**, 205-212.
136. Nozawa, K.; Yuyama, M.; Nakajima, S.; Kawai, K.; Udagawa, S. *J. Chem. Soc., Perkin Trans.1* **1988**, *8*, 2155-2160.
137. Gatenby, W. A. An investigation of some mycotoxins involved in ryegrass staggers. MSc Thesis, University of Waikato, 1997.
138. Saikkonen, K.; Wäli, P.; Helander, M.; Faeth, S. H. *Trends in Plant Science* **2004**, *9*, 275-280.
139. Porter, J. K. *J. Anim. Sci.* **1995**, *73*, 871-880.
140. Rowan, D. D.; Dymock, J. J.; Brimble, M. A. *J. Chem. Ecol.* **1990**, *16*, 1683-1695.
141. Siegel, M. R.; Bush, L. *Phytochem.* **1995**, *21*, 81-119.
142. Tapper, B. A.; Latch, G. C. M. Selection against toxin production in endophyte-infected perennial ryegrass. In *Grassland Research and Practice Series*, 1994; Vol. 7, pp 107-111.
143. Easton, H. S.; Lyons, T. B.; Cooper, B. M.; Mace, W. J. *Proc. N. Z. Grassl. Assoc.* **2009**, *71*, 151-154.
144. Young, C. A.; Tapper, B. A.; May, K.; Moon, C. D.; Schardl, C. L.; Scott, B. *Appl. Environ. Microbiol.* **2009**, *75*, 2200-2211.

145. Dugdale, J. S. *Hepialidae (Insecta: Lepidoptera) Fauna of New Zealand*. Manaaki Whenua Press: Christchurch, 1994; p 164.
146. Brown, B.; Emberson, R. M.; Paterson, A. M. *Bull. Entomol. Res.* **1999**, *89*, 287-293.
147. Richards, N. K.; Mansfield, S.; Townsend, R. J.; Ferguson, C. M. *Pest Manage. Sci.* **2017**, *73*, 2334-2344.
148. Porina *Wiseana* spp. - Identification, monitoring and management options. http://www.beeflambnz.com/ (accessed May 2015).
149. Ferguson, C. M. *N. Z. Plant Prot.* **2000**, *53*, 430-435.
150. Brownbridge, M.; Ferguson, C.; Saville, D. J.; Swaminathan, J.; Hurst, M. R. H.; Jackson, T. A. *N. Z. Plant Prot.* **2008**, *61*, 229-235.
151. Jensen, J. G.; Popay, A. J. *N. Z. Plant Prot.* **2004**, *57*, 323-328.
152. Hennessy, L. M.; Popay, A. J.; Finch, S. C.; Clearwater, M. J.; Cave, V. M. *Front. Plant Sci.* **2016**, *7*, 1097.
153. Popay, A. J. Personal communication. AgReseach Ltd (Hamilton, New Zealand), August 2018.
154. Bultman, T. L.; Borowicz, K. L.; Schneble, R. M.; Coudron, T. A.; Bush, L. P. *Oikos* **1997**, *78*, 170-176.
155. Rasmussen, S.; Lane, G.; Mace, W. J.; Parsons, A. J.; Fraser, K.; Xue, H. *Methods Mol. Biol.* **2012**, *860*, 213-226.
156. Carpenter, A. *N. Z. Entomol.* **1983**, *7*, 466-467.